Technische Universität München

Department Chemie
Lehrstuhl für Biotechnologie

Mechanistic Analysis of Conformational Dynamics of the Molecular Chaperone Hsp90

Franziska Tippel

Vollständiger Abdruck der von der Fakultät für Chemie der Technischen Universität München zur Erlangung des akademischen Grades eines

DOKTORS DER NATURWISSENSCHAFTEN

genehmigten Dissertation.

Vorsitzende: Prof. Dr. Kathrin Lang

Prüfer der Dissertation:

1. Prof. Dr. Johannes Buchner
2. Prof. Dr. Michael Sattler

Die Dissertation wurde am 20.12.2016 bei der Technischen Universität München eingereicht und durch die Fakultät für Chemie am 07.02.2017 angenommen.

“It does not matter if this interpretation was true or false; it was a working link between imagination and reality, like love. “

- Ferruccio Ritossa

CONTENTS

1 Summary

Cellular viability depends on a well-balanced protein homeostasis during physiological and stress conditions. Stress response mechanisms, especially molecular chaperones, help to maintain the proteome integrity. The essential heat shock protein 90 (Hsp90) belongs to these primary guardians in eukaryotic cells. Besides promoting protein folding and preventing protein aggregation, Hsp90 is responsible for the maturation of a variety of client proteins. Hsp90 accomplishes client activation by large conformational rearrangements that are coupled to slow ATP hydrolysis. The Hsp90 ATPase cycle is fine-tuned by a set of co-chaperones and further regulated by post-translational modifications. Comprehensive structural and biochemical studies have contributed to our current knowledge of the mechanism of Hsp90. However, central issues such as isoform specificity and differences between the human and the yeast Hsp90 cycle regarding conformational dynamics are still elusive.

Two isoforms of Hsp90 occur in yeast as well as in humans, a constitutive expressed form (Hsc82, Hsp90β) and a heat-inducible one (Hsp82, Hsp90α), respectively. Little is so far known about mechanistic and functional differences between these isoforms. In the first part of this work, the *in vitro* and *in vivo* properties of Hsp82 and Hsc82 were systematically explored. *In vitro*, the isoforms vary in their ATPase activities and the kinetics of conformational transitions. Specific co-chaperones display different binding affinities for the Hsp90 isoforms and differently impact the ATPase activity and the conformational changes during the ATPase cycle. *In vivo,* the impact of radicicol and amino acid depletion is Hsp90 isoform-dependent. The data thus indicate that subtle but significant differences exist between the Hsp90 isoforms in yeast. Since Hsp90 is highly conserved from bacteria to man, our findings for yeast Hsp90 help to understand the general underlying mechanism.

In a second project, conformational dynamics of the human Hsp90 isoforms, with regard to structural changes and interdomain communication was the focus. To monitor the dynamic Hsp90 machinery, a human Hsp90 FRET system was developed. The premise of a functional FRET setup is how to site-specifically attach a fluorescent dye to human Hsp90. For labeling reactive fluorescent dyes are used

that readily react with thiol groups of cysteines within a protein. As the human Hsp90α/β isoforms carry seven/six natural cysteines it turned out that this is not as simple as for the yeast Hsp90 FRET system. The replacement of all naturally occurring cysteines impacts in particular p23 binding to Hsp90 indicating altered conformational dynamics. The generated Hsp90 variant was used for first FRET experiments and the formation of a FRET competent complex was detected. However, nucleotide-induced closure of Hsp90 could not be observed. In addition, segmental-labeling and domain ligation of Hsp90 mediated by Sortase A (SrtA) was conducted. In this approach, all natural cysteines, located in the MD and CTD of Hsp90, remain intact. While a comprehensive *in vivo* analysis looked promising, p23 binding was once again negatively affected. As an alternative approach, the use of SrtA-mediated domain ligation was successfully applied. This method also enables new possibilities to investigate human Hsp90 dynamics or client binding via efficient segmental-isotope labeling for future NMR experiments. Taken together, it seems indespensible to work with authentic human Hsp90 when analyzing conformational dynamics. For this reason the most attractive way is to utilize the expansion of the genetic code to incorporate unnatural amino acids. To obtain site-specific labeling only one amino acid position has to be changed. To this end, an amber suppression codon was introduced at the respective positions. While the first experiments revealed that unspecific incooperation takes place, the improvement of this method will allow specific incorporation into Hsp90 at different sites.

2 Introduction

Proteins belong to the basic building blocks of life, as they are indispensible for every living cell in terms of structure, regulation, signaling and metabolism. The world of proteins is fascinating due to the fact that they play a role in nearly every biological process and there are so many. An average mammalian cell comprises 10.000 - 28.000 different proteins (Moran et al., 2010; Muller et al., 2002). Proteins are able to fulfill a wide variety of tasks since they contain diverse functional groups. Depending on the arrangement of reactive groups within a protein structure, it is for example able to catalyze a specific enzymatic reaction. Another layer of complexity is the capacity of proteins to interact with other proteins or macromolecules. Larger proteins consist of several modules and every module represents a single protein domain. A protein domain is characterized by an independent, compact structure with individual function. Thus large protein complexes transform to molecular machineries in the cell. A striking feature of proteins is the degree of structural flexibility. Some proteins form rigid entities whereas others are highly flexible and thus are able to adopt different conformational states. Proteins emerge as long linear polypeptide chains, consisting of amino acids connected via peptide bonds, from the ribosome, the birthplace of proteins. After protein synthesis proteins have to adopt a unique three-dimensional structure also termed as fold, to get ready for action. The process from a linear polypeptide chain to a globular 3D structure is called protein folding (Dobson and Karplus, 1999).

2.1 Theory of Protein Folding

For the first time Christian Anfinsen's experiments with ribonuclease had demonstrated that the information of the final folded state is encoded in the amino acid sequence (Anfinsen, 1973). The experiments showed that non-active denatured ribonuclease can fold spontaneously back into its native active state. Similar experiments were applied to many more proteins to illustrate a general mechanism. This also shows that protein folding is a reversible process. In fact, protein folding is not just a two-state process and simple, rather it is a long complex way to the native state of a protein. This goes along with another important aspect; the time a protein needs to fold depends on the conformational states a protein can adopt during the process. Levinthal calculated for a rather small protein, consisting of 100 amino acids, a folding reaction time of 1.6×10^{27} years (Dill and Chan, 1997). This points out that proteins have to fold in a directed way to ensure structure formation in a

biologically relevant timescale. The driving force in this process is the decrease of free enthalpy of the folding reaction. To visualize the energy landscape of the folding process one can imagine a folding funnel (*Figure 1*) (Onuchic and Wolynes, 2004) with a rough and hilly surface. The top of the funnel describes the highest entropy states of an unfolded protein. On the way down towards the native folded structure, most proteins undergo a fast hydrophobic collapse and form intermediate states, which are stabilized by intra-molecular contacts. From here a protein can adopt less possible conformations and faces new energy barriers which cause the formation of kinetically trapped intermediate species (Brockwell and Radford, 2007). Finally, the global energy minimum of the correctly folded state is reached at the deepest point of the funnel. However, the native state of a protein is not a definite frozen state rather as mentioned before it exhibits a highly dynamic nature, which is one of the important features of proteins (Onuchic and Wolynes, 2004).

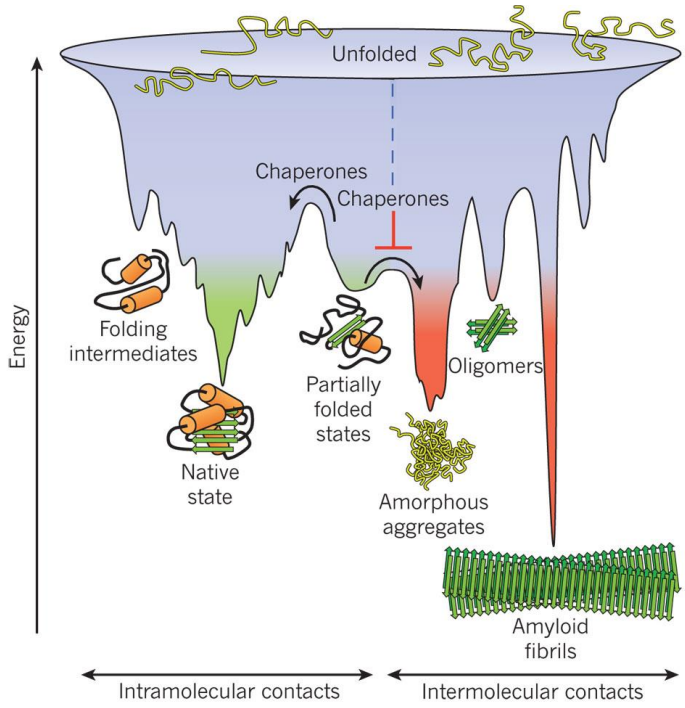

Figure 1: **The energy landscape of protein folding pathways illustrated by a folding funnel.** The folding funnel describes the unfolded state of a protein with the highest free energy at the top and the finally folded state of a protein with lower free energy represents the minimum. The way down a protein reaches its native state or can be kinetically trapped in stable partially folded states via intramolecular contacts. Chaperones assist protein folding or prevent the formation of intermolecular contacts that results in amorphous aggregates, higher oligomers or amyloid fibrils *in vivo*. ((Hartl et al., 2011) Rights and permission order number 3984780919955)

Additionally, the native structure is only marginally stable, and slight changes in the primary amino acid sequence can lead to a protein structure that results in an unstable form. At several stages of the folding pathway, a protein can form kinetically stable but not correctly folded states, termed misfolded proteins. These intermediate states or partially unfolded often expose hydrophobic patches that tend to aggregate and form larger oligomer complexes. The larger a protein the more likely such folding intermediates are (Bartlett and Radford, 2009). As this is the case for many proteins, there is generally a high risk of unspecific interaction resulting in misfolded proteins and amorphous aggregates. Furthermore, protein aggregation of a native protein also arises when exposed to several stresses, like increased temperature, pH shifts or heavy metals (Dobson, 2003; Richter et al., 2010).

In the recent past, it became clear that protein misfolding and aggregation leads to an imbalance in protein homeostasis in the cell and is linked to several diseases like neurodegenerative diseases, myopathies and even cancer (Balch et al., 2008; Powers et al., 2009). Although correct protein folding occurs for some proteins spontaneously and within microseconds, another layer of regulation is needed in the cell. To monitor the faith of proteins and to guarantee well balanced proteostasis the cell evolved a complex protein quality control network accomplished by the guardians of the proteome comprising chaperones, co-chaperones and adapter proteins providing a link to the protein degradation machinery.

2.2 Protein Folding in the Cell

To investigate and understand protein folding in a clear and simplified way, experiments were performed with isolated, diluted proteins *in vitro*. This is in contrast to how protein folding occurs in a cellular environment. Newly synthesized proteins as well as already folded proteins face several issues in the cytosol, such as macromolecular crowding (Ellis, 2001) with a protein concentration in the cell of 300 – 400 mg/ml (Zimmerman and Trach, 1991), a compartmentalized environment, hindered mobility and sticky neighbors (Gershenson and Gierasch, 2011). A crowded cellular environment causes the excluded volume effect where the volume of solvent is reduced (Minton, 2001). The large amount of proteins and other marcomolecules engage most of the volume in the cell therby reducing the volume of solvent for others. Hence, the concentration of proteins increases the chance of non-native and flexible protein structures to aggregate. Additionally, an emerging polypeptide chain at the ribosome can start to fold co-translational during protein synthesis

(Frydman et al., 1999). The cell offers spatial organization due to membranes and compartmentalization that allow establishing microenvironments and reaction compartments. Together, these aspects offer different topologies for protein folding, transport and additional protein modifications in the cell but raise new challenges on the other hand to ensure proteome integrity and healthy protein homeostasis. Hence, protein folding in the cell is complex than in the test tube and thus a higher potential for aberrant protein folding and aggregation exists. To ensure controlled and efficient protein folding, the cell is equipped with folding assistants called molecular chaperones.

2.3 Role of Molecular Chaperones in Protein Folding and Maintenance of Proteostasis

Besides promoting protein folding molecular chaperones prevent protein aggregation, recognize misfolded proteins and some have the ability to refold them (Hartl and Hayer-Hartl, 2009). Molecular chaperones were first described in the early 1990s (Ellis, 1987; Georgopoulos and Welch, 1993; Hartl, 1996). Many of them are also termed heat shock proteins (Hsps) as their up-regulation in cells was observed by exposure to elevated temperatures (Lindquist, 1980). Way earlier Ritossa and colleagues observed by serendipity heat shock response in drosophila chromosome puffs (Ritossa and Vonborstel, 1964). Later it was shown that these expression patterns belong to Hsps and other chaperones (Lindquist, 1980). Furthermore it was approved to be a general mechanism to cope with several cellular stresses (Richter et al., 2010). The picture became clearer as it was shown that molecular chaperones are ubiquitously expressed under physiological conditions at high levels. This points out the importance of molecular chaperones in protein folding. The cell evolved a complex chaperone network consisting of several highly conserved heat shock protein families (*Figure 2*).

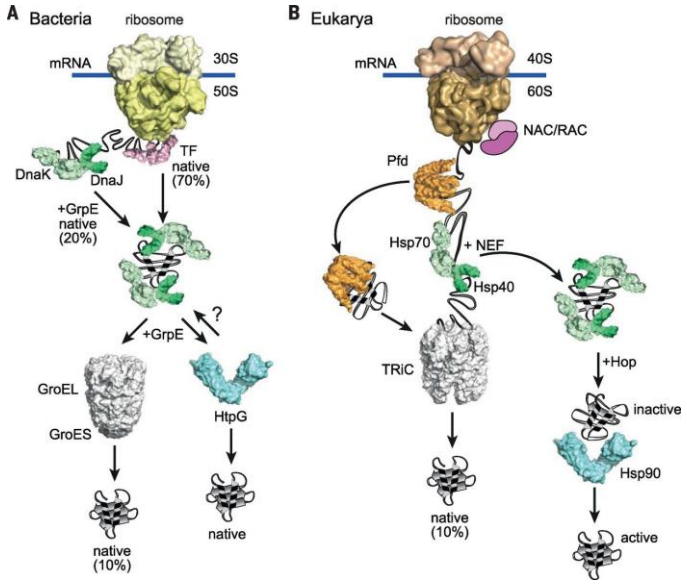

Figure 2: **Chaperone pathways of protein folding in the cytosol.** Nascent chains emerge from the exit tunnel of the ribosome and interact with **A**) trigger factor (TF) in bacteria and **B**) with the nascent-chain associated complex (NAC) and ribosome-associated complex (RAC) in eukaryotic cells. Protein Folding is ensured in a sequential manner by DnaK together with DnaJ and GrpE that assist folding and prevent protein aggregation. The GroEL and GroES complex facilitates folding and activation of larger and more complex proteins. Hsp70 acts together with Hsp40 and nucleotide exchange factors (NEFs) downstream of the ribosome in eukaryotes. Some nascent polypeptides are transferred directly to TCP-1 Ring complex (TRiC) by prefoldin (Pfd). The Hsp90 machinery interacts with metastable proteins and activates a broad spectrum of client proteins with the help of a cohort of co-chaperones. Client transfer from Hsp70 to Hsp90 is facilitated by Hop. In bacteria the Hsp90 homolog HtpG seems to act more generally without known co-chaperones. ((Balchin et al., 2016) Rights and permission order number 3984790152822)

The Hsps are classified by molecular weight (Hsp40, Hsp60, Hsp70, Hsp90, Hsp100 and the small Hsps). The business of chaperones starts already during synthesis at the ribosome. The guidance of assisted protein folding (70 % of proteins) is executed by a chaperone called trigger factor in bacteria (*Figure 2A*) (Oh et al., 2011). In eukaryotic cells, factors called nascent-chain associated complex (NAC) and ribosome-associated complex (RAC) cooperate together with the ribosome to ensure folding of larger emerging polypeptides (Figure 2*B*) (Preissler and Deuerling, 2012). Subsequently, the Hsp70 system has a pivotal role in the folding pathway (Calloni et al., 2012). Hsp70 (DnaK in bacteria) together with Hsp40 (DnaJ in bacteria) and nucleotide exchange factors NEFs (GrpE in bacteria) ensure proper protein folding of about 20 % of the proteome (*Figure 2A-B*) (Hartl and Hayer-Hartl, 2002; Willmund et al., 2013). The remaining 10 % of the proteome comprises even more complex proteins or need further assistance for full activation. To complete folding, some proteins are transferred either directly or via Hsp70 to the chaperonin TRiC (GroEL/ES in bacteria) or to the Hsp90 system (HtpG in bacteria) (*Figure 2A-B*) (Hartl and Hayer-Hartl, 2002; Langer et al., 1992; Rohl et al.,

2013). Some chaperones interact with the substrate protein via recruiter or adapter proteins (Rohl et al., 2013). This illustrates a sequential principle of several folding pathways in the cytosol and thus provides constant protection of newly synthesized proteins against aberrant misfolding, aggregation or subsequent degradation *in vivo* (Duttler et al., 2013).

The maintenance of a well-balanced proteome in terms of properly folded and regulated proteins under physiological and stress conditions is essential for cell viability (Balch et al., 2008). A disruption within the protein homeostasis network is associated with a number of misfolding diseases including lysosomal storage diseases (Sawkar et al., 2006), cystic fibrosis (Koulov et al., 2010), neurodegenerative diseases, such as Alzheimer, Parkinson's and Huntington's diseases and even cancer (Labbadia and Morimoto, 2015). A decline in proteostasis performance goes along with ageing (Taylor and Dillin, 2011). The cell responds with specialized proteins, such as molecular chaperones remodeling factors, the ubiquitin-protesom-system and autophagy involved proteins (Doyle et al., 2007), to restore the balance after a shift in protein homeostasis occurs (Hartl and Hayer-Hartl, 2009). All processes and involved proteins in protein homeostasis are summarized under the term proteostasis (*Figure 3*).

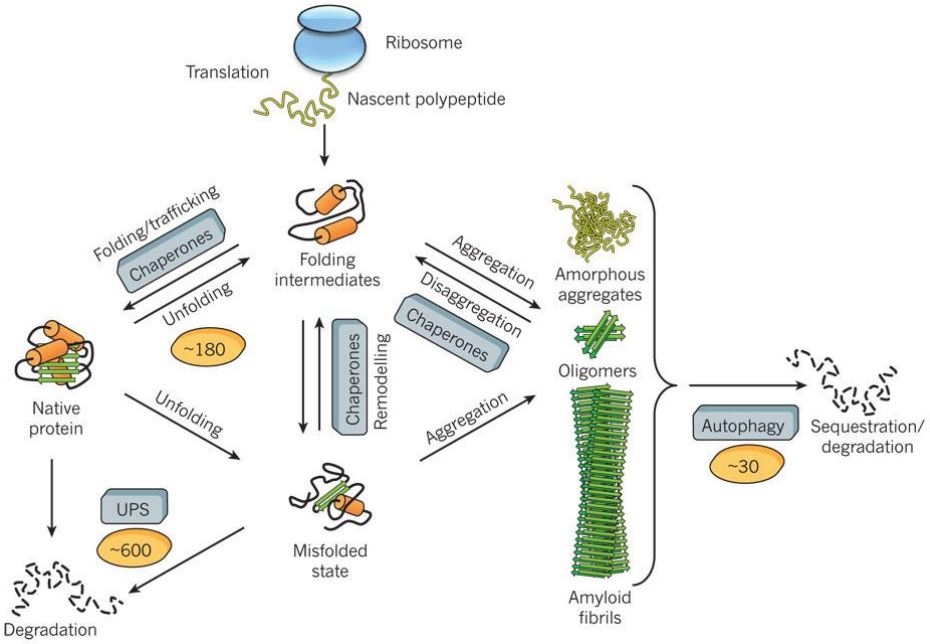

Figure 3: **Strategies to maintain protein homeostasis in the cell.** To ensure a balanced proteostasis a chaperone network employs serveral protein quality control strategies. Besides promoting protein-folding chaperones are able to unfold misfolded states. Molecular chaperones prevent aggregation and facilitate disaggregation in an ATP-dependent manner. To remove misfolded proteins via sequestration and degradation the chaperone network is linked to the ubiquitin-proteasome system (UPS) and autophagy. ((Hartl et al., 2011) Rights and permission order number 3990150117204)

Molecular chaperones constantly monitor the status of the proteome by recognizing misfolded proteins and further have to decide the fate of the aberrant protein (Chen et al., 2011). As a first line of defense, chaperones utilize ATP for refolding (*Figure 3*). Further, they are linked to the ubiquitin-proteasome system to promote their degradation in case refolding is not successful (*Figure 3)* (Chen et al., 2011; McClellan and Frydman, 2001; McClellan et al., 2005). Previous fluorescence microscopy studies have revealed another parallel strategy, namely spatial organization of protein quality control (Kaganovich et al., 2008). Sequestration of deleterious species into specialized cell compartments ensures proteostasis in case of an overload (Kaganovich et al., 2008). It is assumed that the strategy of sequestration is used to protect the cell from toxic misfolded amyloids (Chen et al., 2011). The compartments are visible under physiological as well as under stress conditions (*Figure 3*) (Kaganovich et al., 2008). Facilitating aggregate clearance and protecting the cell from toxic protein species was observed from yeast to mammals and seems to have a benefit for the cell. Hence, the organization of protein aggregation is much higher than previously assumed and is part of the regulation of protein homeostasis. Altogether, we have gotten an idea how the cell manages its proteostasis. However, new questions arise and still it is not understood which underlying mechanisms qualified chaperones as decision maker within the protein triage and protein quality control network.

2.4 Heat shock protein (Hsp)90 – Key Regulator of Protein Homeostasis

Hsp90 is ubiquitously expressed and a highly conserved ATP-dependent molecular chaperone that is required for cell viability in eukaryotes (Borkovich et al., 1989). As many chaperones, Hsp90 recognizes and binds misfolded proteins and thereby prevents protein aggregation. In contrast to other folding machineries, Hsp90 interacts with partially folded or intrinsically instable proteins. The broad spectrum of substrate proteins, termed clients, that only achieves full activity in an Hsp90-dependent mechanism makes the chaperone outstanding. Many Hsp90 clients belong to diverse signal protein families, such as kinases (Xu and Lindquist, 1993), E3 ligases (Taipale et al., 2012), transcription factors (Minet et al., 1999; Sepehrnia et al., 1996), hormone receptors (Sanchez et al., 1985) and other related proteins. 20 % of the proteome seems to interact direct or indirectly with Hsp90 and many of them are known whose activation is regulated by this special chaperone (Taipale et al., 2010). Hence, Hsp90 is described in the literature as a hub of the proteostasis network (McClellan et al., 2007; Taipale et al., 2010). Hsp90 is also involved in many different biological processes such as telomere maintenance (Holt et al., 1999), vesicular transport and trafficking (Chen and Balch, 2006), immune response (Li et al., 2002), viral infections (Geller et al., 2012) and cancer (Miyata et al., 2013; Whitesell and Lindquist, 2005). Recently, an extensive study indicated a role of Hsp90 as a nucleating site for the formation of larger complexes involved in cancer development (Rodina et al., 2016). Moreover, Hsp90 is known to be implicated in neurodegenerative diseases such as Alzheimer, Parkinson's and Huntington's diseases (Pratt et al., 2015; Reis et al., 2016). For this reason, Hsp90 became an attractive drug target for several applications. Currently, 13 specific Hsp90 inhibiors are tested in clinical trials (Gewirth, 2016; Neckers and Workman, 2012). Unlike other chaperones, the Hsp90 dimer functions as a late acting chaperone in cooperation with the Hsp70 system. Clients are transferred from Hsp70 via the adapter protein Hop (Sti1 in yeast) to Hsp90 (Wegele et al., 2006). To serve the needs of diverse clients, Hsp90 exhibits key features. A basic principle of client interaction is that Hsp90 recognizes exposed hydrophobic residues independent of the folding state. It is assumed that the binding strength seems to be strongly influenced by structurally flexibility of the substrate protein (Wandinger et al., 2008). Hsp90 differs from other chaperones in terms of binding sites. It does not seem to have a specific one, rather a wide interaction surface throughout the whole protomer (Mayer and Le Breton, 2015). Furthermore, Hsp90 undergoes large conformational changes driven by ATP binding and hydrolysis. This conformational cycle is regulated in a sequential manner by a set of co-chaperones, influenced by post-translational modifications and affected by clients itself (Pearl, 2016; Rohl et al., 2013).

Although the underlying mechanism of Hsp90 as a molecular chaperone has been studied now over a few decades, it is still enigmatic how Hsp90 copes with the variety of clients and how the conformational dynamics within Hsp90 is coupled to client activation. The following sections will describe these aspects in more detail.

2.4.1 Hsp90 Isoforms

The Hsp90 family is highly conserved in all kingdoms of life with the exception of archea where no Hsp90 was found yet (*Figure 4A*) (Chen et al., 2006). Most bacteria contain a single Hsp90 form, termed HtpG (Bardwell and Craig, 1987). During evolution, multiple gene duplications have led to variations in the Hsp90 isoform number among species (Chen et al., 2006; Gupta, 1995; Pantzartzi et al., 2013). In eukaryotes, Hsp90 is essential and in most vertebrates four isoforms exist: two major cytoplasmic Hsp90 isoforms, namely Hsp90α (Hsp90AA1) and Hsp90β (Hsp90AB1), as well as organelle-specific Hsp90 isoforms found in mitochondria (Trap1) and in the endoplasmic reticulum (Grp96). In humans, these isoforms share 85 % sequence identity, but differ in their expression and secretion pattern (Eustace et al., 2004; Ghaemmaghami et al., 2003; Metchat et al., 2009; Sreedhar et al., 2004), co-chaperone binding and N-terminal domain inhibitor specificity (Millson et al., 2007). Moreover, the activation of client proteins is also differentially affected by the isoforms (Millson et al., 2007). In contrast, the model organisms *Drosophila melanogaster* (Hsp83) and *Ceanorhabditis elegans* (Daf-21) comprise only one gene encoding Hsp90. *Saccharomyces cerevisiae* stand out by being one of the rare fungal species that possess two cytoplasmic isoform (Borkovich et al., 1989), the constitutively expressed Hsc82 and the stress-inducible Hsp82. At the amino acid level, the isoforms share 97 % identity and resemble more closely vertebrate Hsp90β than Hsp90α. Hsc82 and Hsp82 have been extensively used to study various general and yeast-specific aspects of Hsp90 biology, but beyond their deviating expression pattern, mechanistic and biological differences have remained largely enigmatic.

2.4.2 Hsp90 Domain Architecture and Specific Structural Key Features

Hsp90 masters its function as a dimer with identical subunits. The domain architecture is conserved among species with each monomer consisting of three domains: a N-terminal domain (NTD), followed by a long charged linker connecting it to the middle domain (MD) and a C-terminal domain

(CTD) (*Figure 4A-B*). The NTD comprises the ATPase binding site. The middle domain completes the ATPase domain and exhibits the major client-binding site. Dimerization is facilitated by the CTD.

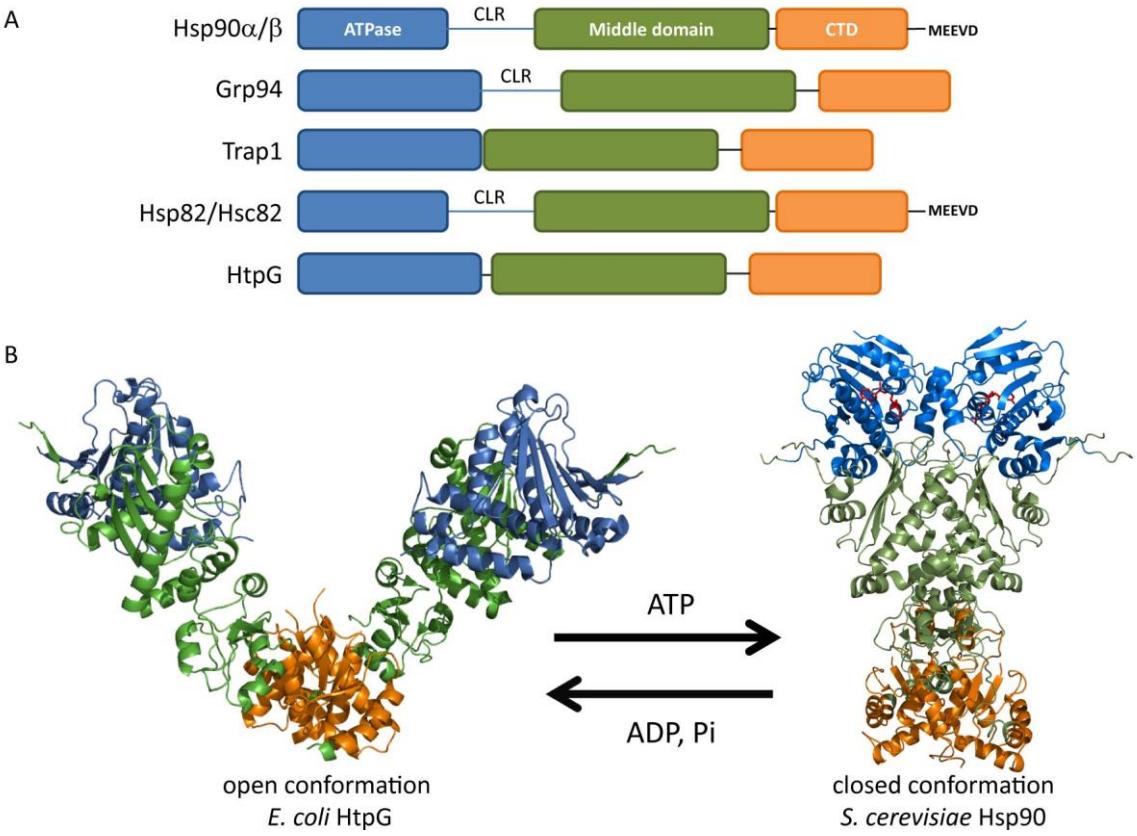

Figure 4: **Conserved Hsp90 domain structure. A**) Schematic presentation of the domain structure of different Hsp90 homologs. The N-terminal domain (NTD) is illustrated in blue, the middle domain (MD) in green and the C-terminal domain (CTD) in orange. The NTD is connected via a flixible charged linker (CLR) to the MD. **B**) The open V-shaped conformation with CTDs dimerized of Hsp90 (PDB 2IOQ). After ATP (depicted in red) binding Hsp90 undergoes large conformational changes and forms a compact closed conformation (PDB 2CG9) with dimerized NTDs and association of the MDs with NTDs.

Sequence homology between the NTD of Hsp90 with type II topoisomerases and MutL mismatch repair proteins revealed that Hsp90 belongs to the same domain family as it comprises a typical fold termed Bergerat fold (Bergerat et al., 1997). A first glimpse in Hsp90 mechanism was provided by crystal structures of the NTD (Prodromou et al., 1997; Stebbins et al., 1997) in the presense of ATP/ADP (*Figure 5* PDB 1AM1). Several natural compounds like geldanamycin (Stebbins et al., 1997) can occupy the ATP binding site and thereby inhibit Hsp90 ATPase activity. Further, this pioneer work identified key residues in the ATP binding pocket (Leu34, Asn37, Asp79, Asn92, Lys98, Gly121 and Phe124) (*Figure 5*). In the presence of Mg^{2+} ions and water molecules, electrostatic and hydrogen

bonds are formed between Hsp90 and the nucleotide. The residue Asp79 is one of only few that interact directly with the adenine base of ATP (*Figure 5*) and a substitution against asparagine (D79N) causes loss of viability in yeast due to loss of the ability to bind the nucleotide (Obermann et al., 1998; Panaretou et al., 1998).

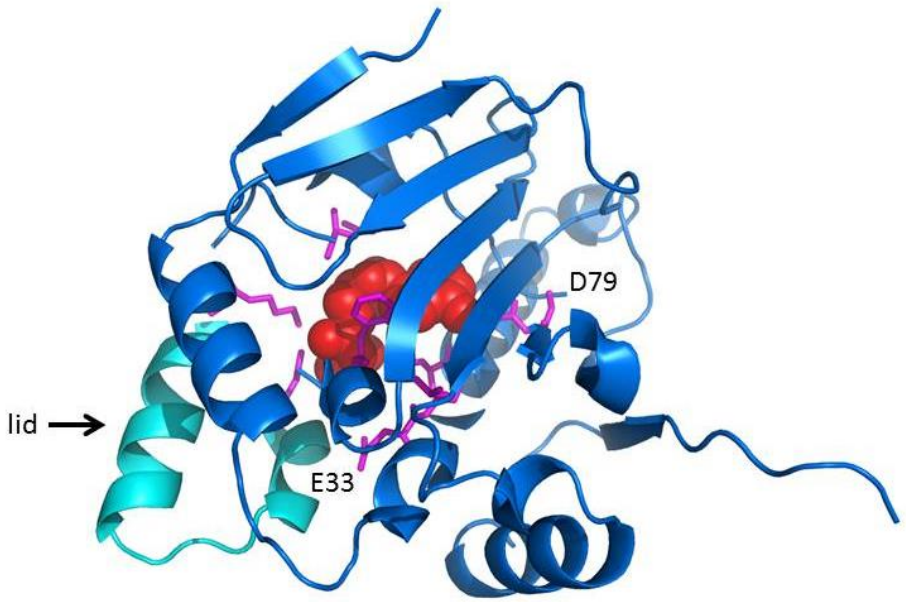

Figure 5 **The N-terminal domain of Hsp90.** The NTD of Hsp90 comprises the ATP binding pocket (PDB 1AM1). Key residues involved in ATP binding are marked in pink and the lid that closes over the pocket is depicted in cyan.

Additionally, the key residue Glu33 is required to hydrolyze ATP (*Figure 5*). An Hsp90 variant, where this particular residue is mutated against alanine (E33A), still binds ATP but cannot hydrolyze ATP anymore (Obermann et al., 1998; Panaretou et al., 1998). Another functional element is a helix-loop-helix (yeast Hsp82 Lys98-Gly121) element within the NTD (*Figure 5*), so-called lid that changes its position upon nucleotide binding and is involved in N-terminal dimerization (Prodromou et al., 1997; Stebbins et al., 1997).

The middle domain consists of a large $\alpha\beta\alpha$ domain followed by a smaller $\alpha\beta\alpha$ domain connected by short α helices. Like for other GHKL proteins, the Hsp90 MD contributes specific residues, termed the catalytic loop (Pro375-Ile388), required for full ATPase activity. Located within the catalytic loop, a conserved arginine residue Arg380 (*Figure 6*) was found to be stabilizing the γ-phosphate of the nucleotide (Cunningham et al., 2012). A mutation of this residue against alanine, R380A, exhibits lower ATPase and causes lethality in yeast (Cunningham et al., 2012; Meyer et al., 2003).

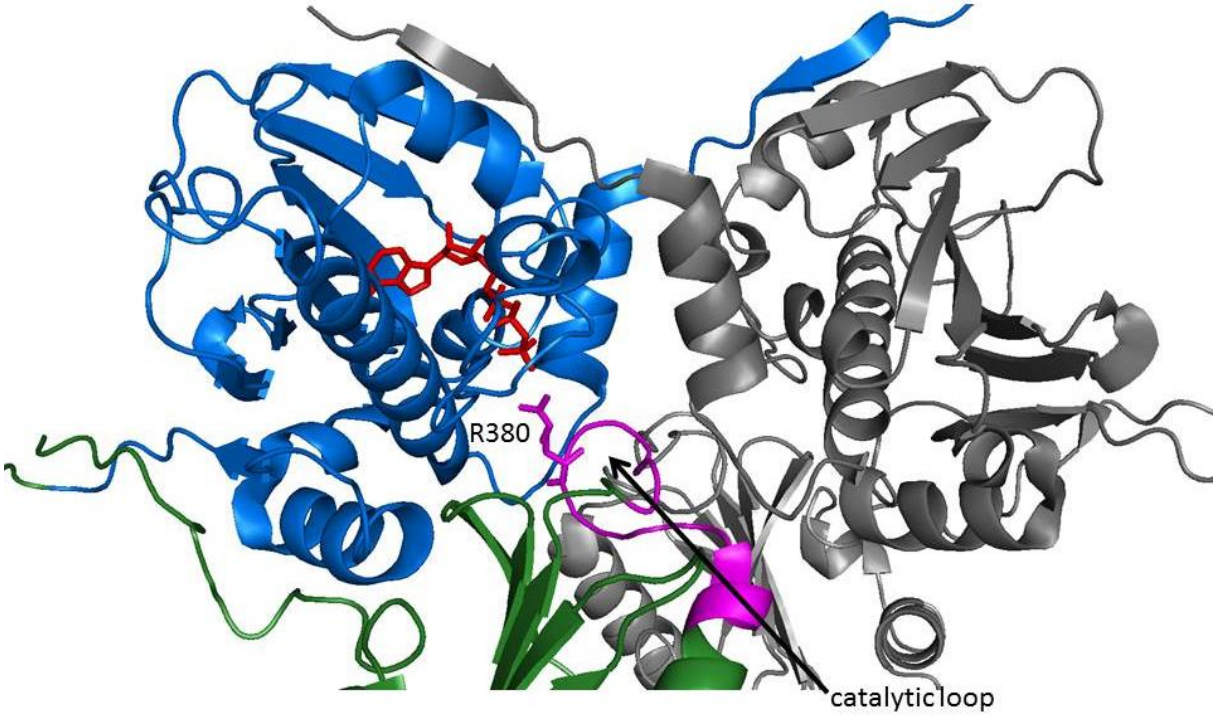

Figure 6: **The middle-domain of Hsp90 contributes to full ATPase activity.** In the closed conformation of Hsp90 the middle domains (green) get in close contact with the ATP binding site and the NTD (blue, one promoter is depicted in grey) (PDB 2CG9). The catalytic loop (pink) comprises a specific residue R380 that stabilizes the γ-phosphate of ATP.

The major site for client interactions is located in the MD with a conserved hydrophobic patch around residue W300 (refers to yHsp82) and a larger amphiphatic stretch between residues 327-340. A pair of helices forms the Hsp90 dimer at the very end of the CTD resulting in a four-helix bundle (*Figure 7*). Overall the CTD is similar among species but more divergent compared to the other Hsp90 domains. C-terminal dimerization is essential for Hsp90 function (Minami et al., 1994). The last five amino acids of the CTD form the MEEVD motif required for interaction with tetratricopeptide-domain containing co-chaperones (Scheufler et al., 2000). Bacteria are an exception; here, Hsp90 is lacking this motif. Due to flexibility of Hsp90, structural analysis of full-length Hsp90 was difficult. In the late 1990's first results were published that showed an open V-shaped Hsp90 (HtpG) (Shiau et al., 2006) and a closed compact structure of Hsp90 (yHsp82) (Ali et al., 2006).

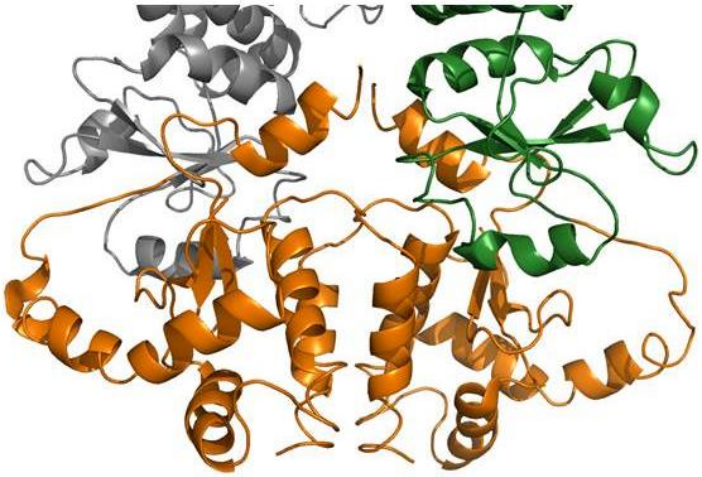

Figure 7: **The C-terminal domain of each promoter facilitates dimerization.** The zoom presents the dimerization's interface of the CTDs (orange) of Hsp90 (PDB 2CG9).

An important aspect of Hsp90 function seems to be the dynamic nature of the open state in the absence of nucleotide, where only the CTDs bind to each other. It was shown that the conformational heterogeneity of the open state seems a universal feature of Hsp90 to serve a wide range of client proteins (Krukenberg et al., 2009; Krukenberg et al., 2008). In contrast, the closed state of Hsp90 involves additional N-terminal dimerization and association with the MD to hydrolyze ATP. Indeed these findings shed light on the large conformational changes Hsp90 can adopt.

Altogether, the comprehensive structural analysis combined with mutagenesis studies *in vitro* and *in vivo* has provided a better understanding of the Hsp90 machinery. Structural data has provided snap shoots of the both extreme Hsp90 conformational states but further work was necessary to gain more insight into the conformational cycle. In particular, how the structural changes and ATP hydrolysis are coupled with Hsp90 function.

2.4.3 Conserved Mechanism of Conformational Changes in Hsp90

Each Hsp90 domain is highly structured but the domain boundaries are flexible hinges that allow domain-domain rearrangements and large conformational transitions. ATP binding and a low hydrolysis rate (McLaughlin et al., 2002; Panaretou et al., 1998; Richter et al., 2008) are thought to drive local and global conformational changes (*Figure 4B*) (Pearl, 2016). Comprehensive FRET analysis provided further insights into the molecular mechanism of the Hsp90 machinery revealing that the conformational transitions are the rate-limiting step within the cycle (Hessling et al., 2009; Street et

al., 2011). Furthermore, the Hsp90 FRET-based system is able to dissect the conformational changes between the open until the fully closed state (*Figure 8*). Hence, several intermediates states were observed. Upon ATP binding, fast structural rearrangements in the NTD occur involving the lid segment which folds over the binding pocket (I1). Further restructuring takes place in the NTD where one β-strand swaps over to the other β-strand of the opposite subunit and the movement of an α-helix results in the exposure of hydrophobic residues. Together, these structural changes build up the dimer interface within the NTDs (closed-1). In a second step, the MDs interact with the N domains and form the active "split" ATPase (closed-2) to allow hydrolysis. In isolation, some of the structural states appear to be iso-energetic, thus random fluctuations between these states are possible (Krukenberg et al., 2008; Mickler et al., 2009).

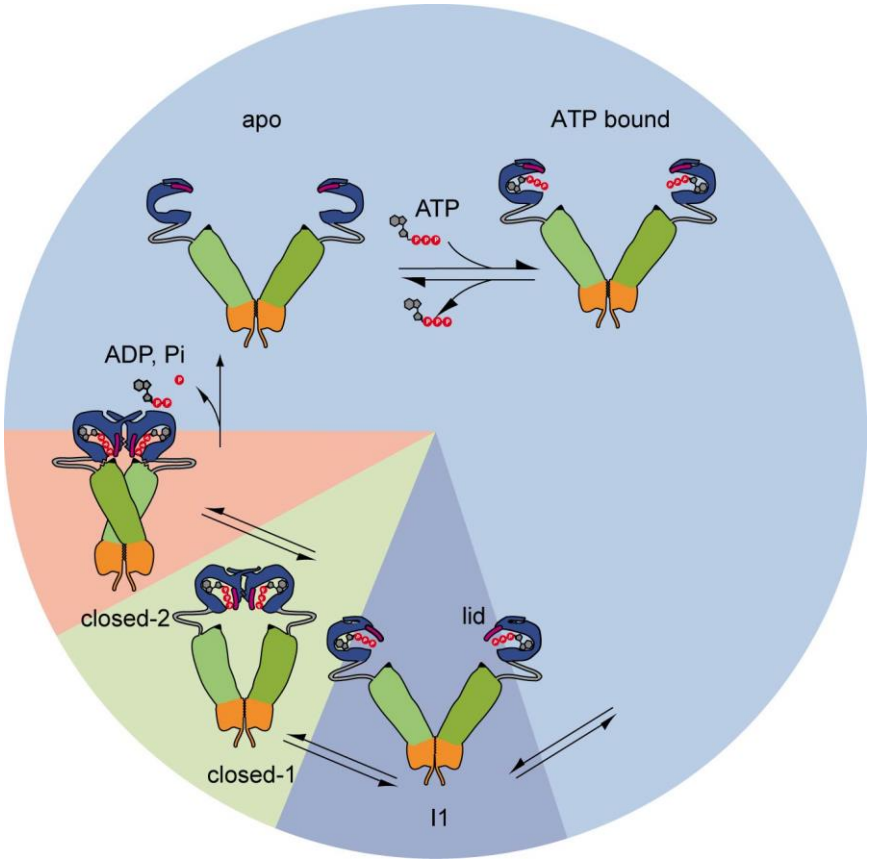

Figure 8: **Hsp90 undergoes large conformational rearrangements upon ATP binding.** The conformational states are in equilibrium and Hsp90 is mostly populated in an open conformation in the presence of ATP. The scheme illustrates the differences in dwelling times in different states (open = blue, I1 = violet, closed-1 = green, closed-2 = orange) for wildtype yeast Hsp90. The apo v-shaped conformation of Hsp90 binds ATP that induces fast conformational changes within the NTDs. Subsequently, the lid within the NTDs closes over the ATP binding pocket (I1). Next, the NTDs associate termed closed-1 state. The ATP hydrolysis competent state is reached when the NTDs are dimerized and associate with the MDs (closed-2).

The defined distinct states, in particular early events in the N-terminal domain of Hsp90, have not been monitored in solution. More recently a study revealed cooperation of local motion within the Hsp90 dimer by applying one-nanometer fluorescence probes based on fluorescence quenching (Schulze et al., 2016). They identified a two-step mechanism for how lid closure takes place (Schulze et al., 2016).

Moreover, molecular dynamic simulations of full-length Hsp90 in the absence and presence of nucleotide demonstrated signal propagation and long-range communication within the dimer. The study identified several “hot spots” involved in inter-domain communication ranging from the ATP binding site up to the CTD. These communicating residues differ depending on the bound nucleotide suggesting distinct conformations (Morra et al., 2009). Moreover, the computational dynamics-based approach was used to discover selectively allosteric inhibitors of Hsp90 (Morra et al., 2010).

Limited information is available for the human Hsp90 system regarding full-length structural data and mechanistic insights. Despite an overall conserved mechanism among Hsp90 species, including the N-terminal rearrangements upon ATP binding followed by subsequent transitions to the closed state (Richter et al., 2008; Vaughan et al., 2008), significant differences exists between bacteria, yeast and human Hsp90. SAXS, EM and hydrogen exchange mass spectrometry studies demonstrated that the closed state is populated by the bacterial and human Hsp90 homolog although the extent to which theses homologs populate the closed state is variable (yeast > bacteria > human) (Graf et al., 2014; Karagoz et al., 2014; Southworth and Agard, 2008) This is in line with the ATP hydrolysis rate (Richter et al., 2008). Of note, the ATPase rate is generally very slow. With a half time of about 10 min for human Hsp90 isoform it is much slower than that of prokaryotic and fungal Hsp90s (Richter et al., 2008). Although co-chaperone regulation (e.g. Sti1, Aha1) is conserved from yeast to mammals, the human Hsp90 system has an extended set of specific co-chaperones (Table 1). Based on indirect evidence, it seems reasonable to assume that some of them, such as the large PPIases (Cyp40, FKBP51 and FKBP52) may affect the kinetics in specific ways, since they differ in their effects on the activation of specific client proteins (Riggs et al., 2003).

2.4.4 The Role of Co-Chaperones in Regulating the Conformational Dynamics of Hsp90

As Hsp90 takes part in many different cellular processes, it is assumed that Hsp90 forms a central hub of the protein homeostasis system and that the associated co-chaperones create crossroads in this complex network to ensure sufficient maintenance of the proteome (Echtenkamp and Freeman, 2012; Taipale et al., 2010). Approximately ~20 co-chaperones have been found for Hsp90 (*Table 1*) (Johnson and Brown, 2009). Co-chaperones are defined as proteins, which assist or alter the function of Hsp90 but are not client proteins. Some co-chaperones interact via a tetratricopeptide repeat domain (TPR) (Blatch and Lassle, 1999; Young et al., 1998) at the C-terminal end wheras others bind to ND and/or MD of Hsp90 (*Figure 9*). Some Hsp90 co-chaperones function as modulators of the ATPase cycle by stabilizing certain Hsp90 conformational states in a nucleotide-dependent manner (Johnson et al., 2007). Furthermore, they are thought to mediate the specificity of client binding to Hsp90, like Cdc37, which delivers kinases to Hsp90 (MacLean and Picard, 2003). In addition, co-chaperones, like CHIP (Carboxyl terminus of Hsc70 Interacting Protein) exhibits E3 ubiquitin ligase activity in its U-box domain and thereby forms a link between chaperones and the protein degradation system by delivering misfolded proteins to the Ubiquitin Proteasome System (UPS) (McDonough and Patterson, 2003).

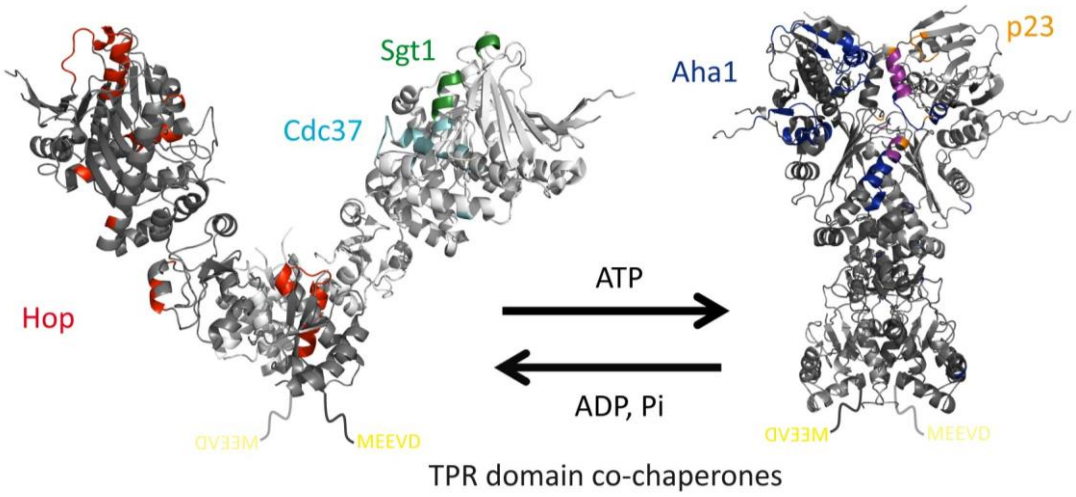

Figure 9: **Co-Chaperone interaction sites of Hsp90.** The structure of open and closed Hsp90 illustrate the binding sites of several co-chaperones that associate to different and overlapping sites to Hsp90. Co-chaperones that contain one or more TPR domains are able to bind to the C-terminal MEEVD motif. Hop (red), Sgt1 (cyan) and Cdc37 (green) bind preferentially to the open state of Hsp90 (PDB 2IOQ). Aha1 (blue) and p23 (orange) favor the compact closed state of Hsp90 (PDB 2CG9). The overlapping binding site of p23 and Aha1 is depicted in pink.

Table 1: List of yeast and human co-chaperones of Hsp90.

Co-Chaperone human/yeast	Effect on ATPase activity	Function
Hop/Sti1	Inhibition	regulator / scaffold of Hsp70 and Hsp90 connection
Aha1	Acceleration	accelerator
p23/Sba1	Inhibition	inhibitor and chaperone / regulator
PP5/Ppt1	none	Phosphatase
TTC4/Cns1	n.d.	essential in yeast / nuclear transport protein
----/Cpr6 Cyp40/Cpr7	weak acceleration	PPIase and regulator/ involved in SHR activation
FKBP51, FKBP52	none	PPIase and regulator/ involved in SHR activation
Cdc37	inhibition	binds kinase clients/involved in kinase activation
Sgt1	none	activation of nucleotide-binding leucine-rich repeat receptors (NLRs) / cell cycle progression
Tah1, Spagh Pih1	weak inhibition	chromatin remodeling / small nuclear ribo- nucleoprotein maturation/adaptor for clients
XAP2	n.d.	signal transduction
AIPL1	n.d.	PPIase and photoreceptor
Chip	none	ubiquitin ligase/interaction with Hsp70
Tpr2	n.d.	Regulator?

(Rohl et al., 2013; Zuehlke and Johnson, 2010) n.d. not determined

Conformation-Sensitive Co-Chaperones Regulate the Hsp90 Cycle

Biochemical and structural analysis indicate that co-chaperones are part of the driving forces within the cycle. They either bind to specific conformations of Hsp90 or induce another. More recently, a study using hetero-oligomeric Hsp90-co-chaperone complexes and applying FRET and analytical ultracentrifugation revealed the underlying regulatory mechanism of the progression through the Hsp90 cycle by co-chaperones (*Figure 10*) (Li et al., 2011b; Li et al., 2012).

Hop/Sti1 Stabilizes Hsp90 Open Conformation

The Hsp70-Hsp90 organizing protein Hop (stress inducible 1-Sti1) is highly conserved and the yeast and human homolog have basically similar properties regarding structure and mechanism (Rohl et al., 2013; Rohl et al., 2015a). The nature of both proteins is very dynamic due to its domain

architecture. Both are elongated proteins consisting of a very flexible N-terminally module (TPR1-DP1) and a more rigid C-terminal module (TPR2A-TPR2B-DP2) (Rohl et al., 2015b). The modules are connected via a flexible linker. The structures of the single domains were determined; however full-length structural data are missing. Hsp70 and Hsp90 bind simultaneously to Hop/Sti1 and thus allow client transfer (*Figure 10*). Hsp70 interacts in a first step with the TPR1 domain in the flexible module of Hop/Sti1 and is subsequently transferred to TPR2B. The transfer is required to bring Hsp90 and Hsp70 in close proximity. Single molecule experiments showed that the binding affinity of Hsp70 to the respective TPR domains is regulated by Hsp90 binding to Hop (Rohl et al., 2015b). TPR2A binds highly specific to the Hsp90 C-terminal end whereas TPR2B binds to the middle domain of Hsp90 (Carrigan et al., 2004; Scheufler et al., 2000; Schmid et al., 2012). Together they inhibit the Hsp90 ATPase activity to the same extent as full-length Sti1/Hop (Rohl et al., 2015a) by preventing nucleotide-induced Hsp90 dimer closure (Hessling et al., 2009).

Aha1 Induces Conformational Changes within Hsp90

Aha1 (Activator of Hsp90 ATPase) binds to the M domain of Hsp90 via its N-terminal domain (Lotz et al., 2003). In contrast to other co-chaperones, Aha1 accelerates the ATP turnover of Hsp90 by bypass slowly structural changes in the Hsp90 cycle (*Figure 10*). Multidimensional NMR analysis revealed the Aha1-mediated activation of the Hsp90 ATPase activity by binding to the MD and NTD in a sequential, asymmetric manner (Retzlaff et al., 2010). Interestingly, the binding of one Aha1 molecule is sufficient to induce the formation of N-terminally dimerized state (Retzlaff et al., 2010). This is in line with accelerated closure kinetics observed by FRET experiments (Hessling et al., 2009). Recently, the combination of FRET and analytical ultracentrifugation in combination with fluorescence detection integrated Aha1 into the Hsp90 cycle (Li et al., 2013). The analysis identified Hsp90 ternary complexes comprising Aha1 and Cpr6 (*Figure 10*). Furthermore, binding of both co-chaperones to Hsp90 synergistically promotes an ATPase –competent state and displaces p23 from Hsp90. Another study engineered fluorescence probes within Hsp90 employed photoinduced electron transfer in combination with stopped-flow to study the influence of Aha1 on fast local structural changes of Hsp90. Their results suggest that Aha1 mobilizes the lid early in the open state of Hsp90 (Schulze et al., 2016).

p23/Sba1 Specifically Binds to the Closed-2 State of Hsp90

Sba1 (increased sensitivity to benzoquinone ansamycins) encodes the yeast Hsp90 co-chaperone that is homologous to the vertebrate p23 protein (Fang et al., 1998; Felts and Toft, 2003). The co-chaperone p23 was first shown in complex with Hsp90 and the progesterone receptor (Smith et al., 1990). It is better known as a non-TPR containing co-chaperone of Hsp90, which binds specifically to the N-terminal closed-2 conformation of Hsp90 in the late phase of the chaperone cycle (*Figure 10*) and promotes stabilization of Hsp90–client complexes (Dittmar et al., 1997; Kosano et al., 1998). The binding of p23 to Hsp90 goes along with a decrease in Hsp90 ATPase activity (Prodromou et al., 2000; Richter et al., 2004). Sba1/p23 stabilizes the pre-hydrolysis closed conformation of Hsp90 (McLaughlin et al., 2006; Prodromou, 2012; Richter et al., 2004). Furthermore, it was observed that p23 has intrinsic chaperone activity (Forafonov et al., 2008). P23 tail is responsible of its chaperone activity (Bose et al., 1996; Weikl et al., 1999). Besides the regulation of the Hsp90 machinery, p23 seems to have additional functions in telomere biology, regulation of transcription and modulation of DNA protein dynamics (Echtenkamp and Freeman, 2012; Toogun et al., 2007; Zelin et al., 2012).

Hsp90 FKBP PPIase Complexes

The FK506 binding proteins FKBP51 and FKBP52 as well as cyclophilin Cyp40 belong to the peptidyl-prolyl-isomerases (PPIases) in vertebrates whereas the Cyclosporin-sensitive proline rotamase 6 (Cpr6) and Cpr7 exist in yeast. Besides binding to Hsp90 this class of proteins comprises isomerase activity and an independent chaperone function (Bose et al., 1996) implying direct interaction with client proteins (Pirkl and Buchner, 2001; Pirkl et al., 2001). Of note, the importance of FKBP51/52 in several diseases raises more attention (Fries et al., 2015; Guy et al., 2015a; Storer et al., 2011). FKBP52 potentiates hormone-dependent reporter gene activation by GR (Davies et al., 2005; Riggs et al., 2003), AR (Cheung-Flynn et al., 2005) and PR (Tranguch et al., 2005). FKBP51 negatively influences GR, PR and MR activation whereas it modulates AR activation (Guy et al., 2015b). To activate a specific receptor depends on the formed Hsp90-PPIase receptor heterocomplex. Hence, elucidating the importance of these co-chaperones in the Hsp90 cycle is still under investigation.

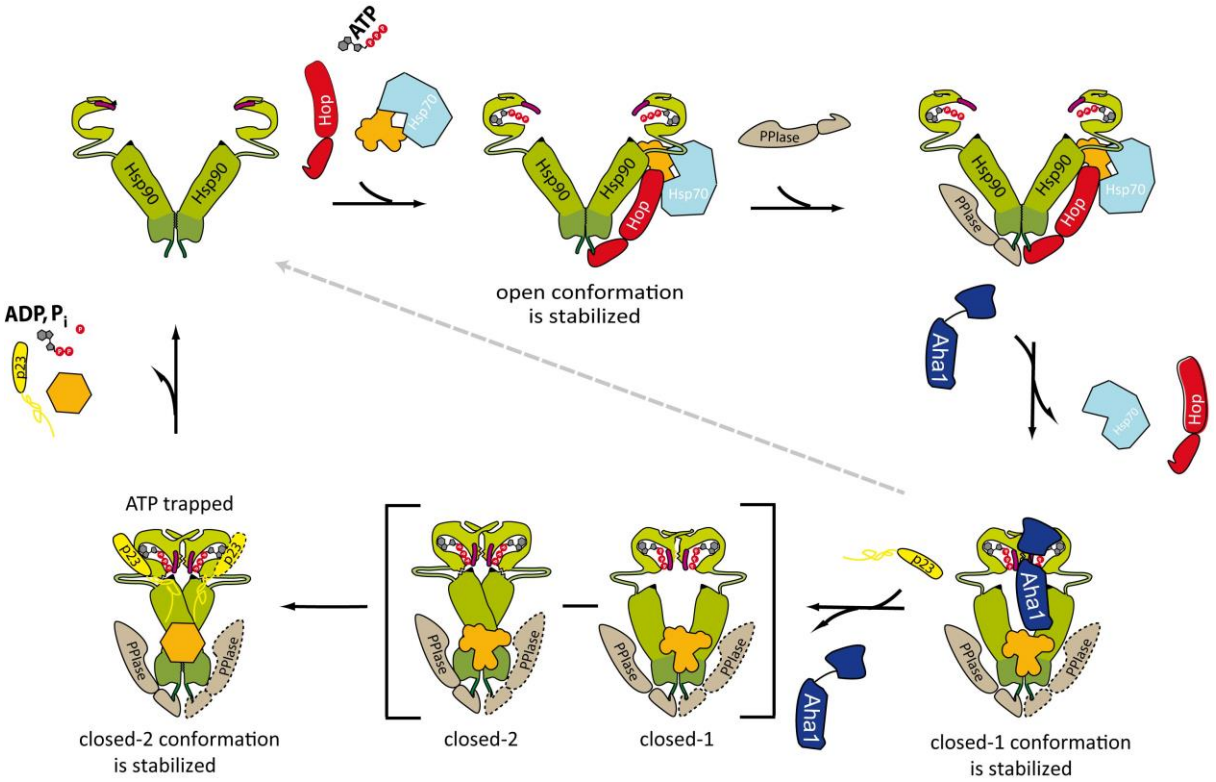

Figure 10: **Integration of co-chaperones in the Hsp90 conformational cycle.** Hop (red) facilitates as adapter protein the transfer of the client protein (orange) from Hsp70 (light blue) to Hsp90 (green). Hop in association with Hsp70 and client binds and stabilizes the open conformation of Hsp90. An asymmetric complex is formed by binding of the PPIase to the other protomer. The Hsp90 ATPase activator Aha1 (dark blue) interacts and thereby induces conformational changes within Hsp90 (closed-1) that results in Hop and Hsp70 release. The client is still bound to Hsp90. The conformational sensitive co-chaperone p23 (yellow) displays Aha1 due to association with Hsp90 (closed-2). ATP hydrolysis takes place and active client as well as bound co-chaperones are released. In the absence of other co-chaperones Aha1 accelerates Hsp90 ATPase activity (depicted by the dashed line). ((Rohl et al., 2013) Order Number 3985331004253)

2.4.5 Influence of Post-Translational Modifications on Hsp90 Dynamics

The modification of Hsp90 at specific residues by post-translational events adds another layer of fine-tuning to the Hsp90 chaperone cycle to ensure sufficient adaption to cell-specific needs. The discovery of a large number of post-translational modifications (PTMs) of Hsp90 in metazoens including phosphorylation (Soroka and Buchner, 2012), acetylation (Scroggins et al., 2007), S-nitrosylation (Martinez-Ruiz et al., 2005), glycosylation (Overath et al., 2012), methylation (Abu-Farha et al., 2011; Donlin et al., 2012), oxidation (Chen et al., 2008) and nitration (Franco et al., 2013) was achieved by several comprehensive proteomics studies (Blank et al., 2003; Mollapour and Neckers, 2012; Wandinger et al., 2008). All PTMs are randomly distributed over the Hsp90 domains and also

found within the flexible linker. Little by little, the influences of these single modifications on Hsp90 were studied and are still under investigation. In general it was shown that PTMs affect several aspects of the Hsp90 machinery in terms of ATPase activity and conformational dynamics resulting in different co-chaperone affinity and client binding (Mollapour and Neckers, 2012). Consequently, this leads to altered client activation both shown *in vitro* and *in vivo* under physiological and for some under non-physiological conditions (Mollapour and Neckers, 2012). Interestingly, phosphorylation events are catalyzed by kinases that are Hsp90-dependent clients suggesting that the client drives Hsp90 conformational changes by phosphorylation (Street et al., 2011). Thereby the cell evolved a feedback mechanism that regulates kinase activity.

Phosphorylation: As many phosphosites have been identified so far at serine-, threonine- and thyrosine residues of Hsp90, phosphorylation is one of its most frequent PTMs. For some specific sites, the responsible kinase is known (Lees-Miller and Anderson, 1989). In addition, phosphatases enable a reversible process. Recently, a mechanistic study revealed insights into the Hsp90 phosphoregulation (Soroka et al., 2012). A comprehensive mutagenesis analysis targeted specific phosphosites in the MD and CTD. To this end, phospho-mimicking mutants were utilized and analyzed *in vivo* and *in vitro* regarding Hsp90 function. For example, phosphorylation at residue Ser379 (refering to yeast Hsp82) influences Hsp90 ATP turnover rate, alters co-chaperone regulation and disrupts client binding. Moreover, mimicking phosphorlyation at this site affects the Hsp90-dependent nucleotide excision repair mechanism. Another important phopho-site is residue Ser485, located in the interface between the MD and CTD. FRET and analytical ultracentrifugation experiments indicate reduced structurally flexibility of Hsp90 accompanied with altered co-chaperone binding. Here, a single substition or phophorylation event is able to disrupt Hsp90 function. The CTD phosphosites S602 and Ser604 seem to play a role under different stress conditions and indicate interdomain comunication to the NTD. Residue Tyr24 is known to be phophorylated by Swe1 (Mollapour et al., 2010). As Tyr24 is located in the hydrophobic area within the NTD, known to be important for N-terminal dimerization, phosphorylation impacts Hsp90 dimer closure and ATPase activity. In addition, the modification of Tyr24 alters Hsp90-dependent kinase activation but not steroid hormone receptor maturation. Taken together, phosphorylation of Hsp90 at specific sites provides a reversible trigger in terms of how Hsp90 dynamics is regulated in the cell. As mentioned above, phosphorylation mediated by Hsp90-dependent clients. Here, one prominent example is c-Src kinase that phosphorylates Hsp90 can be at residue Tyr301. The modification was shown to enhance vascular endothelial growth factor receptor (VEGFR)-2 association to Hsp90

therby increasing nitric oxide synthase (NOS) activity, which in turn produces the signaling molecule nitric oxid (NO) (Duval et al., 2007). Furthermore, the analysis of the influence of post-translational by modified Hsp90 co-chaperones is still in its infancy. However, phosphorylation of co-chaperones (Cdc37, Sgt1, FKBP52, Hop) has been reported to impact the Hsp90 machinery and thus regulate chaperone function (Bansal et al., 2009; Miyata, 2009; Rohl et al., 2015a; Vaughan et al., 2008).

Acetylation: A pivotal role of protein acetylation and deacetylation is known in hisitone modification as part of gene regulation. Histone acetyltransferase (HAT) adds acyl groups to specific lysine residues wheras histone deacetylases (HDAC) facilitate the removing. Since the discovery that HATs and HDACs serve several non-histone targets, such as transcription factors, cytoskeletal proteins and molecular chaperones, acetylation plays a major role in cell regulation (Glozak et al., 2005). Several studies revealed that Hsp90 activity is regulated by acetylation in terms of co-chaperone binding and client maturation (Kekatpure et al., 2009; Kovacs et al., 2005). HDAC6 promotes deacetylation of Hsp90 and inhibition of the deacetylase results in hyperacetylation in the cell (Yu et al., 2002). A mutagenesis study identified acetylation at a specific residue (Lys294 of yeast Hsp82) located in the Hsp90 MD (Scroggins et al., 2007). It was revealed that modification at this position disrupts co-chaperone binding (Aha1, Chip, FKBP52) and alters client association.

S-Nitrosylation: Thiol side chains of cysteine residues can be modified with a nitrogen monoxide group in the process of S-nitrosylation. Recently, S-nitrosylation was observed to modify Hsp90 (Martinez-Ruiz et al., 2005). One conserved residue within the CTD of Hsp90 (Cys597 refered to Hsp90α) was identified as molecular switch point as its modification reduces chaperone activity. When being nitrosylated it was further shown that NO-introduction stabilizes the open v-shape conformation of Hsp90 (Retzlaff et al., 2009). Computational studies proposed unique hot spots in this area that allow long-range-communication from the CTD to the NTD within the Hsp90 dimer (Morra et al., 2009).

Glycosylation: Studies on glycosylation have revealed that modification with N-acetyl glucoseamine (GlcNAc) occurs at the hydroxyl groups of serine and threonine residues of several proteins (O-glycosylation). Glycosylation has been observed at two distinct sites of Hsp90 that can also be phosphorylated which suggests a regulatory function considering Hsp90 activity (Overath et al., 2012). The influence of post-translational modifications is not limited to the chaperone itself but also affects the binding of co-chaperones and client proteins. However, in the case of glycosylation, the influence on the chaperone function is not known yet.

2.4.6 Client Proteins Affect Hsp90 Conformational Changes

Understanding the molecular mechanism of the Hsp90 machinery and in particular how confomational changes are coupled to Hsp90 function is still elusive. To gain insights into this process structural data is neccesary. As mentioned earlier, Hsp90 clients belong to different protein families and it seems that one commom feature is their intrinsic instable nature. To work with those unstable client proteins and a highly dynamic Hsp90 system makes biochemical and structural research difficult. About 60 % of kinases are Hsp90-dependent as their activation is achieved only in the presence of Hsp90 and its co-factor Cdc37. Little is known how the chaperone facilitates kinase function. Single particle electron microscopy had provided the first structural insights of an asymmetric Hsp90 in complex with its co-chaperone Cdc37 and the kinase Cdk4 in 2006 (Vaughan et al., 2006). The data shows that Hsp90 adopts an open conformation with non dimerized NTDs. In comparison to the crystal structure (Ali et al., 2006), conformational rearrangments of the NTD were revealed. The NTD of one subunit is hinged backward and binds Cdc37 between both NTDs. The other subunit makes contacts with the kinase and domain-rearrangments between the MD and CTD were observed (Vaughan et al., 2006).

The most stringent Hsp90 client is the oncogenic viral kinase v-Src (Taipale et al., 2012). In contrast, the activation of the cellular kinase c-Src is not Hsp90 dependent. Of note they share 98% sequence identity. It is unclear why only some kinases are Hsp90-dependent. Boczek *et al.* performed reconstitution assays to elucidate Hsp90 chaperoning action with v-Src. With the help of designed Src kinase mutants and chimeras they could illustrate the correlation between a client and a non-client. The data showed that a Hsp90-dependent client is intrinsically instable that in turn increases hydrophobicity and renders a protein prone to aggregation (Boczek et al., 2015). Furthermore, they propose that Hsp90 recognizes less active states of kinases and shift the equillibrium to an active kinase state via stabilizing metastable folding intermediates.

Recently, Verba and co-workers performed cryo-electron microscopy and determined a 3.9 Å structure of a Hsp90-Cdc37 complex with the kinase Cdk4. The full-length structure revealed that Hsp90 and Cdc37 trap the kinase in an open conformation by stabilizing Cdk4 (Verba et al., 2016). They showed that Hsp90 clamps around the kinase assuming that this prevents the kinase to be trapped in an unfolded state (Verba et al., 2016).

More recently two studies integrated GR, in particular the essential part for association the ligand-binding domain LBD, in the Hsp90 chaperone cycle. Indeed, the experiments illustrate that binding of the client affects Hsp90 conformation. To investigate the modulation of Hsp90 by GR, Lorenz *et al.* utilized several biophysical-, NMR and EM methods. Most evident for structural changes within the Hsp90 dimer is a decline in ATPase activity in the presence of the client protein (Lorenz et al., 2014). Furthermore, they observed a decrease in closure kinetics upon addition of ATPγS (Lorenz et al., 2014). Hsp90 client binding occurs in a nucleotide-dependent manner (Lorenz et al., 2014). Taken together, suggesting GR binds to a preferred open Hsp90 conformation and induces conformational changes that stabilize an intermediate Hsp90 conformation to prolong its association. As the Hsp90-GR hormone-bound complex is known to be transferred to the nucleus, the dwell time seems to be crucial (Harrell et al., 2004). In a second study, the client transfer between Hsp70 and Hsp90 was additionaly investigated in a similar context (Kirschke et al., 2014). Here, Hsp70 keeps GR in a partial unfolded state that is unable to bind hormone. Instead Hsp90 in concert with Hop and p23 is able to induce GR hormone binding activity. Moreover, they illustrate the interplay between to two chaperone systems regarding client maturation.

A completely different story is chaperoning an intrinsically disorded protein, called Tau. In general Tau is involved in microtubules assembly. However, aggregation of Tau into amyoloid fibrils is associated with neurodegenerative diseases, termed also tauopathies (Clavaguera et al., 2014). Several evidence suggest that Hsp90 has an important role in the development of tauopathies (Miyata et al., 2011). Thus it is worthwhile to understand the Hsp90-Tau relationship. Recently, a NMR and SAXS analysis resulted in a structural model of Hsp90 in complex with Tau (Karagoz et al., 2014). To recognize clients, Hsp90 makes several contacts scattered over the NTD and MD. As seen likely for other Hsp90 client complexes, Tau interacts with Hsp90 in an open conformation (Karagoz et al., 2014).

In conclusion, Hsp90 chaperones can handle many different clients probably due to its highly dynamic nature and in complex with recruiting partner co-chaperones. Moreover, clients seem to take part in the Hsp90 conformational cycle but in different ways depending on the client and its folding status (Mayer and Le Breton, 2015).

3 Objectives

3.1 Heat Shock Protein Isoforms in Yeast: Hsp82 versus Hsc82

Hsp90 is one of the most abundant soluble cytosolic proteins (1-2 % of total protein) in the cell and highly conserved among several species. It is known that Hsp90 is essential in all eukaryotes. Its outstanding role as a key factor in protein homeostasis is due to its wide range of binding partners. Hsp90 interacts with about 10 % of the proteome and is crucial for the activation of several cellular key factors involved in cell signaling and regulation like transcription factors or kinases. In *Saccharomyces cerevisiae* two cytoplasmic isoforms exist, the constitutive expressed Hsc82 and the heat- and stress-inducible Hsp82. Of note, at the amino acid level, the isoforms share 97 % sequence identity. Hsc82 and Hsp82 have been extensively used to study various general and yeast-specific aspects of Hsp90 biology, but beyond their deviating expression pattern mechanistic and biological differences have remained largely enigmatic. Previous work has shown a few cases of isoform-specific differences in terms of heat-stress, inhibitor sensitivity and regulation by co-chaperones (Millson et al., 2007; Silva et al., 2013; Sreedhar et al., 2004). The focus of this part of the thesis is to investigate systematically Hsc82 and Hsp82 in terms of their functions *in vitro* and *in vivo* and to test whether they are able to form heterodimers.

3.2 Establishing a Human Hsp90 FRET-System for Montoring Conformation Changes

Little is known about the functional cycle of human Hsp90. Studies on this topic have been mainly performed with prokaryotic and yeast Hsp90. For these species, Hsp90 FRET systems and fluorescence quenching experiments are available to monitor conformational changes within the dimer kinetically (Hessling et al., 2009; Mickler et al., 2009; Schulze et al., 2016; Street et al., 2011). This analysis provided important insights and also allowed to integrate yeast co-chaperones in the conformational cycle. The limited information available for the conformational dynamics of the human system shows that it is clearly different from the yeast Hsp90 cycle, in particular the population of different conformational states such as the N-terminally closed state varies (Karagoz et al., 2014; Southworth and Agard, 2008). Importantly, the reaction cycle is very slow. With a half time

of about 10 min it is much slower than that of prokaryotic and yeast Hsp90s (Richter et al., 2008). It is assumed that this has important functional consequences, such as the availability of acceptor states for co-chaperones and this in turn might affect client interactions. So far it is still enigmatic how the conformation cycle is coupled to Hsp90 function. Therefore, it is of fundamental importance to understand the underlying principles governing this molecular machine. To address these issues, it is instrumental to design a FRET system as a novel tool for the analysis of the conformational dynamics of the human Hsp90 isoforms (Hsp90α and Hsp90β). To this end specific attament points for dyes have to be introduced in Hsp90. Cysteines can be used for example, but this is complicated by the fact that both proteins contain a number of cysteines. In fact, Hsp90 is known to be modifed by a number of post-translational modifications scattered throughout the protomer and these in turn have been shown affect Hsp90 dynamics (Krukenberg et al., 2011; Mollapour and Neckers, 2012). Hence, to utilize a comprehensive characterization of a modified Hsp90 is crucial. Another strategy to introduce dyes is to employ novel protein chemical methods such as protein domain ligation mediated by Sortase A or the incooperation of an unnatural amino acid using the amber suppression codon and the respective aminoacyl tRNA/synthetase pair. This thesis will focus on the different approaches employed here to establish a human Hsp90 FRET-setup to study the conformational cycle.

4 Results

4.1 Hsc82 versus Hsp82 - Same but Different

The baker's yeast *S. cerevisiae* exhibits two cytosolic Hsp90 homologues, encoded by the genes hsc82 and hsp82. The isoforms are differentially expressed: Hsp82 is highly expressed under stress conditions, such as heat; hsc82 transcription is constitutively and only slightly induced by several stresses (Borkovich et al., 1989). The encoded proteins share 97 % sequence identity.

4.1.1 Hsc82 and Hsp82 Differ Slightly in their Amino Acid Sequence

Hsc82 and Hsp82 comprise 16 differences in their amino acid sequences and deviate in the length of the charged linker between the NTD and the MD (*Figure 11A*). In Hsc82, the linker contains 57 amino acids, while in Hsp82 it consists of 61 residues. Most sequence differences between the isoforms cluster in the NTD (8 different residues) and CTD (5 different residues), whereas in the linker a single amino acid substitution is found and the MD contains only two different residues (*Figure 11A*).

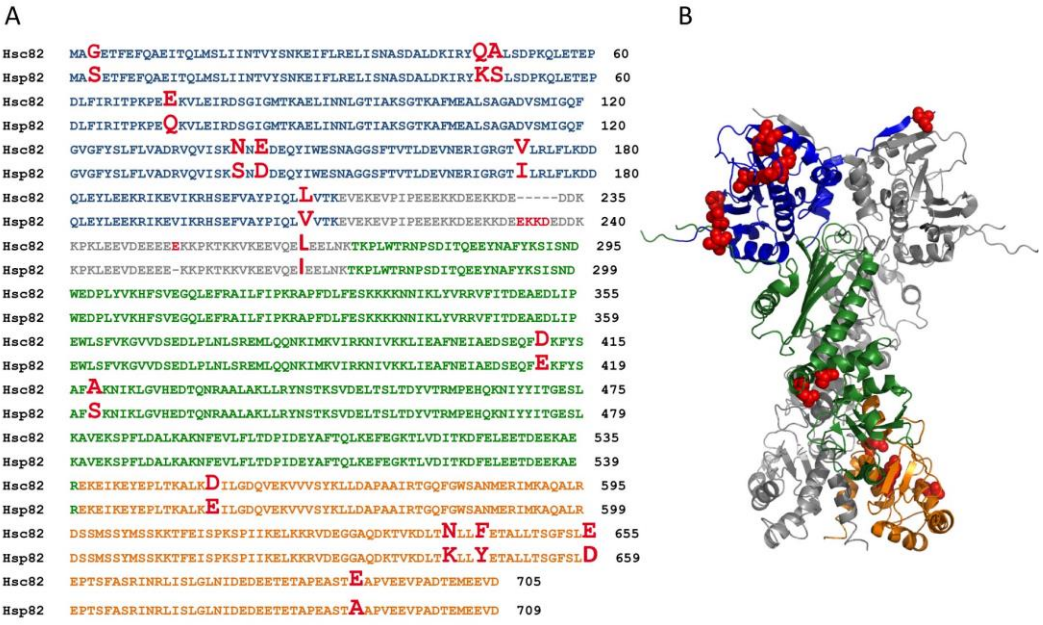

Figure 11: **Comparison of amino acid sequence of the yeast Hsp90 isoforms. A**) Sequence alignment of Hsc82 and Hsp82. The N-terminal domain of the isoforms is depicted in blue, the charged-linker in grey, M-domain in green and the C-terminal domain in orange. **B**) Closed Hsp90 structure (PDB ID: 2CG9 (Ali et al., 2006)) depicting sequence differences between Hsc82 and Hsp82. The differences in amino acid sequence are highlighted in red letters in **A**) and are shown as red spheres in the closed Hsp82 structure in **B**).

The NTD of Hsp90 is a twisted eight-stranded beta-sheet covered on one face by several α-helices (Prodromou et al., 1997). Two helices (helix 2 (residues 28-50) and helix 5 (residues 85-94) together with two mainly unstructured regions (residues 81-85 and 117-124) and residues that protrude from the β -sheet (Ile77, Asp79, Val136, Ser138, Thr171, Ile73) form a pocket that accommodates the nucleotide (Prodromou et al., 1997) (*Figure 11B*). None of the residues directly involved in binding to the nucleotide or to water molecules deviate between Hsc82 and Hsp82 (Prodromou et al., 1997). However, two residues that form part of the binding pocket (Gln48Lys, Ala49Ser) and one residue next to the water-binding Thr171 (Val172Ile) vary (*Figure 11B*). Additionally, Gly3 in Hsc82 is replaced by a serine in Hsp82. Gly3 is part of the region that is swapped between the dimers in the closed conformational state (*Figure 11B*) and impacts the ATPase activity of Hsp90 (Richter et al., 2002).

4.1.2 Hsc82 and Hsp82 Exhibit Similar Structural Stability

Given the sequence differences scattered over all three domains and within the linker region, we wondered if the stabilities differ between Hsc82 and Hsp82. To this end, Hsc82 and Hsp82 were purified to homogeneity. Two purification strategies were used: First both isoforms were recombinantly expressed and purified according to standard lab protocols, resulting in pure N-terminal tagged Hsp90 that comprises six histidines (6xHis-Hsp90). In the second approach, Hsp90 was tagged additionally with the sequence Gly-Gly-Ala-Thr-Tyr at the C-terminal end of the small ubiquitin-like modifier (SUMO) peptide resulting in 6xHis-SUMO-Hsp90, which allows tag removing by cleavage with the Ubiquitin-like protease (ULP1). After protein isolation, a basic structural characterization was performed. To analyze deviations in secondary structure elements far-UV CD spectroscopy was employed. Due to differential absorption of backbone amide groups far-UV CD spectra (260 - 195 nm) of the tagged and untagged Hsp90 isoforms were recorded. The far-UV spectra of the Hsp90 isoforms are typical for a mainly α-helical protein with a maximum at approximately 190 nm and two minima at about 208 nm and 222 nm with an intensity of -10 000 deg cm^2 $dmol^{-1}$ (*Figure 12A*). The far-UV CD spectra indicated that the Hsp90 isoforms are folded properly and that no gross structural alterations exist (*Figure 12A*). The measured CD spectra in the far UV range correspond to absorption spectra of Hsp90 previously published (Richter et al., 2002). CD spectroscopy can also be used to determine thermal transitions by increasing temperature at a constant wavelength (e.g. 208 nm). However, in the case of Hsp90, melting temperatures cannot be determined via CD due to the lack of a significant signal change between the folded and the

unfolded state. Hence, we performed a thermal shift assay using Sypro orange as a fluorescent dye (Lavinder et al., 2009; Niesen et al., 2007). In a thermal shift assay, the isoforms displayed similar thermal stability, with melting temperatures of 57.1 ± 0.2 °C for Hsc82 and 60.4 ± 0.5 °C for Hsp82 in the absence of nucleotide (*Figure 12B*).

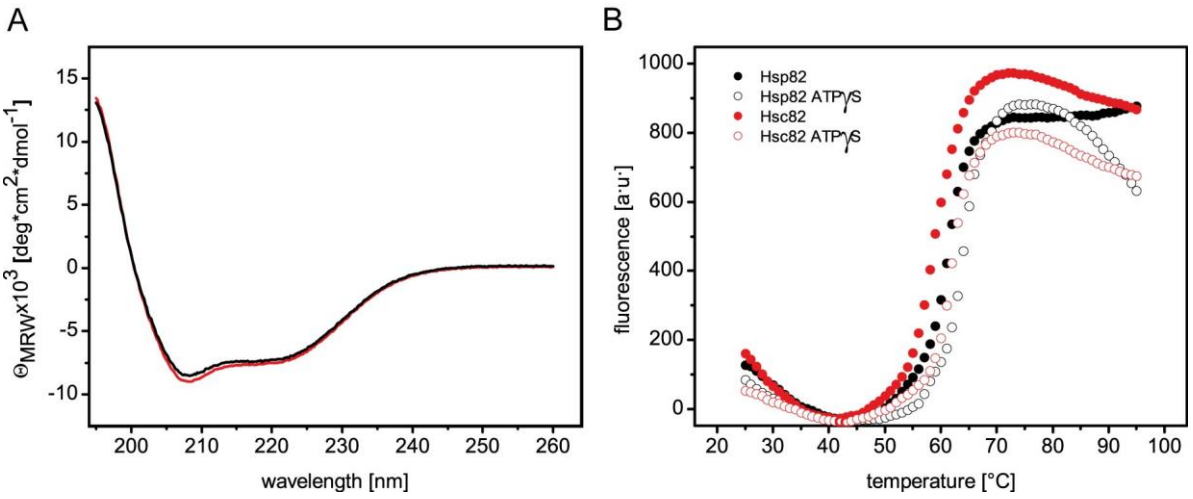

Figure 12: **Stability of yeast Hsp90 isoforms is similar. A**) Far-UV CD spectroscopy of the Hsp90 isoforms. To analyze the secondary structure of the Hsp90 isoforms, far-UV CD spectra were recorded at 20 °C in 50 mM phosphate buffer, pH 7.5 using a protein concentration of 0.2 mg/ml. **B**) Thermal stability was deduced by applying a thermal shift assay in the absence and presence of the nucleotide ATPγS. The protein concentration used was 0.25 mg/ml of protein in a buffer containing 40 mM HEPES, pH 7.5, 150 mM KCl, 5 mM $MgCl_2$ and 2 mM nucleotide.

In the presence of ATPγS, which promotes the formation of the closed Hsp90 conformation, the melting temperature increased by about 3 °C for both isoforms (*Figure 12B and Table 2*) indicating a slight stabilization. In general, this indicates that both isoforms were stable at temperatures up to 55 °C.

Table 2: Melting temperatures of yeast Hsp90 isoforms determined by a thermal stability assay using Sypro Orange. Means of at least three technical replicates and standard derivation (s.d.) are shown.

	T_m [°C]
Hsp82	60.4 ± 0.5
Hsp82 ATPγS	63.3 ± 0.4
Hsc82	57.1 ± 0.2
Hsc82 ATPγS	60.8 ± 0.4

In the past, Hsp90 domain borders were identified using limited proteolysis (Nemoto et al., 2001). When we tested the conformational stability by limited proteolysis with α-chymotrypsin, no difference between the isoforms was observed (*Figure 13*). Hsc82 and Hsp82 displayed a similar digestion pattern with and without nucleotide (*Figure 13*). When incubated with ATPγS prior to digestion, the kinetics of proteolysis was slowed down due to the compact Hsp90 structure, which reduces the accessibility of α-chymotrypsin (*Figure 13*). The observed results indicate that the overall conformational properties of Hsc82 and Hsp82 seem to be similar.

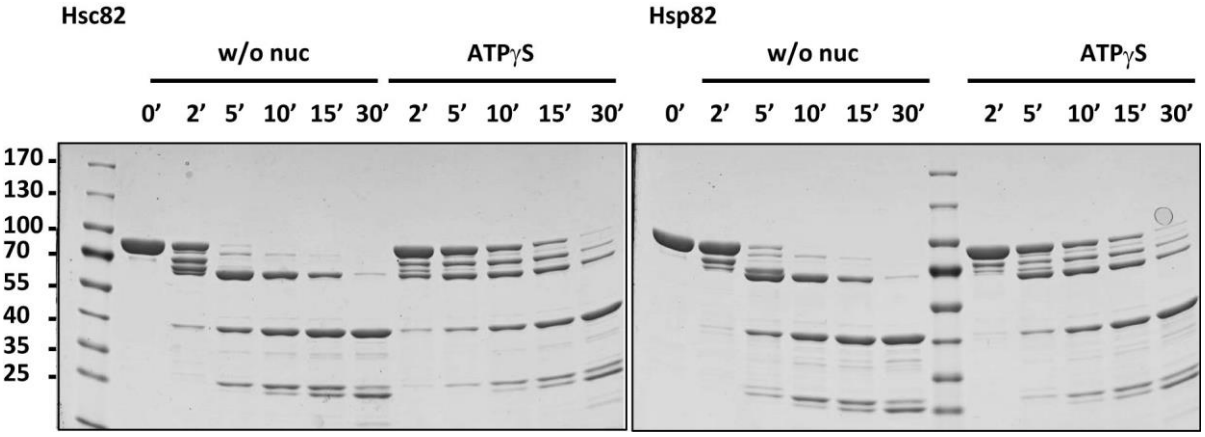

Figure 13: **Analysis of conformational properties of yeast Hsp90 isoforms by using limited proteolysis.** Hsp90 isoforms were treated with α-chymotrypsin in the absence or presence of ATPγS at 20 °C. Proteolysis was stopped with 5x Lämmli supplemented with 2 mM PMSF after several time points and verified by SDS-PAGE analysis. The sample at the start of the raction (time point 0') was included as negative control.

4.1.3 Hsc82 and Hsp82 Differ in their ATPase Activity

Given the sequence differences in the NTD, we wondered if the ATP binding and the ATPase properties vary between Hsc82 and Hsp82. To determine Hsp90 hydrolysis rates, a regenerative enzyme-coupled ATPase assay was carried out. The Hsp82 ATPase rate with a k_{cat} of about 0.52 min^{-1} is in good agreement with published data (Richter et al., 2008). Next ATPase activity of Hsc82 and Hsp82, were compared and found that the enzymatic activity of Hsc82 is approximately 1.3 fold higher at 30 °C and the difference was considerably higher (1.6 fold) at 37°C (*Figure 14A and Table 3*). To exclude differences in the affinity for ATP, ATP binding to the NTD was analyzed in an isothermal titration calorimetry (ITC) experiment (*Figure 14B*). The measurements showed in very similar affinities for ATP with k_D values of approximately <300 mM which is in line with the published data (Richter et al., 2008).

Table 3: ATP hydrolysis rates and ATP binding affinity values.

Hsp90 isoform	k_{cat} [min^{-1}]	x [fold]	ATP K_D [µM]
6xHis-Hsp82	0.75 ± 0.06		
6xHis-Hsc82	1.23 ± 0.10	1.6	
Hsp82 (30 °C)	0.52 ± 0.02		88 ± 14
Hsc82 (30 °C)	0.65 ± 0.02	1.3	151 ± 33
Hsp82 (37 °C)	1.37 ± 0.02		
Hsc82 (37 °C)	2.13 ± 0.13	1.6	

Surprisingly, N-terminal tagging more strongly enhanced the ATPase of Hsc82 (1.9 fold) than of Hsp82 (1.4 fold) (*Figure 14 and Table 3*), thus, suggesting that the difference between the both isoforms seems to be varing in the NTDs.

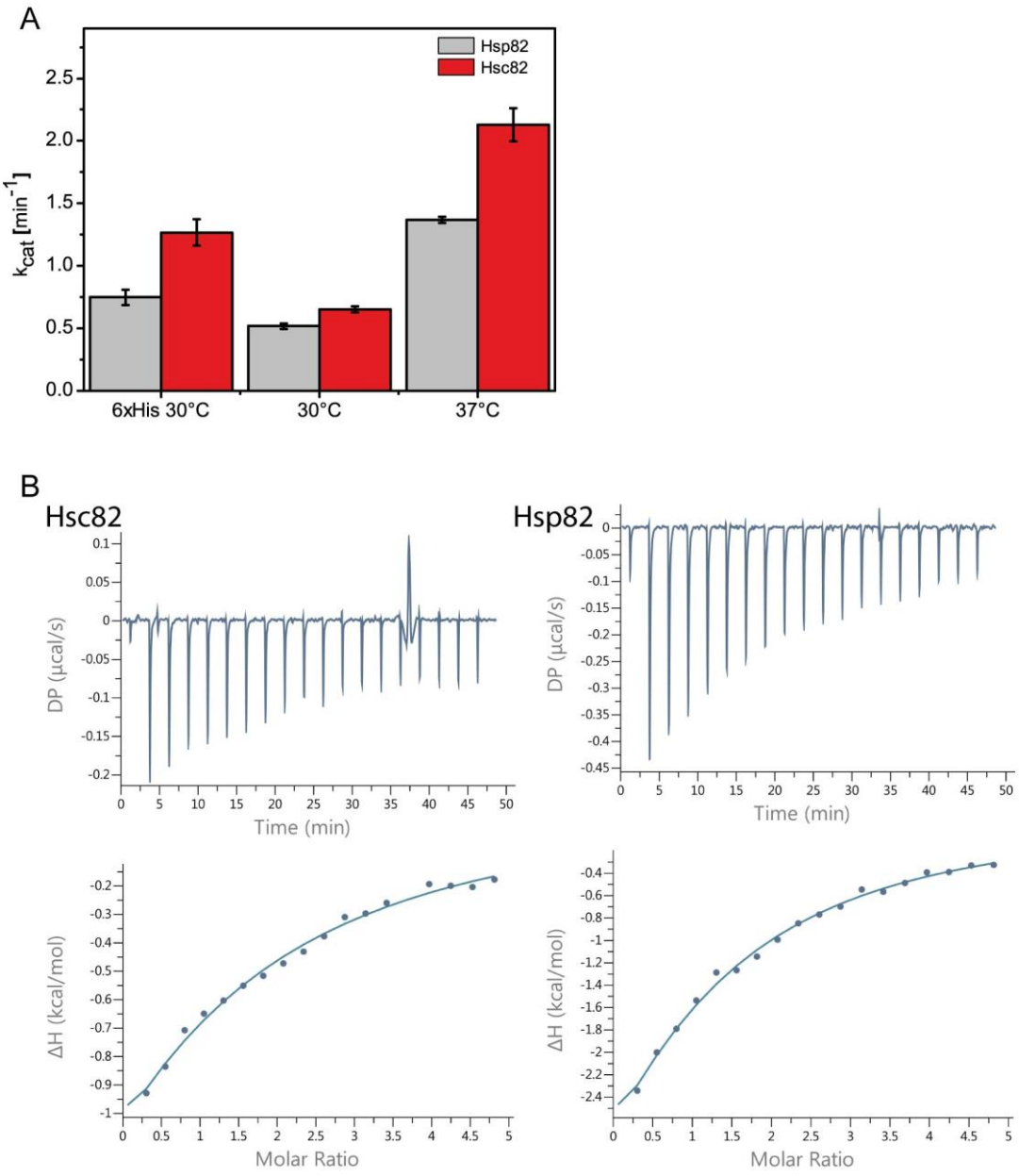

Figure 14: **Analysis of ATPase activity and ATP binding of the Hsp90 isoforms. A**) Comparison of ATPase activity of tagged and untagged Hsp90 isoforms at different temperatures. ATP hydrolysis was measured using an ATP regenerative system. Means and standard deviations (s.d.) were calculated from at least three technical measurements. All values were corrected for background activity using 50 µM radicicol. ATPase assays were performed in a buffer containing 40 mM HEPES, pH 7.5, 150 mM KCl, 5 mM $MgCl_2$, 2 mM ATP and a final Hsp90 concentration of 3 µM at 30 °C and 37 °C. **B**) ATP binding to Hsp90 NTD isoforms was determined using ITC. Measurements were performed in buffer containing 40 mM HEPES, pH 7.5, 150 mM KCl and 5 mM $MgCl_2$ at 25 °C. Hsp90 ND stock solution (20 µM) was filled into the measurement cell and the ATP stock solution (6 mM) into the syringe. The ligand was titrated in until saturation was reached.

4.1.4 Co-Chaperones Differentially Affect the Hsp90 ATPases

Co-chaperones specific take part in the Hsp90 cycle by promoting the progression through stabilizing specific Hsp90 conformations (Li et al., 2011b). Some co-chaperones inhibit or accelerat the Hsp90 ATPase activity. To explore how co-chaperones impact the ATPase of the Hsp90 isoforms, ATPase activity assays in the presence of co-chaperones were performed. First, Aha1, a co-chaperone that stimulates the ATPase activity of Hsp90, was tested (Retzlaff et al., 2010). Aha1 showed a slightly stronger stimulating effect on Hsc82 than on Hsp82 (*Figure 15 and Table 4*). The stimulation of about 24.7 fold by Aha1 of the Hsp82 ATPase is in agreement with previeous results (Retzlaff et al., 2010), whereas Hsc82 ATPase was stimulated up to 26.2 fold (*Figure 15 and Table 4*). The situation was different when Cpr6 was used. Cpr6 also activates Hsp90 ATPase activity although to a differnet extent (Panaretou et al., 2002). Hsp82 (3.1 fold) was slightly more stimulated by Cpr6 than Hsc82 (2.6 fold) (*Figure 15 and Table 4*).

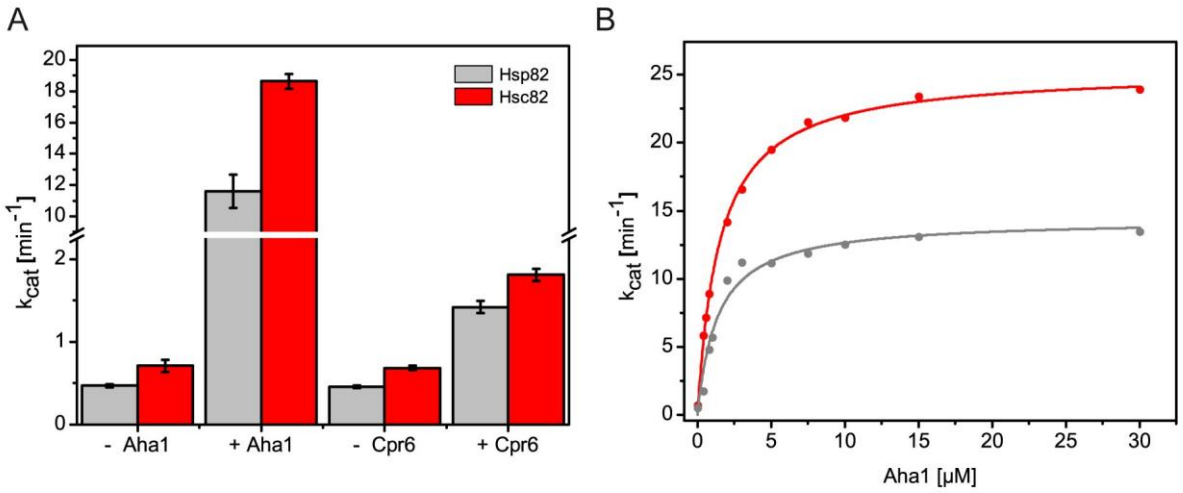

Figure 15: **ATPase activity of Hsp90 isoforms and its modulation by activating co-chaperones**. **A**) Hsp82 (grey bars) and Hsc82 (red bars) ATPase stimulation by Aha1 or Cpr6 were measured in a low salt buffer containing 40 mM HEPES, pH 7.5, 50 mM KCl, 5 mM $MgCl_2$, 2 mM ATP and a final concentration of 1 µM Hsp90 or 3 µM Hsp90 in the presence of 15 µM Aha1 or Cpr6. Measurements were performed at 30 °C. **B**) Different concentrations of Aha1 were added to a constant concentration of Hsp82 (grey curve) or Hsc82 (red curve) and plotted against the determined k_{cat} value.

Table 4: ATP turnover rates of Hsp90 isoforms and its modulation by activating co-chaperones.

Hsp90 isoform	**Aha1**		**Cpr6**	
	k_{cat}max [min^{-1}]	x [fold]	k_{cat}max[min^{-1}]	x [fold]
Hsp82	11.594 ± 1.050	24.7	1.421 ± 0.072	3.1
Hsc82	18.627 ± 0.475	26.2	1.811 ± 0.075	2.6

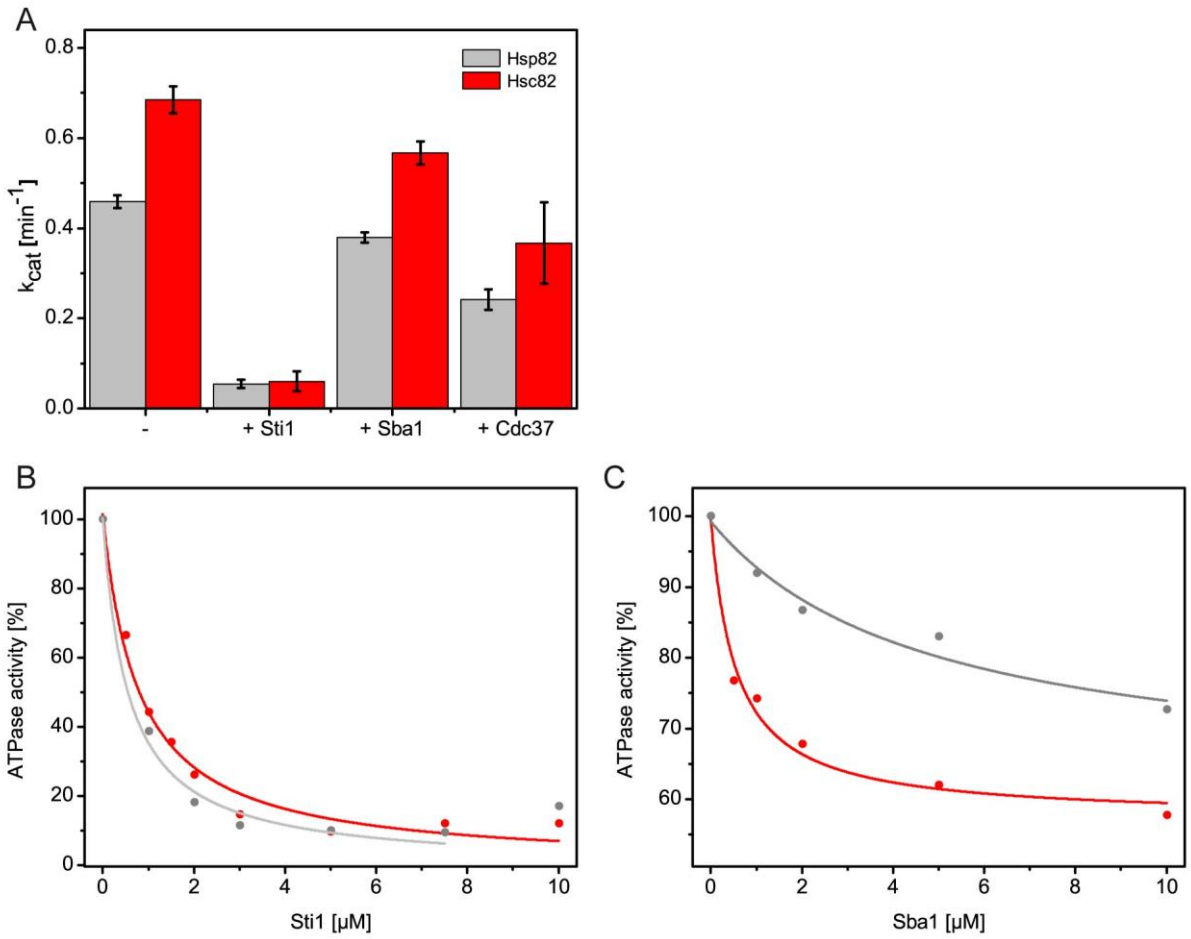

Figure 16: **ATPase activity of Hsp90 isoforms and its modulation by inhibiting co-chaperones**. **A**) Hsp90 ATPase inhibition by Sti1, Sba1 and Cdc37 were measured in a buffer containing 40 mM HEPES, pH 7.5, 40 mM KCl, 5 mM $MgCl_2$, 2 mM ATP and a final concentration of 3 µM Hsp90 in absence of co-chaperone and in presence of 7.5 µM Sti1, 10 µM Sba1 and 20 µM Cdc37 at 30 °C. **B**) Different concentrations of Sti1 were added to a constant concentration of Hsp82 (grey curve) or Hsc82 (red curve) and plotted against the determined k_{cat} value. **C**) Different concentrations of Sba1 were added to a constant concentration of Hsp82 (grey curve) or Hsc82 (red curve) and plotted against the determined k_{cat} value.

Next, co-chaperones that are known to inhibit the Hsp90 ATPase activity, Sba1, Sti1 and Cdc37 were analyzed (Prodromou et al., 2000; Prodromou et al., 1999; Roe et al., 2004). Sba1 was shown to inhibit the Hsp82 ATPase up to 50 % (Richter et al., 2004; Sullivan et al., 2002). Sba1 was approximately two-fold more efficient in inhibiting the ATPase of Hsp82 than of Hsc82 (*Figure 16 and Table 5*), however a reduction of 50 % was not achieved. To exlude the possibility that the difference originates from the tagged-Hsp90 version the experiment was repeated with 6xHis-tagged Hsp82 and Hsc82 resulting in a similar observation (data not shown). No difference could be observed for Cdc37 and Sti1 (*Figure 16 and Table 5*).

Table 5: ATP turnover rates of Hsp90 isoforms and their modulation by inhibiting co-chaperones.

Hsp90 isoform	**Cdc37**		**Sba1**		**Sti1**	
	k_{cat}max [min^{-1}]	Inhibition [%]	k_{cat}max [min^{-1}]	Inhibition [%]	k_{cat}max [min^{-1}]	Inhibition [%]
Hsp82	0.242 ± 0.023	50	0.380 ± 0.012	27	0.055 ± 0.010	90
Hsc82	0.367 ± 0.090	50	0.567 ± 0.025	13	0.060 ± 0.022	90

4.1.5 Specific Co-Chaperones Exhibit Different Affinities for the Hsp90 Isoforms

To better understand the differential impact that some co-chaperones have on the ATPase activities of the yeast Hsp90 isoforms their binding was analyzed by analytical ultracentrifugation. To this end, the Hsp90 isoforms were labeled site-specifically at an engineered cysteine residue (61Cys) with a fluorescent dye (ATTO-Tec 488). No difference was detected in the affinity of Aha1 for Hsc82 or Hsp82 (*Figure 17A*). Conversely, Cpr6 displayed a slightly higher binding for Hsp82 than for Hsc82, indicating that this might be the reason underlying the stronger stimulatory effect of Cpr6 on Hsp82 (*Figure 17B*). Sti1 displayed equal affinities for Hsc82 and Hsp82 (*Figure 17C*). No binding for Cdc37 to both Hsp90 isoforms was observed (*Figure 17D*). Contrary to the stronger inhibitory effect of Sba1 on Hsp82 than on Hsc82, the binding affinity of Sba1 was higher for Hsc82 than for Hsp82 in the presence of ATPγS (*Figure 17E*).

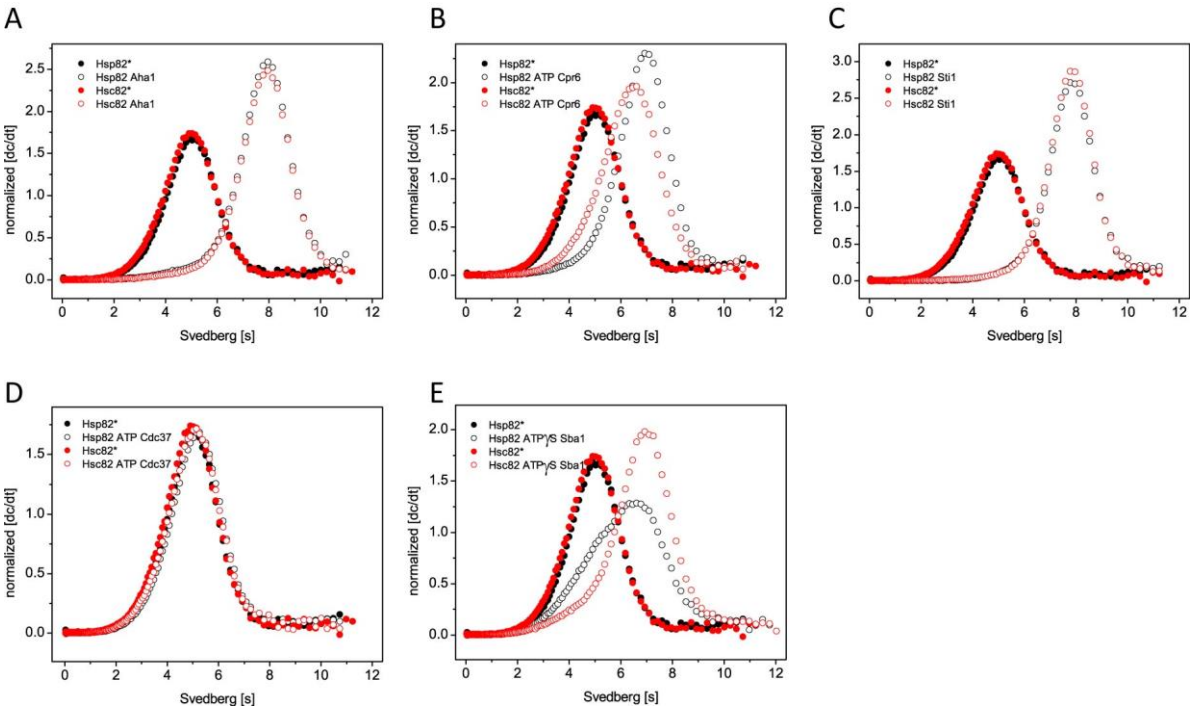

Figure 17: **Formation of complexes between the co-chaperones and labeled Hsp90 isoforms determined by analytical ultracentrifugation.** Normalized sedimentation profiles (dc/dt) of Hsp90 isofoms in the presence and the absence of **A**) Aha1, **B**) Cpr6/ATP, **C**) Sti1 **D**) Cdc37/ATP and **E**) Sba1/ATPγS.

As a control, the experiments were repeated with labeled co-chaperones in the presence of unlabeled Hsp82 or Hsc82. The same results were obtained except for Cdc37 binding (*Figure 18A-D*). Cdc37 displayed equal binding to Hsc82 and Hsp82 (*Figure 18C*) which is in line with similar inhibitory effects on both isoforms. Thus labeling at position 61C of Hsp90 alters Cdc37 binding. Taken together the results indicate that selective co-chaperones differentially bind and impact the ATPase of the Hsp90 isoforms *in vitro*.

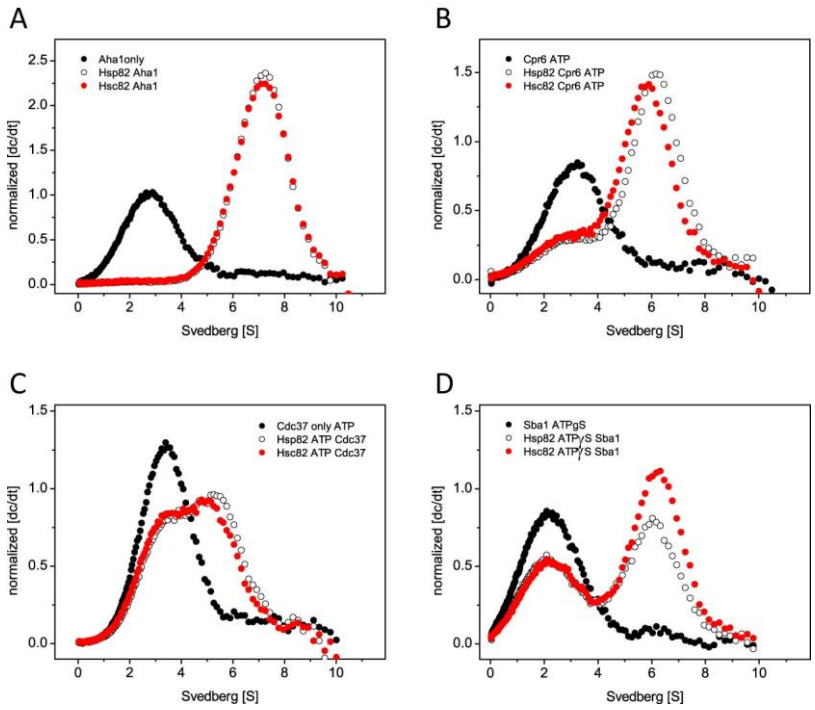

Figure 18: **Formation of complexes between Hsp90 isoforms and labeled co-chaperone determined by analytical ultracentrifugation.** Normalized sedimentation profiles (dc/dt) of Hsp90 isofoms in the presence of **A**) Aha1, **B**) Cpr6/ATP, **C**) Cdc37/ATP and **D**) Sba1/ATPγS.

4.1.6 Establishing a Hsc82 FRET-based System

Hsp90 undergoes conformational transitions from an open to a closed conformation during its ATPase cycle (Hessling et al., 2009). The structural changes to the closed conformation can be tracked with a fluorescent resonance energy transfer (FRET) system, which has been extensively used for Hsp82 (Hessling et al., 2009). For Hsc82, a FRET system was lacking. As yeast Hsp90 isoforms contain no cysteines in their amino acid sequences, the integration of a cysteine by mutagenesis is straightforward (*Figure 19A*). The designed constructs were tested *in vivo* for their activity. In order to verify Hsp90 *in vivo* functionality, plasmids (p423GPD) were transformed in a yeast shuffling strain

(PLCD82α) carrying a wt Hsp90 plasmid with an URA marker. Afterwards, these cells were subjected to a 5'-FOA complementation assay to ensure the loss of the Hsp90 wt plasmid has to be compensated by the cysteine mutants. Both engineered Hsc82 cysteine variants were functional *in vivo* as viability in yeast was supported (*Figure 19B*).

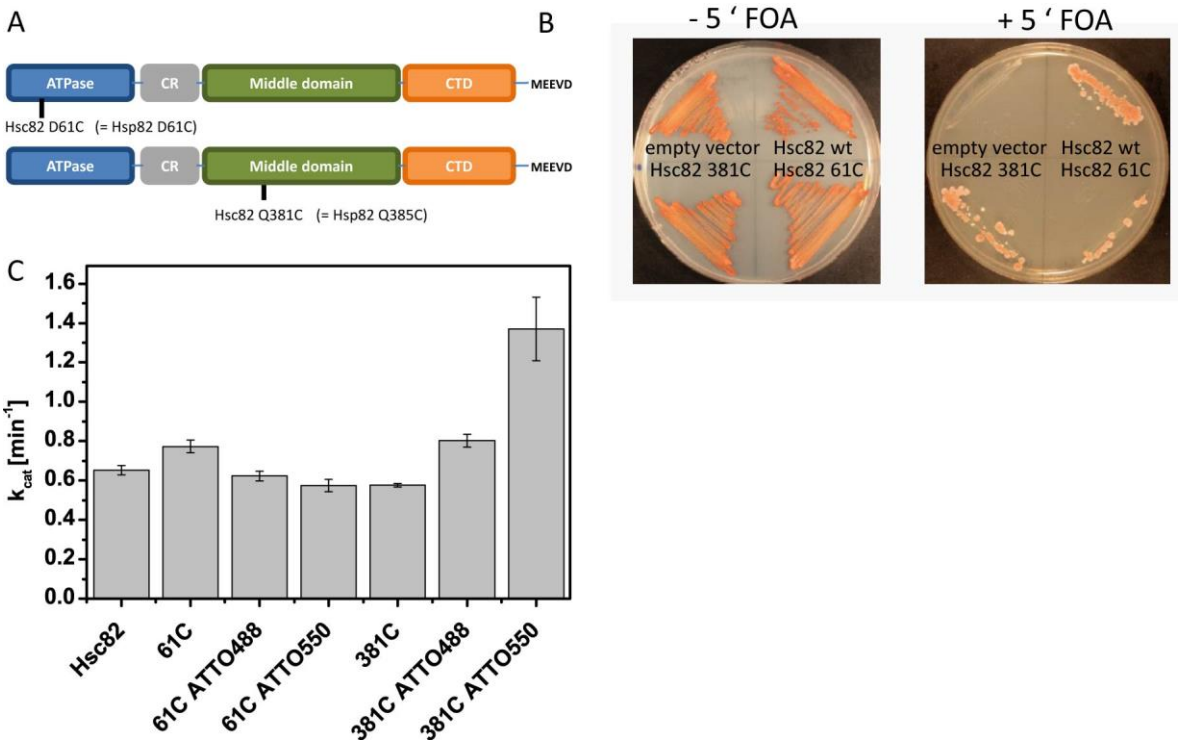

Figure 19: **Establishing an Hsc82 FRET-setup: A**) Design of the Hsc82 FRET constructs. **B**) Viability of the Hsp90 constructs was tested by a 5'-FOA plasmid shuffling approach. Both Hsc82 cysteine variants were able to support yeast viability as sole Hsp90 source in yeast. **C**) Comparison of ATPase activity of Hsc82 wt, cysteine variants and labeled Hsc82. ATP hydrolysis was measured using an ATP regenerative system. Means and standard deviations (s.d.) were calculated from at least three technical replicates. All values were corrected for background activity using 50 µM radicicol. ATPase assays were performed in a buffer containing 40 mM HEPES, pH 7.5, 150 mM KCl, 5 mM $MgCl_2$, 2 mM ATP and a final concentration of 3 µM Hsp90 at 30 °C.

The respective Hsc82 was labeled site-specifically at engineered solvent-exposed cysteine residues on the one hand (61Cys) in the NTD with a fluorescent acceptor dye (ATTO-Tec 550) and on the other hand in the MD (381Cys) with a fluorescence donor dye (ATTO-Tec 488) (*Figure 19*). The selected sites correspond to the sites that have been previously been used for the Hsp82 FRET-setup. To ensure that, similar to Hsp82, the exchange to cysteines and/or the conjugation of fluorophores does not interfere with the conformational cycle of Hsc82, Hsc82 constructs were purified and labeled either with ATTO-dyes at 61Cys or 381Cys. After the labeling procedure, the remaining free label was

separated from the protein-dye conjugate by a size-exclusion HPLC. The degree of labeling for all variants was above 90 % as determined by absorption spectroscopy. The ATPase activities in the absence and presence of conjugated dyes were determined *in vitro*. The cysteines at position 61 and 381 did not alter the ATPase rate of Hsc82 and, except for the attachment of ATTO-550 to 381Cys, all conjugates had an ATPase activity similar to the wt Hsc82 (*Figure 19C*).

4.1.7 Hsp82 and Hsc82 form Hetero-Dimers *in vitro* and *in vivo*

The analysis of Hsp90 dimerization performed by size-exclusion HPLC had revealed a dissociation constant k_d of about 60 nM and furthermore it was stated that dissociation and association in the Hsp90 dimer occur fast (Richter et al., 2001). Constitutive dimerization of Hsp90 is mediated by a three helix-coil motif in the CTD of each monomer. Three of the five residues that vary between Hsc82 and Hsp82 in their CTD are part of this coil (*Figure 20A*). To explore if this impacts the rate of dimerization or hinders the formation of heterodimers, the established FRET systems were employed (Hessling et al., 2009). Subunit exchange by either mixing of NTD and MD labeled protomers of each isoform or formation of hetero-dimers of both isoforms were monitored. Mixing of donor- and acceptor-labeled Hsc82 leads to a formation of a FRET competent hetero-complex indicated by a decrease of donor fluorescence signal and an increase of acceptor fluorescence signal (*Figure 20B*). The subunit exchange rate constants are very similar for both isoforms (*Table 6)* with a k_{se} of 0.02 - 0.04 sec^{-1}. This is in line with published apparent subunit exchange rates for Hsp82 (Hessling et al., 2009).

Moreover, Hsc82 and Hsp82 readily formed heterodimers with equal rate constants (*Table 6*). Wondering if hetero-dimerization of the Hsp90 isoforms also occurs in the cell, an immunoprecipitation assay with differentially tagged Hsp90 was performed in yeast. To this end, yeast strains were constructed in which one isoforms carries a C-terminal GFP-tag and the other isoform an HA-tag. When the GFP-carrying isoforms were immunoprecipitated, the other isoform could be detected in the immunoprecipitation, indicating that Hsc82 and Hsp82 also hetero-dimerize *in vivo* (*Figure 20C*).

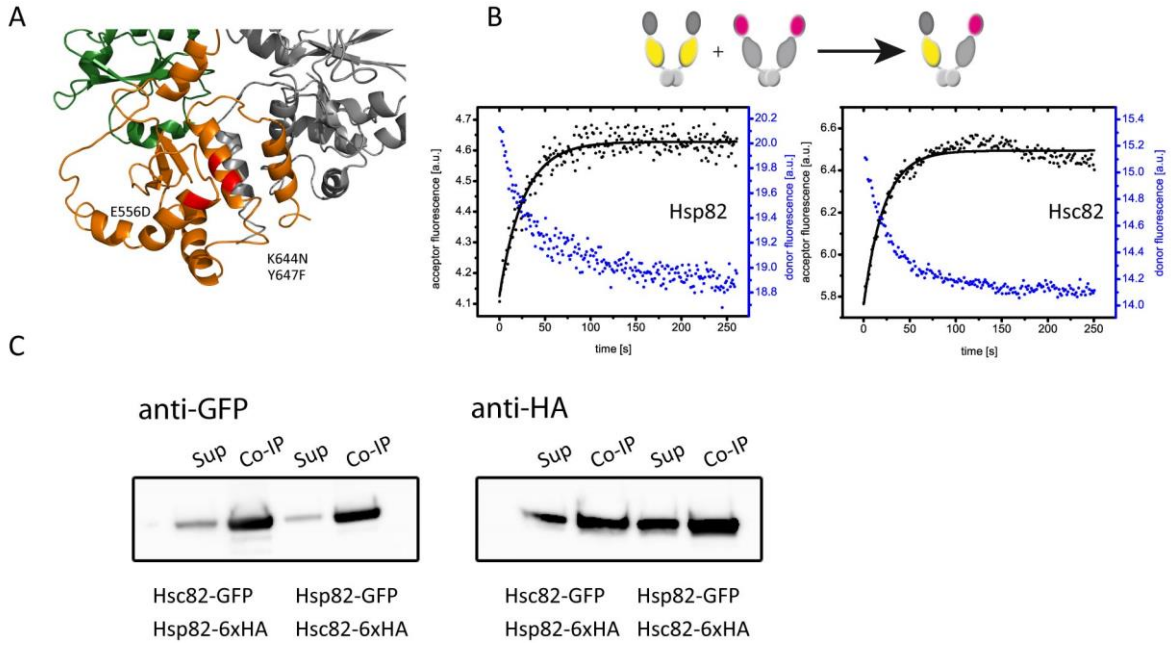

Figure 20: **Analysis of C-terminal dimerization stability and ability to form hetero-dimers of the Hsp90 isoforms. A**) Schematic representation of the dimerized CTDs (orange) of Hsp90. Differences in amino acid sequence between the yeast Hsp90 isoforms are depicted in red. **B**) Dimer-formation of donor- and acceptor-labeled yeast Hsp90 isoforms were followed by FRET subunit-exchange experiments (upper panel). FRET experiments were performed in a buffer containing 40 mM HEPES, pH 7.5, 150 mM KCl and 5 mM $MgCl_2$ at 30 °C. Subunit exchange rates were monitored by increase in acceptor fluorescence (black) and decrease in donor fluorescence (blue) upon mixing (lower panel). The increase in signal was fitted to a mono-exponential function to obtain the apparent rate constants k_{app} (sec^{-1}). **C**) The Co-Immunoprecipitation (Co-IP) assay with differentially tagged Hsp90 (C-terminal HA-tagged and GFP-tagged Hsp82 or Hsc82) was performed in yeast. The pull down was carried out with GFP beads and subsequent analysed by Western Blot. The blot was probed with an specific antybody against GFP and HA.

Table 6: Subunit exchange rates were monitored by increase in acceptor fluorescence and decrease in donor fluorescence upon mixing of donor-and acceptor-labeled yeast Hsp90 isoform. The increase in signal was fitted to a mono-exponential function to obtain the apparent rate constants k_{app} (sec^{-1}). Means and standard derivation (s.d.) were determined by at least three technical replicates.

	k_{se} [sec^{-1}]
6x His Hsp82 (M→N)	0.019 ± 0.002
6x His Hsc82 (M→N)	0.038 ± 0.011
Hsp82 (M→N)	0.034 ± 0.004
Hsc82 (M→N)	0.037 ± 0.006
Hsc82 (N→M)	0.03
Hsp82 (M) Hsc82 (N)	0.03
Hsp82 (N) Hsc82 (M)	0.04

4.1.8 Monitoring Conformational Changes of the Hsp90 Isoforms

The increase in acceptor fluorescence and decrease in donor fluorescence upon addition of ATP analogues presents a read-out for the kinetics of the closing reaction (*Figure 21A*). Comparing the closing kinetics upon addition of ATPγS or AMP-PNP, we observed that Hsp82 molecules convert slower to the closed conformation than Hsc82 dimers (*Figure 21B*). This is in line with their lower ATPase activity (*Figure 14*). In the presence of ATPγS, Hsc82 displayed a k_{app} of 0.522 ± 0.026 and Hsp82 of 0.198 ± 0.009. Likewise, in the presence of AMP-PNP, the k_{app} for Hsc82 was 0.164 ± 0.025 and for Hsp82 it was 0.084 ± 0.004. Furthermore, the closing kinetics, induced either by ATPγS or AMP-PNP, were slower for Hsp82 compared to the N-terminal histidine-tagged Hsp82 version (Hessling et al., 2009). This is in agreement with the observed slightly lower ATPase rate for untagged Hsp82. This is also the case for Hsc82 closing kinetics (*Table 7*). As known before, in the presence of ATP or ADP, Hsp90 mainly populates the open state, indicated by the absence of changes in FRET signals upon nucleotide addition (*Figure 21A-B*).

Table 7: Nucleotide-induced kinetics were monitored upon addition of nucleotide to a pre-formed Hsp90 FRET-complex. The increase in acceptor-fluorescence signal was fitted to a mono-exponential function to obtain the apparent rate constants k_{app} (min^{-1}). Means and standard derivation (s.d.) were determined by at least three technical replicates.

Hsp90 isoform	ATP k_{app} [min^{-1}]	ATPγS k_{app} [min^{-1}]	AMP-PNP k_{app} [min^{-1}]
Hsp82	---	0.198 ± 0.009	0.084 ± 0.004
Hsc82	---	0.522 ± 0.026	0.164 ± 0.025

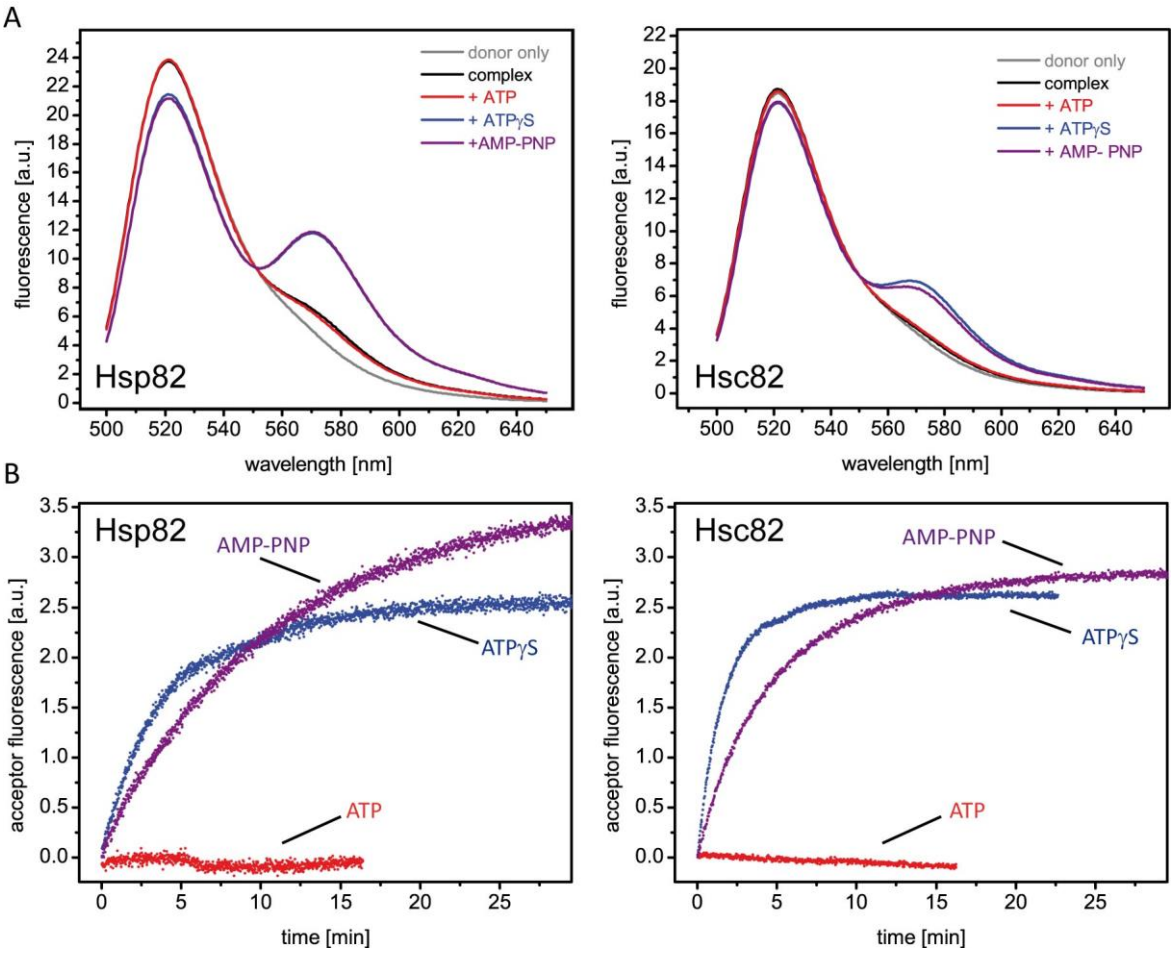

Figure 21: **Monitoring conformational changes within the Hsp90-dimer using FRET. A**) Fluorescence emission spectra of Hsc82 and Hsp82 were recorded and performed in a buffer containing 40 mM HEPES, pH 7.5, 150 mM KCl and 5 mM $MgCl_2$ at 30 °C. Following color-code is used: donor only (grey), the FRET hetero-complex (black), in the presence of 2 mM ATP (red), 2 mM ATPγS (blue) and 2 mM AMP-PNP (purple). **B**) Nucleotide-induced kinetics have been recorded in the presence of 2 mM ATP (red), 2 mM ATPγS (blue) and 2 mM AMP-PNP (purple). The increase in acceptor fluorescence signal was followed and fitted to a mono-exponential function to obtain the apparent rate constants k_{app} (min^{-1}).

To test the influence of different co-chaperones on the closing kinetics, FRET experiments in the presence of co-chaperones were performed. To this end, the FRET-competent heterocomplex was formed and pre-incubated with the co-chaperone to allow binding. Afterwards ATPγS was added to induce conformational changes. In line with what was found for the ATPase activities, Aha1 showed a stronger effect on Hsc82 than that on Hsp82, while Cpr6 stimulated closure of Hsp82 more than of Hsc82 (*Figure 22A-C*). Cpr6 was shown to favor the closing reaction of Hsp82 (Hessling et al., 2009). The observation is in line with the slightly higher ATPase rate and slightly better binding of Cpr6 to Hsp82 compared to Hsc82. The results indicate that Cpr6 differentially alters Hsp90 isoforms. Sti1 is

known to prevent N-terminal dimerization by stabilizing the open conformation (Hessling et al., 2009; Richter et al., 2004). Sti1 inhibited the closed state of both the isoforms to an almost equal extent (*Figure 22A-C*). In contrast, Sba1 is known to stabilize the closed state of Hsp90 by binding to the NTDs. Surprisingly, Sba1 did not effect the closing rate of Hsp82, but inhibited its formation in Hsc82 (*Figure 22A-C*). A possible explanation can be the better binding of Sba1 to Hsc82 shown in analytical ultracentrifugation experiments. Cdc37 inhibited formation of the closed state is more pronounced in Hsc82 than for Hsp82 (*Figure 22A-C*). Taken together, the results indicate that selective co-chaperones differentially alter Hsp90 isoforms *in vitro*.

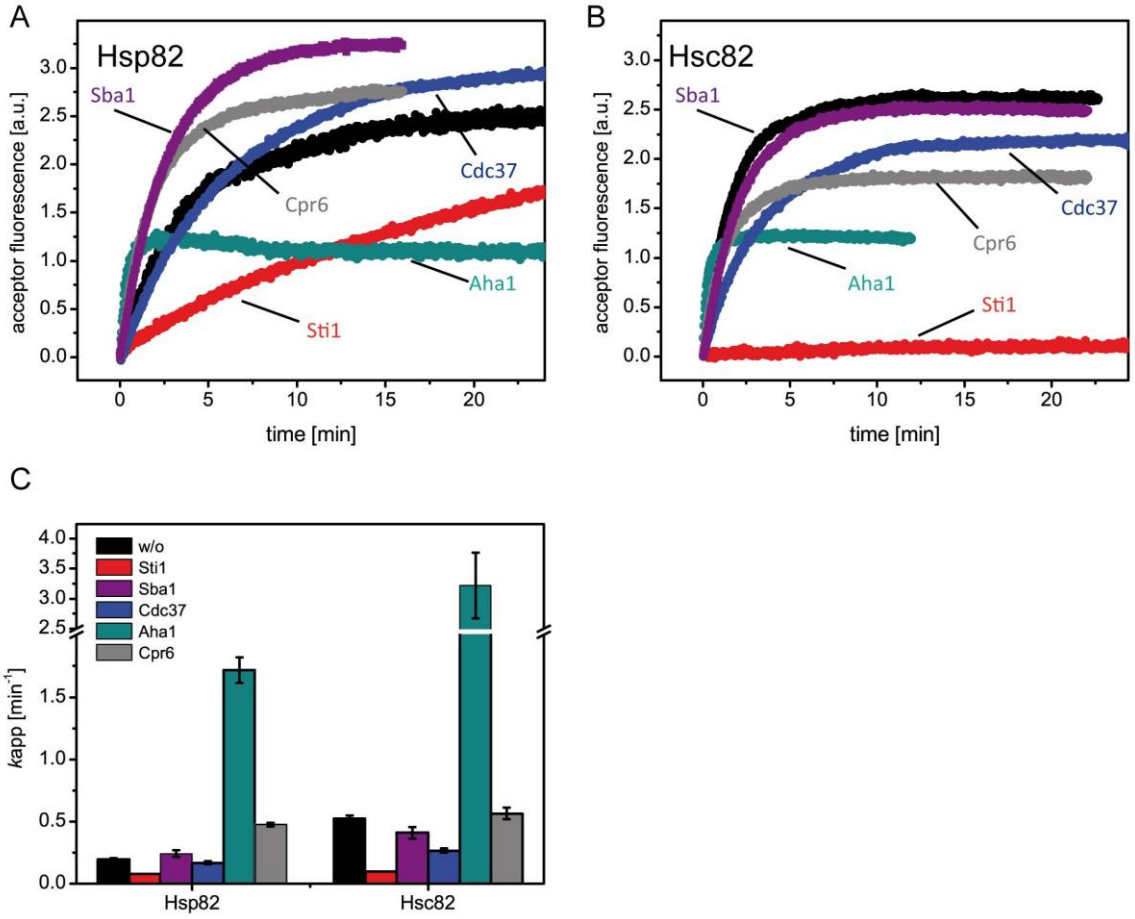

Figure 22: **Effects of co-chaperones on nucleotide-induced kinetics of Hsp90 isoforms determined by FRET. A**) Nucleotide-induced kinetics have been performed in a buffer containing 40 mM HEPES, pH 7.5, 150 mM KCl and 5 mM $MgCl_2$ at 30 °C. FRET kinetics were recorded in the absence of co-chaperone (black) and in the presence of the co-chaperones Sti1 (red), Sba1 (purple), Aha1 (cyan) or Cpr6 (grey). Prior to measurements the Hsp90 FRET-competent complex was pre-incubated with the co-chaperone. The experiment was started by adding 2 mM ATPγS (upper panal). **B**) The increase in acceptor-fluorescence signal was fitted to a mono-exponential function to obtain the apparent rate constants k_{app} (min^{-1}). Means and standard derivation (s.d.) were determined by at least three technical replicates (lower panel).

4.1.9 Hsp90 Isoforms Differ Slightly in N-terminal Dimerization Stability

To further gain insights into the stability of several Hsp90 states in the absence and presence of different nucleotides, FRET chase experiments were employed. The disruption of the FRET-complex depends on N-terminal dimerization stability of the Hsp90 dimer. Thus stability can be determined by FRET chase experiments. In the absence as well as in the presence of ATP the Hsp90 dimer mainly populates the open conformational state (Hessling et al., 2009). The disruption of the FRET-complex is initiated by adding a 10-fold excess of unlabeled Hsp90 and followed by recording the acceptor fluorescence signal. As expected, a fast subunit exchange is observed with a half-life of 0.6 - 0.7 min^{-1} for both isoforms in the presence of ATP and without nucleotide (*Figure 23A and Table 8*). This is in line with the observed subunit exchange rates determined when FRET complexes are formed. In contrast, Hsc82 displayed a slightly more stable N-terminal dimerization compared to Hsp82 in the presence of ATPγS due to slower complex disruption (*Figure 23A and Table 8*). In addition, the difference in NTD association was also observed in the presence of Aha1 and Sba1 (*Figure 23B and Table 8*). For both isoforms, the equilibrium of states is shifted completely towards a stable closed conformation in the presence of AMP-PNP and thus prevents the disruption of the complex (*Figure* 23*A and Table 8*). This is indicated by an unchanged fluorescence signal after chase with the respective unlabeled Hsp90 isoform.

Table 8: Comparison of the N-terminal dimerization stability of the Hsp90 isoforms. Apparent half-lives ($t_{1/2}$) were derived from a non-linear fit of the acceptor signal changes. Means and standard derivation (s.d.) were determined by at least three technical replicates.

Hsp90 isoform	w/o nucleotide k_{app} [min]	ATP k_{app} [min]	ATPγS k_{app} [min]	ATPγS/Aha1 k_{app} [min]	ATPγS/Sba1 k_{app} [min]	AMP-PNP k_{app} [min]
Hsp82	0.564 ± 0.079	0.702 ± 0.073	35.5 ± 3.2	103	47	> 300
Hsc82	0.533 ± 0.085	0.682 ± 0.209	54.2 ± 6.0	160	56	>300

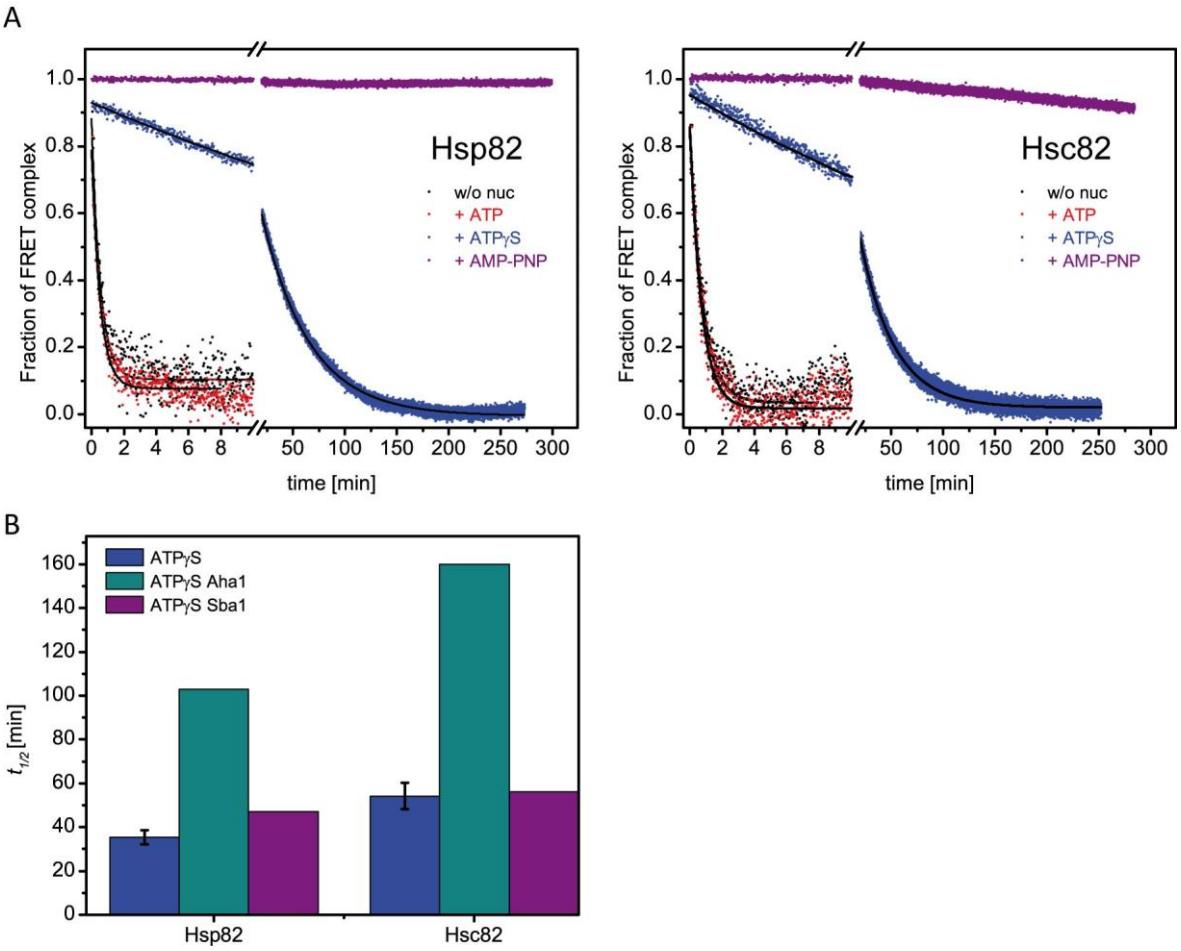

Figure 23: **Comparison of N-terminal dimerization stability of the Hsp90 isoforms. A**) N-terminal dimerization stability was investigated by a FRET chase experiment. FRET chase experiments were performed in a buffer containing 40 mM HEPES, pH 7.5, 150 mM KCl and 5 mM $MgCl_2$ at 30 °C. The chase was induced by adding a 10 x fold excess of unlabeled Hsp90 wt variant to a 400 nM preformed Hsp90 FRET-complex in the absence of nucleotide (black), in the presence of 2 mM ATP (red), 2 mM ATPγS (blue) and 2 mM AMP-PNP (purple). Left panal shows chase experiments with Hsp82 and the results of Hsc82 measurments are depicted in the right panel. **B**) Apparent half-lives of complex in the presence of co-chaperone Aha1 or Sba1.

4.1.10 Hsp90 Isoform *in vivo* Analysis

Although the yeast Hsp90 isoforms share high sequence identity, there is evidence for differences. An *in vivo* analysis was performed to find out which domain is responsible for the differences. To this end we constructed Hsp90 chimera (*Figure 24A*) with both Hsp82 and Hsc82 domains. Via the 5'-FOA-shuffling approach, a copy of wt Hsp82, wt Hs82 or the chimera as the sole source of Hsp90 was introduced into an isogenic *Saccharomyces cerevisiae* background (BY4741). All Hsp90 chimera support yeast viability and the expression levels of the variants were equal (*Figure 24B-C*).

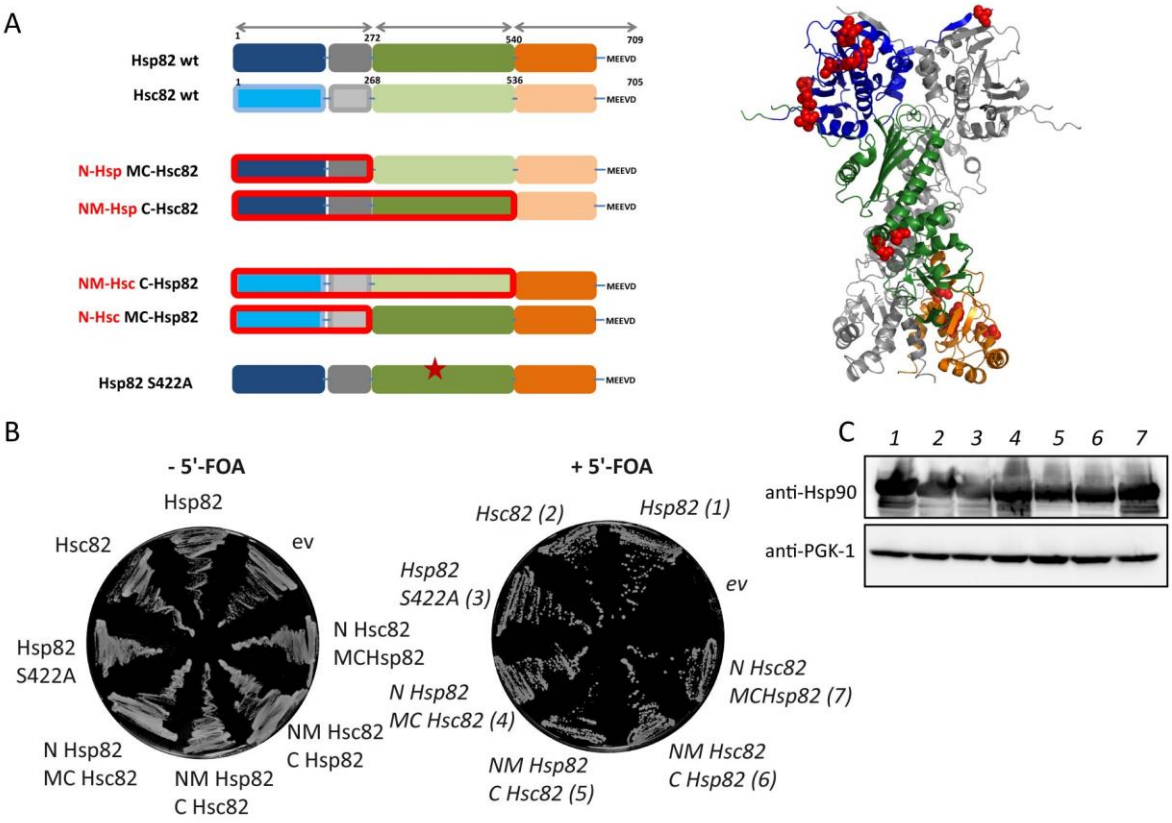

Figure 24: **Studying *in vivo* function of Hsp90 isoforms. A**) Design of yeast Hsp90 chimera (left panel). Most amino acid sequence differences are located in the NTD/linker region and in the CTD as depicted in red spherical elements within the structure (right panel). Domain swapping of the NTD and CTD domain results in four different swapping constructs. A middle domain mutant (S422A) was analyzed in addition. **B**) Hsp90 wt isoforms and chimera were expressed in BY4741 yeast cells. Viability of the Hsp90 chimera was tested by a 5'-FOA plasmid shuffling approach. As negative control yeast cells expressing empty vector GPD423 (e.v.) was used. **C**) Hsp90 variant expression levels were detected by Western Blot analysis. Detection against PGK-1 was used as loading control.

To test for differences in specific functions of the yeast Hsp90 isoforms, cells were subjected to several growth conditions. No differences were observed between the isoforms and chimeras in growth when exposed at elevated temperatures (*Figure 25A*). Yeast cells harboring Hsc82 as the sole Hsp90 source have been reproducible more sensitive to heat stress than Hsp82 carrying cells (Millson et al., 2007). This was not observed in our case, probably due to differences in used promoters. As Hsp90 plays a role in a DNA repair mechanism (McClellan et al., 2007; Toogun et al., 2007), cells were exposed to UV radiation to induce DNA damage. The experiment showed that the Hsp90-dependent nucleotide excision repair mechanism is similarly induced in cells harboring a copy of either Hsc82, Hsp82 or chimera as similar growth was observed after exposure of UV radiation (*Figure 25B*).

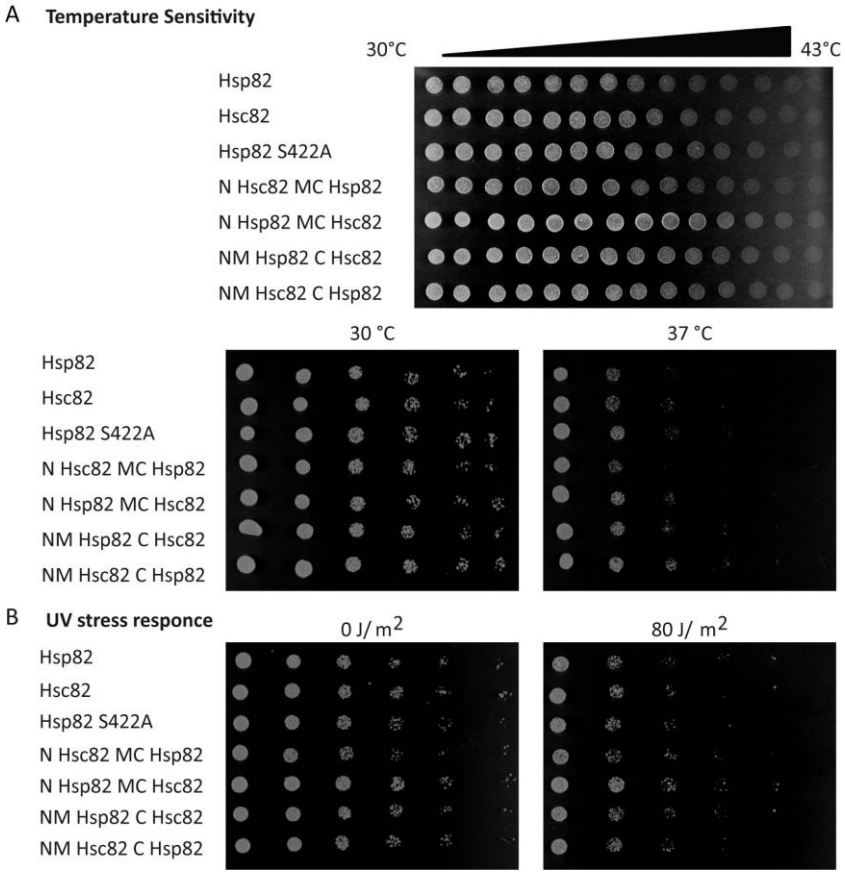

Figure 25: ***In vivo* analysis of Hsp90 isoform chimera. A**) Yeast cell BY4741 expressing a wt Hsp90 isoform or a chimera as the sole Hsp90 source were grown, diluted to an OD_{600}=0.5 and spotted on selective media and placed on a temperature gradient (upper panel). A dilution series starting from OD_{600}=0.5 was prepared and spotted on selective media, placed at 30 °C and 37 °C (lower panel). Cell growth was monitored after 48 h. **B**) A dilution series starting from OD_{600}=0.5 was prepared and spotted on selective media, exposed to UV radiation and incubated at 30 °C. Cell growth was monitored after 48 h.

Given that Hsc82 and Hsp82 deviate in their ATPase activities, we next explored if the isoforms also differ in their affinity to the NTD inhibitor radicicol. Radicicol is a macrocyclic compound, which, similar to the structurally unrelated ansamycin geldanamycin, binds to the nucleotide-binding pocket of Hsp90 and interferes with Sba1 binding and client maturation (Schulte et al., 1998). Applied *in vitro*, radicicol displayed a stronger inhibitory effect on Hsc82 than on Hsp82 in an ATPase assay (*Figure 26A*). This was matched by the *in vivo* findings (*Figure 26B*). Via the shuffling approach a copy of either Hsc82 or Hsp82 as the sole source of Hsp90 into an isogenic *S. cerevisiae* background were introduced. The expression levels of the isoforms were equal, but a much stronger sensitivity to radicicol when Hsc82 was present was observed, in particular in the lower concentration range of the inhibitor (*Figure 26B*). Whereas at 25 µM of radicicol yeast cells expressing Hsc82 were more than 2.5

times stronger inhibited in their growth than Hsp82 expressing cells, at 100 µM of radicicol, the inhibitory influence was almost similar. To obtain domain-specific information we next shuffled the three Hsp90 domains. We found that the higher susceptibility of Hsc82 towards radicicol exclusively relies on the NTD (*Figure 26C*), although the affinities of the NTD of Hsc82 and of Hsp82 turned out to be similar in an ITC experiment (*Figure 26D*).

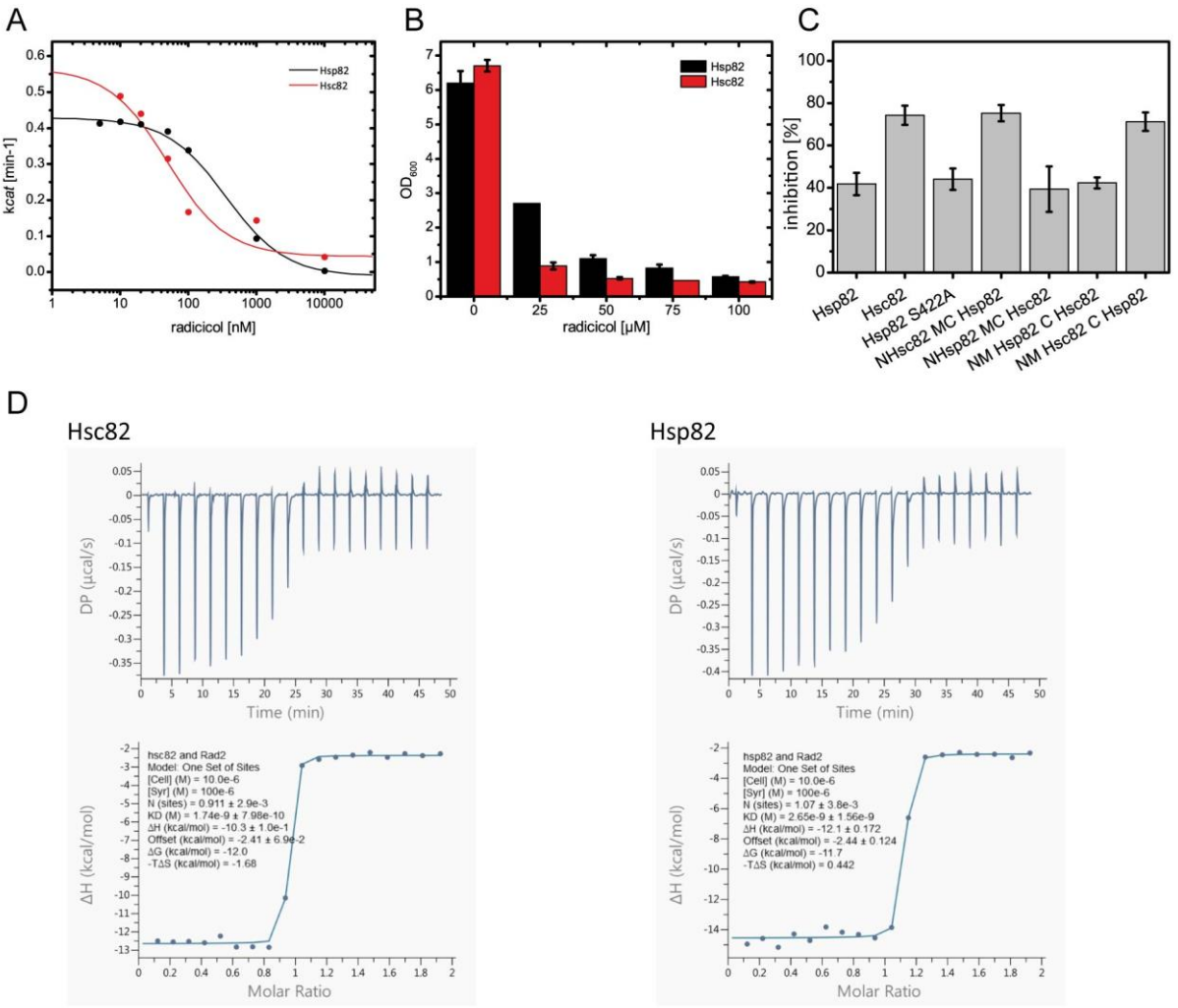

Figure 26: **Effects of Hsp90 chimera on radicicol sensitivity. A)** ATPase assay performed with different concentrations of radicicol were added to a constant concentration of Hsp82 (black curve) or Hsc82 (red curve) and plotted against the determined k_{cat} value. The decrease in signal was fitted to Hill function to obtain the apparent kD to radicicol. **B**) Yeast cells BY4741 expressing a wt Hsp90 isoform, Hsc82 (black bars) and Hsp82 (red bars) as the sole Hsp90 source were grown ON, than diluted to an OD_{600}=0.5 and growth was monitored in the absence and presence of increasing concentration of the Hsp90 inhibitor radicicol. **C**) Experiment was performed as described in B) for Hsp90 isoforms and Hsp90 chimera in the prescence of 25 µM radiciol. Means and standard deviations (s.d.) were calculated from three technical and biological independent replicates. **D**) Affinity for radicicol of Hsp82 and Hsc82 N-domain was determined by ITC.

4.1.11 Isoforms Differ in Client Specificity

Next, client specificity was further investigated since it had previously been shown that client activiation differ for human Hsp90 isoforms (Millson et al., 2007). To this end, a v-Src maturation assay was performed. Yeast cells expressing yeast Hsp90 isoform or Hsp90 chimera as the sole Hsp90 source were transformed with a plasmid encoding for v-Src under a galactose inducible promoter. Cells were selected on respective media and spotted onto media containing glucose as negative control and galactose to induce v-Src expression. The cell growth for all cells expressing different Hsp90 variants is equal indicated by a similar spot pattern and both isoforms activate v-Src displayed by similar inhibition of cell growth (*Figure 27*). In contrast to the human isoforms where Hsp90α is more efficient in activating v-Src, no difference was observed for yeast Hsp90 isoforms (Millson et al., 2007).

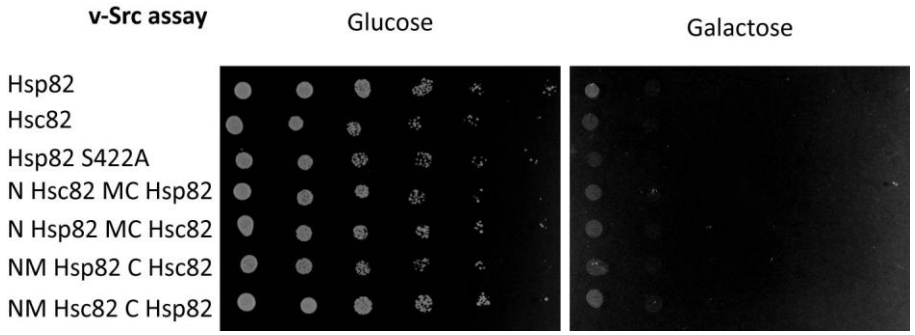

Figure 27: **Analysis of v-Src maturation by yeast Hsp90 isoforms.** Yeast cell BY4741 expressing a wt Hsp90 isoform or a chimera as the sole Hsp90 source and a plasmid encoding for v-Src under a galactose inducible promotor were grown in media contains raffinose. A dilution series starting from OD_{600}=0.5 was prepared and spotted on selective media containing either glucose or galactose and incubated at 30 °C. Cell growth was monitored after 72 h.

Recent data suggest that Hsc82 and Hsp82 have opposing roles in cell death under acetic acid stress, a condition that leads to impairment of general translation via phosphorylation of a subunit of the translation initiation factor eIF2α by Gcn2 (Silva et al., 2013). Gcn2 is a cytoplasmic kinase, which is mainly activated under amino acid starvation and a known Hsp90 client (Baird and Wek, 2012; Donze and Picard, 1999) (*Figure 28A*). Thus we used a yeast strain that either expressed Hsc82 or Hsp82 and explored eIF2α phosphorylation when cells were grown in the presence of 3-aminotriazole, which induces histidine-depletion (*Figure 28A*). Cells expressing Hsc82 as sole Hsp90 source are less

sensitive to amino acid starvation (*Figure 28B*). Furthermore, Hsp90 levels were identical, but the eIF2α phosphorylation was stronger when Hsc82 was present (*Figure 28C*). This is in line with what was found previously (Silva et al., 2013). To narrow this down to a specific domain, the experiment was also applied to the Hsp90 chimera. However, no domain specific relevance could be detected (*Figure 28B-C*).

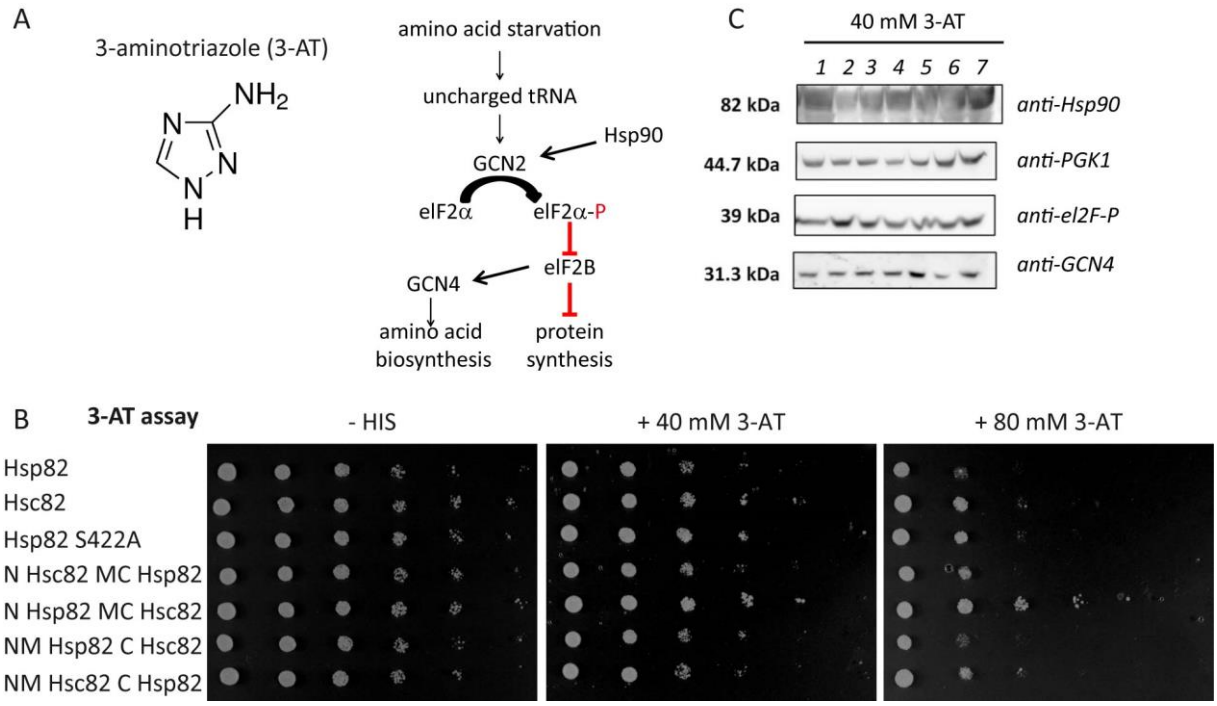

Figure 28: **Analysis of amino acid starvation of yeast Hsp90 isoforms**. **A**) 3-aminotriazole (3-AT) is a competitive inhibitor of the product of the HIS3 gene that leads to amino acid starvation in yeast cells. Overview of the following steps after amino acid starvation. Gcn2 is an Hsp90 client. **B**) Yeast cells BY4741 expressing a wt Hsp90 isoform, Hsc82, Hsp82 or a chimera as the sole Hsp90 source were grown ON, than a dilution series with an starting OD_{600}=0.5 was spotted on selective media containing increasing concentration of 3-AT. Yeast cell growth was monitored after 72 h. **C**) Western Blot analysis of GCN2 processing by Hsp90. Specific antibody was probed against Hsp90, PGK-1 as loading control, phosphorylated el2F and GCN4 levels. Samples were loaded as followed: 1) Hsp82, 2) Hsc82, 3) Hsp82 S422A, 4) N Hsc82 MC Hsp82, 5) N Hsc82 MC Hsp82, 6) NM Hsp82 C Hsc82, 7)NM Hsc82 C Hsp82.

4.2 Establishing a Human Hsp90 FRET-System

Hsp90 is very dynamic molecular machinery and undergoes large conformational changes within the ATPase cycle. Extensive effort was drawn to get structural data that revealed 'snapshots' of two distinct conformations, the open (HtpG) (Shiau et al., 2006) and the closed state (yeast Hsp90) (Ali et al., 2006). A FRET analysis monitored the transitions between both extreme states and indicated intermediate structural rearrangements within the yeast Hsp90 dimer (Hessling et al., 2009). Whether the Hsp90 conformational cycle can be generalized for the entire Hsp90 family is an important unresolved question. Human Hsp90 differs from yeast Hsp90 in that the enzymatic efficiency is significantly lower. As the affinity for ATP is similar, this can not be the reason for lower ATPase activity in human Hsp90 (McLaughlin et al., 2002; Richter et al., 2008). Furthermore the rate limiting step in the ATPase cycle (ATP turnover and N-terminal crosstalk) seems to be conserved (Richter et al., 2008). In addition, the mechanism of several co-chaperones regulating the Hsp90 cycle is conserved. However, crucial mechanistic differences between human Hsp90 and other family members have been reported (Graf et al., 2014; Krukenberg et al., 2011; Southworth and Agard, 2008). Moreover, exclusive human co-chaperones exist and for some their contribution within the Hsp90 cycle is still elusive (Rohl et al., 2013). Because human Hsp90 is an interesting target in cancer therapy, a detailed picture of the ATPase cycle of human Hsp90 is required. To investigate conserved mechanisms of Hsp90 regarding conformational changes and its regulation by co-chaperones, I seeked to establish a human Hsp90 FRET-system. Within this thesis several approaches were followed.

4.2.1 Differences in the Population of the Open vs Closed State of Hsp90

To analyze the dynamics of human Hsp90, limited proteolysis was used to probe structural flexibility. Limited proteolysis provides important information on the structure and dynamics of a protein. It was first used to identify sites of enhanced flexibility (Nemoto et al., 2001). To gain more insights into differences between yeast and human Hsp90, limited proteolysis was employed to probe structural and dynamic differences between the open and the closed state. Here, the conformational stability was tested by proteolysis with α-chymotrypsin.

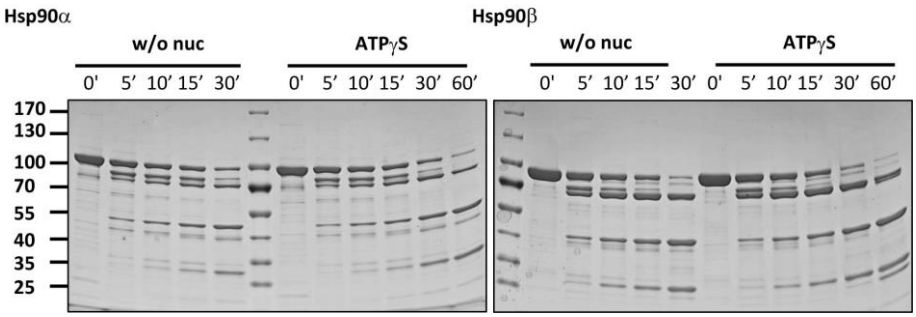

Figure 29: **Analysis of conformational properties of human Hsp90 isoforms by using limited proteolysis.** Hsp90 isoforms were treated with α-chymotrypsin in the absence or presence of ATPγS at 20 °C. The proteolysis reactions were stopped with 5x Lämmli supplemented with 2 mM PMSF after several time points and verified by SDS-PAGE analysis. The sample at the start of the raction (time point 0') was included as negative control.

Hsp90α and Hsp90β displayed a similar digestion pattern with and without nucleotide (*Figure 29*). The digestion pattern is similar between Hsp90α and Hsp82 in the presence of ATPγS. In contrast to yeast Hsp82, human Hsp90α is more protected against α-chymotrypsin in the absence of nucleotide suggesting a more compact structure or less flexible regions (*Figure 30A-B*). For Hsp82 the proteolysis kinetic was slowed down due to the compact Hsp90 structure and thus a lower accessibility of α-chymotrypsin was observed when incubated with ATPγS prior digestion (*Figure 30A-B*). This goes along with the large conformational changes yeast Hsp90 adopt during the ATPase cycle. Indeed, this indicates further that for yeast Hsp90 ATPγS induces larger structural changes than within human Hsp90.

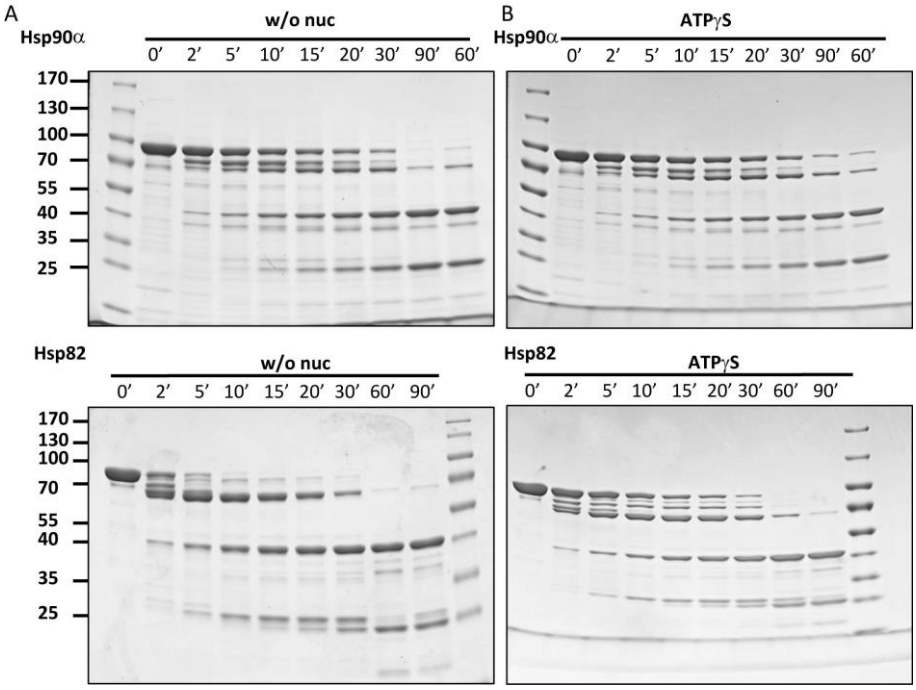

Figure 30: **Comparison of conformational properties of human Hsp90α and Hsp82 by using limited proteolysis.** Human Hsp90 and yeast Hsp90 were treated with α-chymotrypsin **A**) in the absence or **B**) in the presence of ATPγS at 20 °C. The proteolysis reactions were stopped with 5x Lämmli supplemented with 2 mM PMSF after several time points and verified by SDS-PAGE analysis. The sample at the start of the raction (time point 0') was included as negative control.

Likewise, both human Hsp90 isoforms have similar melting temperatures (*Table 9*) determined by a thermal shift assay.

Table 9: Melting temperatures of human Hsp90 isoforms in the absence and presence of ATPγS determined by a thermal shift assay. Means and standard derivation (s.d.) were determined by at least three technical replicates.

	T_m [°C]
Hsp90β	50.6 ± 0.5
Hsp90β ATPγS	55.5 ± 0.6
Hsp90α	50.4 ± 0.5
Hsp90α ATPγS	54.8 ± 1.0

4.2.2 Replacement of Cysteines and Characterization

Given these first hints and further evidence from the literature, a FRET system would be important to shed light on the conformational dynamics of human Hsp90. To this end a donor- and an acceptor-dye needs to be site-specifically attached to an engineered cysteine in the NTD and MD, respectively, similar to those established for the yeast Hsp90 (Hessling et al., 2009). As the human Hsp90α and Hsp90β isoform carries 7 and 6 natural cysteines, respectively, this has to be taken in account. Furthermore, one cysteine is surface-exposed and known to be nitrosylated *in vivo* (Martinez-Ruiz et al., 2005) which allows to regulate conformational changes (Retzlaff et al., 2009). To create a cysteine-free version, the cysteines were replaced on the one hand against serines (all serine) and on the other hand with an amino acid corresponding to naturally occurring amino acids at these positions in other Hsp90 family members (0 Cys) (*Figure 31A-B*). Since the cysteines are not conserved in Hsp90 (yeast Hsp90 has no cysteines), it seems likely, that their replacement can be achieved without affecting the structure and function of Hsp90. To test that the mutations do not affect structure or activity of Hsp90, a comprehensive *in vitro* and *in vivo* characterization was carried out. As it was shown that the human Hsp90 isoforms are able to complement the yeast Hsp90 isoforms *in vivo,* a 5'-FOA-Shuffling approach was employed (Millson et al., 2007). To this end a copy of the engineered Hsp90α and Hsp90β cysteine-free variants as well as the wt isoforms were introduced by the 5'-FOA-shuffling approach as the sole source of Hsp90 into an isogenic *S. cerevisiae* background (PLCD82α). The Hsp90β cysteine free variant is functional in yeast whereas the all serine variant is not able to support viability (*Figure 31C*). The Hsp90α wt as the only Hsp90 source showed severe growth defects but is able to support viability (*Figure 31C*). However, the Hsp90α cysteine-free variant causes lethality of the yeast cells (*Figure 31C*). This indicates that one has to take care when substitute a natural cysteine in human Hsp90.

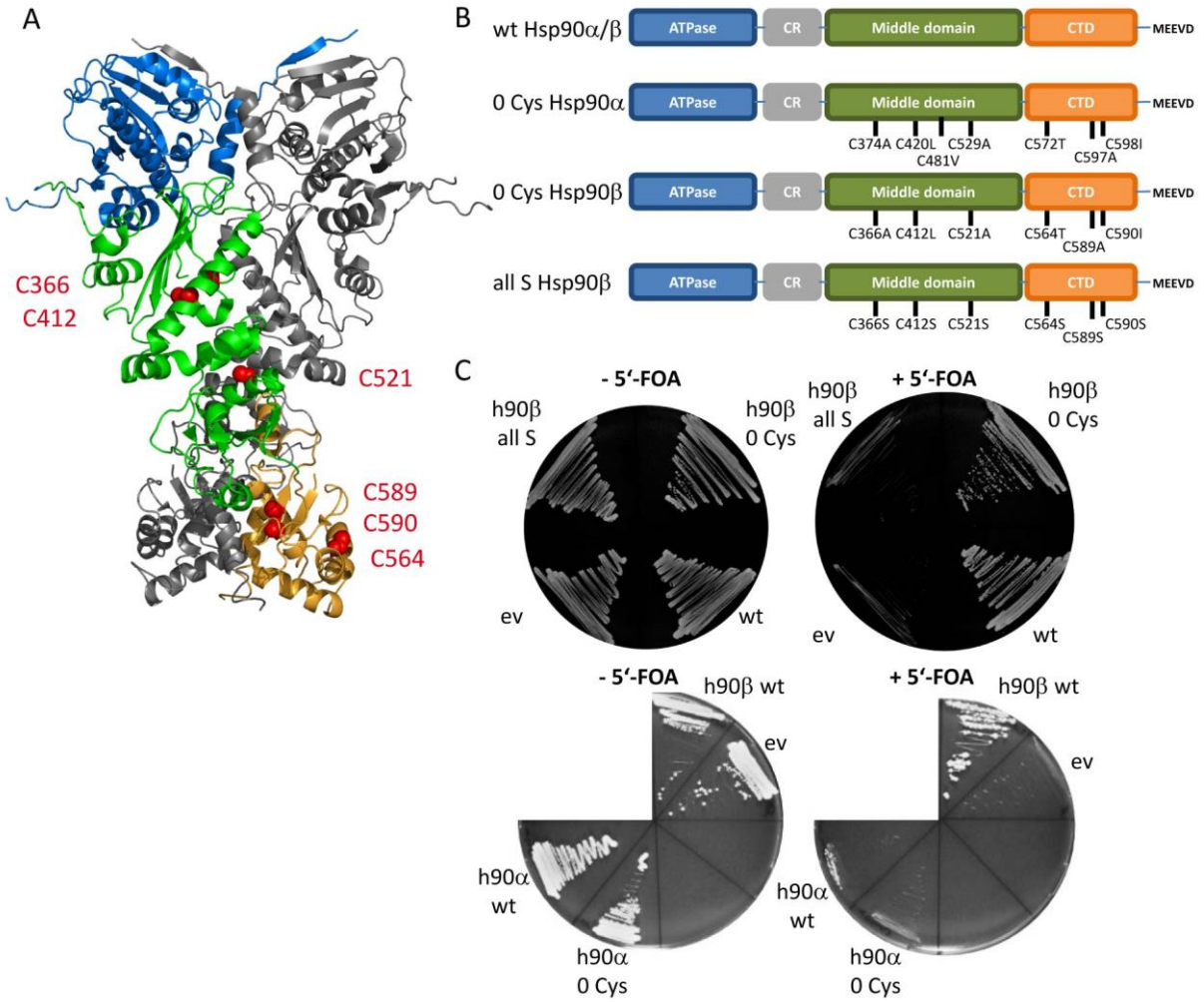

Figure 31: **Design of a cysteine free human Hsp90 variant. A**) Overview of cysteines of Hsp90β illustrated as red spherical elements within the closed yeast Hsp90 structure (PDB ID: 2CG9 (Ali et al., 2006). The cysteines are exlusively located in the middle domain and C-terminal domain of Hsp90. **B**) Schematic representation of generated cysteine-free variants of human Hsp90α/β. **C**) Hsp90 wt isoforms and cys-free variants were expressed in PCLDα yeast cells. Viability of the Hsp90 variants was tested by a 5'-FOA plasmid shuffling approach. As negative control yeast cells expressing empty vector GPD423 (e.v.) was used.

Next, the Hsp90β cysteine-free variant (0 Cys) was validated *in vitro*. The substitution of specific amino acids did not alter the ATPase activity (*Figure 32A*). Moreover, stimulation of the Hsp90β ATPase by Aha1 was tested. The ATPase turnover rate of the Hsp90 cysteine-free variant was stimulated by Aha1 but to a different extent compared to wt (*Figure 32A*). In addition, no structural differences were observed by far-UV CD spectroscopy (*Figure 32B*).

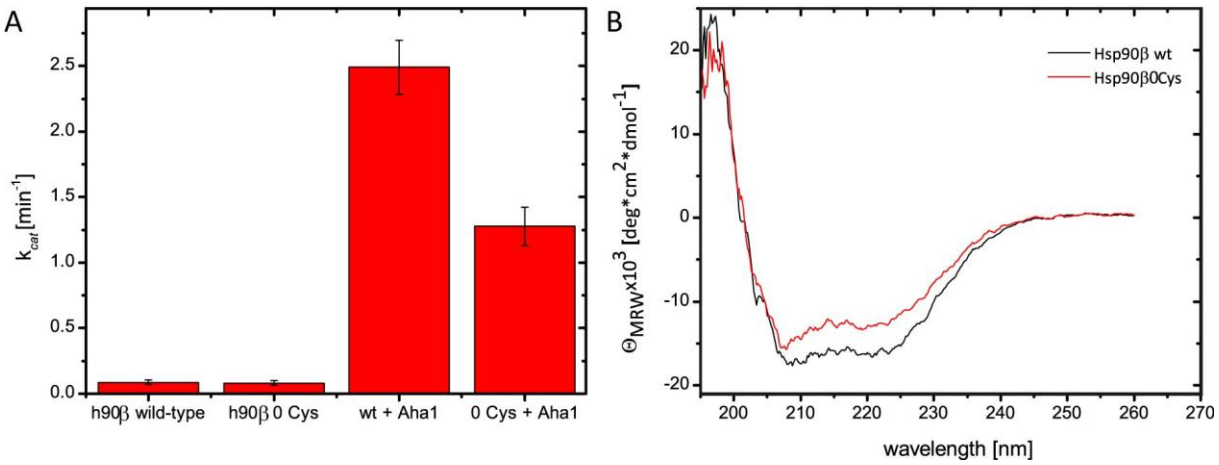

Figure 32: ***In vitro* characterization of generated cys-free Hsp90β (0 Cys). A**) Comparison of ATPase activity of Hsp90β and the cysteine free Hsp90β variant. ATP hydrolysis was measured using an ATP regenerative system. ATPase assays were performed in a buffer containing 40 mM HEPES, pH 7.5, 150 mM KCl, 5 mM $MgCl_2$, 2 mM ATP and a final concentration of 10 µM Hsp90 at 37 °C. The stimulation of Hsp90 ATPase activity was measured in the presence of 30 µM Aha1 in a buffer containing 40 mM HEPES, pH 7.5, 20 mM KCl, 5 mM $MgCl_2$, 2 mM ATP and a final concentration of 1 µM Hsp90 at 37 °C. Means and standard deviations (s.d.) were calculated from at least three technical measurements. All values were corrected for background activity using 100 µM radicicol. **B**) Structural elements of Hsp90 variants were obtained using CD spectroscopy. To analyze the secondary structure far-UV CD spectra were recorded of 0.2 mg/ml Hsp90 variant in 50 mM phosphate buffer, pH 7.5 at 20 °C.

Next, cysteines in the N-terminal domain (63C, 67C, 69C, 70C, 71C) and in the middle domain (383C, 386C, 388C, 390C, 395C, 397C), were introduced by mutagenesis into Hsp90β, lacking all natural occurring cysteines, to allow site-specific labeling (*Figure 33A*). The positions were chosen considering that the Förster–radius of the selected ATTO-dye pair (Donor-ATTO488//Acceptor ATTO 550) is about 63 Angström, to ensure an efficient labeling reaction solvent-exposed residues were chosen. Further, the distance between the donor and acceptor was taken into account. Once again, all Hsp90β cysteine variants were screened for functionality *in vivo* via the 5'-FOA shuffling approach. All variants tested supported growth after complementation, except Hsp90β 395C and Hsp90β 397C (*Figure 33B*). To investigate the influence of the cysteines on Hsp90 function, cells harboring the variant as the sole Hsp90 source were further analyzed regarding temperature sensitivity. All yeast cells expressing the Hsp90 variant, except 383C, displayed no significant difference in growth compared to wt yeast cells under tested stress conditions (*Figure 33C*).

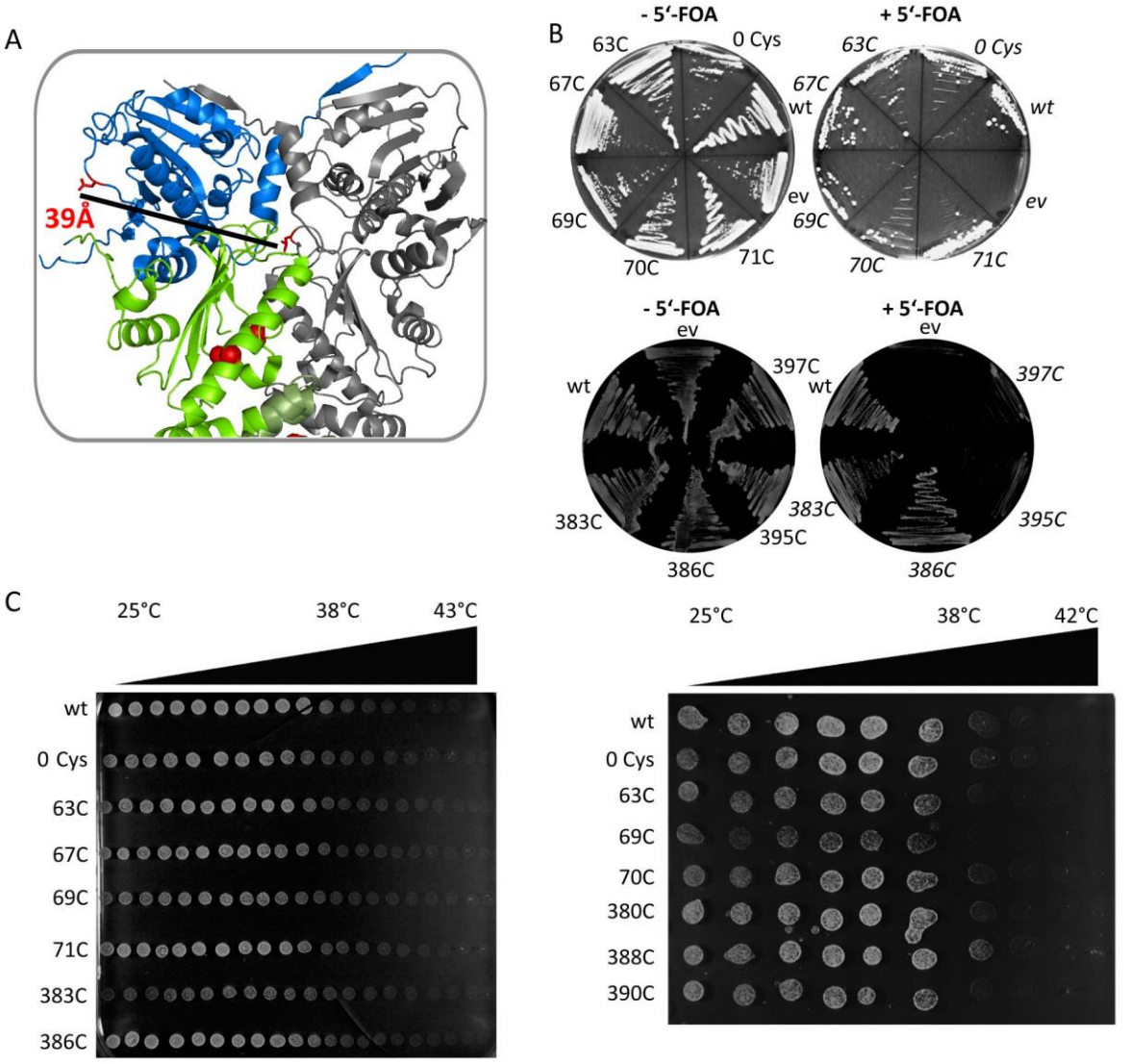

Figure 33: ***In vivo* analysis of generated Hsp90β cysteine variants. A**) Schematic representation of two cysteines of Hsp90β illustrated as red sticks within the closed yeast Hsp90 structure (PDB ID: 2CG9 (Ali et al., 2006). **B**) Hsp90β wt and cysteine variants were expressed in PCLDα yeast cells. Viability of the Hsp90 variants was tested by a 5'-FOA plasmid shuffling approach. As negative control yeast cells expressing empty vector GPD423 (e.v.) was used. **C**) Impacts of generated cysteine variants on temperature sensitivity. Yeast cells expressing an Hsp90 cysteine variant as the sole source of Hsp90 were grown, diluted to an OD_{600} = 0.5 and spotted on selective media and placed on a temperature gradient. Cell growth was monitored after 48 h.

4.2.3 *In vitro* Characterization of Generated Hsp90β Cys-Variants

To analyze the engineered Hsp90 cys-variants regarding structural stability and ATPase activity *in vitro*, the constructs (63C, 67C, 69C, 71C, 386C) were cloned into a pET28 vector, expressed and purified to homogeneity. The ATPase activity is altered in almost every case (*Figure 34A*). It seems

that human Hsp90 is more sensitive against the introduction of cysteines as yeast Hsp90. To point out, due to its low intrinsic ATP turnover rate the used ATPase activity assay faces several difficulties, for example higher error bars. In a thermal shift assay, the stability was determined for wt Hsp90β with a melting temperature of 47.1 ± 0.1 °C (*Figure 34B*). For most variants, the stability is not affected except for 71C with a melting temperature of 39.3 ± 0.6 (*Figure 34B*). This indicates that for most variants human Hsp90β is stable at higher temperatures up to 47 °C.

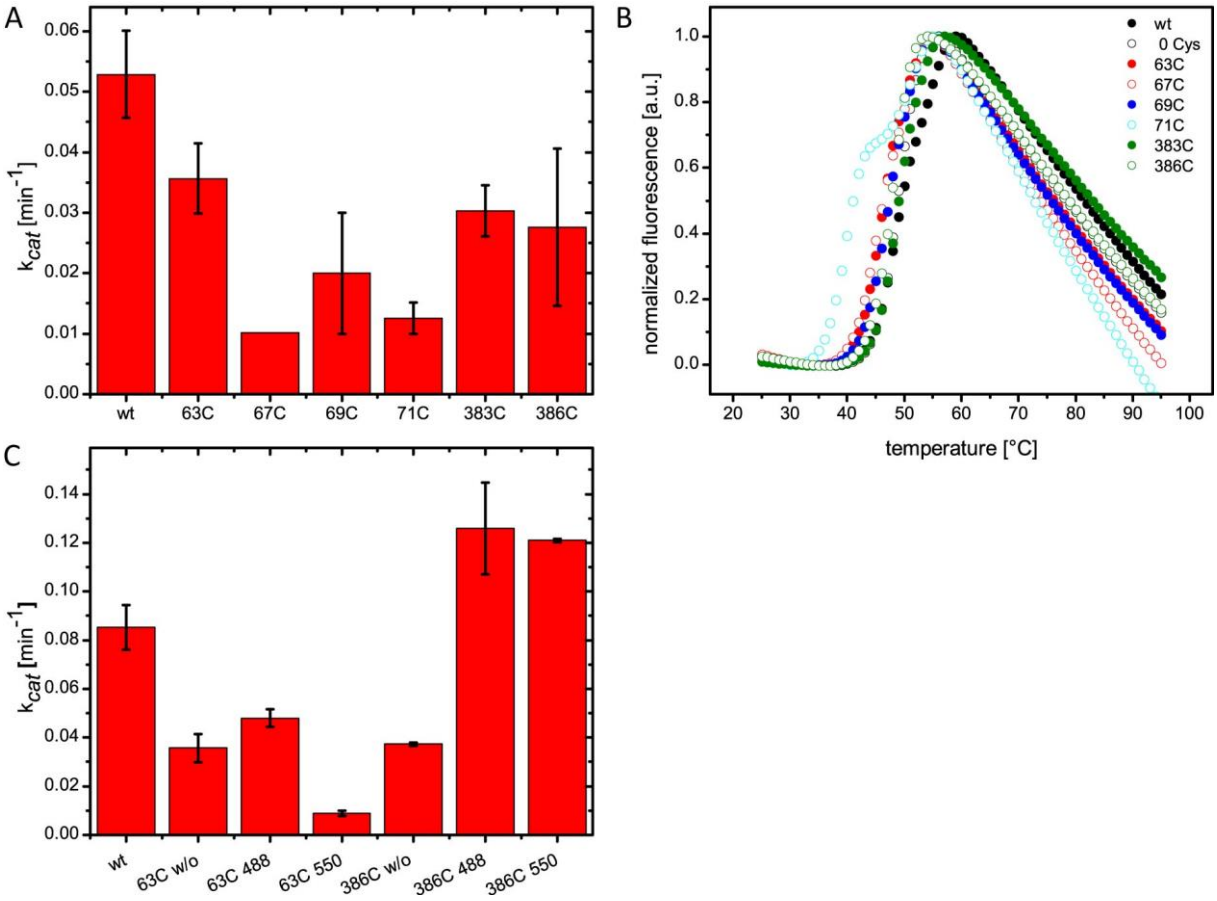

Figure 34: **Basic *in vitro* characterization of generated cysteine Hsp90β variants. A**) Comparison of ATPase activity of Hsp90β wt and the Hsp90β cysteine variants. ATP hydrolysis was measured using an ATP regenerative system. ATPase assays were performed in a buffer containing 40 mM HEPES, pH 7.5, 150 mM KCl, 5 mM $MgCl_2$, 2 mM ATP and a final concentration of 10 µM Hsp90 at 37 °C. All values were corrected for background activity using 100 µM radicicol. **B**) Thermal stability was deduced by applying a thermal shift assay. Sypro Orange fluorescence signal was monitored while temperature was increased 1 °C per minute starting from 25 °C until 95 °C. The assays were performed in a buffer containing 40 mM HEPES, pH 7.5, 150 mM KCl, 5 mM $MgCl_2$, 2 mM ATP and a final concentration of 0.25 mg/µl. **C**) Comparison of ATPase activity of Hsp90β wt and Hsp90β cysteine variants after site-specific labeling with a fluorescent dye (ATTO-488 or ATTO-550). ATP hydrolysis was measured as described in **A**). Means and standard deviations (s.d.) were calculated from at least three technical replicates.

Next, labeling of Hsp90 cysteine variant with fluorescent dyes carrying a reactive maleimide group was performed. The degree of labeling (73-90 %) was in an acceptable range. ATPase assays of the labeled cysteine variants showed that the label also affect the Hsp90 ATPase activity (*Figure 34C*). This was also shown for some cases with yeast Hsp90 (*Figure 19*). One explanation for this observation can be the hydrophobicity of a label that influences protein activity.

4.2.4 Formation of a Hsp90 FRET Hetero-Complex

To monitor a FRET signal, several different combinations of a donor- and an acceptor- labeled Hsp90 variants were tested (*Figure 35A*). Mixing of purified donor-and acceptor-labelled Hsp90 leads to the formation of a hetero-complex due to fast subunit exchange. To determine subunit exchange rates, the decrease of the donor fluorescence signal and the increase in acceptor fluorescence signal were monitored. Furthermore, fluorescence spectra were recorded. The experiments showed that the subunit exchange of the human Hsp90 variants allows producing a FRET complex with rate constants of 0.03-0.04 sec^{-1} were similar to the yeast Hsp90 FRET system (*Figure 35B*) (Hessling et al., 2009). However, the obtained FRET efficiency was very low (*Figure 35B*). To confirm this result, a titration curve was performed. To this end, acceptor-labeled Hsp90 was titrated to a constant amount of donor-labeled Hsp90 in a constant volume and fluorescence spectra were recorded. Indeed, with increasing acceptor concentration, the signal in donor fluorescence constantly decreased and the acceptor fluorescence signal increased (*Figure 35C*). This was further confirmed by a FRET chase experiment. To this end the addition of an excess of non labeled Hsp90 resulting in the disruption of the pre-formed FRET-hetero complex (*Figure 35D)* indeed suggesting formation of a FRET complex.

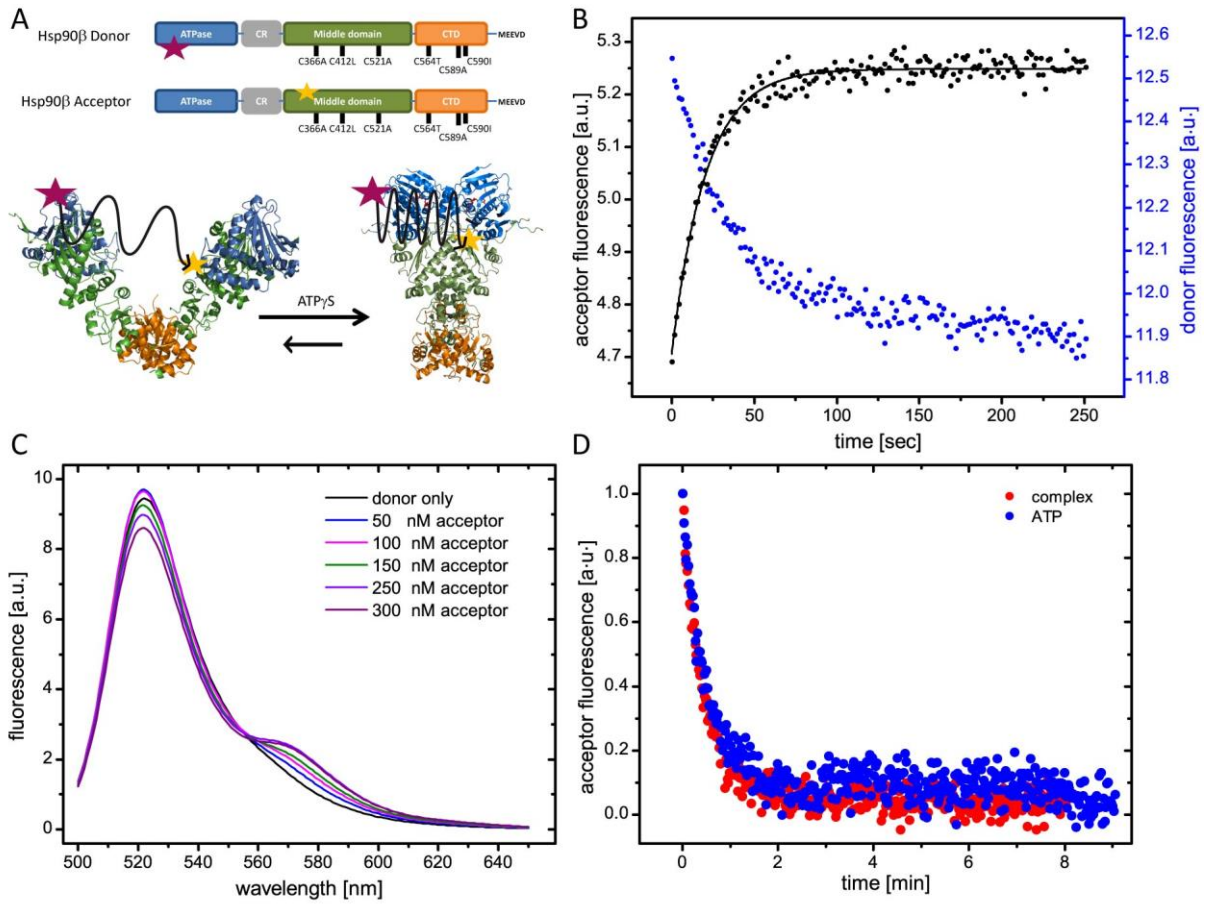

Figure 35: **Hsp90β forms a FRET-competent hetero-complex. A)** The basic principle of the Hsp90 FRET setup. Upon mixing of donor- and acceptor labeled Hsp90 a FRET-competent hetercomplex is formed. The addition of nucleotide induces conformational changes that results in signal changes of the donor and acceptor fluorescences channel. **B**) Dimer-formation of 250 nM donor- and 250 nM acceptor-labeled Hsp90β was followed by FRET subunit-exchange experiments. Subunit exchange rates were monitored by increase in acceptor fluorescence (black) and decrease in donor fluorescence (blue) upon mixing. The increase in signal was fitted to a mono-exponential function to obtain the apparent rate constants k_{app} (sec^{-1}). **C**) Fluorescence emission spectra of Hsp90β with a concentration of 300 nM donor- labeled Hsp90β was constant wherease the concentration of acceptor- labeled Hsp90β varied. **D**) C-terminal dimerization stability was deduced by FRET chase experiments. The chase was induced by adding a 20 x fold excess of unlabeled Hsp90β variant to a 400 nM preformed Hsp90 FRET-complex in the absence of nucleotide (red) and in the presence of ATP (blue).

4.2.5 The Hsp90β Cysteine Variant does not Form a Closed State

ADP or ATP did not induce changes in FRET (*Figure 36A*). This was expected since it is known that in the presence of ATP/ADP, Hsp90 is mostly populated in the open conformation (Hessling et al., 2009; Southworth and Agard, 2008). As nucleotide binding induces conformational rearrangements that result in N-terminal dimerization, a change in FRET efficiency can be monitored in the presence of nucleotide analogues for yeast Hsp90 (Hessling et al., 2009). However, in this setup neither ATPγS, AMP-PNP nor AMP-PNP/p23 shifted the equilibrium to a closed compact state (*Figure 36A-B*).

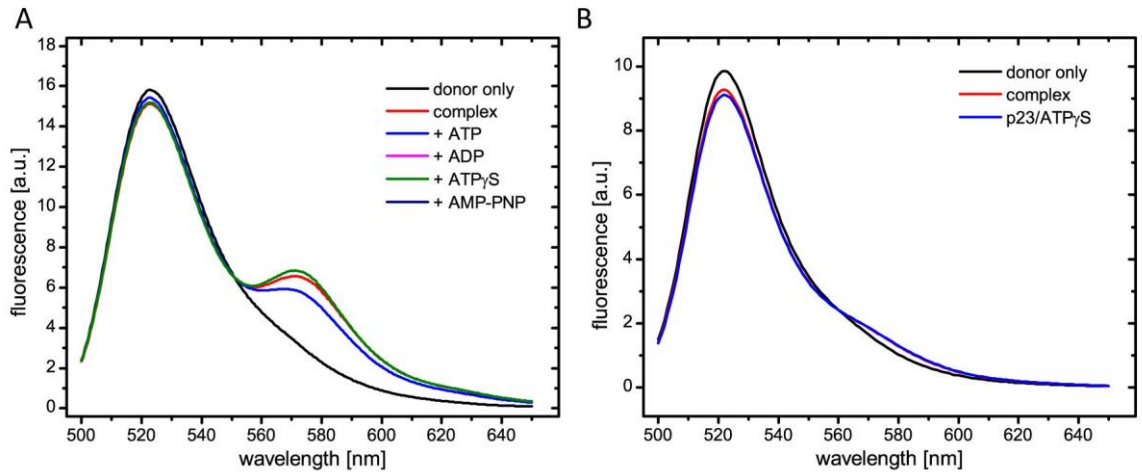

Figure 36: **Hsp90β is not able to form a closed complex.** Prior measurements dimer-formation of 250 nM donor- and 250 nM acceptor-labeled Hsp90β was allowed. **A**) Fluorescence emission spectra of the Hsp90β FRET hetero-complex were recorded in the absence and presence of different nucleotides. **B**) Fluorescence emission spectra of the Hsp90β FRET hetero-complex were recorded in absence and prescence of ATPγS and the co-chaperone p23. All FRET experiments were performed in a buffer containing 40 mM HEPES, pH 7.5, 150 mM KCl and 5 mM $MgCl_2$ at 30 °C.

To confirm this observation, analytical ultracentrifugation with interference optic was performed as recently shown with yeast Hsp90 (Li et al., 2011b; Li et al., 2012). For yeast Hsp90 a shift in the sedimentation coefficient of about 1S can be observed (Li et al., 2012). In contrast, no shift in the sedimentation coefficient was detected in presence of ATPγS (*Figure 37A*). However, binding to p23 was monitored with human Hsp90 wt in complex with ATPγS in analytical ultracentrifugation experiments (*Figure 37B*). In contrast the binding of p23 to the human Hsp90 cysteine-free variant was disturbed (*Figure 37B*). The altered binding of p23 to the Hsp90β cysteine-free variant is one explaination why no conformational changes can be monitored in the FRET setup.

However, the results obtained by limited proteolysis (*Figure 30*) and auc (*Figure 37A*) also indicate that human Hsp90 does not undergo large conformational changes compared to yeast Hsp90.

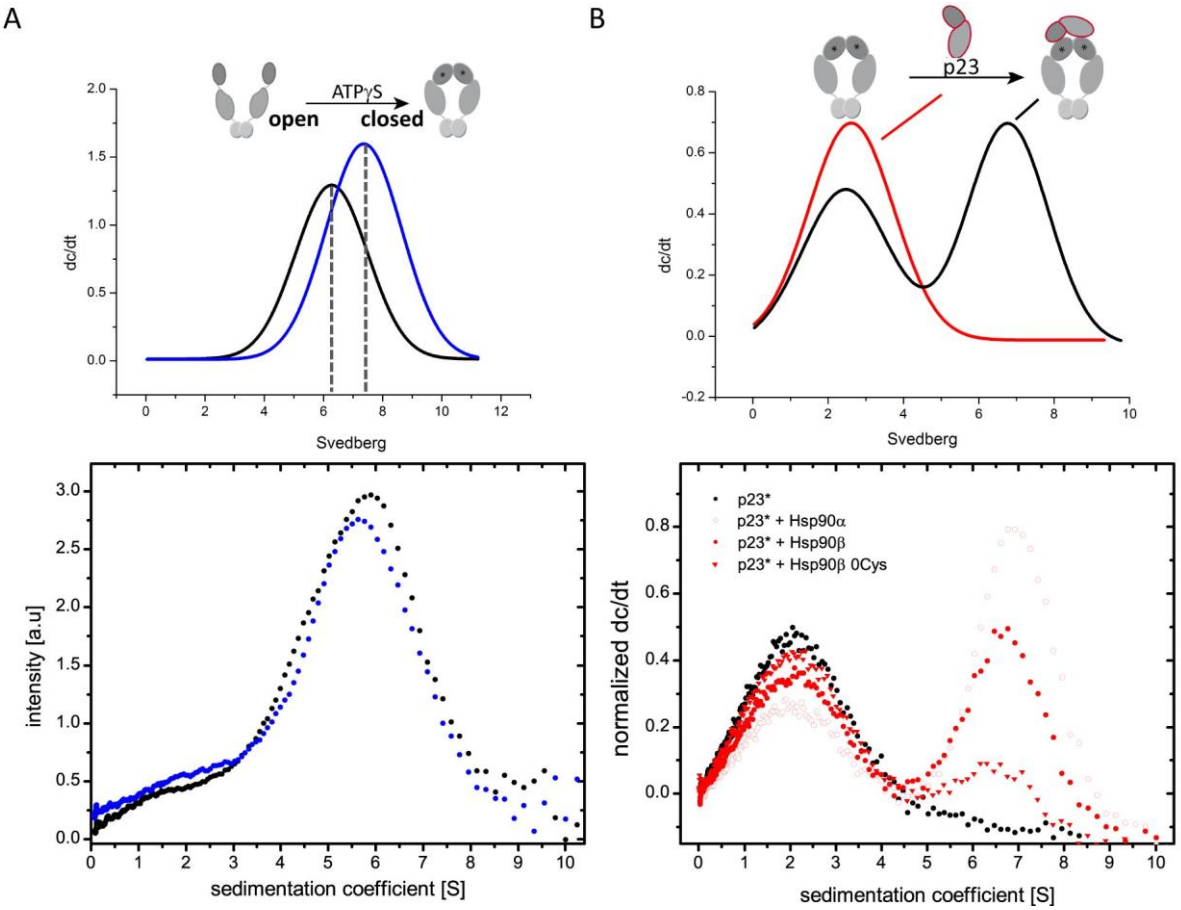

Figure 37: **Analysis of the closed conformation of human Hsp90. A**) Schematic representation of conformational changes of Hsp90 monitored by analytical ultracentrifugation with interference optic (upper panel). Shown are the normalized sedimentation profiles (dc/dt) of wt Hsp90β in the absence and presence of ATPγS. **B**) Schematic representation of complex formation between Hsp90 and labeled co-chaperone p23* determined by analytical ultracentrifugation using a fluorescence detection unit (upper panel). Shown are the normalized sedimentation profiles (dc/dt) of 3 µM Hsp90 isofoms in the presence of 300 nM p23* and 2 mM ATPγS (lower panel).

4.2.6 Segmental Labeling and Domain Ligation of Human Hsp90 Using Sortase A

Recently, the transpepdidase Sortase A was successfully used for segmental labeling and ligation of yeast Hsp90 domains in the context of structural NMR experiments (Freiburger et al., 2015; Lorenz et al., 2014). Sortase A is an enzyme from *Staphylococcus aureus* which usually modifies surface proteins by recognizing and cleaving a carboxyl-terminal sorting signal. For Sortase A, this recognition signal consists of the motif LPXTG (Leu-Pro-any-Thr-Gly). The enzyme allows site-specific ligation of two protein domains. As the natural cysteines are located exclusively in the M- and C-terminal domain of Hsp90α and Hsp90β, we utilized segmental labeling and ligation with Sortase A (*Figure 38A*). To this end the ND with an engineered cysteine was designed, expressed, purified separately and labeled with a fluorescent dye. Afterwards the labeled ND can be ligated, mediated by Sortase A, to the MC-domain of Hsp90 (*Figure 38B*). This allows leaving the natural cysteines intact. Before setting up this method, the constructs were first characterized *in vivo* and *in vitro* regarding functionality. To obtain site-specific labeling in the middle domain, NM-domain can be ligated with the CD, resulting in a full-length construct without affecting the natural cysteines in the CTD (*Figure 38C*).

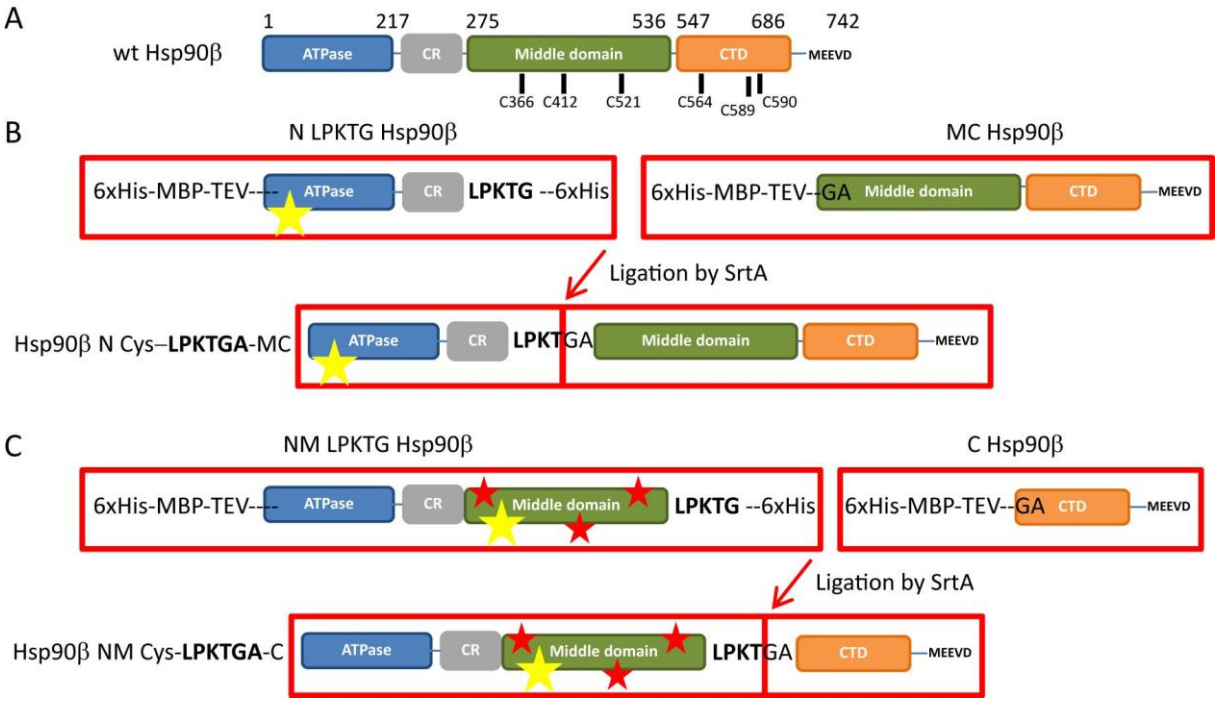

Figure 38: **Overview of the designed Hsp90β constructs for SortaseA (SrtA) mediated domain ligation. A**) Shown is the schematic domain architechture of human Hsp90β with the NTD in blue, followed by a charged linker region (CR) in grey, the middle domain (MD) in green and the C-terminal domain (CTD) depicted in orange. Hsp90β exhibits six natural cysteines located in the MD and CTD. **B**) The N- and MC-domain of Hsp90β are separately expressed and both contain an N-terminal histidine-tag fused to a maltose binding protein (MBP) followed by a TEV protease cleavage site. After cleavage with TEV protease the MC Hsp90β provides an N-terminal glycine required for SrtA ligation. The ND is site-specific labeled with a fluorescence dye (yellow star) and contains the LPKTG motif that is recognized by SrtA at the C-terminal end. The N- and MC-terminal domains are incubated in the presence of SrtA resulting in a ND labeled full-length Hsp90β construct. **C**) The basic principle of SrtA mediated ligation is as in **B**) for NM- and C-domain ligation. Red stars indicate substitution for a natural cysteine. The NM- and C-terminal domains are incubated in the presence of SrtA resulting in a MD-labeled full-length Hsp90β construct.

4.2.7 Comprehensive *in vivo* and *in vitro* Characterization of Hsp90α/β LPKTGA Variants

As the Sortase A requires a recognition motif, the resulting full-length human Hsp90 contains a LPKTGA motif between the domains after ligation (*Figure 38B-C*). First of all, the functionality of the engineered constructs was tested *in vivo*. The 5'-FOA shuffling approach revealed that the incorporation of the motif between the N and M domains did not alter functionality whereas when located between the M and C domains, it caused lethality in yeast cells (*Figure 39A*). Moreover, the N-LPKTGA-MC construct of human Hsp90α/β did not display any difference in temperature sensitivity (*Figure 39B*), UV response repair mechanism (*Figure 39C*) and inhibitor sensitivity (*Figure*

39*D*) compared to the respective wt Hsp90 isoform. Hsp90α shows decreased sensitivity towards the inhibitor radicicol. This is in agreement with a recent publication (Millson et al., 2007).

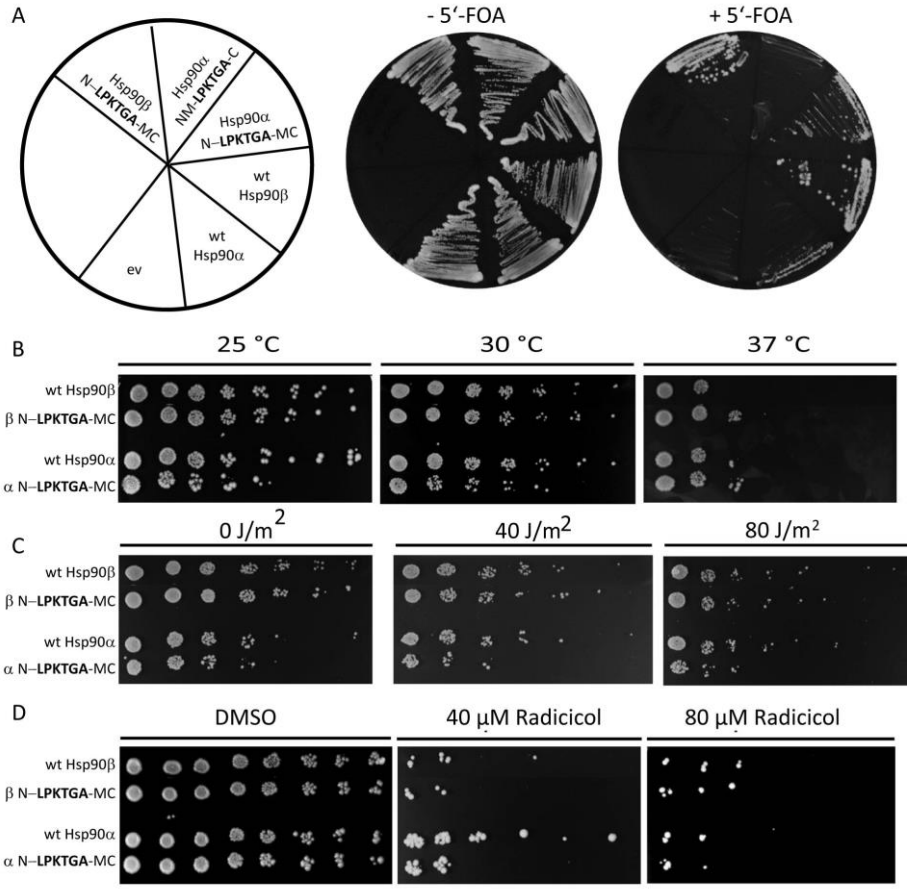

Figure 39: **Summary of *in vivo* analysis of Hsp90 LPKTGA variants.** Hsp90 wt isoforms and LPKTGA variants were expressed in PCLDα yeast cells. The cell growth was monitored after 48 h. **A**) Viability of the Hsp90 variants was tested by a 5'-FOA plasmid shuffling approach. As negative control yeast cells expressing empty vector GPD423 (e.v.) was used. **B**) Impacts of generated Hsp90 variants on temperature sensitivity. A dilution series starting from OD_{600} = 0.5 was prepared and spotted on selective media, placed at 25 °C, 30 °C and 37 °C. **C**) Analysis of generated Hsp90 variants on UV response DNA repair mechanism. A dilution series starting from OD_{600} = 0.5 was prepared and spotted on selective media, exposed to different intensity of UV radiation for a few seconds and incubated at 30 °C. **D**) Analysis of Hsp90 LPKTGA variants regarding inhibitor sensitivity. Yeast cells expressing an Hsp90 variant as the sole source of Hsp90 were grown to stationary phase and diluted to OD_{600} = 0.1 in media containing different concentration of radicicol or DMSO as control. After 24 h a dilution series was prepared and spotted on selective media and incubated at 30 °C.

Next, the Hsp90α/β wt and the respective Hsp90 LPKTGA variants were cloned into a pET-SUMO vector, expressed in *E. coli* and purified. Afterwards, Hsp90 LPKTGA variants were characterized regarding stability and ATPase activity. Far-UV CD spectra displayed that the secondary structure of the human Hsp90 isoforms is not significantly altered by the introduction of the LPKTGA-motif in the

linker region (*Figure 40A*). Furthermore, the ATPase turnover rate of the LPKTGA variants was shown to be comparable to the wt activity (*Figure 40B*).

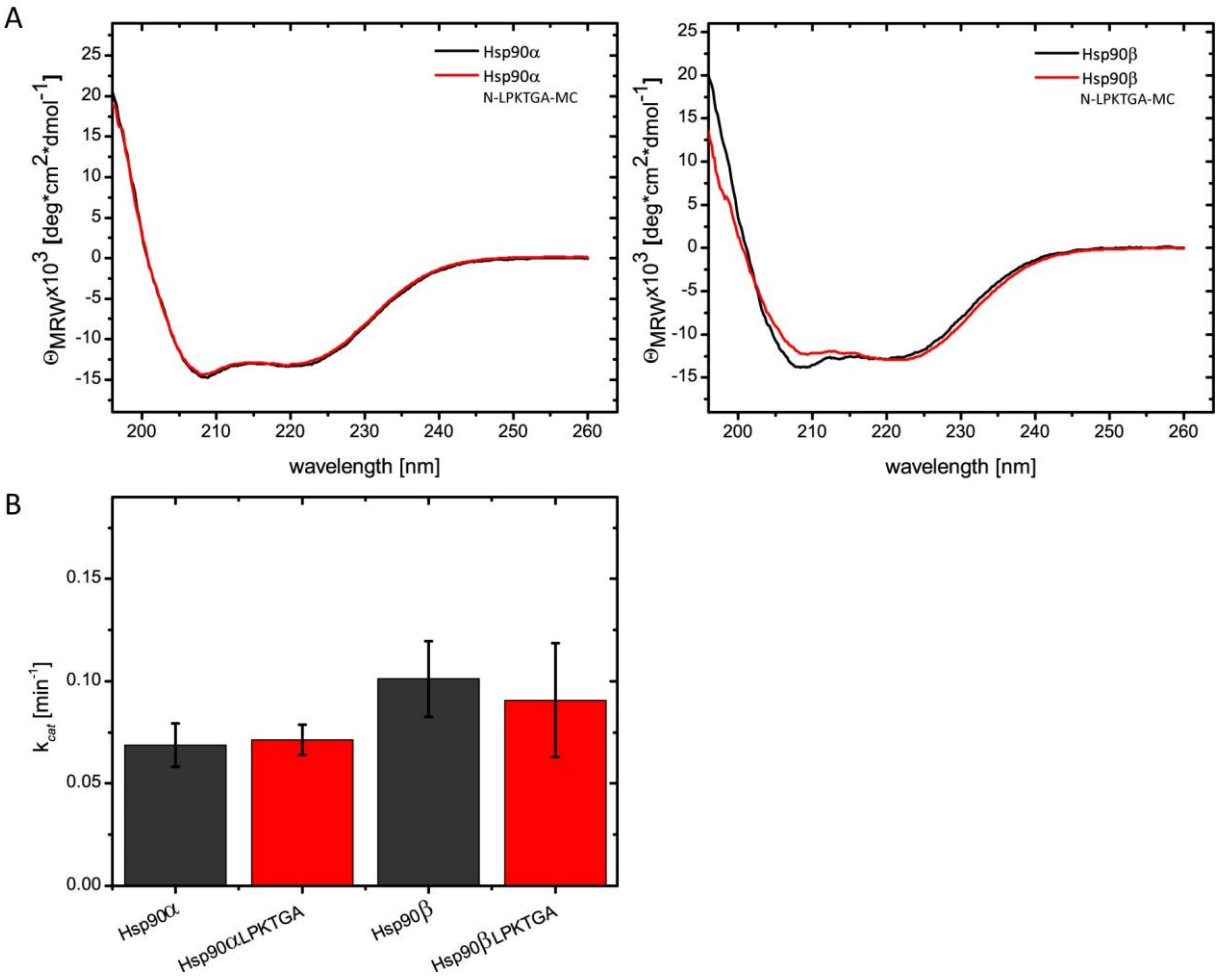

Figure 40: **Hsp90 LPKTGA variants do not differ in stability and ATPase activity**. **A**) Structural elements of Hsp90 isoform wt and variants were obtained using CD spectroscopy. To analyze the secondary structure far-UV CD spectra were recorded of 0.2 mg/ml Hsp90 variant in 50 mM phosphate buffer, pH 7.5 at 20 °C. **B**) Comparison of ATPase activity of Hsp90 wt isoforms with the LPKTG variants. ATP hydrolysis was measured using an ATP regenerative system. ATPase assays were performed in a buffer containing 40 mM HEPES, pH 7.5, 150 mM KCl, 5 mM $MgCl_2$, 2 mM ATP and a final concentration of 10 µM Hsp90 at 37 °C. All values were corrected for background activity using 100 µM radicicol.

To analyze co-chaperone binding to the human Hsp90-LPKTGA variants, analytical ultracentrifugation was applied. The measurements with labeled Aha1 revealed similar binding affinity to the variants (*Figure 41A*) suggesting that the constructs undergo similar conformational changes. In contrast, binding of the conformational sensitive co-chaperone p23 to the LPKTGA variants was impaired (*Figure 41B*). Interestingly, this experiment showed that the binding of p23 to human Hsp90 is affected by the N-terminal histidine-tag (*Figure 41B*). Both tag-less Hsp90 wt

isoforms tested displayed less p23 binding compared to the tagged Hsp90 versions. The p23 binding to the LPKTGA variants was even weaker than to the untagged wt. This is true for both isoforms suggesting that the introduction of a LPKTGA motif in the linker region seems to interfere with the binding of p23 to the Hsp90 dimer. However, the p23 binding was not completely abolished like in the cysteine-free variant of Hsp90 (*Figure 37B*).

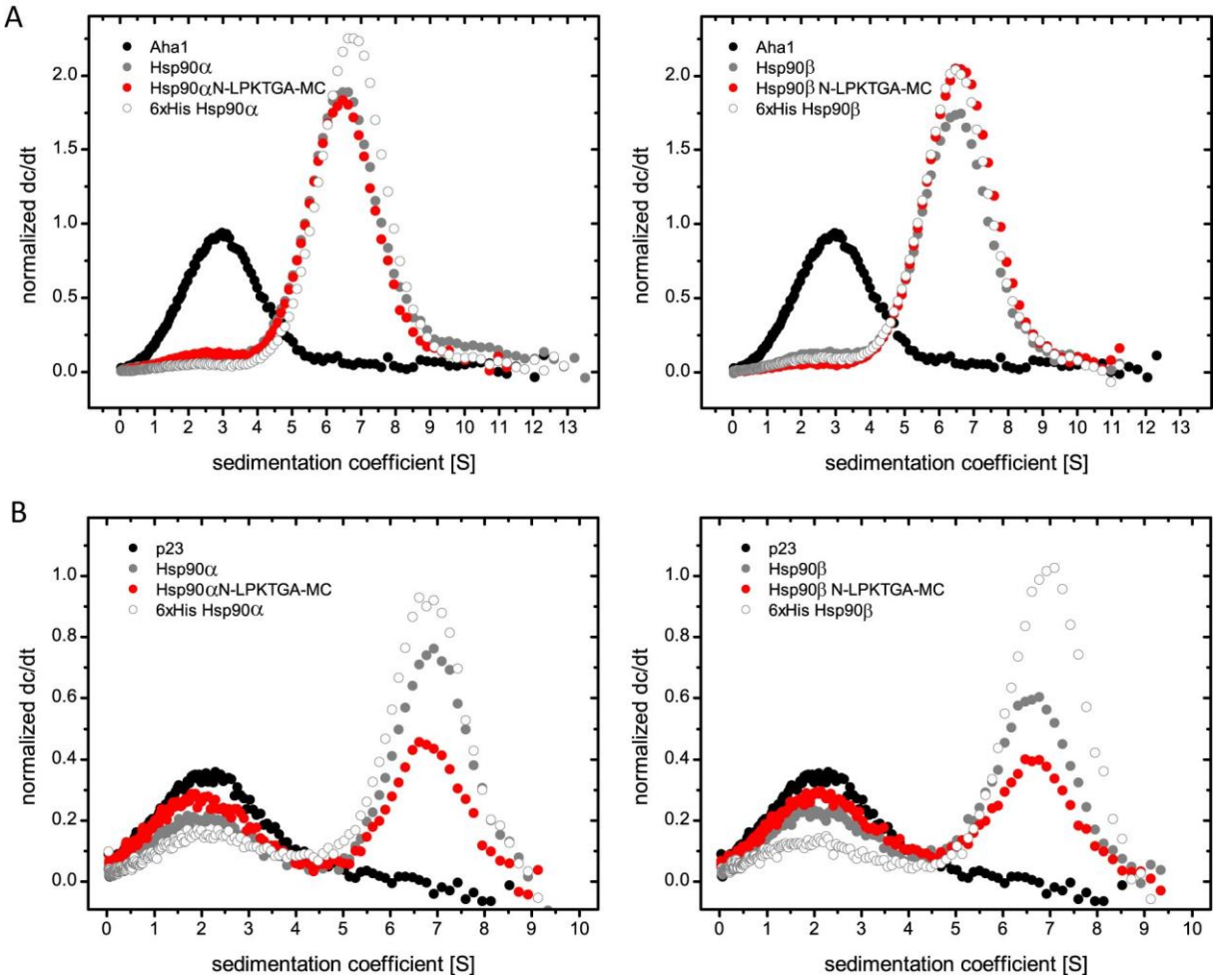

Figure 41: **Analysis of co-chaperone binding to Hsp90 LPKTGA varinats by analytical ultracentrifugation.** Measurments were performed in a buffer containing 40 mM HEPES, pH 7.5, 20 mM KCl, 5 mM $MgCl_2$ in the presence of 2 mM nucleotide at 25 °C. **A**) Formation of complex between 4 µM Hsp90 and 400 nM labeled co-chaperone Aha1* determined by analytical ultracentrifugation with a fluorescence detection unit. Shown are the normalized sedimentation profiles (dc/dt) of Hsp90 isofoms, Hsp90α (left panel) and Hsp90β (right panel) in the presence of Aha1*/ATP. Prior measurments samples were incubated on ice. **B**) Formation of complex between 3 µM Hsp90 and 300 nM labeled co-chaperone p23* determined by analytical ultracentrifugation with a fluorescence detection unit. Shown are the normalized sedimentation profiles (dc/dt) of Hsp90 isofoms, Hsp90α (left panel) and Hsp90β (right panel) in the presence of p23*/ATPγS. Prior measurments samples were incubated for 1 h at 37 °C.

4.2.8 Design and Engineering of Hsp90 Constructs for Sortase A Mediated Ligation

Based on the preliminary work, Sortase A mediated ligation was performed with Hsp90β. The constructs were designed that the recognition motif for SrtA was introduced within the linker region after the NTD. To obtain a human Hsp90 cysteine variant for site-specific labeling, the N-domain and MC-domain were separately expressed, the N-domain site-specifically labeled with a fluorescent dye and ligated together using Sortase A (*Figure 38A*). Several aspects were considered before: For the *S. aureus* Sortase, it has been reported in literature that the X amino acid can be either of D, E, A, N, Q, or K (Mao et al., 2004). To ensure that there is adequate space for recognition of the motif and enzyme binding to the domain, the sequence motif was placed into the linker region of Hsp90. This further allowed expressing and purifying both fragments separately without interfering stability as it was known that individual Hsp90 domains are stable. The sequence of the engineered N-terminal domain of Hsp90 after TEV protease cleavage with the sequence of the ligation motif is underlined and the fusion product of the protein (which is cleaved after ligation) is shown here:

6xHis-MBP-TEV-Hsp90ND-LPKTG

GSSHHHHHHSSGLVPRGSHMKIEEGKLVIWINGDKGYNGLAEVGKKFEKDTGIKVTVEHPDKLEEKFPQVAATGD
GPDIIFWAHDRFGGYAQSGLLAEITPDKAFQDKLYPFTWDAVRYNGKLIAYPIAVEALSLIYNKDLLPNPPKTWEEIP
ALDKELKAKGKSALMFNLQEPYFTWPLIAADGGYAFKYENGKYDIKDVGVDNAGAKAGLTFLVDLIKNKHMNADT
DYSIAEAAFNKGETAMTINGPWAWSNIDTSKVNYGVTVLPTFKGQPSKPFVGVLSAGINAASPNKELAKEFLENYL
LTDEGLEAVNKDKPLGAVALKSYEEELAKDPRIAATMENAQKGEIMPNIPQMSAFWYAVRTAVINAASGRQTVDE
ALKDAQTNSGSGSGSENLYFQGAMPEEVHHGEEEVETFAFQAEIAQLMSLIINTFYSNKEIFLRELISNASDALDKIR
YESLTDPSKLDSGKELKIDIIPNPQERTLTLVDTGIGMTKADLINNLGTIAKSGTKAFMEALQAGADISMIGQFGVGF
YSAYLVAEKVVVITKHNDDEQYAWESSAGGSFTVRADHGEPIGRGTKVILHLKEDQTEYLEERRVKEVVKKHSQFIG
YPITLYLEKEREKEISDDEAEEEKGEKEEEDKDDEEKPKIEDVGSDEEDDSGKDKLPKTG

The C-terminal fragment must contain the N-terminal glycine to be recognized by SrtA for the ligation reaction. As recently reported, multiple glycines increase the activity of SrtA (Mao et al., 2004). Here, only a single N-terminal glycine was introduced to minimize the number of mutations compared to the wt Hsp90. Furthermore, this strategy was shown to be successfully used for yeast Hsp90 in a recent study (Freiburger et al., 2015). A specific cleavage site (TEV) was used to introduce an N-terminal glycine preceded by a solubility tag (MBP) and an affinity tag (6xHis). The design of the CTD resulted in following sequence: 6xHis-MBP-TEV-Hsp90 MC-domain

GSSHHHHHHSSGLVPRGSHMKIEEGKLVIWINGDKGYNGLAEVGKKFEKDTGIKVTVEHPDKLEEKFPQVAATGD
GPDIIFWAHDRFGGYAQSGLLAEITPDKAFQDKLYPFTWDAVRYNGKLIAYPIAVEALSLIYNKDLLPNPPKTWEEIP
ALDKELKAKGKSALMFNLQEPYFTWPLIAADGGYAFKYENGKYDIKDVGVDNAGAKAGLTFLVDLIKNKHMNADT
DYSIAEAAFNKGETAMTINGPWAWSNIDTSKVNYGVTVLPTFKGQPSKPFVGVLSAGINAASPNKELAKEFLENYL
LTDEGLEAVNKDKPLGAVALKSYEEELAKDPRIAATMENAQKGEIMPNIPQMSAFWYAVRTAVINAASGRQTVDE
ALKDAQTNSGSGSGSENLYFQGAIKEKYIDQEELNKTKPIWTRNPDDITQEEYGEFYKSLTNDWEDHLAVKHFSVE
GQLEFRALLFIPRRAPFDLFENKKKKNNIKLYVRRVFIMDSCDELIPEYLNFIRGVVDSEDLPLNISREMLQQSKILKVIR
KNIVKKCLELFSELAEDKENYKKFYEAFSKNLKLGIHEDSTNRRRLSELLRYHTSQSGDEMTSLSEYVSRMKETQKSIYY
ITGESKEQVANSAFVERVRKRGFEVVYMTEPIDEYCVQQLKEFDGKSLVSVTKEGLELPEDEEEKKKMEESKAKFEN
LCKLMKEILDKKVEKVTISNRLVSSPCCIVTSTYGWTANMERIMKAQALRDNSTMGYMMAKKHLEINPDHPIVETL
RQKAEADKNDKAVKDLVVLLFETALLSSGFSLEDPQTHSNRIYRMIKLGLGIDEDEVAAEEPNAAVPDEIPPLEGDED
ASRMEEVD

First the DNA coding for the solubility tag maltose binding protein (MBP) followed by a TEV cleavage site as well as the DNA coding for the Hsp90 segment was amplified via PCR and introduced into a pET28 vector using a site- and ligation-independent cloning strategy. Next, the LPKTG motif was introduced into the DNA sequence coding for the charged linker region after the ND sequence via site-specific mutagenesis. Finally, cysteines were introduced into the N-terminal domain utilizing site-specific mutagenesis. All constructs were successfully obtained and verified by sequencing.

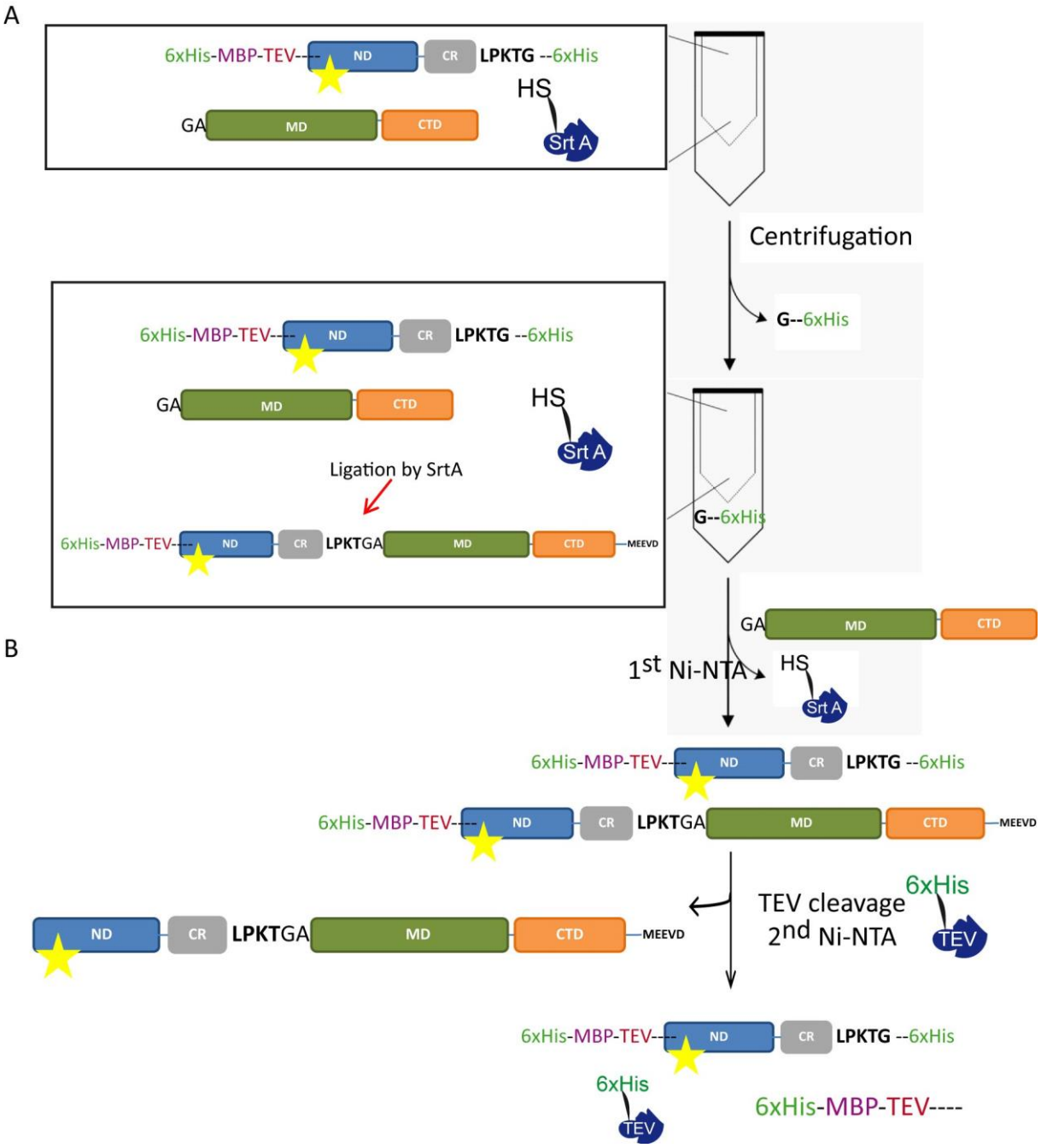

Figure 42: **Schematic representation of the SrtA ligation procedure. A**) The N- and MC-domains are incubated in the presence of SrtA in a centrifugal concentrator unit. The molecular weight cut-off of the centricion allows removing of the cleaved fragment (G-6x-His) during the reaction. The educts and the ligated product remain in the centrifugal concentrator unit. **B**) Purification of the ligated full-length Hsp90. The ligated product is isolated from the non-ligated MC-domain and the SrtA by Ni-NTA affinity chromatography. TEV protease cleavage and a subsequent Ni-NTA column separate the full-length Hsp90 from the unligated ND, the 6xHis-MBP-TEV-tag and the TEV protease. (adapted from (Freiburger et al., 2015))

4.2.9 SrtA Mediated Ligation of Human Hsp90 Fragments

The next step was to perform a test-ligation with the human Hsp90 constructs. An optimized protocol was used for the SrtA ligation reaction (Freiburger et al., 2015). In this improved ligation protocol, the ligation reaction is set up in an amicon ultrafiltration unit at 2000 g in a centrifuge (*Figure 42A*). The amicon filter unit has a molecular cut-off that allows the cleaved residues to be removed from the reaction leading to increased yields, because it prevents the reverse reaction. First, a test-ligation using 5 mg of each fragment and 5 mg of SrtA was performed. The ligation reaction took place in a centrifuge for 8 h at 2000 g at room temperature. The kinetic of the reaction was monitored by SDS-PAGE analysis. Ligated products were obtained after 3 - 4 hours and a decline in the bands for the ND- and MC-domain fragment was observed (*Figure 43*) indicating a successful ligation by SrtA. Besides educts and products, several bands above 80 kDa were visible suggesting that side products were formed (*Figure 43*).

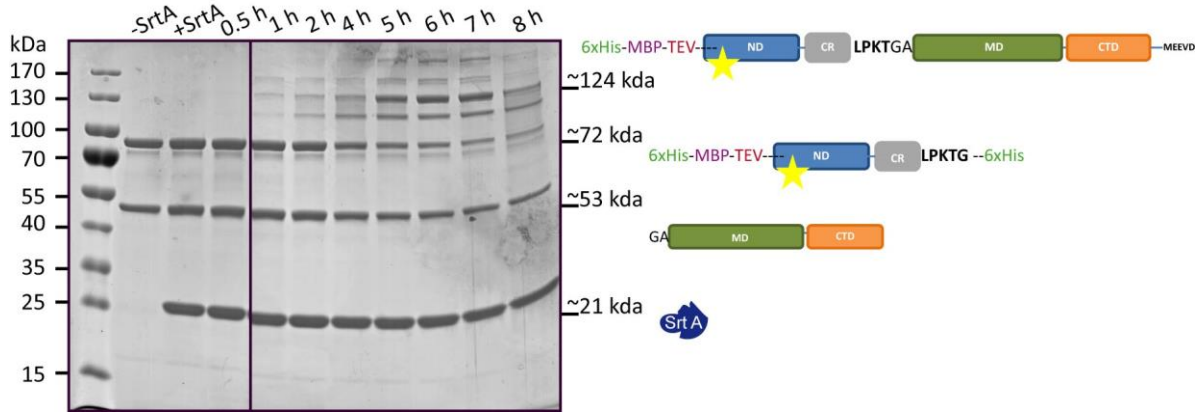

Figure 43: **Monitoring the SrtA mediated domain ligation reaction by SDS-PAGE analysis.** 5 mg of Hsp90β N-domain, 5 mg of Hsp90β MC-domain and 5 mg of SrtA were incubated together in a 15 ml centrifugal concentrator unit at 20 °C. The reaction took place in ligase buffer containing 50 mM Tris, pH 8.0, 150 mM NaCl, 20 mM $CaCl_2$ and 1 mM DTT. Samples were taken at several time points indicated for every lane on top of the SDS-PAGE gradient (4 - 12.5 %) gel. The first lane contains only the ND and MC-domain of Hsp90 without addition of SrtA. The molecular weight of educts and the ligated full-length product is indicated at the right site of the gel.

4.2.10 Purification and Characterization of SrtA Ligated Hsp90β

The ligated product was separated from the educts, the enzyme SrtA and side products using a strategy with cleavable and non-cleavable affinity-tags (*Figure 42B*). To this end, a combination of Ni-

NTA chromatography and TEV cleavage was carried out as shown in the scheme (*Figure 42B*). Analysis of all purification steps showed that the desired product was successfully purified. Besides the correctly ligated full-length Hsp90, the non-ligated MC-fragment was found to be in solution after the purification steps (*Figure 44*). Due to stable C-terminal dimerization between the full-length and the MC-fragment, the separation during Ni-NTA affinity chromatography was not possible. It is known that the affinity of the C-terminal dimerization, deduced by HPLC experiments, is about 50 nM (Richter et al., 2001). This result implies that the purification procedure needs to consider the C-terminal dimerization ability of full-length Hsp90. This was not the case for recent studies as they ligated only the N-domain with the M-domain of yeast Hsp90. Thus the yeast Hsp90 NM construct was not able to form dimers.

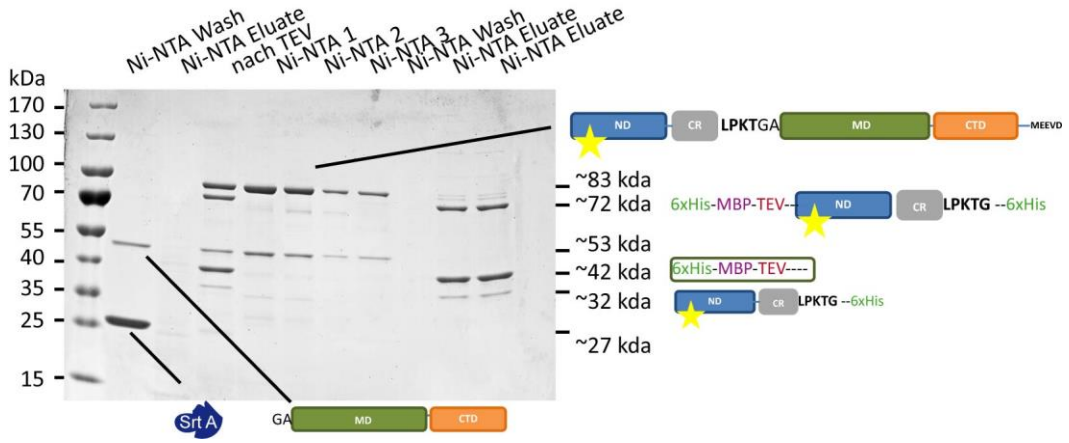

Figure 44: **Monitoring purification steps of ligated full-length Hsp90β.** Samples were taken in every purification step and analyzed by a SDS-PAGE gradient (4 - 12.5 %) gel. In a first step the ligated product was isolated from the non ligated MC-domain (~53 kDa) and the SrtA (~27 kDa) by Ni-NTA affinity chromatography. TEV protease cleavage and a subsequent Ni-NTA column separated the full-length Hsp90β (~83 kDa) from the unligated ND (~72 kDa), the 6xHis-MBP-TEV-tag (~42 kDa) and the TEV protease. The molecular weight of educts and the ligated full-length product is indicated at the right site of the gel.

To test the obtained ligated protein for its *in vitro* functionality several measurements were performed. Far-UV CD spectroscopy displayed no difference in stability and structure compared to wt human Hsp90β (*Figure 45A*). The ATP hydrolysis rate was significantly lower compared to wt protein (*Figure 45B*). Basically, this can be explained by the relatively high amount of non-ligated MC-domain in the protein solution. Heterodimer formation with full-length Hsp90 resulted in reduced ATPase activity. Furthermore, ATPase stimulation of ligated Hsp90 by Aha1 was detected

but significantly reduced (*Figure 45B*). This indicates residual ATPase activity although constrictions in conformational changes. Moreover, p23 binding to ligated Hsp90 was significantly altered (*Figure* 45*C*) suggesting less closed formation due to hetero-dimers of full-length and non-ligated educt.

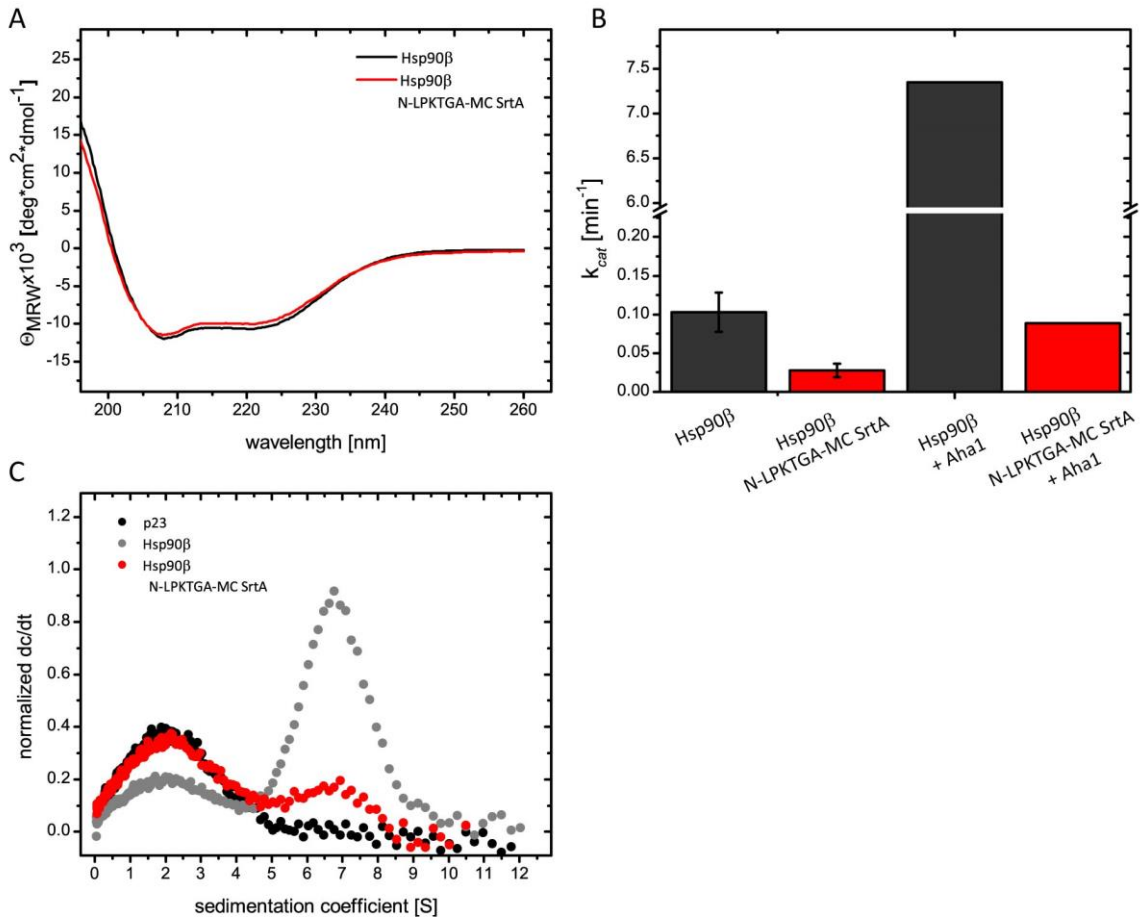

Figure 45: ***In vitro* characterization of the SrtA ligated full-length Hsp90β. A**) Structural elements of Hsp90β wt and ligated Hsp90β were obtained using CD spectroscopy. To analyze the secondary structure far-UV CD spectra were recorded of 0.2 mg/ml Hsp90 variant in 50 mM phosphate buffer, pH 7.5 at 20 °C. **B**) Comparison of ATPase activity of Hsp90β wt and the ligated Hsp90β variant. ATP hydrolysis was measured using an ATP regenerative system. ATPase assays were performed in a buffer containing 40 mM HEPES, pH 7.5, 150 mM KCl, 5 mM $MgCl_2$, 2 mM ATP and a final concentration of 10 µM Hsp90 at 37 °C. The stimulation of Hsp90 ATPase activity was measured in the presence of 30 µM Aha1 in a buffer containing 40 mM HEPES, pH 7.5, 20 mM KCl, 5 mM $MgCl_2$, 2 mM ATP and a final concentration of 1 µM Hsp90 at 37 °C. Means and standard deviations (s.d.) were calculated from at least three technical replicates. All values were corrected for background activity using 100 µM radicicol. **C**) Shown is the complex formation of Hsp90 and labeled co-chaperone p23* determined by analytical ultracentrifugation with a fluorescence detection unit. Shown are the normalized sedimentation profiles (dc/dt) of 3 µM Hsp90β variant in the presence of 300 nM labeled p23* and 2 mM ATPγS. Prior measurments samples were incubated for 1 h at 37 °C.

4.2.11 FRET Experiments with SrtA Ligated Hsp90β

Nevertheless, ND fragments were labeled with the fluorescent dyes and ligated again to the MC-fragment. Subsequent purification resulted in similar problems as described before even though this time stringent washing steps were applied. Several washing steps did not decrease hetero-dimerization. The obtained labeled full-length Hsp90 protein was used for N-N FRET experiments. However, no change in fluorescence signal could be monitored after addition of ATPγS/p23 (*Figure* 46). Taken together, this approach allows segmental and site-specific labeling. However, the recognition motif LPKTGA has to be carefully introduced to obtain a wt like human Hsp90 variant that is able to undergo conformational changes.

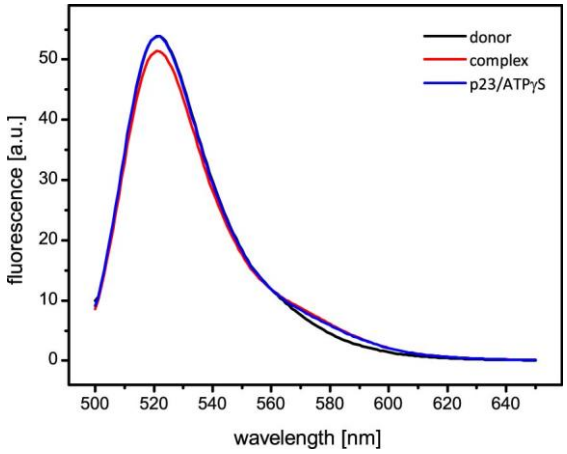

Figure 46: **Fluorescence emission spectra of ligated N-LPKTGA-MC Hsp90β. A**) Dimer-formation of 300 nM donor- and 300 nM acceptor-labeled Hsp90β was allowed by subunit-exchange upon mixing. Fluorescence emission spectra of Hsp90β were recorded and performed in a buffer containing 40 mM HEPES, pH 7.5, 20 mM KCl and 5 mM $MgCl_2$ at 30 °C. Fluorescence emission spectra of Hsp90β were recorded with donor only (black), a FRET hetero-complex (red) in the absence and presence of ATPγS and the co-chaperone p23.

4.2.12 Incorporation of an Unnatural Amino Acid into Human Hsp90

The most elegant way to add site-specifically a fluorescent label in human Hsp90 is the use of the amber suppression system for the incorporation of an unnatural amino acid. In this case only one position has to be modified and the number of cysteines does not play a role. To achieve the incorporation of an unnatural amino acid an orthologue pair of an unnatural amino acid and corresponding aminoacyl tRNA-synthetase is utilized (Liu and Schultz, 2010). Due to generally low yields in protein after expression (ca. 90 % lower) and expensive synthesis of the respective amino acid, the approach may be useful but faces also several difficulties. To encode biophysical probes into human Hsp90, a biorthogonal amino acid such as a strained alkene (CpK) can be incorporated into human Hsp90 site specifically using an orthologue pair of amino acid and corresponding aminoacyl tRNA-synthetase (Lang and Chin, 2014). Afterwards, the alkene can be chemically modified with a tetrazine via a Diels-Alder Cycloaddition. To label human Hsp90 with a fluorescent dye, commercially available dyes can be easily coupled to tetrazine and subsequent used for protein labeling.

To test the incorporations of an unnatural amino acid at a specific position, BocK and the corresponding D4 synthetase was used, as this pair is a well-established system. Furthermore, BocK is cheap and easy to synthesize. The constructs used for expression in BL21 *E. coli* cells were generated by cloning the DNA encoding for human Hsp90 with an N-terminal 6xHisSUMOtag into a pNHD vector. The amber codon TAG was introduced by mutagenesis at specific positions. The corresponding aminoacyl tRNA-synthetase for BocK is D4 wt and for CpK it is pKW synthetase wt. To test the incorporation of an unnatural amino acid into human Hsp90, expression tests were performed. Small cultures were cultivated in the presence of BocK or CpK and in the absence of the unnatural amino acid. The expressions were tested at 25 °C and at 37 °C and samples were taken before induction with IPTG as well as after 4 h and 16 h. As the Hsp90 contains an N-terminal His-tag samples were analyzed by Western Blot and probed with an anti-His antibody (*Figure 47*). The Western Blot analysis showed that the full-length Hsp90 (upper band) was expressed at both tested condition. It turned out that the expression at 25 °C for 16 h full-length Hsp90 is equally expressed compared to the truncated version witch correspond to the lower band in the western blot analysis (*Figure 47*). However, the tests revealed that already in the absence of the unnatural amino acid, the incorporation takes place, suggesting an unspecific incorporation (*Figure 47*). In order to improve the specific incorporation, several sites have to be tested.

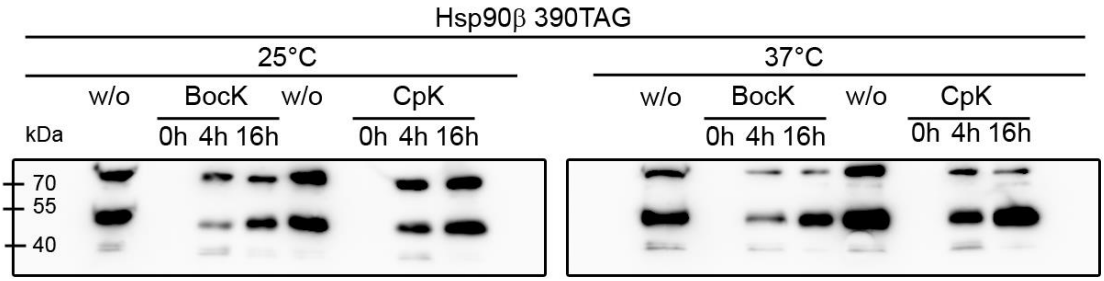

Figure 47: **Test expression and incorporation of an unnatural amino acid at amino acid position 390 of human Hsp90β.** After plasmid transformation *E. coli* cultures were grown to OD_{600} = 0.3 at 37 °C. Cultures were splitted in 5 ml and 1 mM BocK, 1 mM CpK as well as a 0.1 M NaOH (negative control) without amino acid was added and further incubated until OD_{600} = 0.7 was reached at 37 °C. Protein expression was induced by adding 1 mM IPTG to each culture and incubated at 25 °C and 37 °C. At time point 0 h, 4 h and 16 h samples were taken and analyzed by Western Blot and probed with a specific antibody against the 6xHis-tag.

5 Discussion

5.1 Functional Analysis of the Yeast Hsp90 Isoforms

In *Saccharomyces cerevisiae* two cytoplasmic isoforms exist, the constitutively expressed Hsc82 and the heat- and stress-inducible Hsp82. At the amino acid level, the isoforms share 97 % sequence identity. Hsc82 and Hsp82 have been extensively used to study various general and yeast-specific aspects of Hsp90 biology, but beyond their deviating expression pattern mechanistic and biological differences have remained largely enigmatic. Previous work has identified a few cases of isoform-specific differences concerening heat-stress responce, inhibitor sensitivity and regulation by co-chaperones (Millson et al., 2007; Silva et al., 2013; Sreedhar et al., 2004). To obtain a detailed picture about functional differences of Hsc82 and Hsp82, a comprehensive in *vitro* and *in vivo* analysis was systematically performed.

5.1.1 Isoforms Deviate in ATPase Activity

ATPase assays revealed a slightly higher ATPase rate for Hsc82 compared to Hsp82. Furthermore, this observation goes along with an accelerated dimer closure kinetic for Hsc82 compared to Hsp82 determined by FRET experiments. This is in line with the increased ATPase rate for Hsc82 as the conformational changes are the rate-limeting step of the Hsp90 cycle (Hessling et al., 2009). In general, structural stability and ATP binding affinity is not affected. Most prominent differences in the sequence alignment were found in the NTD and charged linker region. The mutations seem to be responsible for deviation in ATPase activity between the Hsp90 isoforms. Ser3Gly is located in the dimerization interface (swapped region) within the first eight amino acids of the unstructured N-terminal region, close to the first β-sheet (*Figure 48*). It was shown, that the deletion of the first eight amino acids results in an increased ATPase activity of Hsp82 implying that N-terminal residues are involved in the catalytic efficiency of Hsp90 (Richter et al., 2002). Furthermore, N-terminal tagging impacts the NTDs of both isoforms indicated by increased ATP turnover rate with Hsc82 being more strongly influenced. The residues Lys48Gln and Ser49Ala are located at the end of the second α-helix (*Figure 48*). Gln72Glu is located in the loop between the 6th and 7th beta stand of the eight-stranded β-sheet (*Figure 48*). Ser140Asn and Asp142Glu are located in the loop between the 3rd and 4th beta stand of the eight-stranded β-sheet (*Figure 48*). Ile 172Val is part of the 5th beta strand of the

eight-stranded β-sheet (*Figure 48*). Val208Leu belongs to the loop adjacenct to the charged linker region (*Figure 48*). None of the amino acids that are directly involved in ATP binding or hydrolysis are affected. However, two residues that form part of the binding pocket (Q48K, A49S) and one residue vary, Val172Ile, that is adjacent next to the water-binding Thr171 (*Figure 48*). Taken together, these observations indicate that slight deviations at the very N-terminal end and within the NTD influence the catalytic activity of the Hsp90 ATPase.

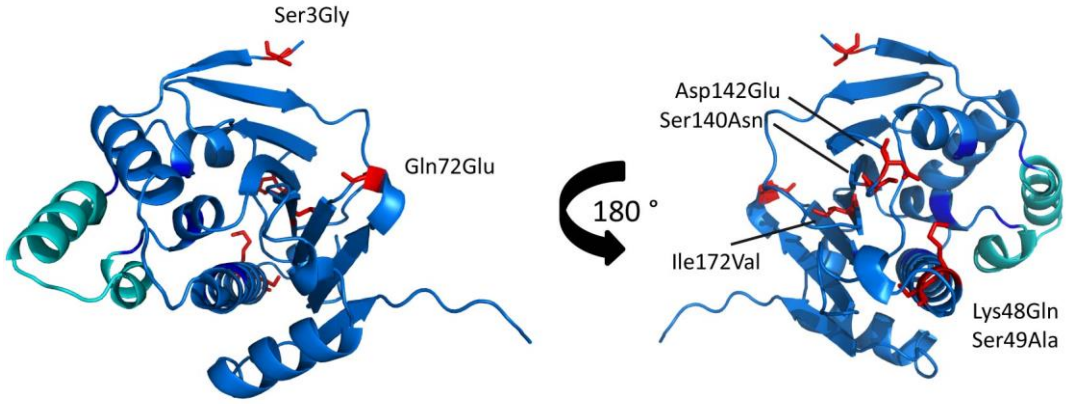

Figure 48: **Cartoon presentation of the NTD of yeast Hsp82**. Th NTD is depicted in blue, the lid region is highlighted in cyan and residues that differ in both isoforms are highlighted as sticks in red (PDB ID: 1AM1 (Prodromou et al., 1997)).

Within the highly charged linker region, a single amino acid substitution is found and the MD contains only two different residues. The residue Ser422Ala is located within the α-helical coil that connects the large α–β–α domain with the smaller α–β–α domain. Interestingly, this position was resently identified as a post-translational modification site and belongs to one of two sites that are shown to be O-glycosylated (O-GlcNAc) on murine Hsp90β (Overath et al., 2012). Post-translational modifications including phosphorylation, S-nitrosylation and glycosylation open up another way of regulating Hsp90 function even though they are far away from the N-terminal ATP binding pocket. For example it has been found that phosphorylation of Hsp90 results in decreased ATPase activity (Soroka and Buchner, 2012) and that S-nitrosylation stabilizes the apo conformation (Retzlaff et al., 2009). Furthermore, Ser422Ala is located next to residue Phe421. This position was identified as a 'hot spot' for allosteric regulation by a Molecular Dynamics computational approach and biochemical methods. This approach revealed that the substitution of Phe421 to alanine results in a slightly

higher ATPase rate and seems to influence the flexibility and dynamics of the entire Hsp90 dimer (Rehn et al., 2016). Biochemical and biophysical experiments revealed that the mutation induce a higher flexibility among the domains, leading to several structural rearrangements that drive the protein toward a different state stabilizing the closed-active conformation (Rehn et al., 2016). The data demonstrate that single residues distal from the ATP binding pocket induce conformational changes and thus modulate the Hsp90 ATPase cycle.

5.1.2 Hsp90 Isoforms Form Hetero-Dimers *in vitro* and *in vivo*

Expression analysis of Hsp90 isoforms had revealed a strong induction of Hsp82 and a moderate induction of Hsc82 under heat stress conditions (Borkovich et al., 1989). Further it was demonstrated that Hsc82 is the most abundant protein in the cell at physiological as well as non-physiolocical conditions. Interestingly, Hsp82 level increased to approximately the same level as Hsc82 under heat stress conditions (Borkovich et al., 1989). This implies that both isoforms could form hetero-dimers *in vivo*. The CTD, which is responsible for dimerization, comprises five residues which differ between the isoforms. Most amino acid substitutions in the CTD between the Hsp90 isoforms in yeast are conservative in terms of amino acid properties and do not influence dimerization or long range communication due to allosteric regulation. The presented FRET and immunoprecipitation experiments revealed for the first time that Hsp82 and Hsc82 are able to form hetero-dimers by subunit-exchange *in vitro* and *in vivo*. Furthermore, the subunit exchange rates are similar to the rate constants of homo-dimerization. Taken together, these data suggest that C-terminal dimerization is not influenced by the substitutions and Hsp82 and Hsc82 can form hetero-dimers *in vivo*.

5.1.3 Co-Chaperones Modulate Hsp90 Isoforms Differentially *in vitro*

In an *in vivo* study the human Hsp90 isoforms had been compared with respect to their interactions with co-chaperones and clients under physiological and stress conditions (Taherian et al., 2008). It was shown that Hsp90α and Hsp90β form similar chaperone complexes and do not differ in co-chaperone interaction with FKBP51, FKBP52 and Hop (Taherian et al., 2008). More recently, Aha1 was shown to bind preferentially to human Hsp90α and that difference in the middle domain are responsible for that (Synoradzki and Bieganowski, 2015). For yeast Hsp90 isoforms, co-chaperone interactions had not been analyzed in a comparative manner. The binding sites and the role of individual yeast co-chaperones within the Hsp90 cycle are studied quiet well. For example, it is

known that the co-chaperones Cpr6 or Sba1 interact in a nucleotide-dependent manner whereas Sti1 associates independent of nucleotide with Hsp90 (Johnson et al., 2007). Within this thesis, Hsp82 and Hsc82 were compared regarding co-chaperone interactions and their influence on the Hsp90 ATPase cycle. Specific co-chaperones displayed different affinities for the Hsp90 isoforms and differently impact the ATPase activity and the conformational changes during the ATPase cycle. Aha1 showed a slightly stronger stimulating effect on Hsc82, whereas Hsp82 was slightly more stimulated by Cpr6 than Hsc82. Regarding co-chaperones that inhibit the ATPase, Sba1 was approximately two-fold more efficient in inhibiting the ATPase of Hsp82 than of Hsc82, whereas no difference could be observed for Cdc37 and Sti1. This is line with the observed nucleotide-induced closing kinetics of Hsp90 in the prescence of the respective co-chaperone. Furthermore, binding was detected with analytical ultracentrifugation. Aha1 showed similar binding for Hsc82 and Hsp82. Conversely, Cpr6 displayed a slightly higher affinity for Hsp82 than Hsc82, indicating that this might be reason underlying the stronger stimulatory effect of Cpr6 on Hsp82. Sti1 and Cdc37 displayed equal binding for Hsc82 and Hsp82. Contrary to the stronger inhibitory effect of Sba1 on Hsp82 than on Hsc82, the binding of Sba1 was slightly stronger for Hsc82 than for Hsp82. The data demonstrate that selective co-chaperones differentially bind and have slightly different preference for Hsp90 isoforms in yeast. However, looking in more detail at the binding sites of the co-chaperones in Hsp90, we found that no substitution directly matches a binding site. Thus, we conclude that the difference in amino acid sequence induces slightly different Hsp90 conformation resulting in Hsp90 isoform-specific co-chaperone modulation. To confirm differences in N-terminal dimerization, FRET chase experiments were employed and we found that the stability of N-terminal assoziation is slightly enhanced for Hsc82. This observation indicates altered populations of the closed states of Hsc82 compared to Hsp82 and can be a possible explanation for the higher ATPase rate as well as increased Sba1 binding to Hsc82.

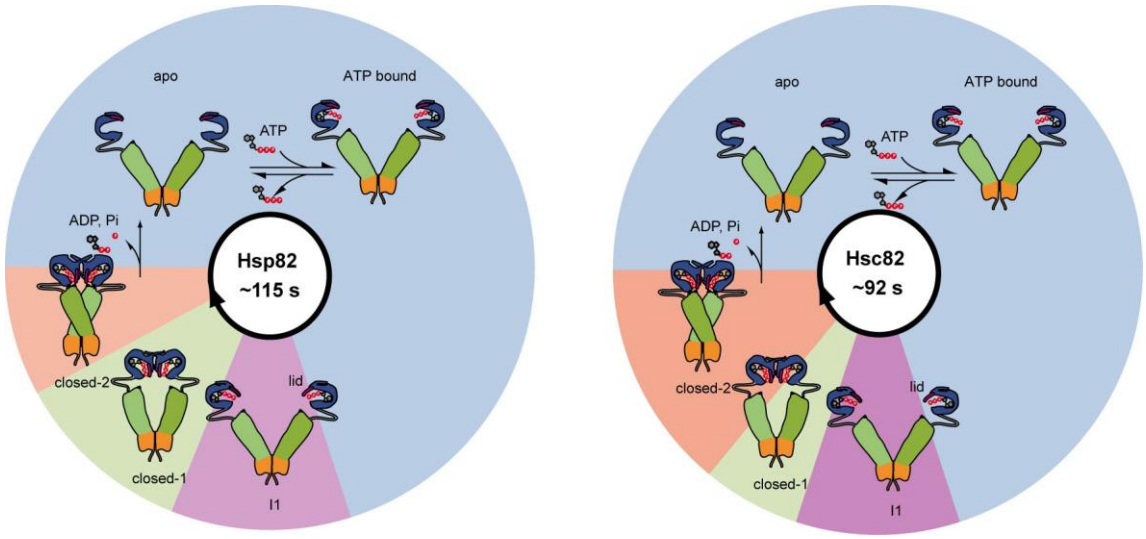

Figure 49: **Hsp82 and Hsc82 slightly differ in the ATPase conformational cycle.** The scheme illustrates the differences in dwell times Hsp90 adopts during the ATPase cycle (open = blue, I1 = violet, closed-1 = green, closed-2 = orange). The dwell times for yeast Hsp90 were deduced from Hessling et al. (Hessling et al., 2009) and are depicted schematically. The conformational states are in equilibrium and both yeast Hsp90 isoforms are mostly populated in an open conformation in the presence of ATP. Hsc82 populates slightly more of the closed-2 state compared to Hsp82. The ATP hydrolysis rate is indicated by the number within the white circle.

Taken together, Hsc82 passes slightly faster through the ATPase cycle indicated by an increased ATPase activity and closing rate. In general both Hsp90 isoforms are mostly populated in an open conformation in the prescence of ATP revealed by nucleotide-induced FRET experiments (*Figure 49*). Furthermore, similar binding and inhibition by Sti1 demonstrate no difference in the open conformation between the isoforms. Hsc82 tends to populate more closed-2 state compared to Hsp82 indicated by slightly stronger Sba1 binding (*Figure 49*). Contrary, Hsp82 slightly bind better and is more affected by Cpr6 suggesting a shift towards the closed-1 state compared to Hsc82 (*Figure* 49). Taken together, the results provide information about differences between the Hsp90 isoforms within the conformational cycle.

5.1.4 Hsp90 Isoform Exhibit Different Sensitivity Towards Radiciol and Differ in Client Specificity

Hsp90 is essential in eukaryotic cells. Yeast cells harboring only one functional gene for Hsp82 or Hsc82 are able to support yeast cell growth under non-stress and stress conditions (Borkovich et al., 1989). This indicates that both isoforms may serve similar functions. However, yeast Hsp90 isoforms display distinct functions in response to acetic acid stress conditions (Silva et al., 2013). We showed that *in vivo,* the impact of radicicol and amino acid depletion is Hsp90 isoform-dependent. To narrow this down, we constructed chimera and found that the higher susceptibility of Hsc82 towards radicicol exclusively relies on the NTD although the affinities of the NTD of Hsc82 and of Hsp82 turned out to be similar. This is in line with the literature, where activiation of certain client proteins by human Hsp90 isoforms was analyzed in yeast cells (Millson et al., 2007). The data revealed that human Hsp90α and Hsp90β expressed as the sole Hsp90 source differ with regard to their capacities for activation of specific clients and only Hsp90β generates sensitivity to radicicol (Millson et al., 2007). Another study using human cell culture showed that the human Hsp90 isoforms behave significantly different regarding client interaction under stress conditions with Hsp90α serving more clients at higher temperatures (Taherian et al., 2008). To study differences in client interaction is important since many Hsp90 clients are involved in diseases like cancer. Thus this isoform-specific aspect has to be considered in development of Hsp90 inhibitors. Recently, it was shown in more detail that human Hsp90 isoforms differ in client and drug preference with regard to different conformational dynamics (Prince et al., 2015). Again, it turned out that Hsp90β is more affected by inhibitors compared to Hsp90α. This goes along with what we found for the yeast Hsp90 isoforms with Hsc82 being more affected by radicicol.

5.1.5 Conclusion and Outlook

In conclusion, although as expected Hsp82 and Hsc82 to behave very similarly due to 97 % sequence identity, we, interestingly found, that both isoforms exhibit slight differences in conformational changes, sensitivity towards radiciol, conformational dynamics and their *in vivo* function. However, the physiological reason for having two isoforms in *S. cerevisiae* remains unclear. One reason why very few *in vivo* differences between the isoforms have been observed might be the expression at much higher level than required for growth at physiological temperature. This might mask differences between the isoforms. Interestingly, no isoform-specific differences during heat stress

where both isoforms were overexpressed were detected while in a previous study, where endogenous promotors were used, this was reported (Borkovich et al., 1989; Millson et al., 2007). In a future study lower expression levels of the isoform should thus be tested.

Gcn2 is an Hsp90 dependent client (Donze and Picard, 1999) that seems to be differentially regulated by the yeast Hsp90 isoforms. Biochemical and biophysical methods would provide further insights into the mechanism. In this context, the role of co-chaperones should be addressed because it would be interesting to decipher if they increase or decrease isoform-specific effects on clients. Moreover, isoform-specific clients should be identified via a global approach, such as co-immunoprecipitation.

5.2 Analysis of Human Hsp90 Dynamics using FRET

Hsp90 is a very dynamic molecular machinery and undergoes large conformational changes within the ATPase cycle revealed by the atomic structures of two distinct conformations, the open (HtpG) (Shiau et al., 2006) and the closed conformation (yeast Hsp82) (Ali et al., 2006). A FRET analysis monitored the transitions between both extreme states and indicated intermediate structural rearrangements within the yeast Hsp90 dimer (Hessling et al., 2009). Whether the Hsp90 conformational cycle can be generalized for the entire Hsp90 family is an important unresolved question. Since Hsp90 is highly conserved from bacteria to man, the findings for yeast Hsp90 will help to understand the general underlying mechanism. Besides common Hsp90 mechanisms for yeast and man (Vaughan et al., 2009), differences in the Hsp90 ATPase cycle (McLaughlin et al. 2004) as well as diverse equilibrium states of the conformational states have been reported (Graf et al., 2014; Krukenberg et al., 2011; Southworth and Agard, 2008). In this context, the ATPase turnover rate of human Hsp90 is 10-fold slower than that of the yeast homolog (Richter et al. 2008). It is assumed that the slow hydrolysis rate results from differences in conformational changes. It is still unknown how the conformational rearrangements and inter-domain communication differ in human Hsp90 compared to yeast Hsp90. It is assumed that in principle the mechanism will be the same, but the level of regulation will be different. Several evidences strengthened the idea that the ATPase cycle of human Hsp90 is similar to that of Hsp90 from simple eukaryotic cell, like yeast. However, human Hsp90 is more tightly regulated by several layers of modulation including a diverse set of co-chaperones, post-tranlational modifications and a larger number of clients. To investigate Hsp90 dynamics potential differences conformational changes and interdomain communication, a human Hsp90 FRET system would be a suitable method.

Within this thesis, several approaches were followed to establish a human Hsp90 FRET system. The experimental strategy was site-specific labeling via thiol-reactive ATTO labels. ATTO maleimides readily react with thiol groups of cysteines within a protein. As the human Hsp90α/β isoforms carry seven/six natural cysteines, this is not as simple as for the yeast Hsp90 FRET system. To obtain an Hsp90 variant for site-specific labeling, three approaches have been conducted:

- Replacement of all natural occurring cysteines
- Segmental labeling and domain ligation of human Hsp90 mediated by Sortase A
- Incorporation of an unnatural amino acid into human Hsp90

5.2.1 Replacement of all Natural Cysteines Affect Hsp90 Dynamics

To generate a cysteine-free Hsp90 variant, all cysteines were replaced with an amino acid corresponding to naturally occurring amino acids at these positions in yeast Hsp90. In a next step, a donor- and an acceptor- dye needs to be site-specifically attached to a cysteine in the NTD and MD, respectively, similar to those established for the yeast Hsp90. A variety of engineered Hsp90β variants were recombinant expressed in *E. coli* and purified. An extensively *in vivo* and *in vitro* characterization addressed stability, ATPase activity and functionality in yeast cells and was aimed to find a human Hsp90β variant that behave like wt. The results are summarized in *Table 10.* Variants that turned out to be suitable were site-specifically labeled with a donor- and an acceptor-fluorescent dye. First FRET measurements revealed that a FRET-competent heterocomplex can be formed although with low FRET efficiency. However, conformational changes, like closing of Hsp90 induced by ATPγS binding could not be observed. Also the prescence of p23, which stabilizes the closed state (Dittmar et al., 1997; Kosano et al., 1998) did not help. To test whether the engineered Hsp90s are able to bind p23, auc was performed with fluorescently-labed p23. Indeed, p23 binding was strongly altered for the cysteine-free Hsp90β variant whereas both Hsp90α and Hsp90β form a complex with p23 in the prescene of ATPγS. Taken together, the data suggest that the cysteines located in the MD and CTD seem to be import for Hsp90 conformational dynamics. With our results we can not narrow down which cysteine particularly is important but it was shown that a cysteine located in the yeast CTD (Cys597 refered to Hsp90α) serves as a molecular switch point when post-translational modified (Retzlaff et al., 2009). Several studies demonstrated that the closed state is populated by the human Hsp90 homolog but to a much lesser extent compared to the yeast homolog (yeast > bacteria > human) (Graf et al., 2014; Karagoz et al., 2014; Southworth and Agard, 2008).

In fact, that p23 binding is observed suggests the formation of a closed state, but to which extent conformational rearrangements occur can not be deduced from that. To exlude the possibility that the the substitutions of the cysteines are responsible for preventing Hsp90 closure another experimental strategy had to be employed.

Table 10: Summary of *in vivo* functionality, ATPase activity and stability of the generated Hsp90β cys-variants. (n.d. = not determined)

Hsp90β variant	**5-FOA Shuffling**	**Stress sensitivity**	**ATPase k_{cat} [min^{-1}]**	**Stability T_m [°C]**
Hsp90 wt	viable	no	0.11 ± 0.03	47.2 ± 0.1
0Cys I (589I)	viable	no	0.08 ± 0.02	48.0 ± 0.0
0Cys II (all serine)	lethal	---	n.d.	n.d.
63C	viable	no	0.03 ± 0.02	45.0 ± 0.1
67C	viable	no	0.01	44.3 ± 0.6
69C	viable	no	0.02 ± 0.01	46.0 ± 0.0
70C	viable	no	n.d.	n.d.
71C	viable	no	0.01 ± 0.003	39.3 ± 0.6
383C	viable	slower growth	0.03 ± 0.004	47.9 ± 0.1
386C	viable	no	0.03 ± 0.013	47.1 ± 0.1
388C	viable	no	n.d.	n.d.
390C	viable	no	n.d.	n.d.
395C	lethal	---	n.d.	48.3 ± 0.4
397C	lethal	---	n.d.	47.4 ± 0.5

5.2.2 Segmental Labeling and Domain Ligation of Human Hsp90 Mediated by Sortase A

As the natural cysteines are located exclusively in the M- and C-terminal domain of Hsp90α and Hsp90β, we utilized segmental labeling and ligation mediated by Sortase A. To this end the ND with an engineered cysteine was designed, expressed, purified separately and labeled with a fluorescent dye. Afterwards the labeled ND can be ligated, mediated by Sortase A, to the MC-domains of Hsp90. This allows leaving the natural cysteines intact. Before setting up the SrtA ligation method, the constructs that result after SrtA ligation, containing the recognition motif LPKTGA, were first

characterized *in vivo* and *in vitro.* The comprehensive *in vivo* analysis with regard to functionality revealed that the introduction of LPKTGA within the linker region did not influence viability or stress response function compared to wt Hsp90. The position in the flexible linker is located close to an important region at the end of the linker (Hsp82 264-272) (Jahn et al., 2014). The supplementation to a glycine-serine linker caused conformational restraints in yeast Hsp90 resulting in a strongly defective client activation (Jahn et al., 2014). Our data demonstrate that client activation is not influenced by the LPKTGA motif. In contrast, when the motif is located between the MD and CTD this caused lethality in yeast obtained by 5'-FOA shuffling. Furthermore, *the vitro* characterization showed that the human Hsp90 isoforms carrying the LPKTGA motif within the linker region behave similarly compared to wt human Hsp90 except for p23 binding. Again, auc experiments demonstrated that binding of p23 to the Hsp90 variant was negatively affected in contrast to that of wt Hsp90. This result suggests that conformational rearrangements are affected but this does not seem to play a role *in vivo* as client maturation was not affected. As the complex formation of p23 to the variants was not completely defective and binding of the co-chaperone Aha1 was not influenced, segmental labeling and domain ligation mediated by SrtA was performed. Correctly ligated full-length Hsp90β was obtained with the optimized strategy using a centrifugal filter unit. The obtained yield of about 45 % ligated full-length product is in good agreement with the literature (Freiburger et al., 2015). However, the non-ligated MC fragment could not be fully removed after ligation during the purification steps due to C-terminal dimerization (*Figure 50*). Stringent washing steps did not improve the purification. The ligated Hsp90 was stable and exhibits ATPase activity althougth to a lower extent but could be stimulated by Aha1. Unfortunately, even less complex formation was detected with the ligated Hsp90 and p23. Again, the binding of the co-chaperone p23 was altered. Taken together, the data suggest that the altered ATPase activity and co-chaperone binding are due the formation of hetero-dimers of the ligated Hsp90 with unligated MC fragment. In general the domain ligation by SrtaA for human Hsp90 domains obtained good yields but subsequent purification needs to be improved to achieve pure full-length Hsp90 homodimer. For future experiments one can test other positions in the linker and between MD and CTD.

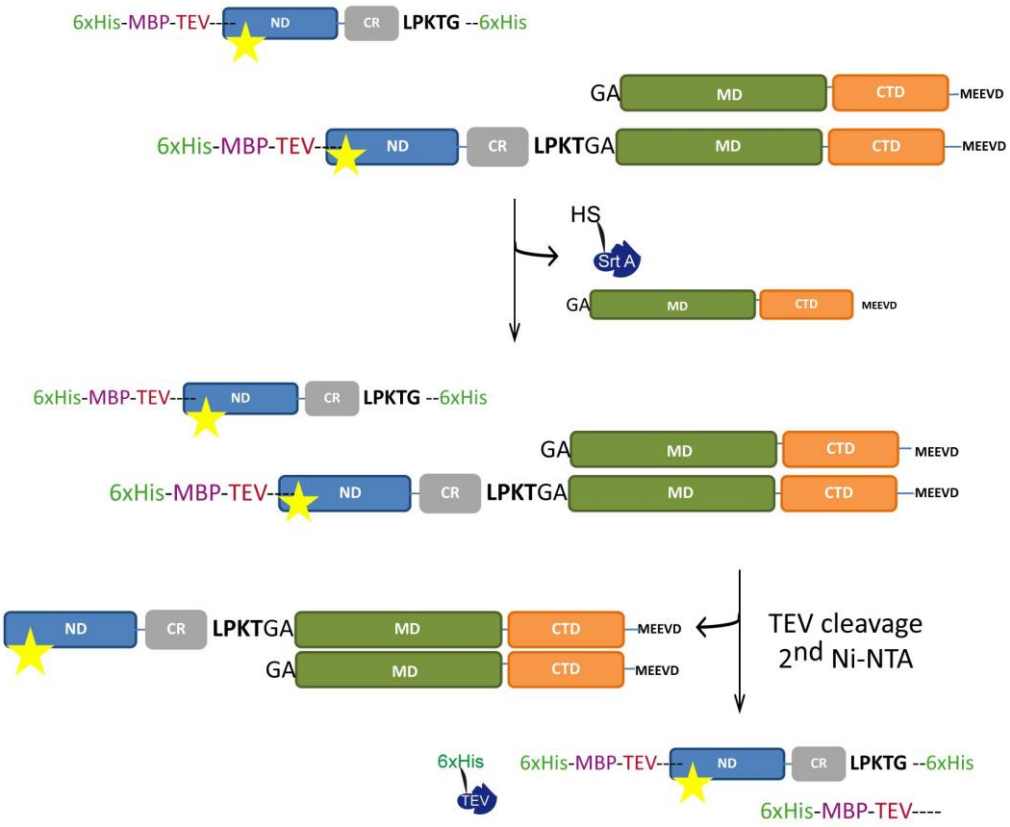

Figure 50: **C-terminal dimerization causes impurity in the purification of ligated full-length Hsp90**. The ligated product is not fully isolated from the non ligated MC-domain by both Ni-NTA affinity chromatography steps. TEV protease cleavage and Ni-NTA column separate the full-length Hsp90 from the unligated ND, the 6xHis-MBP-TEV-tag and the TEV protease.

5.2.3 Future Investigations: Incorporation of an Unnatural Amino Acid into Human Hsp90

The elegant alternative compared to segmental labeling and ligation is the expansion of the genetic code using an unnatural amino acid to incorporate a suitable one to obtain site-specific labeling of human Hsp90 (Lang et al., 2015). To this end, an amber suppression codon was introduced at positions, that had already been characterized *in vitro* and *in vivo*. Using a well established orthogonal amino acid t-RNA synthetase pair, an unnatural amino acid can be introduced at this position. To this end, we used an unnatural amino acid with an alkene as a functional group. After incorporation, a tetrazine-reactive fluorescent dye can be attached via a Diels-Alder reaction. To test the incorporation, expression tests under several conditions were tested. However, the tests revealed that in the absence of the unnatural amino acid, the incorporation takes place, suggesting unspecific incorporation. In order to improve the specific incorporation, several sites have to be tested in the future. Furthermore, a large scale expression has to be performed with BocK, a rather

cheap unnatural amino acid, to estimate the yield that can be obtained. Than the large scale expression can be repeated with CpK and incorporation has to be verified with mass spectrometry to ensure specific incorporation. This method is promising as only one position within the sequence needs to be modified minimizing the effect on the conformational ATPase cycle of Hsp90. Due to generally low protein yields after expression (ca. 90 % lower) and expensive synthesis of the respective amino acid, the approach may be useful but faces also several difficulties. In general, this approach provides a 'toolkit' that expands selective modifications in proteins. It was applied successfully for histone modifications since histones can be stablely expressed and in high yields (Chatterjee and Muir, 2010; Simon et al., 2007; Spicer and Davis, 2014). The method has been extended to other proteins as well. The characterization of an aminoacyl-tRNA synthetase/tRNA pair for the co-translational, site-specific incorporation of 3-nitrotyrosine at genetically encoded sites was established for the first time for manganese superoxide dismutase (Neumann et al., 2008). Recently, the post-translational modification of tyrosine residues in human Hsp90 was performed by recombinant expression using site-specific unnatural amino acid replacement to encode nitrotyrosine genetically (Franco et al., 2013). The data demonstrate that this experimental strategy works out in human Hsp90.

6 Material and Methods

6.1 Material

6.1.1 Chemicals

Chemical	Origin
Acrylamide / Bisacrylamide solution (40%)	Serva (Heidelberg, Germany)
Agar Agar	Serva (Heidelberg, Germany)
Agarose, ultra pure	Serva (Heidelberg, Germany)
Amino acids	Sigma-Aldrich (St Louis, USA)
Adenylyl-imidodiphosphate (AMP-PNP)	Roche (Mannheim, Germany)
Ammoniumpersulfate (APS)	Roth (Karlsruhe, Germany)
Ampicillin	Roth (Karlsruhe, Germany)
Adenosin-5-diphosphate (ADP)	Roche (Mannheim, Germany)
Adenosin-5-triphosphate (ATP)	Roche (Mannheim, Germany)
Adenosin-5-(γ -thio)-triphosphate (ATPγS)	Roche (Mannheim, Germany)
N_{ε}-(tert-Butoxycarbonyl)-L-Lysin (BocK)	Cabolution Chemicals (Saarbrücken, Germany)
Bovine Serume Albumin (BSA)	New England Biolabs (Frankfurt, Germany)
Bromphenolblue S	Serva (Heidelberg, Germany)
Calcium chloride	Roth (Karlsruhe, Germany)
Complete Protease Inhibitor Cocktail HP	Serva (Heidelberg, Germany)
Coomassie Brilliant Blue R-250	Serva (Heidelberg, Germany)
CpK	Prof. Dr Kathrin Lang
11-Deoxycorticosterone (DOC)	Sigma-Aldrich (St Louis, USA)
Deoxyribonucleic acid, single stranded from salmon testis	Sigma-Aldrich (St Louis, USA)
Dimethyl sulfoxide (DMSO)	Sigma-Aldrich (St Louis, USA)
1,4-Dithiothreitol (DTT)	Roth (Karlsruhe, Germany)
DNA stain clear G	Serva (Heidelberg, Germany)
ECL-Westernblot Detection System	GE Healthcare (Munich, Germany)
Ethylendiamintetraacidic acid (EDTA)	Merck (Darmstadt, Germany)
5'-Fluoroorotic acid (5'-FOA)	ThermoFisher Scientific (Paisley, UK)
Galactose	Merck (Darmstadt, Germany)
Glucose	Merck (Darmstadt, Germany)
Glycerol, 99%	Roth (Karlsruhe, Germany)
Hydrochloric acid 32%	Sigma-Aldrich (St Louis, USA)
N-2-Hydroxyethylpiperazin-N'-2-ethansulfonsäure (HEPES)	Roth (Karlsruhe, Germany)
Imidazole	Sigma-Aldrich (St Louis, USA)
Isopropyl-β-D-thiogalactopyranosid (IPTG)	Roth (Karlsruhe, Germany)
Isopropanol	Roth (Karlsruhe, Germany)
Kanamycin	Roth (Karlsruhe, Germany)
LB_0-Media	Serva (Heidelberg, Germany)
Lithium-Acetate	Roth (Karlsruhe, Germany)

Magnesium chloride-hexahydrate	Merck (Darmstadt, Germany)
β-Mercaptoethanol, pure	Sigma-Aldrich (St Louis, USA)
Methanol	Roth (Karlsruhe, Germany)
Milk powder	Roth (Karlsruhe, Germany)
Nicotinamide adenine dinucleotide (NADH)	Roche (Mannheim, Germany)
O-nitropehenyl β-D-galactopyranoside (ONPG)	Sigma-Aldrich (St Louis, USA)
Polyethylene glycol (PEG-4000)	Merck (Darmstadt, Germany)
Potassium chloride	
Phosphoenolpyruvate (PEP)	Roche (Mannheim, Germany)
Radicicol	Sigma-Aldrich (St Louis, USA)
Raffinose	Merck (Darmstadt, Germany)
Sodium chloride	Merck (Darmstadt, Germany)
Sodiumdodecylsulfat (SDS)	Roth (Karlsruhe, Germany)
Sodium hydroxide	Roth (Karlsruhe, Germany)
di-Sodium-hyrogenphosphate	Merck (Darmstadt, Germany)
Sodium-dihydrogenphosphate	Merck (Darmstadt, Germany)
Spectinomycin	AppliChem (Darmstadt, Germany)
Tetracyclin	AppliChem (Darmstadt, Germany)
N,N,N',N'-Tetramethylethylendiamin (TEMED)	Roth (Karlsruhe, Germany)
Tris(hydroxymethyl)-aminomethan (Tris)	Roth (Karlsruhe, Germany)
Polyoxyethylen-Sorbitan-monolaurat (Tween 20)	Merck (Darmstadt, Germany)
Yeast Extract	Difco (Detroit, USA)
Yeast Extract Peptone Dextrose (YPD)	Difco (Detroit, USA)
Yeast Nitrogen Base	Difco (Detroit, USA)

6.1.2 Devices and Additional Materials

Device	**Manufacturer**
Scales	
Sartorius Universal	Sartorius (Göttingen, Germany)
Sartorius BL310	Sartorius (Göttingen, Germany)
Sartorius BP121S	Sartorius (Göttingen, Germany)
Centrifuges	
Beckman J-26 XP, Avanti J25	Beckman Coulter (Krefeld, Germany)
Beckman XL-1 analytical centrifuge	Beckman Coulter (Krefeld, Germany)
Eppendorf-Centrifuge 5415C	Eppendorf (Hamburg, Germany)
Hettich-Centrifuge Mikro 185	Hettich (Tuttlingen, Germany)
Chromatography columns	
His-Trap FF, 5 ml	GE Healthcare (Freiburg, Germany)
His-Trap HP, 5 ml	GE Healthcare (Freiburg, Germany)
ResourceQ , 6 ml	GE Healthcare (Freiburg, Germany)
CFT Hydroxyapatide, 50 ml	BioRAD (Munich, Germany)
Superdex Prep Grade 75 (16/60, 26/60)	GE Healthcare (Freiburg, Germany)
Superdex Prep Grade 200 (16/60)	GE Healthcare (Freiburg, Germany)
PD-10 desalting columns	GE Healthcare (Freiburg, Germany)

Chromatography devices	
Äkta FPLC-System	GE Helthcare (Freiburg, Germany)
Jasco HPLC-System	Jasco (Groß-Umstadt, Germany)
Loop 5ml / 10 ml	GE Helthcare (Freiburg, Germany)
Superloop 150 ml	GE Helthcare (Freiburg, Germany)
Gel electrophoreses and blotting devices	
Bio Doc II detection system	VWR (Radnor, USA)
Electrophorese Power Supply 3501 XL	GE Helthcare (Freiburg, Germany)
Electrophorese Power Supply 601	GE Helthcare (Freiburg, Germany)
Wide Mini-Sub Cell GT	BioRad (München, Germany)
Hoefer Dual Gel Caster	GE Helthcare (Freiburg, Germany)
Hoefer Mighty Small II SE 250 / 260 Mini-Vertical Units	GE Helthcare (Freiburg, Germany)
PCR accessories	
PCR tubes	Nerbe Plus (Winsen, Germany)
Thermocycler T100	BioRad (München, Germany)
Thermocycler MJ Mini	BioRad (München, Germany)
Thermocycler MWG Biotech Primus 25	MWG-Biotech (Ebersberg, Germany)
Absorptions Spectrophotometer	
Varian Cary 50 Bio UV-Vis Spectrophotometer	Varian (Palo Alto, USA)
Quartz Cuvettes High Precision Cell 10 mm	Hellma Analytics (Müllheim, Germany)
Nanodrop ND-1000 UV-Vis	Nanodrop ND-1000 UV-Vis
Tecan Sunrise	Tecan Group (Maennedorf, Schweiz)
UV-Meter Ultrospec 1100 pro	GE Helthcare (Freiburg, Germany)
Circulardichroism spectropolarimeter	
Jasco J715	Jasco (Groß-Umstadt, Germany)
CD cuvette	Hellma Analytics (Müllheim, Germany)
PTC 343 Peltier temperature device	Jasco (Groß-Umstadt, Germany)
Fluoroescence spectrophotometer	
FluoroMax 2	Horiba Scientific (München, Germany)
FluoroMax 3	Horiba Scientific (München, Germany)
Quartz Cuvettes High Precision Cell 10 mm (3 windows)	Hellma Analytics (Müllheim, Germany)
Additional devises and materials	
Advansta WesternBright ECL Spray	Advansta (Menlo Park, USA)
Amicon Ultra MWCO 3k/10k/30K	Merck (Darmstadt, Germany)
Amicon Ultra-15 centrifuge filtermembran	Merck (Darmstadt, Germany)
Dialysis Slide-A-Lyzer™	Thermo Fisher Scientific
Eppendorf Thermomixer Compact	Eppendorf (Hamburg, Germany)
Eppendorf-Tubes	Eppendorf (Hamburg, Germany)
Fast-Blot B44 Apparat	Biometra (Göttingen, Germany)
Image Quant LAS 4000	GE Helthcare (Freiburg, Germany)
Incubators	New Brunswick Scientific (Nürtingen, Germany)
Magnet stirrer MR2000	Heidolph (Melsungen, Germany)
pH-meter WTW pH526	WTW (Weilheim, Germany)
Plastic cuvettes	Sarstedt (Nümbrecht, Germany)

Roti®-PVDF Membran	Roth (Karlsruhe, Germany)
Serva SDS-Gel TG PRiME 4 - 20 %	Serva (Heidelberg, Germany)
Spectra/Por Biotech-Grade membrane dialysis	Spectrum Labs (Breda, Niederlande)
Temperature Gradiente TGGE Maxi System	Biometra (Göttingen, Germany)
Varioklav	HP-Medizintechnik (Oberschleißheim, Germany)
Vortexer REAX top	Heidolph (Kehlheim, Germany)
Whatman Chromatography paper (3mm)	Whatman (Maidstone, England)
Cell disruption apparatus Basic Z Constant system	Constant Sysetms (Warwick, USA)

6.1.3 Enzymes

Name	Origin
Alkaline Phosphatase	New England Biolabs (Frankfurt, Germany)
BamHI-HF	New England Biolabs (Frankfurt, Germany)
Chymotrypsin Sequencing Grade (from bovine pancrease)	Roche (Mannheim, Germany)
DNAseI	Invitrogen Life Sciences (Paisley, UK)
DpnI	New England Biolabs (Frankfurt, Germany)
GoTaq DNA-Polymerase	Promega (Madison, USA)
KLD enzyme mix	New England Biolabs (Frankfurt, Germany)
Lactate-Dehydrogenase (2750 U/ml in 3,2 M $(NH_4)_2SO_4$	Roche (Mannheim, Germany)
NdeI-HF	New England Biolabs (Frankfurt, Germany)
Not1-HF	New England Biolabs (Frankfurt, Germany)
Pfu DNA-Polymerase	Promega (Madison, USA)
Pyruvat Kinase (2000 u/ml in 3,2 M $(NH_4)_2SO_4$	Roche (Mannheim, Germany)
Q5 DNA-Polymerase	New England Biolabs (Frankfurt, Germany)
SalI-HF	New England Biolabs (Frankfurt, Germany)
SpeI-HF	New England Biolabs (Frankfurt, Germany)
T4 DNA-Ligase	Promega (Madison, USA)
T4 DNA-Polymerase	New England Biolabs (Frankfurt, Germany)
Thermosensitive alkaline Phosphatase (TSAP)	Promega (Madison, USA)
Xho1-HF	New England Biolabs (Frankfurt, Germany)

6.1.4 Antibodies

Name	Origin	Dilution
anti-Glucocorticoid-Receptor (GR) IgG (rabbit)	Invitrogen (Eugene, USA)	1:5000
anti-His_6-HRP IgG (monoclonal, rabbit)	Roche (Mannheim, Germany)	1:10000
anti-Hsp90 (polyclonal, rabbit)	Pineda (Berlin, Germany)	1:40000
anti-3-Phosphoglyceratkinase (yeast PGK) IgG (mouse)	Invitrogen (Eugene, USA)	1:10000
anti-Phosphotyrosine IgG, clone 4G10 (mouse)	Millipore (Temecula, USA)	1:1000
anti-mouse IgG (HRP, monoclonal)	Sigma-Aldrich (St Louis, USA)	1:20000
anti-rabbit IgG (HRP, monoclonal)	Sigma-Aldrich (St Louis, USA)	1:20000

6.1.5 Fluorophores

Name	Ex_{max} (nm)	Em_{max} (nm)	ε (M^{-1} cm^{-1})	Origin
5(6)-FAM	492	515	78.000	Invitrogen/Life Technologies (Paisley, UK)
ATTO 488-maleimid	501	523	90.000	Atto-Tec (Siegen, Germany)
ATTO 550-maleimid	554	576	120.000	Atto-Tec (Siegen, Germany)

*Ex_{max}: Spectral excitation maximum, Em_{max}: Spectral emission maximum, ε: molar extension coefficient

6.1.6 Size and Molecular Mass Standard Kits

Name	Origin
Q5®-Site-Directed Mutagenesis Kit	New England Biolabs (Frankfurt, Germany)
Wizard SV Gel and PCR Clean-Up System	Promega (Madison, USA)
Wizard *Plus* SV Minipreps DNA Purification System	Promega (Madison, USA)
Page Ruler Prestained Protein Ladder	ThermoFisher Scientific (Waltham, USA)
SDS PAGE Molecular Weight Standard Low Range	BioRad (Munich, Germany)
Serva FastLoad 1 kb DNA Ladder	Serva (Heidelberg, Germany)

6.1.7 Strains

Organism	Strain	Genotype	Origin
E. coli	BL21 DE3	B F^- *dcm ompT hsd*S(r_B^-, m_B^-) *gal* λ(DE3)	Stratagene (La Jolla, USA)
E. coli	Mach1	F^- Φ80*lac*ZΔM15 Δ*lac*X74 *hsd*R(r_K^-, m_K^+) Δ*rec*A1398 *end*A1 *ton*A	Invitrogen (Karlsruhe, Germany)
E. coli	XL1 Blue	*rec*A1 *end*A1 *gyr*A96 *thi-1 hsdR17 supE44 relA1* lac F'[*proAB*$^+$ *lacI*^{q} *ZΔM15] Tn10*(Tet^r)]	Stratagene (La Jolla, USA)
S. cerevisiae	PCLDα	Hsp82::Leu hsc82::Leu2 ade2 his3 leu2 trp1 ura3	Nathan und Lindquist, 1995
S. cerevisiae	BY4741	arg4::kanMX hsc82::kanMX hsp82::natMX lys2Δ0 his3Δ1 met15Δ0 MATa [HSP82]URA3 ura3Δ0 leu2Δ0	Florian Schopf

6.1.8 DNA Oligonucleotide

All used DNA oligonucleotides were synthesized by *Eurofins Genomics* (Ebersberg, Germany) and dissolved in $H20_{dd}$ to a final concentration of 100 pmol/µl.

Primer for introducing cysteines into human Hsp90β	
h90bT60C rev	TAGCGAATCTTGTCCAAG
h90bT60C fwd	TGAGAGCCTGtgtGACCCTTCGAAG
h90bT60C_rev_long	TAGCGAATCTTGTCCAAGGCATCAGAAG
h90bT60C_fwd_long	TGAGAGCCTGTGTGACCCTTCGAAGTTG
h90bI390C rev	AGATCCTCAGAGTCAACC
h90bI390C fwd	GCCCCTGAACtgtTCCCGAGAAATG
h90bL388C rev	TCAGAGTCAACCACACCAC
h90bL388C fwd	GGATCTGCCCtgtAACATCTCCCGAGAAATG
h90bE70C rev	TCCAACTTCGAAGGGTCTG
h90bE70C fwd	CAGTGGTAAAtgtCTGAAAATTGACATCATCCC
Primer for re-cloning of Hsp90β cys-variants into a yeast vector backbone (p423GPD)	
h90a SpeI fwd	CGGACTAGTATGCCTGAGGAAACCCAGACCC
h90a Sal1 rev	CGCGTCGACTTAGTTACTTCTTCCATGCGTGATGTGT
h90b SpeI fwd	CGGACTAGTATGCCTGAGGAAGTGCACCATG
h90b SalI rev	CGCGTCGACCTAATCGACTTCTTCCATGCGAGAC
Primer for cloning of the domain fragments for SrtA ligation	
MBP_TEV fwd	gccgcgcggcagccatatgATGAAAATCGAAGAAGGTAAAC
MBP_TEV N278 rev	tcaggcatGGCGCCCTGAAAATAAAG
N278_h90alpha fwd	agggcgccATGCCTGAGGAAACCCAG
MBP_TEV MCh90a rev	ccttaatcttGGCGCCCTGAAAATAAAG
MC_h90alpha fwd	agggcgccAAGATTAAGGAAAAGTACATCG
MBP_TEV CDh90a fwd	tctggaagGGCGCCCTGAAAATAAAG
CD h90alpha fwd	agggcgccCTTCCAGAGGATGAAGAAG
N278_h90alpha rev	tcagtggtggtggtggtggtgctcgagtgcggccgcCTTCTTCTTCTTCTTGTCACC
MC_h90alpha rev	tcagtggtggtggtggtggtgctcgagtgcggccgcTTAGTCTACTTCTTCCATGC
NM_h90alpha rev	tcagtggtggtggtggtggtgctcgagtgcggccgcTTCCAGGCCTTCTTTGGTG
petsumo GGA fwd	ggaTCCACTAGTAACGGCCGC
petsumo GGA rev	TCCACCAATCTGTTCTCTGTG
MBP_TEV Nh90 rev	tcaggcatGGCGCCCTGAAAATAAAG
N271_h90b fwd	agggcgccATGCCTGAGGAAGTGCAC
MBP_TEV MCh90b rev	ctctttgatGGCGCCCTGAAAATAAAG
MC h90beta fwd	agggcgccATCAAAGAGAAATACATTGATCAG
MBP_TEV Ch90b rev	tcaggcagGGCGCCCTGAAAATAAAG
CD h90beta fwd	agggcgccCTTCCAGAGGATGAAGAAG
N271 h90beta rev	tcagtggtggtggtggtggtgctcgagtgcggccgcCTTAGTTTTCTTCTTCTTATCCTTACC
MC h90beta rev	tcagtggtggtggtggtggtgctcgagtgcggccgcCTAATCGACTTCTTCCATGC
NM h90beta rev	tcagtggtggtggtggtggtgctcgagtgcggccgcCTCCAGACCCTCCTTGGT
Primer for introducing the LPKTG motif into the SrtA	
Nh90 LPKTG fwd	gaccggcGCGGCCGCACTCGAGCAC

Nh90a LPKTG rev	ttgggcagGTCACCATCCTTCTTTTCTTCTTCCTCATCAGAAC
NMh90a LPKTG rev	ttgggcagGGTGACTGACACTAAAGTCTTCCCCTC
Nh90b LPKTG rev	ttgggcagCTTATCCTTACCGCTGTCATCCTCCTC
NMh90be LPKTG rev	ttgggcagGGTAACTGAGACCAGGCTCTTCCC
Primer for re-cloning of the SrtA constructs into a yeast vector (p423GPD)	
NLPKTG h90b fwd	TagtttcgacggatcTagaacTagtATGCCTGAGGAAGTGCACC
NLPKTG h90b rev	ctttgatggcGCCGGTCTTGGGCAGCTT
MC + G h90b fwd	caagaccggcGCCATCAAAGAGAAATACATTG
MC + G h90b rev	actaattacatgactcgaggtcgacCTAATCGACTTCTTCCATGC
NM_LPKTG h90b fwd	TagtttcgacggatcTagaacTagtATGCCTGAGGAAGTGCACCATG
NM_LPKTG h90b rev	caggcagggcGCCGGTCTTGGGCAGGGT
C +G h90b fwd	caagaccggcGCCCTGCCTGAGGATGAG
C +G h90b rev	actaattacatgactcgaggtcgacCTAATCGACTTCTTCCATGCGAG
N LPKTGA h90a fwd	TagtttcgacggatcTagaacTagtATGCCTGAGGAAACCCAGAC
N LPKTGA h90a rev	taatcttggcGCCGGTCTTGGGCAGGTC
MC + G h90a fwd	caagaccggcGCCAAGATTAAGGAAAAGTAC
MC + G h90a rev	actaattacatgactcgaggtcgacTTAGTCTACTTCTTCCATGC
NM_LPKTG h90a fwd	TagtttcgacggatcTagaacTagtATGCCTGAGGAAACCCAGACC
NM_LPKTG h90a rev	ctggaagggcGCCGGTCTTGGGCAGGGT
C +H h90a fwd	caagaccggcGCCCTTCCAGAGGATGAAG
C +H h90a rev	actaattacatgactcgaggtcgacTTAGTCTACTTCTTCCATGCG
BNM-C in Wt fwd	accggcgccCTGCCTGAGGATGAGGAG
BNM-C in Wt rev	cttgggcagGGTAACTGAGACCAGGCTC
Primer for re-cloning of SrtA constructs from p423GPD into a expression pETSUMO vector	
h90b fwd	tcacagagaacagattggtggatccATGCCTGAGGAAGTGCAC
h90b rev	actggcggccgttacTagtggatccCTAATCGACTTCTTCCATGC
h90a fwd	tcacagagaacagattggtggatccATGCCTGAGGAAACCCAG
h90a rev	actggcggccgttacTagtggatccTTAGTTACTTCTTCCATGCG
Primer for Sequenzing by GATC	
T7	TAATACGACTCACTATAGGG
pET-RP	CTAGTTATTGCTCAGCGG
GATC-GPD_FW-228935	aaagacggTaggtattg
GATC-CYCterm_rev-313905	taaaTagggaccTagac
GATC-hHsp90a_163-1398531	GTCCTCAGCAGGGGGATC
GATC-Hsp82-500-fwd-1123598	ttcttgaccgacccaattga
GATC-Hsp82-1-fwd-1123595	ATGGCTAGTGAAACTTTTGAAT
GATC-MBPTEVfwd-1461890	GACAAACCGCTGGGTGCCG
GATC-SynthetasePromotor7-26-1475303	CGGGAGTTGTCAGCCTGTCC
GATC-Synthetaserev-1480355	CCGGCCTACAAAAGCACGC
GATC-D4fwd2-1509897	cttttgctgagttgaagga
GATC-h90alpha328-1478930	CGCCAAGTCTGGGACCAAAG
GATC-hHsp90B_fwd233-665967	GAAAGGTGAGAAAGAAGAGG
GATC-petSUMO_fwd-endofSumo-1479095	CTCACAGAGAACAGATTG

6.1.9 Plasmids

Vector/Plasmid	Description	Origin
pET28b+	Expression in *E.coli* Kana^{R}	Merck Bioscience GmbH (Schwalbach, Germany)
pET28bSUMO	Expression in *E.coli,* N-term Sumotag, Kana^{R}	Dr. Oliver Lorenz
pET28b+ Hsp82	Expression of yeast 6xHis Hsp82 WT	Dr. Klaus Richter
pET28b+ Hsp82 D61C	Cysteine variant D61C	Dr. Martin Hessling
pET28b+ Hsp82 Q385C	Cysteine variant Q385C	Dr. Martin Hessling
pET28b+ Hsc82	Expression of yeast 6xHis Hsc82 WT	this work
pET28b+ Hsc82 D61C	Cysteine variant D61C	this work
pET28b+ Hsc82 Q381C	Cysteine variant Q381C	this work
pET28bSUMO Hsp82	Expression of SUMO-tagged yeast Hsp82 WT	this work
pET28bSUMOHsp82 D61C	Cysteine variant D61C	this work
pET28bSUMO Hsp82 Q385C	Cysteine variant Q385C	this work
pET28bSUMO Hsc82	Expression of SUMO-tagged yeast Hsc82 WT	this work
pET28bSUMO Hsc82 D61C	Cysteine variant D61C	this work
pET28bSUMO Hsc82 Q381C	Cysteine variant Q381C	this work
p423 GPD	Expression in yeast under GPD promotor, Amp^{R}, HIS	ATCC (Manassas, USA)
p423 GPD Hsc82	Hsc82 WT	this work
p423 GPD Hsc82 D61C	Cysteine variant D61C	this work
p423 GPD Hsc82 Q381C	Cysteine variant Q381C	this work
		this work
Co-chaperone		
pET28b+ Aha1	Expression of the yeast co-chaperone Aha1	Dr. Klaus Richter
pET28b SUMO Sti1	Expression of the yeast co-chaperone Sti1	Dr. Andreas Schmid
pET28b+ Sba1	Expression of the yeast co-chaperone Sba1	Dr. Martin Hessling

Vector/Plasmid	Description	Origin
pET28b+	Expression in *E.coli* Kana^R	Merck Bioscience GmbH (Schwalbach, Germany)
pET28bSUMO	Expression in *E.coli,* N-term SUMO-tag, Kana^R	Dr. Oliver Lorenz
pET28b Hsp90β	Expression of 6xHis Hsp90β	Dr. Klaus Richter
pET28b Hsp90β 0CysI	C366A, C412L, C521A, C564T,C589A, C590I	this work
pET28b Hsp90β 0CysII	C366A, C412L, C521A, C564T,C589A, C590S	this work
pET28b Hsp90β 0Cys T60C	0 Cysteine variant T60C	this work
pET28b Hsp90β 0Cys S63C	0 Cysteine variant S63C	this work
pET28b Hsp90β 0Cys S67C	0 Cysteine variant S67C	this work
pET28b Hsp90β 0Cys K69C	0 Cysteine variant K69C	this work
pET28b Hsp90β 0Cys E70C	0 Cysteine variant E70C	this work
pET28b Hsp90β 0Cys L71C	0 Cysteine variant L71C	this work
pET28b Hsp90β 0Cys S383C	0 Cysteine variant S383C	this work
pET28b Hsp90β 0Cys L386C	0 Cysteine variant L386C	this work
pET28b Hsp90β 0Cys L388C	0 Cysteine variant L388C	this work
pET28b Hsp90β 0Cys I390C	0 Cysteine variant I390C	this work
pET28b Hsp90β 0Cys Q397C	0 Cysteine variant Q397C	this work
pET28b+ MBP-TEV	Solubility tag maltose binding protein, TEV cleavage site	Dr. Lee Freiburger
pET28b MBP-TEV-Hsp90β - ND	MBP-TEV Hsp90β N-Domain (1-271)-6xHis	this work
pET28b MBP-TEV-Hsp90β - NM	MBP-TEV Hsp90β NM-Domain (1-543)-6xHis	this work
pET28b MBP-TEV-Hsp90β - MC	MBP-TEV Hsp90β MC-Domain (272-End)	this work
pET28b MBP-TEV-Hsp90β - CD	MBP-TEV Hsp90β C-Domain (544-End)	this work
pET28b MBP-TEV-Hsp90β - ND LPKTG	MBP-TEV Hsp90β N-Domain (1-LPKTG)-6xHis	this work
pET28b MBP-TEV-Hsp90β - NM LPKTG	MBP-TEV Hsp90β NM-Domain (1-LPKTG)-6xHis	this work
pET28b MBP-TEV-Hsp90β - ND 70C	MBP-TEV Hsp90β N-Domain (1-LPKTG)-6xHis E70C	this work
pET28b MBP-TEV-Hsp90β - NM 390C	MBP-TEV Hsp90β NM-Domain (1-LPKTG)-6xHis 390C	this work
pET28 SUMO Hsp90β WT	Expression of SUMO-tagged Hsp90β WT	this work
pET28 SUMO Hsp90β N-LPKTGA-MC	Expression of SUMO-tagged Hsp90β N-LPKTGA-MC	this work
pET28b Hsp90α		Dr. Klaus Richter
pET28b Hsp90α 0Cys	C374A, C420L, C481V,C529A C572T,C597A, C598I	Eurofins genomics
pET28b MBP-TEV-Hsp90α - ND	MBP-TEV Hsp90α N-Domain (1-278)-6xHis	this work
pET28b MBP-TEV-Hsp90α - NM	MBP-TEV Hsp90α NM-Domain (1-550)-6xHis	this work
pET28b MBP-TEV-Hsp90α - MC	MBP-TEV Hsp90α MC-Domain (279-End)	this work
pET28b MBP-TEV-Hsp90α - CD	MBP-TEV Hsp90α C-Domain (551-End)	this work
pET28b MBP-TEV-Hsp90α - ND LPKTG	MBP-TEV Hsp90α N-Domain (1-LPKTG)-6xHis	this work
pET28b MBP-TEV-Hsp90α - NM LPKTG	MBP-TEV Hsp90α NM-Domain (1LPKTG)-6xHis	this work
pET28SUMO Hsp90α WT	Expression of SUMO-tagged Hsp90α WT	this work
pET26SUMO Hsp90α LPKTGA	Expression of SUMO-tagged Hsp90α N-LPKTGA-MC	this work
pET28SUMO hChip	Expression of the human co-chaperone Chip	this work
pET28SUMO FKBP51	Expression of the human co-chaperone FKBP51	this work
pET28SUMO FKBP51	Expression of the human co-chaperone FKBP52	this work

pET28b+ Hop	Expression of the human co-chaperone Hop	Dr Andreas Schmid
pET28b+ Aha1	Expression of the human co-chaperone Aha1	Dr Marco Retzlaff
pET28b+ p23	Expression of the human co-chaperone p23	Dr Martin Hessling
p423 GPD	Expression in yeast under GPD promotor, Amp^R, HIS	
p423 GPD Hsp90β WT		Dr. Alexandra Rehn
p423 GPD Hsp90β 0CysI	C366A, C412L, C521A, C564T,C589A, C590I	this work
p423 GPD Hsp90β 0CysII	C366A, C412L, C521A, C564T,C589A, C590S	this work
p423 GPD Hsp90β 0Cys T60C	0 Cysteine variant T60C	this work
p423 GPD Hsp90β 0Cys S63C	0 Cysteine variant S63C	this work
p423 GPD Hsp90β 0Cys S67C	0 Cysteine variant S67C	this work
p423 GPD Hsp90β 0Cys K69C	0 Cysteine variant K69C	this work
p423 GPD Hsp90β 0Cys E70C	0 Cysteine variant E70C	this work
p423 GPD Hsp90β 0Cys L71C	0 Cysteine variant L71C	this work
p423 GPD Hsp90β 0Cys S383C	0 Cysteine variant S383C	this work
p423 GPD Hsp90β 0Cys L386C	0 Cysteine variant L386C	this work
p423 GPD Hsp90β 0Cys L388C	0 Cysteine variant L388C	this work
p423 GPD Hsp90β 0Cys I390C	0 Cysteine variant I390C	this work
p423 GPD Hsp90β 0Cys Q397C	0 Cysteine variant Q397C	this work
p423 GPD Hsp90β N-LPKTGA-MC	Hsp90β N-Domain (LPKTGA)MC	this work
p423 GPD Hsp90β NM-LPKTGA-C	Hsp90β NM-Domain (LPKTGA)C	this work
p423 GPD Hsp90α WT	Expression in yeast under GPD promotor, Amp^R, HIS	this work
P423 GPD Hsp90α 0Cys	C374A, C420L, C481V,C529A C572T,C597A, C598I	Eurofins genomics
P423 GPD Hsp90α N-LPKTGA-MC	Hsp90α N-Domain (LPKTGA)MC	this work
p423 GPD Hsp90α NM-LPKTGA-C	Hsp90α NM-Domain (LPKTGA)C	this work
p426 Gal v-Src	Expression of v-Src under a Gal inducible promotor, Amp^R, URA marker	Dr. Joanna Soroka, TUM
p2A rat GR-lacZ	Expression of rat GR under a constitutive promotor, Amp^R, ADE marker	Nathan und Lindquist (1995)

Plasmids incorporation of an unnatural amino acid into human Hsp90

pNHD	Expression in E. coli (tetR)	Prof. Kathrin Lang
pNHD Hsp90α WT	Expression in E. coli (tetR)	this work
pNHD Hsp90β WT	Expression in E. coli (tetR)	this work
pNHD Hsp90β TAA WT	(tetR) mit Stoppcodon TAA	this work
pNHD Hsp90β TAA E20TAG	E20 amber Stopp codon (tetR) mit Stoppcodon TAA	this work
pNHD Hsp90β TAA E63TAG	E63 amber Stopp codon (tetR) mit Stoppcodon TAA	this work
pNHD Hsp90β TAA E67TAG	E67 amber Stopp codon (tetR) mit Stoppcodon TAA	this work
pNHD Hsp90β TAA K69TAG	K69 amber Stopp codon (tetR) mit Stoppcodon TAA	this work
pNHD Hsp90β TAA I390TAG	I390 amber Stopp codon (tetR) mit Stoppcodon TAA	this work
pKW1	Synthetase	Prof. Kathrin Lang
pNHD GFP 150TAG		this work

6.1.10 Media und Antibiotics

The following media were used for cultivation of *E.coli* or *S. cerevisiae*. The media were prepared with $_{dd}H_20$ and for solid media 20 g/l Agar were used.

Name	Compounds
LB_0	20 g/l LB_0
dYT	5 g/l NaCl 10 g/l Yeast Extract 16 g/l Bacto Pepton
YPD	50 g/l Yeast Extract Peptone Dextrose (YPD)
Yeast selection media	6.7 g/l Yeast Nitrogen Base 20 g/l sugar source (glucose/raffinose or galactose) 2 g/l selective amino acid mix

The used selective antibiotic concentration were 35 µg/ml kanamycin, 200 µg/ml ampillicin, 12.5 µg/ml tetracyclin or 50 µg/ml spectinomycin.

6.1.11 Buffers for Molecular Biological Methods

All buffers were prepared with $_{dd}H_20$ and the pH was adjusted at 20°C.

Buffer	Compounds
Agarose Solution	1 g Agarose 100 ml TAE (1x) 1 µl DNA Stain Clear G (SERVA)
DNA loading buffer 5x	50 % (v/v) Glycerol 10 mM EDTA (pH 8.0) 0.2 % (w/v) Bromphenolblue 0.2 % (w/v) Xylencyanol
TAE-Buffer 50x	2 M Tris/Acetate, pH = 8.0 50 mM EDTA 0.11 % (v/v) Acetic acid
NEB-Buffer 2.1 10x	100 mM Tris/HCl, pH = 7.9 0.5 M NaCl 100 mM $MgCl_2$ 1 mg/ml BSA
NEB-Buffer Cutsmart 10x	0.2 M Tris/Acetat, pH = 7,9 0.5 M $C_2H_3KO_2$ 0.1 M $C_4H_6MgO_4$ 1 mg/ml BSA

6.1.12 Computer Software

Programm	Origin
Adobe Illustrator CS3	Adobe System (San Jose, USA)
Adobe Photoshop	Adobe System (San Jose, USA)
BioEdit	Ibis Biosciences (Carlsbad, USA)
Endnote X7	Adept Scientific (Herts, GB)
Microsoft Office 2011	Microsoft Corporation (Redmond, USA)
NEBaseChanger™	NEBaseChanger.neb.com
NEBuilder	NEBuilder.neb.com
OligoCalc	www.basic.northwestern.edu/biotools/oligocalc
Origin 8.6	Originlab (Northhampton, USA)
ProtParam Tool	ExPasy (www.expasy.org)
PyMol	Schrödinger (Mannheim, Germany)
Sedview	Hayes D.B. & Stafford W.F. (Hayes and Stafford, 2010)

6.2 Methods in Molecular Biology

6.2.1 Storage and Cultivation of *E. coli*

E. coli cells were cultivated either on LB agar plates or in liquid LB media at 37 °C. The incubation of liquid cultures took place at constant shaking at 180 rpm. The selection was carried out via media containing the respective antibiotic to select for transfomants harboring the resistance gene on a plasmid. A 5 ml or 100 ml liquid culture was inoculated with freshly transformed cells of a single colony. The inoculation of a 2 l liquid culture was carried out via 1:100 dilution of a fresh over night culture. To monitor the growth of the bacteria culture the optical densitiy (OD_{600}) of the cell suspension was measured at 600 nm (OD_{600}=1 correspond to a cell amount of 8 x 10^8 cell per ml). For long-term storage cells were stored in media containing 15 % glycerol at -80 °C.

6.2.2 Storage and Cultivation of *S. cerevisiae*

For yeast meadia and yeast cultivation standard protocols were used (methods in Yeast Genetics: a Cold spring Harbor Laboratory Course manual, 2005 Edition). *S. cerevisiae* were cultivated either on YPD agar plates or in liquid YPD media at 30 °C. The incubation of liquid cultures took place at constant shaking at 180 rpm. The selection of the yeast strains was guaranteed via auxotrophy. The media contained the respective amino acid mixture. A 5 ml or 100 ml liquid culture was inoculated with freshly transformed cells of a single colony. To monitor the growth of the yeast culture the optical densitiy (OD_{595}) of the cell suspension was measured at 595 nm (OD_{595}=1 correspond to a cell amount of 2 x 10^7 cell per ml). For long-term storage cells were stored in media containing 15 % glycerol at -80 °C.

6.2.3 Transformation of Plasmid DNA into *E. coli* Cells

Chemically competent *E.coli* cells were prepared according to Sambrook et al. (Sambrook, 1989), shock frozen into 100 µl aliquots and stored until use at -80 °C. For the transformation of DNA an aliquot of competend cells were mixed with 100 ng of plasmid DNA and incubated on ice for 30 min. Next, a heat shock, 1 min at 42 °C, was applied to the cells and afterwards chilled on ice for 5 min. To recover the cells 1 ml of LB_0 was added and incubated for 1 h at 37°C while shaking. Cells were spun

down (3 min, 5000 rpm), resuspended in 100 µl sterile $_{dd}H_20$ and streaked out on selective media followed by cultivation over night at 37 °C.

6.2.4 Yeast High Efficiency Lithium Acetate Transformation

A 5 ml YPD liquid culture was inoculated with cells of a single colony and incubated over night at 30 °C. The next day the OD_{595} of the pre-culture was measured. 50 ml of fresh media was inoculate (OD_{595}=0.15) and incubated for 4 h at 30 °C. Afterwards cells were spun down (3 min, 4500 rpm), supernatant was discarded and washed in 25 ml sterile H_2O. Next, the cell pellet was carefully resuspended in 1 ml 0.1 M lithiumacetate (LiOAc) and transferred to a fresh tube. The cells were again harvested (1 min, 7000 rpm) and resuspended in 0.5 ml 0.1 M LiOAc. 50 µl of the cell suspension were used per transformation. Again, cells were spun down (1 min, 7000 rpm), supernatant was discarded and the cell pelett was carefully resuspended with 360 µl PLATE mixture:

PEG 3000 50 % (w/v)	240 µl
LiOAc (1 M)	36 µl
Salmon ssDNA	10 µl
Plasmid-DNA	2 µl
H_2O sterile	72 µl

After 30 min incubation time at 30 °C cells were applied to a heat shock for 30 min at 42 °C. Cells were spun down (1 min, 7000 rpm) and washed with 1 ml sterile H_2O. 150 µl of the yeast cell suspension was plated onto selective media and incubated for several days (2-4) at 30 °C.

6.2.5 Amplification and Isolation of Plasmid DNA of *E. coli*

To amplify plasmid DNA, DNA was transformed into chemically competent *E. coli* (MACH1) cells as described above. A single colony was used to inoculate a 5 ml over night culture. To isolate the plasmid DNA from *E. coli* cells the *Wizard® PLUS SV Minipreps DNA purification system* kit was used according to the manufacturer's protocol. The concentration and purity of the DNA sample was determined using a NanoDrop device by recording an absorption spectrum. All newly constructed

plasmids were verified by sequencing with GATC Biotech (Konstanz, Germany). The plasmids were stored at -20°C.

6.2.6 Polymerase-Chain-Reaction for Amplification of DNA Fragments

The Polymerase-Chain-Reaction (PCR) is a specific method to amplify DNA fragments from genomic DNA or plasmids using the enzyme DNA-polymerase. Depending on the cloning strategy, either the program *NEBuilder Assembly Tool* (SLIC-cloning) or *NEBase Changer* (Insertion or Substitution) were used to design appropriate primers. The NEBtools calculated the melting temperatures T_m of the primers. All PCR components were combined in a reaction tube on ice and the reactions were carried out in a thermal cycler with a heated lid. The paramaters of a standard PCR were following:

Template-DNA (100 ng/µl)	1 µl
Primer fwd (10 µM)	2 µl
Primer rev (10 µM)	2 µl
Polymerase	0.5 µl
10 x Polymerase-reaction buffer	5 µl
dNTPs (10 mM)	1.5 µl
H_2O sterile	38 µl

A PCR program was set up according to the manufacturer's protocol in which some parameters were adjusted to the respective primers, length of amplified DNA fragment and needs of the used polymerase:

Step	Temperature	Time	Number of cycles
Initial Denaturation	95°C	2 min	1x
Denaturation	95°C	0.5 min	
Annealing	42-65°C	0.5-1 min	30x
Extention	72°C	2 min/kb	
Final Extention	72°C	10 min	1x
Soak	4°C	until use	

6.2.7 Separation of DNA via Agarose Gel Electrophoresis

PCR products or otherwise obtained DNA samples were separated by agarose gel electrophoresis to verifiy the size of the DNA fragments. The agarose gels were prepared with 1 % (w/v) agarose and 0.002 % Stain G in TAE-buffer. The gel was transferred into a gel electrophoresis chamber and filled up with 1x TAE buffer. For analytical use a small amount of DNA samples were mixed with 6x DNA loading buffer and loaded into the gel chambers. The gel electrophoresis was carried out at constant voltage of 120 V for 30 min. Afterwards the separation of the DNA fragments was detected by excitation of the stain G fluorescence in a *BioDoc II System.* For preparative use, the complete PCR product was applied and separated. The respective gel piece was cutted out and purified with the *Wizard® SV Gel Clean-Up System* Kit.

6.2.8 Purification and Storage of DNA-Fragments

DNA fragments or plasmids were purified with *Wizard® SV Gel and PCR Clean-Up System* Kits according to the manufacturers protocols. The concentration and purity of the DNA sample was determined using a NanoDrop device by recording an absorption spectrum. All newly constructed plasmids were verified by sequencing with GATC Biotech (Konstanz, Germany). The plasmids were stored at -20°C.

6.2.9 Re-Cloning of DNA Fragments

To create a new DNA fragment several cloning strategies can be used. Here, a conventional method was used to clone a gene of interest into a new vector-backbone. To this end the DNA region of interest from plasmids or genomic DNA was amplified via Polymerase-Chain-Reaction (PCR). Via the designed primers specific restriction sites can be introduced. The amplification product and the vector-backbone were digested via respective restictition enzymes. The restriction digest were carried out according to the manufactures protocol (NEB), combined in a reaction tube and incubated for 2 h at 37 °C.

Setting up a restriction enzyme digest:

Insert-DNA	5 µg
RE 10X buffer	5 µl
Restriction enzyme	2 µl
H_2O	Add 50 µl

Vektor-backbone	5-30 µg
RE 10X buffer	5 µl
Restriction enzyme	2 µl
H_2O	Add 50 µl

The vector-backbone was treated with alkaline phosphatase to avoid re-ligation. To remove the enzymes, the digested insert as well as the vector were purified with the *Wizard® SV Gel and PCR Clean-Up Systems* Kit according to the manufacturer's protocol. Next, the insert-DNA and the vector-DNA were ligated with T4 DNA Ligase. For the ligation reaction 100 ng of vector-DNA were used. The amount of insert-DNA was calculated with the following equation:

$$insert\ (ng) = \frac{vector\ DNA\ (ng) \cdot size\ of\ insert\ (bp)}{size\ of\ vector\ (bp)} \cdot ratio\ (\frac{insert}{vector})$$

Equation 1

Setting up a ligation reaction:

Vector-DNA	100 ng
Insert-DNA	X µl
T4 DNA Ligase	1 µl
5x T4 DNA Ligase-Buffer	2 µl
H_2O sterile	add 20 µl

The assembled reaction was incubated over night at 16 °C in a water bath. Afterwards the ligation product was transformed into chemically competent *E. coli* (MACH1 or XL1 blue) cells and selected on media containing appropriate antibiotics. A colony PCR was applied to screen for positive clones after transformation by using specific primers. To this end a small amount of single colonies were suspended in 10 ml of PCR master mix:

5 x GoTaq® buffer	2 µl
dNTPs (10 mM each)	0.3 µl
Upstream Primer (10 µM)	0.4 µl
Downstream Primer (10 µM)	0.4 µl
GoTaq® Polymerase (5 U/l)	0.1 µl
H_2O sterile	7 µl

A PCR program was set up according to the manufacturer's protocol:

Step	Temperature	Time	Number of Cycles
Initial Denaturation	95°C	5 min	1x
Denaturation	95°C	0.5 mn	
Annealing	42-65°C	0.5-1 min	30x
Extention	72°C	1 min/kb	
Final Extention	72°C	5 min	1x
Soak	4°C	until use	

Afterwards the whole PCR reaction was loaded onto a 1% agarose gel for verification. For positive hits the plasmids were re-isolated and the cloning success was verified via sequencing.

6.2.10 Site-Specific Blunt-End-Mutagenesis

To introduce site-specific point mutations or short insertions within a gene of interest the *Q5 Site-Directed MuTagenesis Kit* was used according to the manufacturer's protocol. To this end, two non-overlapping primers were designed with the help of the NEB online tool NEBase Changer™. The reverse Primer contains the complementary upstream sequence of the gene and the specific mutation and the reverse primer starts exactly at the 5' site of the specific mutation site. The whole plasmid was amplified by PCR and afterwards analyzed via gel electrophoresis. The linear PCR product was treated with the KDL enzyme-reaction-mix for 5 min at RT. The kinase phosphorylates the 5' ends of DNA to ensure the ligation by the ligase. The enzyme Dpn1 recognizes methylated DNA and digests the plasmid, which was added used for the amplification. 10 µl of the KDL-mix were mixed with 100 µl chemically competent cells and transformed.

6.2.11 Sequenz- and Ligations-Independent Cloning (SLIC)

To introduce one or more fragments into a vector-backbone sequence- and ligation- independend cloning was carried out (Li et al., 2011a; Li and Elledge, 2012). First, all DNA fragments were amplified by a PCR with primers whose 5' ends have 25 bp overlaps with the vector backbone or with the other DNA fragments. The vector backbone was linerazied by restriction digest. Afterwards, 100 ng of linearized vector and purified PCR products in a ratio of 1:2 -1:5 were mixed and incubated with T4-ligase for 2.5 min at RT.

The standard SLIC-assembly reaction was following:

Linearized vector DNA	100 ng
Insert fragments	1:2 – 1:5
T4-DNA-Ligase	0.4 µl
NEB-Buffer 2.1	1 µl
H_2O (nucleasefree)	add 10 µl

The reaction was stopped by incubation on ice for 10 min. Afterwards 5 µl of the assembly reaction were mixed with 100 µl chemically competent cells (XL1 blue) and transformed. Thus up to 5 fragments can be inserted into a vector-backbone by designing primers with 25 bp overlapping overhangs corresponding to the fragments and vector.

6.3 Methods in Protein Expression and Purification

6.3.1 Protein Expression in *E. coli*

Recombinant protein expression was carried out in Bl21 *E. coli* cells. To this end, a plasmid (pET28 or pet28SUMO) containing the gene of interest was transformd into chemically competent BL21 cells. A single colony was used to inoculate a 150 ml pre-culture and incubated while shaking at 180 rpm at 37 °C over night. Pre-warmed media (4 x 2 l dYT) was inoculated with 25 ml pre-culture (~OD_{600} = 0.1) and incubated at 37°C. Protein expression was induced by adding 1 mM Isopropyl-β-D-thiogalactopyranoside (IPTG) to each flask at OD_{600} = 0.8. Hsp90 wt and Hsp90 variants were incubated at 37 °C for 4h. Protein expression of co-chaperones took place at 30°C after induction with IPTG. Cells were harvested (12 min, 6000 rpm) and the cell pellet was suspended in buffer A and a protease inhibitor mix HP was added before shock freezing them in liquid nitrogen. All cells were stored at -80 °C until use. All subsequent steps were carried out on ice or at 4 °C.

6.3.2 Purification of Hsp90, Hsp90 Variants and Co-Chaperones

For protein purification, the cell suspension was thawed and DNase was added. Cell disruption was performed with a french press at 1.8 kbar. To separate cell fragments from soluble proteins, the cell lysate was centrifuged at high speed (45 min, 18000 rpm, 6°C).

All buffers were freshly prepared, filtered and degased prior use. As required, 1 mM DTT was added prior to use.

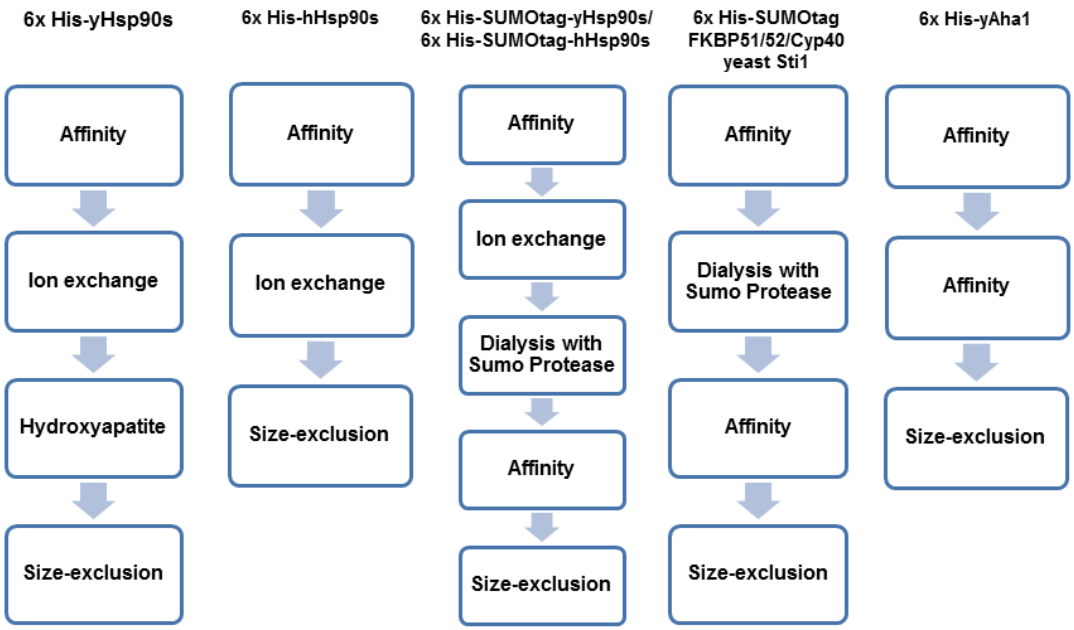

Figure 51: **Overview of different purification strategies of several Hsp90s and co-chaperones.**

List of Hsp90 purification buffers

Buffer	Compounds
Ni NTA - Buffer A	50 mM Na_2HPO_4, pH = 7.8 300 mM NaCl
Ni NTA - Buffer B	50 mM Na_2HPO_4, pH = 7.8 300 mM NaCl 500 mM Imidazol
ResQ – Buffer A	40 mM Hepes, pH = 7.5 20 mM KCl 1 mM EDTA 1 mM DTT
ResQ - Buffer B	40 mM Hepes, pH = 7.5 1 M KCl 1 mM EDTA 1 mM DTT
HAT Buffer A	20 mM KP, pH 7.5
HAT Buffer B	500 mM KP, pH 7.5
SEC - Buffer (yHsp90s)	40 mM Hepes, pH = 7.5 150 mM KCl 5 mM $MgCl_2$
SEC - Buffer (hHsp90s)	40 mM Hepes, pH = 7.5 150 mM KCl 5 mM $MgCl_2$ 1 mM DTT

List of Co-Chaperone purification buffers

Buffer	Compounds
Ni NTA - Buffer A (Aha1)	50 mM Na_2HPO_4, pH = 8.5 300 mM NaCl
Ni NTA - Buffer B (Aha1)	50 mM Na_2HPO_4, pH = 8.5 300 mM NaCl 500 mM Imidazol
SEC - Buffer (Aha1)	40 mM Hepes, pH = 8.5 300 mM KCl 1 mM DTT
Dialyse (Aha1)	40 mM Hepes, pH = 8.5 20 mM KCl 1 mM DTT
Ni NTA - Buffer A (Sti1)	50 mM Na_2HPO_4, pH = 7.8 300 mM NaCl
Ni NTA - Buffer B (Sti1)	50 mM Na_2HPO_4, pH = 7.8 300 mM NaCl 500 mM Imidazol
SEC - Buffer (Sti1)	40 mM Hepes, pH = 7.5 150 mM KCl 5 mM $MgCl_2$ 1 mM DTT

The purification of Hsp90 wt, Hsp90 variants and co-chaperones from *E.coli* lysate was achieved by several chromatography techniques depending on the used tag, cleavage site, molecular weight or chemical parameters like isoelectric point (pI) of the protein (*Figure 51*).

Affinity Chromatography

As all used constructs were N-terminally tagged with 6 histidines (6xHis), the initial step of the purification procedure was an affinity chromatography performed with a 5 ml packed *HisTrap FF* (GE Healthcare) column. The column was equilibrated, cleaned and stored according to the manufacturer's instructions (GE Healthcare). The histidine-tagged proteins were immobilized by nickel ions affinity chromatography and separated from other proteins in the lysate. To ensure removing of unspecific bound proteins to the column material, a washing step with 30 column volume of 6 % buffer B was performed. The histidine-tagged proteins were eluted by setting up a step-gradient with 10 column volume to 60 % of buffer B. The increase in imidazole competes with the histidine-tagged protein for the binding site to the nickel ions and thereby displaces the protein. The elution was collected in 5 ml fractions (note: 1 mM EDTA was added prior use to the tubes) and the fractions containing protein were detected by UV absorption at 280 nm. The column was finally washed with 10 column volume of 100 % of buffer B. The fractions containing the protein were analyzed by SDS-PAGE, then pooled and diluted in ResoureceQ buffer A to a volume of max. 150 ml.

Ion-Exchange Chromatography

Next, the protein was further purified by ion-exchange chromatography. The basic principle of ion-exchange chromatography is the reversible adsorption of macromolecules to the immobilized ion-exchange groups of opposite charge. For the purification of Hsp90, a ResourceQ (6 ml) column was applied. The column was equilibrated, cleaned and stored according to manufacturer's instructions (*GE Healthcare*). The protein was loaded on the pre-equilibrated column and washed with 10 column volumes at a flow of 4 ml/min. In a fast first step, the salt gradient was increased from 0 mM to 100 mM KCl within 10 ml, followed by a slow linear gradient by increasing the salt concentration from 100 mM KCl to 500 mM KCl within 150 ml. Here, the elution of the protein from the column takes place. Finally, the column was washed by 100 % ResourceQ buffer B. Samples were taken from the collected fractions (5 ml) containing protein and were verified via SDS-PAGE analysis. The protein containing fractions were pooled and dialyzed in a dialysis tube (Spectra/Por®; molecular porous membrane tubing; *Spectrum laboratories Inc.,* MWCO 6-8 kDa) twice for 1h against HAT buffer A at 4 °C.

Hydroxyapatite Chromatography

The hydroxyapatite chromatography is a “mixed mode” ion exchange chromatography since both anionic (Ca^{2+}, NH_4^+) and cationic groups (PO_4^{3-}, COO^-) are involved (Bernardi, 1973). The HAT column (CV 30 ml) was equilibrated with 5 column volumes of HAT buffer A. The protein was loaded onto the column and washed with 5 column volumes of HAT buffer A. Next, a linear gradient from 0 mM KP to 400 mM within 200 ml was set up to ensure separation and elution of the proteins. The protein containing fractions were analysed, pooled and concentrated by centrifugation (3800 rpm, 20 min, 4 °C) with an Amicon filter unit up to a final volume of 5 ml.

Size-Exclusion-Chromatography

Finally, size-exclusion chromatography (SEC) or also called gel-filtration chromatography was used as the last purification step for all proteins. The principle of SEC is to separate proteins in solution according to their size and shape. Small macromolecules retain longer in the matrix pores and elute later compared to larger ones. The SEC column was equilibrated, cleaned and stored according to the manufacturer’s protocol (*Pharmacia Biotech*). The column size was chosen according the size of the protein: for Hsp90 and Sti1: HiLoad 16/60 Superdex 200 prep grade; *Pharmacia Biotech*// for Aha1: HiLoad 16/60 Superdex 75 prep grade; *Pharmacia Biotech*). The concentrated protein solution was injected and the column was washed with 1 column volume of SEC buffer. The fraction size was 5 ml per fraction and the flow rate 1 ml/min. The protein-containing fractions were analysed, pooled and concentrated by centrifugation (3800 rpm, 20 min, 4 °C) with an Amicon filter unit (*Millipore*) up to a final concentration of about 100 µM. The pure protein was aliquoted, shock frozen in liquid nitrogen and kept at -80 °C until further use.

Dialysis

To exchange buffers, the protein was dialyzed against the respective buffer in a dialysis tube (Spectra/Por®; molecular porous membrane tubing; *Spectrum laboratories Inc.,* MWCO 6-8 kDa) over night at 4 °C. For smaller volumes (100 - 500 µl) a Dialysis Slide-A-Lyzer™ cassette was used.

Proteolytic Digest with SUMO Protease

In the case of N-terminal 6xHis-SUMO-tagged Hsp90, the SUMO-tag was removed after the ion-exchange chromatography. The Ubiquitin-like protease (ULP1/SUMO protease) hydrolyses a peptide bond in the sequence Gly-Gly-|-Ala-Thr-Tyr at the C-terminal end of the small ubiquitin-like modifier (SUMO) peptide (Li and Hochstrasser, 1999). To this end, 100 µl yeast SUMO protease (Ulp1) was added to the pooled fractions after IEX and at the same time the protein was dialyzed against Ni NTA buffer A over night. After cleavage, the SUMOtag and the protease were removed by a subsequent affinity chromatography. The untagged Hsp90 was collected, concentrated by centrifugation (3800 rpm, 20 min, 4 °C) with an Amicon filter unit up to a final volume of 5 ml and applied to a size-exclusion column.

6.3.3 Preparation of Yeast Cell Lysates

To determine protein levels in yeast cells, Western Blot analysis was performed. To this end, yeast cell lysates were prepared as followed. Single clones were grown at 30 °C in minimal medium (5 ml) to stationary phase. An OD_{595} of 5 of each sample were harvested (4500 rpm, 5 min). The cell pellets were washed with H_2O and the OD_{595} was measured again. Cells were spun down (4500 rpm, 5 min) and resuspended in 200 µl H_20 and 200 µl of 0.2 M NaOH were added and incubated for 3 min at RT. Cells were harvested again (13 000 rpm, 1 min) and supernatant was discarded. The pellet was resuspended in 100 µl (= OD_{600} of 5) sample buffer and boiled for 5 min at 95 °C. Proteins were separated by SDS-PAGE and blotted on a PVDF membrane for 1 h.

6.4 Protein Chemical Methods

6.4.1 Bradford Assay

The Bradford Assay is a spectroscopic method, based on the absorbance shift from 465 nm (red) to 595 nm (blue) of the chromophore upon protein binding. Here, the commercially available solution 5x Coomassie Protein Assay Reagent was diluted 1:5 in $_{dd}H_2O$. For the BSA standard curve 0, 1, 3, 5, 10, 15 and 20 µg BSA (2 mg/ml) were added to 100 µl $_{dd}H_2O$ in an eppendurf tube, respectively. To determine the protein concentrations several dilutions of the cell extract were prepared (volume of 100 µl). 1 ml of 1x Coomassie Protein Assay Reagent was added to each tube. The samples were incubated for 10 min at RT. The BSA standard curve was recorded with a spectrophotometer at 595 nm. The standard curve was used to determine the protein concentration of each sample.

6.4.2 Bicinchoninic Acid Protein Assay (BCA)

The BCA assay was performed using the Pierce^R BCA assay Kit to determine protein concentrations in a cell lysate. For the BSA standard curve 0, 1, 3, 5, 10, 15 and 20 µg BSA (2 mg/ml) were added to 10 µl $_{dd}H_2O$ in an eppendurf tube, respectively. To determine the protein concentration of the sample, 2 µl of the cell extract were added to 10 µl of $_{dd}H_2O$. Reagent A and B (Pierce) were mixed in a ratio 50:1 and 1 ml of the mixture was added to to each tube. The samples were incubated for 30 min at 37°C. The BCA standard curve was recorded with a spectrophotometer at 562 nm. The standard curve was used to determine the protein concentration of each sample.

6.4.3 SDS-Polyacrylamid-Gelelektrophoresis (SDS-PAGE)

To analyze the size of a protein and to verify its purity after purification, SDS-PAGE according to Laemmli and Fling & Gregerson was applied (Fling and Gregerson, 1986; Laemmli, 1970). The amphiphile, anionic detergent SDS attaches to the denatured protein and renders it negatively charged. The separation of a protein mixture by SDS-PAGE is based on the different time a protein, depending on the size and charge, migrates through the acrylamide gel within an electic field. A SDS-PAGE either consists of a fixed acrylamide concentration or a gradient of varying acrylamide

concentrations (4 %- 12 %). The gels were used depending on the size of the analyzed protein mixture. The composition of a self-casted gel was as followed:

	resolving gel (12.5 %)	**stacking gel (5 %)**
Acrylamid / Bisacrylamid 19:1 (40 % w/v)	3.125 ml	0.625 ml
Resolving gel-Buffer (4x)	2.5 ml	-
Stacking gel-Buffer (2x)	-	2.5 ml
APS	100 µl	100 µl
TEMED	10 µl	10 µl
H_2O	1.875	4.375

The gels were fresh prepared, placed into the electrophoresis chamber and 1x SDS running buffer was added. For sample preaparation the protein solution was mixed with 5x reducing Laemmli loading buffer and incubated at 95 °C for 5 min. 15 -20 µl prepared sample as well as a moleculare size standard mixture were loaded onto the pockets of the gel and electrophoresis was carried out at 25 mA per gel for 1h.

All buffers were prepared with H_20_{dd}.

Buffer	Compounds
SDS Running Buffer 10x	0.25 M Tris/HCl, pH = 8.0 2 M Glycine 1 % (w/v) SDS
5x Laemmli Loading Buffer	0.3 M Tris/HCl, pH = 6.8 50 % (v/v) glycerole 10 % (w/v) SDS 5 % (w/v) β-Mercaptoethanol 0.5 % (w/v) Bromphenolblue
Resolving gel-Buffer (4x)	1.5 M Tris/HCl, pH = 8.8 0.8 % (w/v) SDS
Stacking gel-Buffer (2x)	0.25 M Tris/HCl, pH = 6.8 0.4 % (w/v) SDS

Proteins were either visualized by Coomassie staining or the target protein was detected with a specific antibody by Western Blot analysis.

6.4.4 Coomassie-Staining of SDS-Gels

Coomassie Brilliant blue R binds to hydrophobic areas of a protein. After electrophoreses gels were stained according to a modified protocol provided by Fairbanks *el al.* (Fairbanks et al., 1971). To this end, the gels were heated up in Fairbanks A solution and incubated for 30 min at RT. After staining gels were rinsed with water and de-stained with Fairbanks D solution. The gels were pivotd on a shaker until stained bands became visible. Shorter destaining times were achieved by heating up the gels in Fairbanks D solution.

Buffer	Compounds
Fairbanks A	25 % (v/v) Isopropanol 10 % (v/v) Acetic acid 0.05 % (w/v) Coomassie Brilliantblue R
Fairbanks D	10 % (v/v) Acetic acid

6.4.5 Western-Blotting and Detection

To confirm the presence or absence of a specific protein, a Western Blot was performed. Proteins were separated according to their electrophoretic mobility via SDS-PAGE and transferred to a PVDF-membrane. The membrane was activated in methanol for 30 sec. The membrane, the polyacrylamide gel and the filter papers were pre-equilibrated in Western Blot Transfer Buffer for 5 min prior to stack assembly. The transfer stack consisted of three pieces of Whatman filter paper, the PVDF membrane, the polyacrylamide gel and three additional filter papers. This stack was placed on the semi-dry blotting device. Protein transfer was performed at 72 mA per gel for 1-2 h according the size of the protein. Afterwards, the membrane was blocked in blocking solution 5 % milk in PBS-T for 30 min at RT to prevent non-specific background binding of the antibodies. After blocking the membrane was briefly rinsed with PBS-T buffer and washed three times with PBS-T for 10 min at RT. Next, the blot was incubated with the primary antibody 1 h or overnight at 4 °C. After a repeated wash step as described above the membrane was incubated with horseradish peroxidase (HRP) labeled secondary antibody diluted in 1 % milk PBS-T buffer for 1 h at RT. Prior detection of the protein the membrane was rinsed and washed one more time as described above. The Western Blot was developed by using WesternBright ECL spray and an *ImageQuant LAS 4000 Imaging System* according to the manufacturer's protocol.

Buffer	**Compounds**
PBS 10x	160 mM Na_2HPO_4 , pH = 7.4 40 mM KH_2PO_4 1.15 M NaCl 27 mM KCl
PBS-Tween	PBS 1x 0.1 % Tween-20
Western-Blotting Transfer-Buffer	0.025 M Tris/HCl, pH = 8.3 192 mM Glycine 20 % (v/v) Methanol 0.12 g/l SDS

6.4.6 Protein Domain Ligation Mediated by Sortase A SrtA

Protein Expression and Purification of the N-terminal Hsp90β LPKTG-containing domain

The N-terminal domain was expressed and purified according to the standard protocol via Ni-NTA affinity chromatography and a final size-exlusion chromatography to ensure high purity.

Protein Expression and Purification of the Hsp90β MC domain

The MC-terminal protein was expressed according to the standard protocol. The expressed protein was purified using standard Ni-NTA affinity chromatography. The column was equilibrated with 50 mM Tris, pH 8.0, 150 mM NaCl, 10 mM imidizole, before loading the protein onto the column. In order to remove unspecific bound proteins and nucleic acids, the column was wash with washing buffer (50 mM Tris, pH 8.0, 150 mM NaCl, 25 mM imidazole). The bound protein was eluted with high imidazole concentration. After the first Ni-NTA column, all fractions containing the Hsp90β MC-domain (verified by SDS PAGE), are applied to TEV cleavage and dialysed against 50 mM Tris, pH 8.0, 150 mM NaCl, 2.5 mM DTT overnight at 4 °C. Subsequent, a second Ni-NTA affinity chromatography stepwas performed to remove TEV protease and the cleaved tag which bound to the column. All Hsp90β MC-domain fractions (checked by SDS PAGE) were pooled and subjected to gel filtration chromatography using a Hi-Load Superdex 75 16/60 column. The column was equilibrated with 50 mM Tris, pH 8.0, 150 mM NaCl. Finally the pure protein was pooled, concentrated up to 100 µM and and stored until use at -80 °C.

SrtA mediated Domain Ligation and Isolation of the ligated Product

The ligation of multi-domains proteins can be achieved by using the *S. aureus* transpeptidase Sortase A (SrtA) (Freiburger et al., 2015; Kobashigawa et al., 2009; Levary et al., 2011). The SrtA is a membrane-ancored protein which catalysis a reaction at a Leu-Pro-Xxx-Thr-Gly motif of a protein (Mao et al., 2004). This motif is cleaved by SrtA between threonine and glycine and then covalently linked to the carboxyl group of threonine to an amino group of glycine of a peptidoglycan located at the cell wall. The reaction takes place in two steps: First, the SrtA recognizes the LPXTG motif N-terminal of a peptide or protein and binds to it by forming a reactive thioester –acyl-intermediate between the threonine of the motif and a cysteine located in the active center of the enzyme. The thioester-intermediate is attacked by a nucleophile amnio group of a glycine of the second peptide or protein and forms a peptide bond.

Freiburger *et al.* (Freiburger et al., 2015; Lorenz et al., 2014) earlier described an optimized strategy for segmenetal labeling of yeast Hsp90 mediated by SrtA. The protein domains (human Hsp90β N-domain and human Hsp90 MC-domain) were purified as described above. The ligation reaction was performed in a Amicon centrifugation filter unit (cut off 10 kDa) with 5 mg of each domain, as well as 5 mg of SrtA in Ligation buffer (50 mM Tris, pH 8.0, 150 mM NaCl, 20 mM $CaCl_2$,) in a final volume of 15 ml). The ligation was started by adding 10 mM $CaCl_2$ and was incubated while concentrated (2.000 rpm) over 4 h at 20 °C. Every 20 min ligation buffer was added to a final volume of 15 ml. Afterwards, affinity chromatography was applied to separate educts and ligation products. The purification of the ligated product was performed by a Ni-NTA affinity chromatography as described earlier. The column was equilibrated with 50 mM Tris, pH 8.0, 150 mM NaCl before loading the protein solution onto the column. The column was washed with wash buffer (50 mM Tris, pH 8.0, 150 mM NaCl, and containing 20 mM and 500 mM imidazole) before eluting the bound ligated protein with high imidazole. All fractions containing mostly ligated protein were subjected to TEV protease cleavage and dialysed against 50 mM Tris, pH 8.0, 150 mM NaCl, and 2.5 mM DTT overnight at 4 °C. Afterwards the ligated protein was separated from the TEV protease and the N-terminal 6x Histag by a second Ni-NTA column. All fractions containing solely the ligated product were pooled and concentrated up to desired concentration. The ligation kinetics, efficiency and subsequent purification steps were determined by SDS-PAGE analysis.

6.4.7 Incorporation of an Unnatural Amino Acid

To test the incorporation of an unnatural amino acid (UAA) into human Hsp90, a small-scale approach was applied. To this end, chemically competent BL21 *E. coli* cells were transformed with two plasmids. One encodes the N-terminal histidine-tagged gene of interest (goi), containing the amber stop codon (TAG) at the respective position, and the other plasmid (pKW1) provided the wt synthetase/tRNA pair. After the transformation the cells were directly transferred into 50 ml LB_0 media supplied with the respective antibiotics and was incubated over night at 37 °C. Next, a fresh 50 ml culture was inoculated with the pre-culture to an OD_{600} of 0.1 and was further incubated at 37 °C until OD_{600} of 0.3 was reached. Then, the culture was split into 5 ml cultures and the respective UAA (1-2 mM UAA in NaOH) was added. As a negative control one culture was treated with the same volume of solvent (50 µl NaOH). Before induction, a sample was taken (0 h). The induction of expression was induced at OD_{600} of 0.7 with 1 mM IPTG and the cultures were incubated either at 25°C or 37°C. Further samples were taken at 4 h and 16 h. For sample preparation, 1 ml of the cell

suspension was taken and OD_{600} was measured. An OD_{600} of 0.5 was transferred into an Eppendorf tube and harvested by centrifugation (4500 rpm, 5 min). The supernatant was removed, the pellet was resuspended in 50 µl 5x Laemmli, boiled for 5 min at 95 °C and stored at -20°C until use. Before analysis of protein expression samples were further diluted in 1x Laemmli (1:5) and 20 µl of each sample was applied to a precast SERVAGel™ TG PRiME™ SDS-PAGE (4-12 %). Electrophoresis was carried out at 20 mA per gel for 1.5 h. Afterwards, the proteins were transferred on a activated PVDF membrane for Western Blotting. The presence of the respective proteins, full-length as well as the truncated version was detected with an HRP-coupled antibody against the histidine-tag.

6.4.8 Protein Labeling with Fluorocent Dyes

To ensure specific and high sensitive fluorescence detection, proteins can be modified with commercially available fluorescenct dyes by protein chemistry. To this end, the dye is covalenty coupled site-specifically to a side chain of a protein.

Protein Labeling with 5-Carboxyfluorescine (5(6)-FAM)

Aha1 and Sti1 were labeled with 5(6)-FAM via a reactive succimidyl ester group to lysine (Invitrogen, Karlsruhe, Germany) according to the manufacturer's protocol. In brief, the protein was dialyzed against labeling buffer A over night at 4 °C. The protein was diluted in buffer A to a volume of 1 ml. Next, labeling buffer B was added in a ration of 1:20. The dye was diluted in DMSO and a 2-fold excess of dye was added to the protein solution. The labeling reaction either took place 2 h at RT or over night at 4 °C. Free label was removed via a Superdex 75 FPLC (Pharmacia Biotech). The labeled protein was concentrated and the degree of labeling (DOL) was determined by UV-VIS spectroscopy:

$$DOL\ [\%] = \frac{A_{max} \cdot \varepsilon_{Protein}}{(A_{280} - A_{max} \cdot CF_{280}) \cdot \varepsilon_{max}}$$

Equation 2

$\varepsilon_{Protein}$ = molare extinctioncoeffizient of the protein at 280 nm

ε_{max} = molare extinctioncoeffizient of the label A_{max}

A_{max} = Absorption at λ_{max}

A_{280} = Absorption at 280 nm

CF_{280} = correction factor of the label at 280 nm

Protein Labeling with Atto-Maleimid-Conjugates

Labeling of the Hsp90 cysteine variants was performed with ATTO-488 maleimid and ATTO- 550 maleimid (ATTO-TEC, Siegen, Germany) according to the manufacturer's protocol. p23 was labeled via an engineered cysteine at position 2 with 5-iodacetamido-fluorescein (Invitrogen, Karlsruhe, Germany). In brief, in a first step DTT was eliminiated via a Superdex 75 FPLC system to ensure free cysteines. The DTT-free protein sample was mixed with an excess of the ATTO-dye and incubated for 1.5 h at RT according to the ATTO-TEC manual. To stop the labeling reaction 5 mM of DTT was added to each sample followed by further incubation and shaking of the labeled proteins (30 min; RT). Remaining free label and excess DTT were removed by applying the samples to the HPLC column. The labeled protein was distinguished from the free label according to size and detection of the UV signal (280 nm) as well as of the fluorescence signal (Jasco FP 1520S) of the used label. The labeled protein was concentrated and the degree of labeling (DOL) was determined by UV-VIS spectroscopy as described above.

6.4.9 Limited Proteolysis

Hsp90 (10 µM) was incubated with 1:25 (w:w) α-chymotrypsin (Sigma) in 100 mM Tris, 100 mM NaCl, 10 mM $CaCl_2$, pH 7.8 at 25°C for 90 min. Proteolysis reactions were terminated with 2 mM phenylmethylsulfonyl fluoride (Sigma) after various time points and analyzed by SDS-PAGE on 4-12 % acrylamide gels followed by Coomassie blue staining.

6.5 Biophysical Methods

Spectroscopic methods provide a wide range of different tools to characterize proteins. The principle is based on electromagnetic raddiation of a typical wavelength and intensitiy which is exposed on atoms, ions and molecules, that either absorbs, scatter or emits it.

6.5.1 Absorbance Spectroscopy

Proteins have two functional groups that absorb UV light. On the one hand the peptide bonds (180-220 nm) and on the other hand the aromatic amino acids tryptophan, thyrsoine and phenylalanin, which have their highest absorptions peak at 280 nm. To determine the concentration of a purified protein, a UV spectrum of a diluted protein solution as well as the buffer solution was recorded (200-340 nm) using a Varian Cary50 UV-Vis spectrophotometer. The buffer spectrum was substracted from the protein spectrum. The protein concentration can be estimated at the wavelength 280 nm using the law of Lambert-Beer:

$$A_{280} = \varepsilon_{280} \cdot c \cdot d$$

Equation 3

with A: Absorbance, ε_{280}: molar extinction coefficient (M^{-1} cm^{-1}), c: molar protein concentration (M) and d: thickness of the cuvette (cm). The used extinction coefficient ε_{280} of all proteins were calculated by the online tool protparam (www.expasy.org).

6.5.2 Circular Dicroism Spectroscopy

Circular dicroism (CD) spectroscopy is a specific form of absorbance spectroscopy that relies on the interaction with chiral macromolecules. Due to differences in absorbance, of right- or left-circular polarized light, by an analyzed protein, secondary structure elements can be determined. For recording spectra, the proteins were dialyzed overnight against CD buffer (50 mM NaP, pH 7.5) and diluted to a final concentration of 0.2 mg/ml. For Far-UV analysis, spectra were measured at 20 °C between 260 nm and 195 nm and the data was corrected by the absorption of the corresponding buffer spectrum. For normalization the measured ellipticity was converted into the residual ellipticity $[\Theta]_{MRW}$ with the following equation:

$$[\Theta_{MRW}] = \frac{[\Theta] \cdot M_r \cdot 100}{d \cdot c \cdot (N_{aa} - 1)}$$

Equation 4

Here, [Θ] is the measured ellipticity in degree, M_r is moleculare weight of the protein in g/mol, d the thickness of the cuvette, c the concentration in mg/ml and *Naa* the number of amino acids.

6.5.3 Thermo Shift Assay

The thermo shift assay (TSA) is a tool to determine the change in thermal denaturation temperature of a protein. The dye Sypro^R Orange binds non-specifically to hydrophobic areas of proteins and in water its fluorescence is quenched. Due to increasing temperature a protein unfolds and exposes these hydrophobes patches where Sypro^R Orange starts to bind which results in an increase in the fluorescence signal. The thermo shift assay was performed with a real time PCR-cycler (Agilent Technologies Stratagene Mx3000P). 5 µg of each Hsp90 variant was used in a total reaction volume of 20 µl in the presence of Sypro^R Orange (5x). The change of the sypro-orange fluorescence signal after excitation at 475 nm and emission at 590 nm with increasing temperature (1 °C per minute) was monitored. The measurements were performed in 40 mM Hepes/KOH pH 7.5, 150 mM KCl, and 5 mM $MgCl_2$. The melting temperatures were calculated by using the 2nd derivative. For each Hsp90 variant, at least triplicate measurements were performed.

6.5.4 Fluorescence Spectroscopy

After excitation of a molecule in its higher energy state, it ends up in its ground state via different possibilities: One important process is fluorescence ($S_1 \rightarrow S_0$). A molecule loses energy as heat by going through all vibronic levels of all excited singlet states (vibrational relaxtion). Another type of nonradiative transition, called internal conversion (IC), occurs when a molecule returns from the excited vibrational level (S_1) to its ground state (S_0) or converts to a triplet state which is called intersystem crossing (ISC).

Fluorescence Resonance Energy Transfer

A specific tool of fluorescence spectroscopy called fluorescence resonance energy transfer (FRET) is used to study protein-protein interactions and conformational changes within a protein. Here, an excited fluorescent molecule (donor) transfers energy non-radiative in close proximity (<10 nm) to a second fluorophor (acceptor). In order for FRET to occur, dipole-dipole interaction have to take place between the two fluorophores. Another requirement for FRET is an overlap of the emission spectrum of the donor with the absorption spectrum of the acceptor. The FRET efficiency (ET) is strongly dependent on the distance between the donor and the acceptor fluorophor (r). R_0 is for each donor-acceptor fluorophor pair the typical distance at which the FRET efficiency is 50 %.

$$\mathrm{E}_T = \frac{1}{\left(1 + \left(\frac{r}{R_0}\right)^6\right)}$$

Equation 5

The Hsp90 FRET-System

To monitor conformational changes within the Hsp90 dimer and upon nucleotide and/or co-chaperone binding, a previously established yeast Hsp82 FRET setup was used (Hessling et al., 2009). To this end, both yeast Hsp90 isoforms and human Hsp90 were site-specifically labeled as descibed in section 4.4.8 with a donor dye (ATTO-488 maleimide) and an acceptor dye (ATTO-550 maleimide). To form a hetero-competent Hsp90 FRET complex, the donor- and acceptor labeled Hsp90 were mixed (400 nM) in standard FRET buffer (40 mM Hepes, pH = 7.5, 150 mM KCl, 5 mM $MgCl_2$) in a total volume of 150 µl. All measurements were recorded at 30 °C.

To analyze the conformational rearrangements after nucleotide binding, Hsp90 heterodimers (400 nM) were formed by mixing an equal amount of donor-labeled and acceptor-labeled Hsp90 in standard buffer as described above. The experiment was started by addition of 2 mM nucleotide (ATP, ATPγS, AMP-PNP) and the increase of fluorescence intensity was recorded using a Fluoromax 3 or Fluoromax 2 fluorescence spectrophotometer with detection at 575 nm after excitement at 490 nm. All measurments were performed at 30 °C. The apparent rate constants of the conformational changes were determined by fitting the data to mono-exponential function using the Origin software (OriginLab Corporation, Northhampton, USA).

Chase experiments were performed to determin N-terminal or C-terminal dimerization stability. After heterodimer formation, the subunit exchange was recorded by addition of a 10-20 fold excess

of unlabeled Hsp90 wt and the decay of fluorescence intensity was recorded using a Fluoromax 3 or Fluoromax 2 fluorescence spectrophotometer at 575 nm after excitement at 490 nm at 30 °C. For experiments in the presence of different nucleotides (ATP, ATPγS, AMP-PNP) and/or 4 µM co-chaperone, Hsp90 variants were pre-equilibrated 30 min in the presence of 2 mM of the respective nucleotide to allow the formation of the closed state. The apparent half-life of the reaction was determined by fitting the data using the function for exponential decay in the Origin software (OriginLab Corporation, Northhampton, USA).

6.5.5 Isothermal Titration Calorimetry

To determine the binding affinity, enthalphy changes and binding stoichiometry of the interaction between small molecules, like nucleotides, and Hsp90, isothermal titration calorimetry (ITC) was applied. Prior to measurements, Hsp90 N-domain was dialyzed against freshly prepared ITC buffer (40 mM Hepes, pH 7.5, 150 mM KCl, 5 mM $MgCl_2$). The same buffer was used to prepare the ligand stock solution. The concentration of the Hsp90 ND stock solution was 20 - 40 µM (10 µM) and the ATP stock solution was 6 mM (100 µM radiciol). The measurements were performed with a MicroCal PEAQ ITC (Malvern Instruments Ltd, Malvern, UK). To record a binding curve between Hsp90 and the small molecule, the ligand was titrated in precisely known aliquots into the raction chamber containing Hsp90 N-domain. A reference cell was filled up with the same buffer except Hsp90. To run an experiment the MicroCal ITC control software and the proposed setup of the software was used. All ITC measurements were carried out at 25 °C. Data analyzis was carried out with the MicroCal user software.

6.5.6 Analytical Ultracentrifugation

To analyze the binding of Fluorescein-Sba1, 5(6-)FAM-Aha1 and ATTO 488-GR to Hsp90, analytical ultracentrifugation was performed in a Beckman ProteomeLab XL-A (Beckman, Krefeld, Germany) equipped with a fluorescence-detection system (Aviv Biomedica, Lakewood, USA). Sedimentation-velocity experiments were performed with labeled protein supplemented with various combinations of unlabeled proteins in standard low salt AUC buffer (40 mM Hepes, pH = 7.5, 20 mM KCl, 5 mM $MgCl_2$) in a total volume of 350 µl at 42,000 rpm. A Ti-50 Rotor (Beckman) was used and all measurements were performed at 20 °C. To determine the size of complexes, the raw data were

converted to *dc/dt* profiles by subtracting nearby scans and converting the difference into *dc/dt* plots as described (Stafford, 1992). The plots generally correlated with those from the SEDVIEW dc/dt program (Hayes and Stafford, 2010). *dc/dt* profiles were analyzed to determine the *s*-values and the areas of the corresponding peaks.

6.5.7 Small Angle X-Ray Scattering (SAXS)

SAXS data for solutions of the nucleotide-free, ATP-, and ATPγS bound forms of wt yeast Hsp90 and Hsp90 mutants were recorded with the help of Dr. Tobias Madl on an in-house SAXS instrument (SAXSess mc2, Anton Paar, Graz, Austria) equipped with a Kratky camera, a sealed X-ray tube source and a two-dimensional Princeton Instruments PI•SCX:4300 (Roper Scientific) CCD detector. The scattering patterns were measured with a 60-min exposure time (360 frames, each 10 seconds) for several solute concentrations in the range from 0.8 to 3.3 mg/ml. Radiation damage was excluded based on a comparison of individual frames of the 60-min exposures, where no changes were detected. A range of momentum transfer of $0.012 < s < 0.63$ Å^{-1} was covered

$$s = \frac{4\pi * \sin(\theta)}{\lambda}$$

Equation 6

2 θ is the scattering angle and λ = 1.5 Å is the X-ray wavelength.

All SAXS data were analyzed with the package ATSAS (version 2.5). The data were processed with the SAXSQuant software (version 3.9), and desmeared using the program GNOM (Svergun, 1992). The forward scattering, I(0), the radius of gyration, Rg, the maximum dimension, D_{max}, and the inter-atomic distance distribution functions, (P(R)), were computed with the program GNOM (Svergun, 1992). The masses of the solutes were evaluated by comparison of the forward scattering intensity with that of a human serum albumin reference solution (molecular mass 69 kDa).

6.6 Activity Assays for Proteins *in vitro*

6.6.1 Regenerative ATPase Assay

The ATPase activities of all Hsp90 variants were determined using an enzymatic-coupled regenerative ATPase assay (Richter et al., 2008). To ensure the presence of a constant amount of ATP an ATP-regenerative system with the enzymes pyruvate kinase (PK), lactate dehydrogenase (LDH) and the co-factors phosphoenolpyruvate (PEP) and NADH was used.

$$ATP + H_2O \xrightarrow{Hsp90} ADP + P_i$$

$$PEP + ADP \xrightarrow{pyruvate\ kinase} Pyruvate + ATP$$

$$Pyruvate + NADH \xrightarrow{lactate\ dehydrogenase} Lactate + NAD^+$$

The ATPase activity is measuread indirectly via the NADH concentration at 340 nm. The consumption in NADH is directly proportional to the decrease in ATP concentration. For all ATPase measurements, standard buffer (40 mM Hepes, pH = 7.5, 150 mM KCl, 5 mM $MgCl_2$) was used.

First, a 2 x ATPase premix was prepared as followes:

4328 µl	Assay-Buffer (HKM)
240 µl	Phosphoenolpyruvate (100 mM in HKM)
48 µl	NADH (50 mM in HKM)
44 µl	Lactatdehydrogenase solution
12 µl	Pyruvatkinase solution

Before starting, all components except ATP were mixed in a cuvette and incubated for 5 min at 30 °C for yeast Hsp90 and for human Hsp90 at 37 °C as followes:

75 µl	2x ATPase Premix
3 µM or 10 µM	yHsp90 or hHsp90
2 mM	ATP
fill up to 150 µl	standard buffer

In general, adding ATP to the cuvettes started the reaction and the absorbance of NADH at 340 nm was followed for 30-45 min in a *Varian Cary 50 UV-Vis-Spectrophotometer*. To verifiy specific Hsp90 ATPase activity, the Hsp90 inhibitor radicicol (100 nM) was added to the reaction and a second slope

was monitiored and substracted from the first one. The data was analyzed using linear regression and the specific enzymatic Hsp90 activity was calculated using the extinction coefficient of NADH of 6200 $M^{-1}cm^{-1}$, the respective Hsp90 concentration and the following equation:

$$k_{cat} = -\frac{dA}{dt} \cdot \frac{1}{\varepsilon_{NADH} \cdot c(Hsp90) \cdot d}$$

Equation 7

k_{cat} =specific activity in min^{-1}

ε(NADH) = molar extinction coefficient of NADH in $M^{-1}cm^{-1}$

c(Hsp90) = concentration of Hsp90 in M

d = thickness of the cuvette in cm

For analysis of a k_d value, the determined k_{cat} values were plotted as a function of the used concentrations using the following equation:

$$k_{cat} = A \cdot \frac{x}{x + k_d} + c$$

Equation 8

6.7 Activity Assays for Proteins *in vivo*

Hsp90 is essential in yeast. Hence, to analyze Hsp90 variants *in vivo*, the respective Hsp90 plasmids were introduced by a yeast shuffling approach in *S. cerevisiae*. Afterwards, yeast cells carring the plasmid containing the Hsp90 variant as sole Hsp90 source, cells were exposed to several stress factors such as heat stress, UV radiation or known Hsp90 inhibitors. Furthermore, the activation of known Hsp90 clients was investigated.

6.7.1 5'-FOA Plasmid Shuffling Assay

The *in vivo* functionality of the different Hsp90 variants was tested using a plasmid shuffling approach, based on the system described previously (Nathan and Lindquist, 1995). The ΔPCLDα *Saccharomyces cerevisiae* strain (a derivative of W303) obtained from Susan Lindquist's lab (Nathan and Lindquist, 1995) was used. This yeast strain is deficient for genomic hsp82 and hsc82 and contains a plasmid coding for hsp82 wt to rescue lethality. This plasmid pKAT6 carries an URA selection marker, which enables a selection for cells that had lost the wt hsp82 plasmid in the medium supplemented with 5-FOA. Hsp90 wt and the Hsp90-variants were constitutively expressed

from a 2 micron high-copy number plasmid under the control of a constitutive glyceraldehyde-3-phosphate dehydrogenase gene (GPD) promotor (p423GPD vector). The cells surviving the shuffling were tested for loss of the URA-plasmid by plating out on respective selection media lacking URA.

6.7.2 Temperature Sensitivity

Drop dilution assays were performed in order to study the influence of various Hsp90 mutants on the growth of *S. cerevisiae* cells. After 5-FOA, a few colonies were plated onto histidine and leucine (-His/-Leu)-depleted media. After a two-day incubation time at 30 °C liquid –His/-Leu media were inoculated and incubated again (30 °C; 18 h). The OD_{600} of the cultures were measured and set to 0.5 by diluting with –His/-Leu medium. The first dilution sample had a total volume of 1 mL. Based on this first dilution sample, a serial dilution consisting of five more 1:5 dilutions with a sample volume of 200 µL each were created. The serial dilution was finally plated on –His/-Leu medium, using 5 µL of sample per drop. Every dilution step 1-6 per mutant is plated when studying the growth at different temperatures (24 °C, 30 °C and 37 °C).

6.7.3 Radicicol Sensitivity

Radicicol is a natural inhibitor that competes with ATP for the Hsp90 ATP binding pocket and thereby inhibits its ATPase activity (Roe et al., 1999). To investigate the inhibitor sensitivity of Hsp90 variants, yeast cells were grown in liquid –His/-Leu media and incubated at 30 °C over night. The OD_{600}s of the cultures were measured and set to 0.1 (sample volume 2 ml) by diluting with –His/-Leu medium containing different radicicol concentrations. As a control, a sample was treated with DMSO. Next, yeast cells were further incubated at 30 °C until the next morning. A serial dilution was prepared as described above and spotted onto -His/-Leu medium, using 5 µL of sample per drop. The difference in yeast growth was obtained after incubation at least 48 h at 30 °C.

6.7.4 Nucleotide Excision Repair Assay

To study the Hsp90 nucleotide excision repair process, yeast cells were grown and serial dilutions were prepared as described previously (Soroka et al., 2012). In brief, yeast cells were spotted onto media and plates were exposed (without the lid of the petri dish) to UV-light radiation (80 x 100 $\mu J/cm^2$, 10 seconds) with a CL-100 Ultraviolet Crosslinker devise (UVP, inc.). As a control, one plate was not exposed to UV-light. The growth of each Hsp90 variant was compared to wt Hsp90 present on every plate. Yeast cell growth was documented after 48 h.

6.7.5 Glucocorticoid Receptor Activity Assay

To study *in vivo* functionality of Hsp90, client processing was investigated in more detail. The clients used are strictly Hsp90-dependent. One of the best studied Hsp90 clients is the glucocorticoid receptor (GR), which is strongly dependent on Hsp90 activity (Nathan and Lindquist, 1995).

Here, GR processing by Hsp90 was measured indirectly via a β-galactosidase reporter assay. The β-galactosidase gen (lacZ) is regulated by three hormone response elements (HRE). Binding of mature hormone-bound-GR to the HREs induce the expression of β-galactosidase from the lacZ gen. β-galactosidase hydrolyzes the artificial substrate ortho-nitrophenyl-β-D-galactopyranoside (ONPG) to galactose and ortho-nitrophenol which can be used to quantifiy enzyme activity and therefore GR processing by Hsp90. To this end, yeast cells expressing the Hsp90 variant as the sole Hsp90 source were transformed with a plasmid containing the GR gene and selected for positive yeast colonies. Single colonies were used to inoculate 400 µl selective yeast media in a 96-well plate and incubated over night at 30 °C. Next, the pre-cultures were diluted 1:20 in 200 µl selective media containing 10 µM of the receptor-activating hormone-analogon 11-Desoxycorticosterone (DOC) and yeast cells were further incubated for 4 h (log-phase) or over night (stationary phase) at 30 °C. To quantify β-galactosidase activity, 50 µl yeast cell suspension was harvested (4500 rpm, 5 min, RT), the supernatant was discarded and cells were lysed in 150 µl SDS-Buffer for 10 min under constant shaking (850 rm). Afterwards 50 µl of the substrate ONPG (4 mg/ml in Z-Buffer) was added to each well. Subsequently, the change in absorbance of the solution was measured at 405 nm in a Teacan Plate-Reader for 30 min at RT. Furthermore, the cell density was obtained. The GR activity was divided by the cell density and all values were normalized to the wt levels. For the determination of the GR activity at least five technical replicates starting from single colonies were carried out.

Buffer	Compounds
SDS-Buffer (GR-Assay)	82 mM Na_2HPO_4, pH = 7.5 12 mM NaH_2PO_4 0,1 % (w/v) SDS
Z-Buffer (GR-Assay)	100 mM Na_2HPO_4, pH = 7.0 15 mM KCl 5 mM $MgSO_4$

6.7.6 v-Src Maturation Assay

To further investigate *in vivo* functionality of Hsp90 in terms of client processing, viral Src kinase (v-Src) activation was tested. The kinase v-Src is known as a retro-viral oncogen whose expression in host cells causes unspecific phosphorylation of the host proteome (Vogt, 2012). As yeast cells exhibit less intrinsic tyrosine kinase activity (Xu et al., 1999), expression of v-Src leads to hyperphosphyrolation of the yeast proteins and thereby induces lethality (Brugge et al., 1987). v-Src activation in yeast is strongly Hsp90-dependent and a well-established tool to study Hsp90 client maturation (Xu and Lindquist, 1993). The assay was performed as described in the literature (Nathan and Lindquist, 1995). In brief, yeast cells carring the respective plasmid as the sole Hsp90 source were transformed with an additional plasmid containing the v-Src gene under the control of a galactose-inducible promotor and a URA selection marker. Single colonies were used to inoculate an over night pre-culture in -URA/-His/-Leu media. Next, the pre-culture was diluted in medium containing raffinose as sugar source and further incubated at 30 °C until the stationary growth phase was reached. Afterwards, cell cultures were serially diluted as described above and spotted on media containing glucose (control) and on media plates containing galactose as the sugar source (v-Src expression).

References

Abu-Farha, M., Lanouette, S., Elisma, F., Tremblay, V., Butson, J., Figeys, D., and Couture, J.F. (2011). Proteomic analyses of the SMYD family interactomes identify HSP90 as a novel target for SMYD2. Journal of molecular cell biology *3*, 301-308.

Ali, M.M., Roe, S.M., Vaughan, C.K., Meyer, P., Panaretou, B., Piper, P.W., Prodromou, C., and Pearl, L.H. (2006). Crystal structure of an Hsp90-nucleotide-p23/Sba1 closed chaperone complex. Nature *440*, 1013-1017.

Anfinsen, C.B. (1973). Principles that govern the folding of protein chains. Science *181*, 223-230.

Baird, T.D., and Wek, R.C. (2012). Eukaryotic initiation factor 2 phosphorylation and translational control in metabolism. Advances in nutrition *3*, 307-321.

Balch, W.E., Morimoto, R.I., Dillin, A., and Kelly, J.W. (2008). Adapting proteostasis for disease intervention. Science *319*, 916-919.

Balchin, D., Hayer-Hartl, M., and Hartl, F.U. (2016). In vivo aspects of protein folding and quality control. Science *353*, aac4354.

Bansal, P.K., Mishra, A., High, A.A., Abdulle, R., and Kitagawa, K. (2009). Sgt1 dimerization is negatively regulated by protein kinase CK2-mediated phosphorylation at Ser361. The Journal of biological chemistry *284*, 18692-18698.

Bardwell, J.C., and Craig, E.A. (1987). Eukaryotic Mr 83,000 heat shock protein has a homologue in Escherichia coli. Proceedings of the National Academy of Sciences of the United States of America *84*, 5177-5181.

Bartlett, A.I., and Radford, S.E. (2009). An expanding arsenal of experimental methods yields an explosion of insights into protein folding mechanisms. Nature structural & molecular biology *16*, 582-588.

Bergerat, A., de Massy, B., Gadelle, D., Varoutas, P.C., Nicolas, A., and Forterre, P. (1997). An atypical topoisomerase II from Archaea with implications for meiotic recombination. Nature *386*, 414-417.
Bernardi, G. (1973). Chromatography of proteins on hydroxyapatite. Methods in enzymology *27*, 471-479.

Blank, M., Mandel, M., Keisari, Y., Meruelo, D., and Lavie, G. (2003). Enhanced ubiquitinylation of heat shock protein 90 as a potential mechanism for mitotic cell death in cancer cells induced with hypericin. Cancer research *63*, 8241-8247.

Blatch, G.L., and Lassle, M. (1999). The tetratricopeptide repeat: a structural motif mediating protein-protein interactions. BioEssays : news and reviews in molecular, cellular and developmental biology *21*, 932-939.

Boczek, E.E., Reefschlager, L.G., Dehling, M., Struller, T.J., Hausler, E., Seidl, A., Kaila, V.R., and Buchner, J. (2015). Conformational processing of oncogenic v-Src kinase by the molecular chaperone Hsp90. Proceedings of the National Academy of Sciences of the United States of America *112*, E3189-3198.

Borkovich, K.A., Farrelly, F.W., Finkelstein, D.B., Taulien, J., and Lindquist, S. (1989). hsp82 is an essential protein that is required in higher concentrations for growth of cells at higher temperatures. Molecular and cellular biology *9*, 3919-3930.

Bose, S., Weikl, T., Bugl, H., and Buchner, J. (1996). Chaperone function of Hsp90-associated proteins. Science *274*, 1715-1717.

Brockwell, D.J., and Radford, S.E. (2007). Intermediates: ubiquitous species on folding energy landscapes? Current opinion in structural biology *17*, 30-37.

Brugge, J.S., Jarosik, G., Andersen, J., Queral-Lustig, A., Fedor-Chaiken, M., and Broach, J.R. (1987). Expression of Rous sarcoma virus transforming protein pp60v-src in Saccharomyces cerevisiae cells. Molecular and cellular biology *7*, 2180-2187.

Calloni, G., Chen, T., Schermann, S.M., Chang, H.C., Genevaux, P., Agostini, F., Tartaglia, G.G., Hayer-Hartl, M., and Hartl, F.U. (2012). DnaK functions as a central hub in the E. coli chaperone network. Cell reports *1*, 251-264.

Carrigan, P.E., Nelson, G.M., Roberts, P.J., Stoffer, J., Riggs, D.L., and Smith, D.F. (2004). Multiple domains of the co-chaperone Hop are important for Hsp70 binding. The Journal of biological chemistry *279*, 16185-16193.

Chatterjee, C., and Muir, T.W. (2010). Chemical approaches for studying histone modifications. The Journal of biological chemistry *285*, 11045-11050.

Chen, B., Retzlaff, M., Roos, T., and Frydman, J. (2011). Cellular strategies of protein quality control. Cold Spring Harbor perspectives in biology *3*, a004374.

Chen, B., Zhong, D., and Monteiro, A. (2006). Comparative genomics and evolution of the HSP90 family of genes across all kingdoms of organisms. BMC genomics *7*, 156.

Chen, C.Y., and Balch, W.E. (2006). The Hsp90 chaperone complex regulates GDI-dependent Rab recycling. Molecular biology of the cell *17*, 3494-3507.

Chen, W.Y., Chang, F.R., Huang, Z.Y., Chen, J.H., Wu, Y.C., and Wu, C.C. (2008). Tubocapsenolide A, a novel withanolide, inhibits proliferation and induces apoptosis in MDA-MB-231 cells by thiol oxidation of heat shock proteins. The Journal of biological chemistry *283*, 17184-17193.

Cheung-Flynn, J., Prapapanich, V., Cox, M.B., Riggs, D.L., Suarez-Quian, C., and Smith, D.F. (2005). Physiological role for the cochaperone FKBP52 in androgen receptor signaling. Molecular endocrinology *19*, 1654-1666.

Clavaguera, F., Grueninger, F., and Tolnay, M. (2014). Intercellular transfer of tau aggregates and spreading of tau pathology: Implications for therapeutic strategies. Neuropharmacology *76 Pt A*, 9-15.

Cunningham, C.N., Southworth, D.R., Krukenberg, K.A., and Agard, D.A. (2012). The conserved arginine 380 of Hsp90 is not a catalytic residue, but stabilizes the closed conformation required for ATP hydrolysis. Protein science : a publication of the Protein Society *21*, 1162-1171.

Davies, T.H., Ning, Y.M., and Sanchez, E.R. (2005). Differential control of glucocorticoid receptor hormone-binding function by tetratricopeptide repeat (TPR) proteins and the immunosuppressive ligand FK506. Biochemistry *44*, 2030-2038.

Dill, K.A., and Chan, H.S. (1997). From Levinthal to pathways to funnels. Nature structural biology *4*, 10-19.

Dittmar, K.D., Demady, D.R., Stancato, L.F., Krishna, P., and Pratt, W.B. (1997). Folding of the glucocorticoid receptor by the heat shock protein (hsp) 90-based chaperone machinery. The role of p23 is to stabilize receptor.hsp90 heterocomplexes formed by hsp90.p60.hsp70. The Journal of biological chemistry *272*, 21213-21220.

Dobson, C.M. (2003). Protein folding and misfolding. Nature *426*, 884-890.

Dobson, C.M., and Karplus, M. (1999). The fundamentals of protein folding: bringing together theory and experiment. Current opinion in structural biology *9*, 92-101.

Donlin, L.T., Andresen, C., Just, S., Rudensky, E., Pappas, C.T., Kruger, M., Jacobs, E.Y., Unger, A., Zieseniss, A., Dobenecker, M.W.*, et al.* (2012). Smyd2 controls cytoplasmic lysine methylation of Hsp90 and myofilament organization. Genes & development *26*, 114-119.

Donze, O., and Picard, D. (1999). Hsp90 binds and regulates Gcn2, the ligand-inducible kinase of the alpha subunit of eukaryotic translation initiation factor 2 [corrected]. Molecular and cellular biology *19*, 8422-8432.

Doyle, S.M., Hoskins, J.R., and Wickner, S. (2007). Collaboration between the ClpB AAA+ remodeling protein and the DnaK chaperone system. Proceedings of the National Academy of Sciences of the United States of America *104*, 11138-11144.

Duttler, S., Pechmann, S., and Frydman, J. (2013). Principles of cotranslational ubiquitination and quality control at the ribosome. Molecular cell *50*, 379-393.

Duval, M., Le Boeuf, F., Huot, J., and Gratton, J.P. (2007). Src-mediated phosphorylation of Hsp90 in response to vascular endothelial growth factor (VEGF) is required for VEGF receptor-2 signaling to endothelial NO synthase. Molecular biology of the cell *18*, 4659-4668.

Echtenkamp, F.J., and Freeman, B.C. (2012). Expanding the cellular molecular chaperone network through the ubiquitous cochaperones. Biochimica et biophysica acta *1823*, 668-673.

Ellis, J. (1987). Proteins as molecular chaperones. Nature *328*, 378-379.

Ellis, R.J. (2001). Macromolecular crowding: obvious but underappreciated. Trends in biochemical sciences *26*, 597-604.

Eustace, B.K., Sakurai, T., Stewart, J.K., Yimlamai, D., Unger, C., Zehetmeier, C., Lain, B., Torella, C., Henning, S.W., Beste, G.*, et al.* (2004). Functional proteomic screens reveal an essential extracellular role for hsp90 alpha in cancer cell invasiveness. Nature cell biology *6*, 507-514.

Fairbanks, G., Steck, T.L., and Wallach, D.F. (1971). Electrophoretic analysis of the major polypeptides of the human erythrocyte membrane. Biochemistry *10*, 2606-2617.

Fang, Y., Fliss, A.E., Rao, J., and Caplan, A.J. (1998). SBA1 encodes a yeast hsp90 cochaperone that is homologous to vertebrate p23 proteins. Molecular and cellular biology *18*, 3727-3734.

Felts, S.J., and Toft, D.O. (2003). p23, a simple protein with complex activities. Cell stress & chaperones *8*, 108-113.

Fling, S.P., and Gregerson, D.S. (1986). Peptide and protein molecular weight determination by electrophoresis using a high-molarity tris buffer system without urea. Analytical biochemistry *155*, 83-88.

Forafonov, F., Toogun, O.A., Grad, I., Suslova, E., Freeman, B.C., and Picard, D. (2008). p23/Sba1p protects against Hsp90 inhibitors independently of its intrinsic chaperone activity. Molecular and cellular biology *28*, 3446-3456.

Franco, M.C., Ye, Y., Refakis, C.A., Feldman, J.L., Stokes, A.L., Basso, M., Melero Fernandez de Mera, R.M., Sparrow, N.A., Calingasan, N.Y., Kiaei, M.*, et al.* (2013). Nitration of Hsp90 induces cell death. Proceedings of the National Academy of Sciences of the United States of America *110*, E1102-1111.

Freiburger, L., Sonntag, M., Hennig, J., Li, J., Zou, P., and Sattler, M. (2015). Efficient segmental isotope labeling of multi-domain proteins using Sortase A. Journal of biomolecular NMR *63*, 1-8.

Fries, G.R., Gassen, N.C., Schmidt, U., and Rein, T. (2015). The FKBP51-Glucocorticoid Receptor Balance in Stress-Related Mental Disorders. Current molecular pharmacology *9*, 126-140.

Frydman, J., Erdjument-Bromage, H., Tempst, P., and Hartl, F.U. (1999). Co-translational domain folding as the structural basis for the rapid de novo folding of firefly luciferase. Nature structural biology *6*, 697-705.

Geller, R., Taguwa, S., and Frydman, J. (2012). Broad action of Hsp90 as a host chaperone required for viral replication. Biochimica et biophysica acta *1823*, 698-706.

Georgopoulos, C., and Welch, W.J. (1993). Role of the major heat shock proteins as molecular chaperones. Annual review of cell biology *9*, 601-634.

Gershenson, A., and Gierasch, L.M. (2011). Protein folding in the cell: challenges and progress. Current opinion in structural biology *21*, 32-41.

Gewirth, D.T. (2016). Paralog Specific Hsp90 Inhibitors - A Brief History and a Bright Future. Current topics in medicinal chemistry *16*, 2779-2791.

Ghaemmaghami, S., Huh, W.K., Bower, K., Howson, R.W., Belle, A., Dephoure, N., O'Shea, E.K., and Weissman, J.S. (2003). Global analysis of protein expression in yeast. Nature *425*, 737-741.

Glozak, M.A., Sengupta, N., Zhang, X., and Seto, E. (2005). Acetylation and deacetylation of non-histone proteins. Gene *363*, 15-23.

Graf, C., Lee, C.T., Eva Meier-Andrejszki, L., Nguyen, M.T., and Mayer, M.P. (2014). Differences in conformational dynamics within the Hsp90 chaperone family reveal mechanistic insights. Frontiers in molecular biosciences *1*, 4.

Gupta, R.S. (1995). Phylogenetic analysis of the 90 kD heat shock family of protein sequences and an examination of the relationship among animals, plants, and fungi species. Molecular biology and evolution *12*, 1063-1073.

Guy, N.C., Garcia, Y.A., and Cox, M.B. (2015a). Therapeutic Targeting of the FKBP52 Co-Chaperone in Steroid Hormone Receptor-Regulated Physiology and Disease. Current molecular pharmacology *9*, 109-125.

Guy, N.C., Garcia, Y.A., Sivils, J.C., Galigniana, M.D., and Cox, M.B. (2015b). Functions of the Hsp90-binding FKBP immunophilins. Sub-cellular biochemistry *78*, 35-68.

Harrell, J.M., Murphy, P.J., Morishima, Y., Chen, H., Mansfield, J.F., Galigniana, M.D., and Pratt, W.B. (2004). Evidence for glucocorticoid receptor transport on microtubules by dynein. The Journal of biological chemistry *279*, 54647-54654.

Hartl, F.U. (1996). Molecular chaperones in cellular protein folding. Nature *381*, 571-579.

Hartl, F.U., Bracher, A., and Hayer-Hartl, M. (2011). Molecular chaperones in protein folding and proteostasis. Nature *475*, 324-332.

Hartl, F.U., and Hayer-Hartl, M. (2002). Molecular chaperones in the cytosol: from nascent chain to folded protein. Science *295*, 1852-1858.

Hartl, F.U., and Hayer-Hartl, M. (2009). Converging concepts of protein folding in vitro and in vivo. Nature structural & molecular biology *16*, 574-581.

Hayes, D.B., and Stafford, W.F. (2010). SEDVIEW, real-time sedimentation analysis. Macromolecular bioscience *10*, 731-735.

Hessling, M., Richter, K., and Buchner, J. (2009). Dissection of the ATP-induced conformational cycle of the molecular chaperone Hsp90. Nature structural & molecular biology *16*, 287-293.

Holt, S.E., Glinsky, V.V., Ivanova, A.B., and Glinsky, G.V. (1999). Resistance to apoptosis in human cells conferred by telomerase function and telomere stability. Molecular carcinogenesis *25*, 241-248.

Jahn, M., Rehn, A., Pelz, B., Hellenkamp, B., Richter, K., Rief, M., Buchner, J., and Hugel, T. (2014). The charged linker of the molecular chaperone Hsp90 modulates domain contacts and biological function. Proceedings of the National Academy of Sciences of the United States of America *111*, 17881-17886.

Johnson, J.L., and Brown, C. (2009). Plasticity of the Hsp90 chaperone machine in divergent eukaryotic organisms. Cell stress & chaperones *14*, 83-94.

Johnson, J.L., Halas, A., and Flom, G. (2007). Nucleotide-dependent interaction of Saccharomyces cerevisiae Hsp90 with the cochaperone proteins Sti1, Cpr6, and Sba1. Molecular and cellular biology *27*, 768-776.

Kaganovich, D., Kopito, R., and Frydman, J. (2008). Misfolded proteins partition between two distinct quality control compartments. Nature *454*, 1088-1095.

Karagoz, G.E., Duarte, A.M., Akoury, E., Ippel, H., Biernat, J., Moran Luengo, T., Radli, M., Didenko, T., Nordhues, B.A., Veprintsev, D.B*., et al.* (2014). Hsp90-Tau complex reveals molecular basis for specificity in chaperone action. Cell *156*, 963-974.

Kekatpure, V.D., Dannenberg, A.J., and Subbaramaiah, K. (2009). HDAC6 modulates Hsp90 chaperone activity and regulates activation of aryl hydrocarbon receptor signaling. The Journal of biological chemistry *284*, 7436-7445.

Kirschke, E., Goswami, D., Southworth, D., Griffin, P.R., and Agard, D.A. (2014). Glucocorticoid receptor function regulated by coordinated action of the Hsp90 and Hsp70 chaperone cycles. Cell *157*, 1685-1697.

Kobashigawa, Y., Kumeta, H., Ogura, K., and Inagaki, F. (2009). Attachment of an NMR-invisible solubility enhancement tag using a sortase-mediated protein ligation method. Journal of biomolecular NMR *43*, 145-150.

Kosano, H., Stensgard, B., Charlesworth, M.C., McMahon, N., and Toft, D. (1998). The assembly of progesterone receptor-hsp90 complexes using purified proteins. The Journal of biological chemistry *273*, 32973-32979.

Koulov, A.V., LaPointe, P., Lu, B., Razvi, A., Coppinger, J., Dong, M.Q., Matteson, J., Laister, R., Arrowsmith, C., Yates, J.R., 3rd*, et al.* (2010). Biological and structural basis for Aha1 regulation of Hsp90 ATPase activity in maintaining proteostasis in the human disease cystic fibrosis. Molecular biology of the cell *21*, 871-884.

Kovacs, J.J., Murphy, P.J., Gaillard, S., Zhao, X., Wu, J.T., Nicchitta, C.V., Yoshida, M., Toft, D.O., Pratt, W.B., and Yao, T.P. (2005). HDAC6 regulates Hsp90 acetylation and chaperone-dependent activation of glucocorticoid receptor. Molecular cell *18*, 601-607.

Krukenberg, K.A., Bottcher, U.M., Southworth, D.R., and Agard, D.A. (2009). Grp94, the endoplasmic reticulum Hsp90, has a similar solution conformation to cytosolic Hsp90 in the absence of nucleotide. Protein science : a publication of the Protein Society *18*, 1815-1827.

Krukenberg, K.A., Forster, F., Rice, L.M., Sali, A., and Agard, D.A. (2008). Multiple conformations of E. coli Hsp90 in solution: insights into the conformational dynamics of Hsp90. Structure *16*, 755-765.

Krukenberg, K.A., Street, T.O., Lavery, L.A., and Agard, D.A. (2011). Conformational dynamics of the molecular chaperone Hsp90. Quarterly reviews of biophysics *44*, 229-255.

Labbadia, J., and Morimoto, R.I. (2015). The biology of proteostasis in aging and disease. Annual review of biochemistry *84*, 435-464.

Laemmli, U.K. (1970). Cleavage of structural proteins during the assembly of the head of bacteriophage T4. Nature *227*, 680-685.

Lang, K., and Chin, J.W. (2014). Bioorthogonal reactions for labeling proteins. ACS chemical biology *9*, 16-20.

Lang, K., Davis, L., and Chin, J.W. (2015). Genetic encoding of unnatural amino acids for labeling proteins. Methods in molecular biology *1266*, 217-228.

Langer, T., Lu, C., Echols, H., Flanagan, J., Hayer, M.K., and Hartl, F.U. (1992). Successive action of DnaK, DnaJ and GroEL along the pathway of chaperone-mediated protein folding. Nature *356*, 683-689.

Lavinder, J.J., Hari, S.B., Sullivan, B.J., and Magliery, T.J. (2009). High-throughput thermal scanning: a general, rapid dye-binding thermal shift screen for protein engineering. Journal of the American Chemical Society *131*, 3794-3795.

Lees-Miller, S.P., and Anderson, C.W. (1989). The human double-stranded DNA-activated protein kinase phosphorylates the 90-kDa heat-shock protein, hsp90 alpha at two NH2-terminal threonine residues. The Journal of biological chemistry *264*, 17275-17280.

Levary, D.A., Parthasarathy, R., Boder, E.T., and Ackerman, M.E. (2011). Protein-protein fusion catalyzed by sortase A. PloS one *6*, e18342.

Li, C., Wen, A., Shen, B., Lu, J., Huang, Y., and Chang, Y. (2011a). FastCloning: a highly simplified, purification-free, sequence- and ligation-independent PCR cloning method. BMC biotechnology *11*, 92.

Li, J., Richter, K., and Buchner, J. (2011b). Mixed Hsp90-cochaperone complexes are important for the progression of the reaction cycle. Nature structural & molecular biology *18*, 61-66.

Li, J., Richter, K., Reinstein, J., and Buchner, J. (2013). Integration of the accelerator Aha1 in the Hsp90 co-chaperone cycle. Nature structural & molecular biology *20*, 326-331.

Li, J., Soroka, J., and Buchner, J. (2012). The Hsp90 chaperone machinery: conformational dynamics and regulation by co-chaperones. Biochimica et biophysica acta *1823*, 624-635.

Li, M.Z., and Elledge, S.J. (2012). SLIC: a method for sequence- and ligation-independent cloning. Methods in molecular biology *852*, 51-59.

Li, S.J., and Hochstrasser, M. (1999). A new protease required for cell-cycle progression in yeast. Nature *398*, 246-251.

Li, Z., Dai, J., Zheng, H., Liu, B., and Caudill, M. (2002). An integrated view of the roles and mechanisms of heat shock protein gp96-peptide complex in eliciting immune response. Frontiers in bioscience : a journal and virtual library *7*, d731-751.

Lindquist, S. (1980). Translational efficiency of heat-induced messages in Drosophila melanogaster cells. Journal of molecular biology *137*, 151-158.

Liu, C.C., and Schultz, P.G. (2010). Adding new chemistries to the genetic code. Annual review of biochemistry *79*, 413-444.

Lorenz, O.R., Freiburger, L., Rutz, D.A., Krause, M., Zierer, B.K., Alvira, S., Cuellar, J., Valpuesta, J.M., Madl, T., Sattler, M.*, et al.* (2014). Modulation of the Hsp90 chaperone cycle by a stringent client protein. Molecular cell *53*, 941-953.

Lotz, G.P., Lin, H., Harst, A., and Obermann, W.M. (2003). Aha1 binds to the middle domain of Hsp90, contributes to client protein activation, and stimulates the ATPase activity of the molecular chaperone. The Journal of biological chemistry *278*, 17228-17235.

MacLean, M., and Picard, D. (2003). Cdc37 goes beyond Hsp90 and kinases. Cell stress & chaperones *8*, 114-119.

Mao, H., Hart, S.A., Schink, A., and Pollok, B.A. (2004). Sortase-mediated protein ligation: a new method for protein engineering. Journal of the American Chemical Society *126*, 2670-2671.

Martinez-Ruiz, A., Villanueva, L., Gonzalez de Orduna, C., Lopez-Ferrer, D., Higueras, M.A., Tarin, C., Rodriguez-Crespo, I., Vazquez, J., and Lamas, S. (2005). S-nitrosylation of Hsp90 promotes the inhibition of its ATPase and endothelial nitric oxide synthase regulatory activities. Proceedings of the National Academy of Sciences of the United States of America *102*, 8525-8530.

Mayer, M.P., and Le Breton, L. (2015). Hsp90: breaking the symmetry. Molecular cell *58*, 8-20.

McClellan, A.J., and Frydman, J. (2001). Molecular chaperones and the art of recognizing a lost cause. Nature cell biology *3*, E51-53.

McClellan, A.J., Tam, S., Kaganovich, D., and Frydman, J. (2005). Protein quality control: chaperones culling corrupt conformations. Nature cell biology *7*, 736-741.

McClellan, A.J., Xia, Y., Deutschbauer, A.M., Davis, R.W., Gerstein, M., and Frydman, J. (2007). Diverse cellular functions of the Hsp90 molecular chaperone uncovered using systems approaches. Cell *131*, 121-135.

McDonough, H., and Patterson, C. (2003). CHIP: a link between the chaperone and proteasome systems. Cell stress & chaperones *8*, 303-308.

McLaughlin, S.H., Smith, H.W., and Jackson, S.E. (2002). Stimulation of the weak ATPase activity of human hsp90 by a client protein. Journal of molecular biology *315*, 787-798.

McLaughlin, S.H., Sobott, F., Yao, Z.P., Zhang, W., Nielsen, P.R., Grossmann, J.G., Laue, E.D., Robinson, C.V., and Jackson, S.E. (2006). The co-chaperone p23 arrests the Hsp90 ATPase cycle to trap client proteins. Journal of molecular biology *356*, 746-758.

Metchat, A., Akerfelt, M., Bierkamp, C., Delsinne, V., Sistonen, L., Alexandre, H., and Christians, E.S. (2009). Mammalian heat shock factor 1 is essential for oocyte meiosis and directly regulates Hsp90alpha expression. The Journal of biological chemistry *284*, 9521-9528.

Meyer, P., Prodromou, C., Hu, B., Vaughan, C., Roe, S.M., Panaretou, B., Piper, P.W., and Pearl, L.H. (2003). Structural and functional analysis of the middle segment of hsp90: implications for ATP hydrolysis and client protein and cochaperone interactions. Molecular cell *11*, 647-658.

Mickler, M., Hessling, M., Ratzke, C., Buchner, J., and Hugel, T. (2009). The large conformational changes of Hsp90 are only weakly coupled to ATP hydrolysis. Nature structural & molecular biology *16*, 281-286.

Millson, S.H., Truman, A.W., Racz, A., Hu, B., Panaretou, B., Nuttall, J., Mollapour, M., Soti, C., and Piper, P.W. (2007). Expressed as the sole Hsp90 of yeast, the alpha and beta isoforms of human Hsp90 differ with regard to their capacities for activation of certain client proteins, whereas only Hsp90beta generates sensitivity to the Hsp90 inhibitor radicicol. The FEBS journal *274*, 4453-4463.

Minami, Y., Kimura, Y., Kawasaki, H., Suzuki, K., and Yahara, I. (1994). The carboxy-terminal region of mammalian HSP90 is required for its dimerization and function in vivo. Molecular and cellular biology *14*, 1459-1464.

Minet, E., Mottet, D., Michel, G., Roland, I., Raes, M., Remacle, J., and Michiels, C. (1999). Hypoxia-induced activation of HIF-1: role of HIF-1alpha-Hsp90 interaction. FEBS letters *460*, 251-256.

Minton, A.P. (2001). The influence of macromolecular crowding and macromolecular confinement on biochemical reactions in physiological media. The Journal of biological chemistry *276*, 10577-10580.

Miyata, Y. (2009). Protein kinase CK2 in health and disease: CK2: the kinase controlling the Hsp90 chaperone machinery. Cellular and molecular life sciences : CMLS *66*, 1840-1849.

Miyata, Y., Koren, J., Kiray, J., Dickey, C.A., and Gestwicki, J.E. (2011). Molecular chaperones and regulation of tau quality control: strategies for drug discovery in tauopathies. Future medicinal chemistry *3*, 1523-1537.

Miyata, Y., Nakamoto, H., and Neckers, L. (2013). The therapeutic target Hsp90 and cancer hallmarks. Current pharmaceutical design *19*, 347-365.

Mollapour, M., and Neckers, L. (2012). Post-translational modifications of Hsp90 and their contributions to chaperone regulation. Biochimica et biophysica acta *1823*, 648-655.

Mollapour, M., Tsutsumi, S., Donnelly, A.C., Beebe, K., Tokita, M.J., Lee, M.J., Lee, S., Morra, G., Bourboulia, D., Scroggins, B.T*., et al.* (2010). Swe1Wee1-dependent tyrosine phosphorylation of Hsp90 regulates distinct facets of chaperone function. Molecular cell *37*, 333-343.

Moran, U., Phillips, R., and Milo, R. (2010). SnapShot: key numbers in biology. Cell *141*, 1262-1262 e1261.

Morra, G., Neves, M.A., Plescia, C.J., Tsustsumi, S., Neckers, L., Verkhivker, G., Altieri, D.C., and Colombo, G. (2010). Dynamics-Based Discovery of Allosteric Inhibitors: Selection of New Ligands for the C-terminal Domain of Hsp90. Journal of chemical theory and computation *6*, 2978-2989.

Morra, G., Verkhivker, G., and Colombo, G. (2009). Modeling signal propagation mechanisms and ligand-based conformational dynamics of the Hsp90 molecular chaperone full-length dimer. PLoS computational biology *5*, e1000323.

Muller, A., MacCallum, R.M., and Sternberg, M.J. (2002). Structural characterization of the human proteome. Genome research *12*, 1625-1641.

Nathan, D.F., and Lindquist, S. (1995). Mutational analysis of Hsp90 function: interactions with a steroid receptor and a protein kinase. Molecular and cellular biology *15*, 3917-3925.

Neckers, L., and Workman, P. (2012). Hsp90 molecular chaperone inhibitors: are we there yet? Clinical cancer research : an official journal of the American Association for Cancer Research *18*, 64-76.

Nemoto, T.K., Ono, T., Kobayakawa, T., Tanaka, E., Baba, T.T., Tanaka, K., Takagi, T., and Gotoh, T. (2001). Domain-domain interactions of HtpG, an Escherichia coli homologue of eukaryotic HSP90 molecular chaperone. European journal of biochemistry / FEBS *268*, 5258-5269.

Neumann, H., Hazen, J.L., Weinstein, J., Mehl, R.A., and Chin, J.W. (2008). Genetically encoding protein oxidative damage. Journal of the American Chemical Society *130*, 4028-4033.

Niesen, F.H., Berglund, H., and Vedadi, M. (2007). The use of differential scanning fluorimetry to detect ligand interactions that promote protein stability. Nature protocols *2*, 2212-2221.

Obermann, W.M., Sondermann, H., Russo, A.A., Pavletich, N.P., and Hartl, F.U. (1998). In vivo function of Hsp90 is dependent on ATP binding and ATP hydrolysis. The Journal of cell biology *143*, 901-910.

Oh, E., Becker, A.H., Sandikci, A., Huber, D., Chaba, R., Gloge, F., Nichols, R.J., Typas, A., Gross, C.A., Kramer, G.*, et al.* (2011). Selective ribosome profiling reveals the cotranslational chaperone action of trigger factor in vivo. Cell *147*, 1295-1308.

Onuchic, J.N., and Wolynes, P.G. (2004). Theory of protein folding. Current opinion in structural biology *14*, 70-75.

Overath, T., Kuckelkorn, U., Henklein, P., Strehl, B., Bonar, D., Kloss, A., Siele, D., Kloetzel, P.M., and Janek, K. (2012). Mapping of O-GlcNAc sites of 20 S proteasome subunits and Hsp90 by a novel biotin-cystamine tag. Molecular & cellular proteomics : MCP *11*, 467-477.

Panaretou, B., Prodromou, C., Roe, S.M., O'Brien, R., Ladbury, J.E., Piper, P.W., and Pearl, L.H. (1998). ATP binding and hydrolysis are essential to the function of the Hsp90 molecular chaperone in vivo. The EMBO journal *17*, 4829-4836.

Panaretou, B., Siligardi, G., Meyer, P., Maloney, A., Sullivan, J.K., Singh, S., Millson, S.H., Clarke, P.A., Naaby-Hansen, S., Stein, R.*, et al.* (2002). Activation of the ATPase activity of hsp90 by the stress-regulated cochaperone aha1. Molecular cell *10*, 1307-1318.

Pantzartzi, C.N., Drosopoulou, E., and Scouras, Z.G. (2013). Assessment and reconstruction of novel HSP90 genes: duplications, gains and losses in fungal and animal lineages. PloS one *8*, e73217.

Pearl, L.H. (2016). Review: The HSP90 molecular chaperone-an enigmatic ATPase. Biopolymers *105*, 594-607.

Pirkl, F., and Buchner, J. (2001). Functional analysis of the Hsp90-associated human peptidyl prolyl cis/trans isomerases FKBP51, FKBP52 and Cyp40. Journal of molecular biology *308*, 795-806.

Pirkl, F., Fischer, E., Modrow, S., and Buchner, J. (2001). Localization of the chaperone domain of FKBP52. The Journal of biological chemistry *276*, 37034-37041.

Powers, E.T., Morimoto, R.I., Dillin, A., Kelly, J.W., and Balch, W.E. (2009). Biological and chemical approaches to diseases of proteostasis deficiency. Annual review of biochemistry *78*, 959-991.

Pratt, W.B., Gestwicki, J.E., Osawa, Y., and Lieberman, A.P. (2015). Targeting Hsp90/Hsp70-based protein quality control for treatment of adult onset neurodegenerative diseases. Annual review of pharmacology and toxicology *55*, 353-371.

Preissler, S., and Deuerling, E. (2012). Ribosome-associated chaperones as key players in proteostasis. Trends in biochemical sciences *37*, 274-283.

Prince, T.L., Kijima, T., Tatokoro, M., Lee, S., Tsutsumi, S., Yim, K., Rivas, C., Alarcon, S., Schwartz, H., Khamit-Kush, K.*, et al.* (2015). Client Proteins and Small Molecule Inhibitors Display Distinct Binding Preferences for Constitutive and Stress-Induced HSP90 Isoforms and Their Conformationally Restricted Mutants. PloS one *10*, e0141786.

Prodromou, C. (2012). The 'active life' of Hsp90 complexes. Biochimica et biophysica acta *1823*, 614-623.

Prodromou, C., Panaretou, B., Chohan, S., Siligardi, G., O'Brien, R., Ladbury, J.E., Roe, S.M., Piper, P.W., and Pearl, L.H. (2000). The ATPase cycle of Hsp90 drives a molecular 'clamp' via transient dimerization of the N-terminal domains. The EMBO journal *19*, 4383-4392.

Prodromou, C., Roe, S.M., O'Brien, R., Ladbury, J.E., Piper, P.W., and Pearl, L.H. (1997). Identification and structural characterization of the ATP/ADP-binding site in the Hsp90 molecular chaperone. Cell *90*, 65-75.

Prodromou, C., Siligardi, G., O'Brien, R., Woolfson, D.N., Regan, L., Panaretou, B., Ladbury, J.E., Piper, P.W., and Pearl, L.H. (1999). Regulation of Hsp90 ATPase activity by tetratricopeptide repeat (TPR)-domain co-chaperones. The EMBO journal *18*, 754-762.

Rehn, A., Moroni, E., Zierer, B.K., Tippel, F., Morra, G., John, C., Richter, K., Colombo, G., and Buchner, J. (2016). Allosteric Regulation Points Control the Conformational Dynamics of the Molecular Chaperone Hsp90. Journal of molecular biology.

Reis, S.D., Pinho, B.R., and Oliveira, J.M. (2016). Modulation of Molecular Chaperones in Huntington's Disease and Other Polyglutamine Disorders. Molecular neurobiology.

Retzlaff, M., Hagn, F., Mitschke, L., Hessling, M., Gugel, F., Kessler, H., Richter, K., and Buchner, J. (2010). Asymmetric activation of the hsp90 dimer by its cochaperone aha1. Molecular cell *37*, 344-354.

Retzlaff, M., Stahl, M., Eberl, H.C., Lagleder, S., Beck, J., Kessler, H., and Buchner, J. (2009). Hsp90 is regulated by a switch point in the C-terminal domain. EMBO reports *10*, 1147-1153.

Richter, K., Haslbeck, M., and Buchner, J. (2010). The heat shock response: life on the verge of death. Molecular cell *40*, 253-266.

Richter, K., Muschler, P., Hainzl, O., and Buchner, J. (2001). Coordinated ATP hydrolysis by the Hsp90 dimer. The Journal of biological chemistry *276*, 33689-33696.

Richter, K., Reinstein, J., and Buchner, J. (2002). N-terminal residues regulate the catalytic efficiency of the Hsp90 ATPase cycle. The Journal of biological chemistry *277*, 44905-44910.

Richter, K., Soroka, J., Skalniak, L., Leskovar, A., Hessling, M., Reinstein, J., and Buchner, J. (2008). Conserved conformational changes in the ATPase cycle of human Hsp90. The Journal of biological chemistry *283*, 17757-17765.

Richter, K., Walter, S., and Buchner, J. (2004). The Co-chaperone Sba1 connects the ATPase reaction of Hsp90 to the progression of the chaperone cycle. Journal of molecular biology *342*, 1403-1413.

Riggs, D.L., Roberts, P.J., Chirillo, S.C., Cheung-Flynn, J., Prapapanich, V., Ratajczak, T., Gaber, R., Picard, D., and Smith, D.F. (2003). The Hsp90-binding peptidylprolyl isomerase FKBP52 potentiates glucocorticoid signaling in vivo. The EMBO journal *22*, 1158-1167.

Ritossa, F.M., and Vonborstel, R.C. (1964). Chromosome Puffs in Drosophila Induced by Ribonuclease. Science *145*, 513-514.

Rodina, A., Wang, T., Yan, P., Gomes, E.D., Dunphy, M.P., Pillarsetty, N., Koren, J., Gerecitano, J.F., Taldone, T., Zong, H.*, et al.* (2016). The epichaperome is an integrated chaperome network that facilitates tumour survival. Nature.

Roe, S.M., Ali, M.M., Meyer, P., Vaughan, C.K., Panaretou, B., Piper, P.W., Prodromou, C., and Pearl, L.H. (2004). The Mechanism of Hsp90 regulation by the protein kinase-specific cochaperone p50(cdc37). Cell *116*, 87-98.

Roe, S.M., Prodromou, C., O'Brien, R., Ladbury, J.E., Piper, P.W., and Pearl, L.H. (1999). Structural basis for inhibition of the Hsp90 molecular chaperone by the antitumor antibiotics radicicol and geldanamycin. Journal of medicinal chemistry *42*, 260-266.

Rohl, A., Rohrberg, J., and Buchner, J. (2013). The chaperone Hsp90: changing partners for demanding clients. Trends in biochemical sciences *38*, 253-262.

Rohl, A., Tippel, F., Bender, E., Schmid, A.B., Richter, K., Madl, T., and Buchner, J. (2015a). Hop/Sti1 phosphorylation inhibits its co-chaperone function. EMBO reports *16*, 240-249.

Rohl, A., Wengler, D., Madl, T., Lagleder, S., Tippel, F., Herrmann, M., Hendrix, J., Richter, K., Hack, G., Schmid, A.B.*, et al.* (2015b). Hsp90 regulates the dynamics of its cochaperone Sti1 and the transfer of Hsp70 between modules. Nature communications *6*, 6655.

Sambrook, J., Fritsch, E., Maniatis, T. (1989). Molecular Cloning: a laboratory Manual. (Cold spring Harbor Laboratory Press).

Sanchez, E.R., Toft, D.O., Schlesinger, M.J., and Pratt, W.B. (1985). Evidence that the 90-kDa phosphoprotein associated with the untransformed L-cell glucocorticoid receptor is a murine heat shock protein. The Journal of biological chemistry *260*, 12398-12401.

Sawkar, A.R., D'Haeze, W., and Kelly, J.W. (2006). Therapeutic strategies to ameliorate lysosomal storage disorders--a focus on Gaucher disease. Cellular and molecular life sciences : CMLS *63*, 1179-1192.

Scheufler, C., Brinker, A., Bourenkov, G., Pegoraro, S., Moroder, L., Bartunik, H., Hartl, F.U., and Moarefi, I. (2000). Structure of TPR domain-peptide complexes: critical elements in the assembly of the Hsp70-Hsp90 multichaperone machine. Cell *101*, 199-210.

Schmid, A.B., Lagleder, S., Grawert, M.A., Rohl, A., Hagn, F., Wandinger, S.K., Cox, M.B., Demmer, O., Richter, K., Groll, M.*, et al.* (2012). The architecture of functional modules in the Hsp90 co-chaperone Sti1/Hop. The EMBO journal *31*, 1506-1517.

Schulte, T.W., Akinaga, S., Soga, S., Sullivan, W., Stensgard, B., Toft, D., and Neckers, L.M. (1998). Antibiotic radicicol binds to the N-terminal domain of Hsp90 and shares important biologic activities with geldanamycin. Cell stress & chaperones *3*, 100-108.

Schulze, A., Beliu, G., Helmerich, D.A., Schubert, J., Pearl, L.H., Prodromou, C., and Neuweiler, H. (2016). Cooperation of local motions in the Hsp90 molecular chaperone ATPase mechanism. Nature chemical biology *12*, 628-635.

Scroggins, B.T., Robzyk, K., Wang, D., Marcu, M.G., Tsutsumi, S., Beebe, K., Cotter, R.J., Felts, S., Toft, D., Karnitz, L.*, et al.* (2007). An acetylation site in the middle domain of Hsp90 regulates chaperone function. Molecular cell *25*, 151-159.

Sepehrnia, B., Paz, I.B., Dasgupta, G., and Momand, J. (1996). Heat shock protein 84 forms a complex with mutant p53 protein predominantly within a cytoplasmic compartment of the cell. The Journal of biological chemistry *271*, 15084-15090.

Shiau, A.K., Harris, S.F., Southworth, D.R., and Agard, D.A. (2006). Structural Analysis of E. coli hsp90 reveals dramatic nucleotide-dependent conformational rearrangements. Cell *127*, 329-340.

Silva, A., Sampaio-Marques, B., Fernandes, A., Carreto, L., Rodrigues, F., Holcik, M., Santos, M.A., and Ludovico, P. (2013). Involvement of yeast HSP90 isoforms in response to stress and cell death induced by acetic acid. PloS one *8*, e71294.

Simon, M.D., Chu, F., Racki, L.R., de la Cruz, C.C., Burlingame, A.L., Panning, B., Narlikar, G.J., and Shokat, K.M. (2007). The site-specific installation of methyl-lysine analogs into recombinant histones. Cell *128*, 1003-1012.

Smith, D.F., Faber, L.E., and Toft, D.O. (1990). Purification of unactivated progesterone receptor and identification of novel receptor-associated proteins. The Journal of biological chemistry *265*, 3996-4003.

Soroka, J., and Buchner, J. (2012). Mechanistic aspects of the Hsp90 phosphoregulation. Cell cycle *11*, 1870-1871.

Soroka, J., Wandinger, S.K., Mausbacher, N., Schreiber, T., Richter, K., Daub, H., and Buchner, J. (2012). Conformational switching of the molecular chaperone Hsp90 via regulated phosphorylation. Molecular cell *45*, 517-528.

Southworth, D.R., and Agard, D.A. (2008). Species-dependent ensembles of conserved conformational states define the Hsp90 chaperone ATPase cycle. Molecular cell *32*, 631-640.

Spicer, C.D., and Davis, B.G. (2014). Selective chemical protein modification. Nature communications *5*, 4740.

Sreedhar, A.S., Kalmar, E., Csermely, P., and Shen, Y.F. (2004). Hsp90 isoforms: functions, expression and clinical importance. FEBS letters *562*, 11-15.

Stafford, W.F., 3rd (1992). Boundary analysis in sedimentation transport experiments: a procedure for obtaining sedimentation coefficient distributions using the time derivative of the concentration profile. Analytical biochemistry *203*, 295-301.

Stebbins, C.E., Russo, A.A., Schneider, C., Rosen, N., Hartl, F.U., and Pavletich, N.P. (1997). Crystal structure of an Hsp90-geldanamycin complex: targeting of a protein chaperone by an antitumor agent. Cell *89*, 239-250.

Storer, C.L., Dickey, C.A., Galigniana, M.D., Rein, T., and Cox, M.B. (2011). FKBP51 and FKBP52 in signaling and disease. Trends in endocrinology and metabolism: TEM *22*, 481-490.

Street, T.O., Lavery, L.A., and Agard, D.A. (2011). Substrate binding drives large-scale conformational changes in the Hsp90 molecular chaperone. Molecular cell *42*, 96-105.

Sullivan, W.P., Owen, B.A., and Toft, D.O. (2002). The influence of ATP and p23 on the conformation of hsp90. The Journal of biological chemistry *277*, 45942-45948.

Svergun, D.I. (1992). Determination of the regularization parameter in indirect-transform methods using perceptual criteria. .

Synoradzki, K., and Bieganowski, P. (2015). Middle domain of human Hsp90 isoforms differentially binds Aha1 in human cells and alters Hsp90 activity in yeast. Biochimica et biophysica acta *1853*, 445-452.

Taherian, A., Krone, P.H., and Ovsenek, N. (2008). A comparison of Hsp90alpha and Hsp90beta interactions with cochaperones and substrates. Biochemistry and cell biology = Biochimie et biologie cellulaire *86*, 37-45.

Taipale, M., Jarosz, D.F., and Lindquist, S. (2010). HSP90 at the hub of protein homeostasis: emerging mechanistic insights. Nature reviews Molecular cell biology *11*, 515-528.

Taipale, M., Krykbaeva, I., Koeva, M., Kayatekin, C., Westover, K.D., Karras, G.I., and Lindquist, S. (2012). Quantitative analysis of HSP90-client interactions reveals principles of substrate recognition. Cell *150*, 987-1001.

Taylor, R.C., and Dillin, A. (2011). Aging as an event of proteostasis collapse. Cold Spring Harbor perspectives in biology *3*.

Toogun, O.A., Zeiger, W., and Freeman, B.C. (2007). The p23 molecular chaperone promotes functional telomerase complexes through DNA dissociation. Proceedings of the National Academy of Sciences of the United States of America *104*, 5765-5770.

Tranguch, S., Cheung-Flynn, J., Daikoku, T., Prapapanich, V., Cox, M.B., Xie, H., Wang, H., Das, S.K., Smith, D.F., and Dey, S.K. (2005). Cochaperone immunophilin FKBP52 is critical to uterine receptivity for embryo implantation. Proceedings of the National Academy of Sciences of the United States of America *102*, 14326-14331.

Vaughan, C.K., Gohlke, U., Sobott, F., Good, V.M., Ali, M.M., Prodromou, C., Robinson, C.V., Saibil, H.R., and Pearl, L.H. (2006). Structure of an Hsp90-Cdc37-Cdk4 complex. Molecular cell *23*, 697-707.

Vaughan, C.K., Mollapour, M., Smith, J.R., Truman, A., Hu, B., Good, V.M., Panaretou, B., Neckers, L., Clarke, P.A., Workman, P*., et al.* (2008). Hsp90-dependent activation of protein kinases is regulated by chaperone-targeted dephosphorylation of Cdc37. Molecular cell *31*, 886-895.

Vaughan, C.K., Piper, P.W., Pearl, L.H., and Prodromou, C. (2009). A common conformationally coupled ATPase mechanism for yeast and human cytoplasmic HSP90s. The FEBS journal *276*, 199-209.

Verba, K.A., Wang, R.Y., Arakawa, A., Liu, Y., Shirouzu, M., Yokoyama, S., and Agard, D.A. (2016). Atomic structure of Hsp90-Cdc37-Cdk4 reveals that Hsp90 traps and stabilizes an unfolded kinase. Science *352*, 1542-1547.

Vogt, P.K. (2012). Retroviral oncogenes: a historical primer. Nature reviews Cancer *12*, 639-648.

Wandinger, S.K., Richter, K., and Buchner, J. (2008). The Hsp90 chaperone machinery. The Journal of biological chemistry *283*, 18473-18477.

Wegele, H., Wandinger, S.K., Schmid, A.B., Reinstein, J., and Buchner, J. (2006). Substrate transfer from the chaperone Hsp70 to Hsp90. Journal of molecular biology *356*, 802-811.

Weikl, T., Abelmann, K., and Buchner, J. (1999). An unstructured C-terminal region of the Hsp90 co-chaperone p23 is important for its chaperone function. Journal of molecular biology *293*, 685-691.

Whitesell, L., and Lindquist, S.L. (2005). HSP90 and the chaperoning of cancer. Nature reviews Cancer *5*, 761-772.

Willmund, F., del Alamo, M., Pechmann, S., Chen, T., Albanese, V., Dammer, E.B., Peng, J., and Frydman, J. (2013). The cotranslational function of ribosome-associated Hsp70 in eukaryotic protein homeostasis. Cell *152*, 196-209.

Xu, Y., and Lindquist, S. (1993). Heat-shock protein hsp90 governs the activity of pp60v-src kinase. Proceedings of the National Academy of Sciences of the United States of America *90*, 7074-7078.

Xu, Y., Singer, M.A., and Lindquist, S. (1999). Maturation of the tyrosine kinase c-src as a kinase and as a substrate depends on the molecular chaperone Hsp90. Proceedings of the National Academy of Sciences of the United States of America *96*, 109-114.

Young, J.C., Obermann, W.M., and Hartl, F.U. (1998). Specific binding of tetratricopeptide repeat proteins to the C-terminal 12-kDa domain of hsp90. The Journal of biological chemistry *273*, 18007-18010.

Yu, X., Guo, Z.S., Marcu, M.G., Neckers, L., Nguyen, D.M., Chen, G.A., and Schrump, D.S. (2002). Modulation of p53, ErbB1, ErbB2, and Raf-1 expression in lung cancer cells by depsipeptide FR901228. Journal of the National Cancer Institute *94*, 504-513.

Zelin, E., Zhang, Y., Toogun, O.A., Zhong, S., and Freeman, B.C. (2012). The p23 molecular chaperone and GCN5 acetylase jointly modulate protein-DNA dynamics and open chromatin status. Molecular cell *48*, 459-470.

Zimmerman, S.B., and Trach, S.O. (1991). Estimation of macromolecule concentrations and excluded volume effects for the cytoplasm of Escherichia coli. Journal of molecular biology *222*, 599-620.

Zuehlke, A., and Johnson, J.L. (2010). Hsp90 and co-chaperones twist the functions of diverse client proteins. Biopolymers *93*, 211-217.

Abbreviations

5‘-FOA	5’-fluoroorotic acid
A	ampere
A_{280}	absorption at 280 nm
Å	Ångström
AA	amino acid
ADP	adenosindiphosphate
amp	ampicillin
AMP-PNP	adenylyl-imidodiphosphate
APS	ammoniumpersulfate
ATP	adenosintriphosphate
ATPγS	adenosin-5-(γ -thio)-triphosphate
a.u.	arbitrary units
aUC	analytical ultracentrifugation
BSA	bovine serume albumin
CD	circular dicroism
CTD	C-terminal domain
CV	column volume
Da	dalton
DNA	deoxyribonucleic acid
dNTPs	deoxynucleoside triphosphate
DOC	11-deoxycorticosterone
DTT	1,4-dithiothreitol
E. coli	*Escherichia coli*
EM	electron microscopy
ER	endoplasmic reticulum
FPLC	fast protein liquid chromatography
FRET	Fluorescence Resonance Energy Transfer
GHKL	gyrase, hsp90, histidine kinase, mutL
GR	glucocorticoid receptor
HAT	hydroxyapatite
HPLC	high performance liquid chromatography
Hsp	Heat schock protein
IC_{50}	half maximal inhibitory concentration
IEC	ion exchange chromatography
IPTG	isopropyl-β-D-thiogalactopyranosid
kana	kanamycin
k_{cat}	unimolecular rate constant
k_D	dissociation constant
kDa	kilo dalton
LB_0	Luria-Bertani media without antibiotics
LDH	lactate dehydrogenase
LiAc	lithium acetate
MD	middle domain
MS	mass spectrometry
MW	molecular weight
NAC	nacent chain associated complex
NADH	nicotinamide adenine dinucleotide
ND	N-terminal domain
NEF	nucleotide exchange factor
NMR	nuclear magnetic resonance
OD_{600}	optical density at 600 nm
ONPG	O-nitropehenyl β-D-galactopyranoside

ON	over night
PCR	polymerase chain reaction
P_i	orthophosphate
$_P$I	isoelectric point
PEP	phosphoenolpyruvate
PK	pyruvate kinase
POD	peroxidase
PPIase	Peptidyl-prolyl-isomerase
PTM	post-translational modification
RAC	ribosome associated complex
Rpm	revolution per minute
RT	room temperature
S. cerevisiae	*Saccharomyces cerevisiae*
SAXS	Small Angle X-ray Scattering
SDS-PAGE	Sodium dodecyl sulfate polyacrylamid gel electrophoresis
SEC	size exclusion chromatography
sHsp	small heat schock protein
SLIC	sequence- and ligation independent cloning
SrtA	Sortase A
tet	tetracyclin
TF	trigger factor
TPR	tetratricopeptide repeat
UV	ultra-violet
vSrc	viral Src kinase
wt	wild type
YNB	yeast nitrogen base
YPD	yeast extract peptone dextrose

Publications

- Zierer BK*, Rübbelke M*, **Tippel F***, Madl T, Schopf FH, Rutz DA, Richter K, Sattler M, Buchner J. Importance of cycle timing for the function of the molecular chaperone Hsp90. ***Nat Struct Mol Biol***. 2016 Nov 23 (*These authors contributed equally to this work.)

- Rehn AB, Moroni E, Zierer BK, **Tippel F**, Morra G, John C, Richter K, Colombo G, Buchner J. Allosteric regulation points control the conformational dynamics in the molecular chaperone Hsp90. ***J Mol Biol.*** 2016 Nov 6

- Röhl A, Wengler D, Madl T, Lagleder S, **Tippel F**, Herrmann M, Hendrix J, Richter K, Hack G, Schmid AB, Kessler H, Lamb DC, Buchner J. Hsp90 regulates the dynamics of its cochaperone Sti1 and the transfer of Hsp70 between modules**.** ***Nat Commun***. 2015 Apr 8.

- Röhl A, **Tippel F**, Bender E, Schmid AB, Richter K, Madl T, Buchner J. Hop/Sti1 phosphorylation inhibits its co-chaperone function. ***EMBO Rep.*** 2015 Feb 16.

Acknowledgements

First, I would like to thank my Professor, Johannes Buchner, for the possibility to prepare my thesis in an exiting research environment. Furthermore, I like to thank him for his guidance during the whole time working on my thesis. I would like to thank him for the interesting and challenging research topic and for his confidence and belief that he showed to me. Also, for giving me the opportunity to attend many exciting conferences.

Special thanks apply to Alina Röhl, Bettina Zierer, Alexandra Rehn, Tobias Madl, Michael Sattler and Giorgio Colombo for productive and perfect cooperation on several Hsp90 projects during my thesis work.

I would like to thank my office members Hannah Girstmair, Florian Schopf and Daniel Rutz for helpful support and intensive discussions. Special thanks goes to all members of the Buchner group, in particular my lab members Priyanka Sahasrabudhe and Sandrine Stiegler, for the daily good working atmosphere.

I am grateful that I had the opportunity to supervise wonderful interns and master thesis students, Katha Lamm, Melly Breintner, Louise Funke, Barbara Tremmel and Sophie Flommersfeld, who participated in both projects.

In addition, I thank our lab technicians, Hasi and Margot Rubinstein for a smooth lab and bureaucracy everyday life.

Also, Marina Daaka, Christine John, Chrissy Stutzer and Pamina Kazman, who went for running with me even in winter times during our “lunch break”.

For generous financial and ideally support I would like to thank the Studienstiftung des Deutschen Volkes and the TUM graduate school.

Finally, great thanks to my family, friends and last but not least my boyfriend Oliver Süßmuth, for their constant encouragement and support.

Declaration

Hereby I declare that this thesis was written independently, without use of other resources or references than the stated ones. This work has not been presented to any examination broad yet.

Hiermit erkläre ich, Franziska Tippel, dass die vorliegende Arbeit selbstständig verfasst wurde. Dabei wurden keine anderen als die hier angegebenen Hilfsmittel oder Quellen verwendet. Diese Arbeit wurde bisher keiner anderen Prüfungsbehörde vorgelegt.

Franziska Tippel

München, Dezember